

AD-A126 689

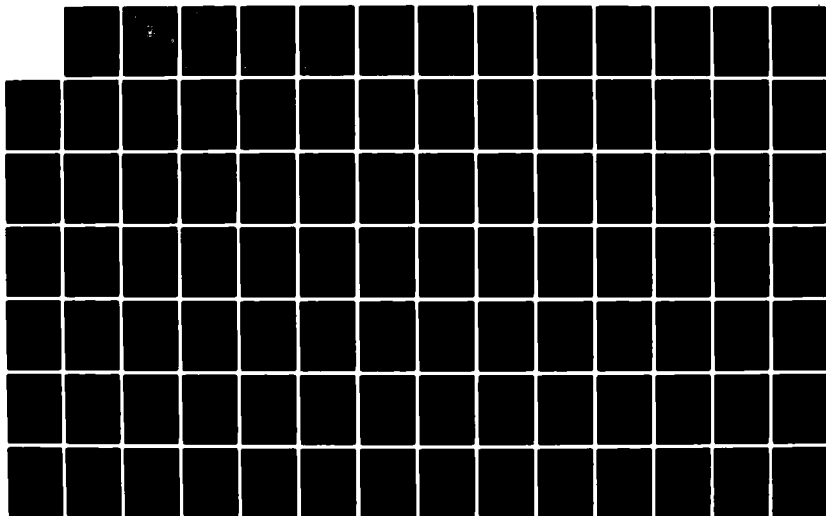
INERTIAL NAVIGATION SYSTEMS AIDED BY GPS(U) NAVAL
POSTGRADUATE SCHOOL MONTEREY CA C C SAFLIANIS DEC 82

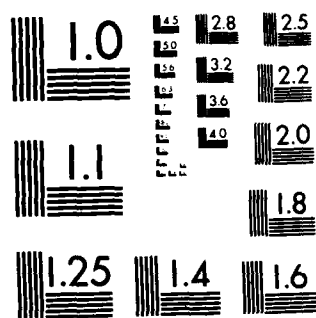
1/4

UNCLASSIFIED

F/G 17/7

NL





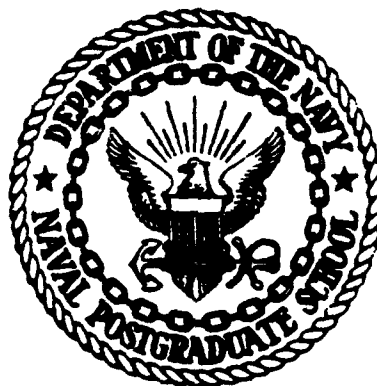
MICROCOPY RESOLUTION TEST CHART
NATIONAL BUREAU OF STANDARDS-1963-A

2

NAVAL POSTGRADUATE SCHOOL

Monterey, California

ADA 126689



THESIS

DTIC
ELECTE
APR 11 1983
S H D

INERTIAL NAVIGATION SYSTEMS

AIDED BY G.P.S.

by

Constantinos Christou Saflianis

December 1982

Thesis Advisor:

D. Collins

DTIC FILE COPY

Approved for public release; distribution unlimited

83 04 11 041'

UNCLASSIFIED

SECURITY CLASSIFICATION OF THIS PAGE (When Data Entered)

REPORT DOCUMENTATION PAGE		READ INSTRUCTIONS BEFORE COMPLETING FORM
1. REPORT NUMBER	2. GOVT ACCESSION NO.	3. RECIPIENT'S CATALOG NUMBER
4. TITLE (and Subtitle) INERTIAL NAVIGATION SYSTEMS AIDED BY G.P.S.		5. TYPE OF REPORT & PERIOD COVERED Master's Thesis; December 1982
7. AUTHOR(s) Constantinos Christou Saflianis		6. PERFORMING ORG. REPORT NUMBER
8. PERFORMING ORGANIZATION NAME AND ADDRESS Naval Postgraduate School Monterey, California 93940		9. CONTRACT OR GRANT NUMBER(s)
11. CONTROLLING OFFICE NAME AND ADDRESS Naval Postgraduate School Monterey, California 93940		10. PROGRAM ELEMENT, PROJECT, TASK AREA & WORK UNIT NUMBERS
14. MONITORING AGENCY NAME & ADDRESS (if different from Controlling Office)		12. REPORT DATE December 1982
		13. NUMBER OF PAGES 306 pages
		15. SECURITY CLASS. (of this report) Unclassified
		16a. DECLASSIFICATION/DOWNGRADING SCHEDULE
16. DISTRIBUTION STATEMENT (of this Report) Approved for public release; distribution unlimited		
17. DISTRIBUTION STATEMENT (of the abstract entered in Block 20, if different from Report)		
18. SUPPLEMENTARY NOTES		
19. KEY WORDS (Continue on reverse side if necessary and identify by block number) Inertial Navigation Systems Global Positioning System		
20. ABSTRACT (Continue on reverse side if necessary and identify by block number) The present work is a Kalman filter study, in indirect feedback configuration, for a proposed integrated inexpensive Inertial Navigation System/Global Positioning System (I.N.S./G.P.S.). A one nautical mile per hour, local-level, two-accelerometer I.N.S. is used where the errors are represented by a 7 state linear model.		

DD FORM 1 JAN 73 1473

EDITION OF 1 NOV 65 IS OBSOLETE
S/N 0102-014-6601

UNCLASSIFIED

SECURITY CLASSIFICATION OF THIS PAGE (When Data Entered)

UNCLASSIFIED

SECURITY CLASSIFICATION OF THIS PAGE/When Data Entered

20. (Continued)

G.P.S. is assumed to provide four range measurements from an equal number of satellites with the best relative position among those in view.

I.N.S. error analysis showed error dependence on Schuler frequency and that it was possible to neglect Foucault modulation for navigation purposes.

The present I.N.S./G.P.S. system has been shown to be quite effective since the navigation errors are reduced quickly for both short and long term periods without any divergence.

Accession For	
NTIS GRA&I	<input checked="checked" type="checkbox"/>
DTIC TAB	<input type="checkbox"/>
Unannounced	<input type="checkbox"/>
Justification	
By _____	
Distribution/	
Availability Codes	
Dist	Avail and/or Special
A	



Approved for public release; distribution unlimited

Inertial Navigation Systems Aided by G.P.S.

by

Constantinos Christou Saflianis
Lieutenant, Hellenic Navy
B.S., Naval Postgraduate School, 1981

Submitted in partial fulfillment of the
requirements for the degrees of

MASTER OF SCIENCE IN ELECTRICAL ENGINEERING

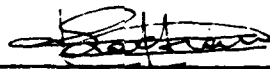
and

MASTER OF SCIENCE IN ENGINEERING SCIENCE

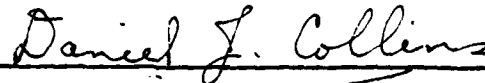
from the

NAVAL POSTGRADUATE SCHOOL
December 1982

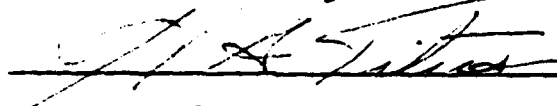
Author:



Approved by:



Thesis Advisor



Co-Advisor



Chairman, Department of Electrical Engineering



Chairman, Department of Aeronautics



Dean of Science and Engineering

ABSTRACT

The present work is a Kalman filter study, in indirect feedback configuration, for a proposed integrated inexpensive Inertial Navigation System/Global Positioning System (I.N.S./G.P.S.).

A one nautical mile per hour, local-level, two-accelerometer I.N.S. is used where the errors are represented by a 7 state linear model.

G.P.S. is assumed to provide four range measurements from an equal number of satellites with the best relative position among those in view.

I.N.S. error analysis showed error dependence on Schuler frequency and that it was possible to neglect Foucault modulation for navigation purposes.

The present I.N.S./G.P.S. system has been shown to be quite effective since the navigation errors are reduced quickly for both short and long term periods without any divergence.

TABLE OF CONTENTS

I.	INTRODUCTION	19
	A. OVERVIEW OF AN INERTIAL NAVIGATION SYSTEM (I.N.S.)	19
	B. OVERVIEW OF THE G.P.S.	20
	C. I.N.S OPTIMAL AIDING	22
	D. KALMAN FILTER	24
	1. Type of Filter Implementation	25
	2. Assumptions	26
II.	KALMAN FILTER EQUATIONS	30
	A. GENERAL	30
	B. SYSTEM MODEL EQUATIONS	31
	C. FILTER EQUATIONS	33
III.	I.N.S. ERROR ANALYSIS	40
	A. GENERAL	40
	B. GENERAL I.N.S ASSUMPTIONS	42
	C. LOCAL-LEVEL TERRESTRIAL NAVIGATOR	43
	D. THE TWO-ACCELEROMETER LOCAL-LEVEL SYSTEM	44
	1. Error Model Equations	45
	2. Error Equations Solution	51
	a. Constant Gyro Drift Errors	52
	b. Accelerometer Bias Errors	56
	c. Initial Conditions Errors	57

IV.	I.N.S./G.P.S. SYSTEM MODEL AND EQUATIONS SOLUTION	59
A.	SYSTEM MODEL	59
1.	State Variable Definition and Initial Conditions	59
2.	Plant Error States	61
B.	EQUATIONS, SOLUTION AND COMPUTER SIMULATION . .	61
C.	I.N.S. COMPONENT ERROR MODELS	77
1.	Gyro Drift Uncertainties	77
2.	Accelerometer Measurement Uncertainties . .	78
3.	Computer Simulation Results	78
V.	CONCLUSIONS AND RECOMMENDATIONS	80
A.	CONCLUSIONS	80
B.	RECOMMENDATIONS	82
APPENDIX A:	A Simple Example: Kalman Filter Application to a Radar Position Aided Inertial Navigation System	181
APPENDIX B:	Satellite Geometry, View and Range Errors	251
APPENDIX C:	I.N.S. Error Analysis Computer Programs . .	274
APPENDIX D:	RICATI Computer Program Data	292
APPENDIX E:	I.N.S./G.P.S. Error Analysis Computer Programs	293
	LIST OF REFERENCES	302
	BIBLIOGRAPHY	303
	INITIAL DISTRIBUTION LIST	305

LIST OF TABLES

I.	I.N.S. System Model Matrices F_e and G_e	50
II.	Computer Simulation Parameters	53
III.	I.N.S./G.P.S. System State Vector Definition	62
IV.	Computer Simulation Variables and Constants	65
V.	Numerical Values for RICATI Program	68
VI.	Kalman Filter Gains for a 4 Hour Process	70
VII.	Summary of State Errors for the I.N.S./G.P.S. System Model	76
VIII.	Computer Runs Summary	198
IX.	Orbital Design Constants	262
X.	Satellite Initial Conditions	263
XI-1 through 6.	Satellite Position and Observability Criterion for Times 30 sec, 60 sec, 120 sec, 360 sec, 1200 sec, 3600 sec	263

LIST OF FIGURES

1.	Typical Gimbaled Inertial Measurement Unit	21
2.	NAVSTAR/G.P.S. Phases	23
3.	Indirect Feedback Kalman Filter	27
4.	Stationary Case. North Level Error [Rad/meru] for Constant North Gyro Drift [1 meru]	84
5.	Stationary Case. East Level Error [Rad/meru] for Constant North Gyro Drift [1 meru]	85
6.	Stationary Case. Azimuth Level Error [Rad/meru] for Constant North Gyro Drift [1 meru]	86
7.	Stationary Case. Latitude Error [Rad/meru] for Constant North Gyro Drift [1 meru]	87
8.	Stationary Case. Longitude Error [Rad/meru] for Constant North Gyro Drift [1 meru]	88
9.	Stationary Case. Latitude Rate Error [Rad/hour*meru] for Constant North Gyro Drift [1 meru]	89
10.	Stationary Case. Longitude Rate Error [Rad/hour*meru] for Constant North Gyro Drift [1 meru]	90
11.	Easterly Flight at 600 ft/sec. North Level Error [Rad/meru] for Constant North Gyro Drift [1 meru]	91
12.	Easterly Flight at 600 ft/sec. East Level Error [Rad/meru] for Constant North Gyro Drift [1 meru]	92
13.	Easterly Flight at 600 ft/sec. Azimuth Level Error [Rad/meru] for Constant North Gyro Drift [1 meru]	93
14.	Easterly Flight at 600 ft/sec. Latitude Error [Rad/meru] for Constant North Gyro Drift [1 meru]	94

15.	Easterly Flight at 600 ft/sec. Longitude Error [Rad/meru] for Constant North Gyro Drift [1 meru]	95
16.	Easterly Flight at 600 ft/sec. Latitude Rate Error [Rad/hour meru] for Constant North Gyro Drift [1 meru]	96
17.	Easterly Flight at 600 ft/sec. Longitude Rate Error [Rad/hour meru] for Constant North Gyro Drift [1 meru]	97
18.	Westerly Flight at 600 ft/sec. North Level Error [Rad/meru] for Constant North Gyro Drift [1 meru]	98
19.	Westerly Flight at 600 ft/sec. East Level Error [Rad/meru] for Constant North Gyro Drift [1 meru]	99
20.	Westerly Flight at 600 ft/sec. Azimuth Level Error [Rad/meru] for Constant North Gyro Drift [1 meru]	100
21.	Westerly Flight at 600 ft/sec. Latitude Error [Rad/meru] for Constant North Gyro Drift [1 meru]	101
22.	Westerly Flight at 600 ft/sec. Longitude Error [Rad/meru] for Constant North Gyro Drift [1 meru]	102
23.	Westerly Flight at 600 ft/sec. Latitude Rate Error [Rad/hour meru] for Constant North Gyro Drift [1 meru]	103
24.	Westerly Flight at 600 ft/sec. Longitude Rate Error [Rad/hour meru] for Constant North Gyro Drift [1 meru]	104
25.	Stationary Case. North Level Error [Rad/200ug] for Constant North Accelerometer Bias [200ug] . . .	105
26.	Stationary Case. East Level Error [Rad/200ug] for Constant North Accelerometer Bias [200ug] . . .	106
27.	Stationary Case. Azimuth Level Error [Rad/200ug] for Constant North Accelerometer Bias [200ug]	107

28.	Stationary Case. Latitude Error [Rad/200 μ g] for Constant North Accelerometer Bias [200 μ g] . . .	108
29.	Stationary Case. Longitude Error [Rad/200 μ g] for Constant North Accelerometer Bias [200 μ g] . . .	109
30.	Stationary Case. Latitude Rate Error [Rad/hour \cdot 200 μ g] for Constant Accelerometer Bias [200 μ g]	110
31.	Stationary Case. Longitude Rate Error [Rad/hour \cdot 200 μ g] for Constant Accelerometer Bias [200 μ g]	111
32.	Easterly Flight at 600 ft/sec. North Level Error [Rad/200 μ g] for Constant North Accelerometer Bias [200 μ g]	112
33.	Easterly Flight at 600 ft/sec. East Level Error [Rad/200 μ g] for Constant North Accelerometer Bias [200 μ g]	113
34.	Easterly Flight at 600 ft/sec. Azimuth Level Error [Rad/200 μ g] for Constant North Accelerometer Bias [200 μ g]	114
35.	Easterly Flight at 600 ft/sec. Latitude Error [Rad/200 μ g] for Constant North Accelerometer Bias [200 μ g]	115
36.	Easterly Flight at 600 ft/sec. Longitude Error [Rad/200 μ g] for Constant North Accelerometer Bias [200 μ g]	116
37.	Easterly Flight at 600 ft/sec. Latitude Rate Error [Rad/hour \cdot 200 μ g] for Constant North Accelerometer Bias [200 μ g]	117
38.	Easterly Flight at 600 ft/sec. Longitude Rate Error [Rad/hour \cdot 200 μ g] for Constant North Accelerometer Bias [200 μ g]	118
39.	Westerly Flight at 600 ft/sec. North Level Error [Rad/200 μ g] for Constant North Accelerometer Bias [200 μ g]	119
40.	Westerly Flight at 600 ft/sec. East Level Error [Rad/200 μ g] for Constant North Accelerometer Bias [200 μ g]	120

41.	Westerly Flight at 600 ft/sec. Azimuth Level Error [Rad/200 μ g] for Constant North Accelerometer Bias [200 μ g]	121
42.	Westerly Flight at 600 ft/sec. Latitude Error [Rad/200 μ g] for Constant North Accelerometer Bias [200 μ g]	122
43.	Westerly Flight at 600 ft/sec. Longitude Error [Rad/200 μ g] for Constant North Accelerometer Bias [200 μ g]	123
44.	Westerly Flight at 600 ft/sec. Latitude Rate Error [Rad/hour*200 μ g] for Constant North Accelerometer Bias [200 μ g]	124
45.	Westerly Flight at 600 ft/sec. Longitude Rate Error [Rad/hour*200 μ g] for Constant North Accelerometer Bias [200 μ g]	125
46.	Stationary Case. North Level Error [Rad/140 μ rad] for Initial North Level Error [140 μ rad]	126
47.	Stationary Case. East Level Error [Rad/140 μ rad] for Initial North Level Error [140 μ rad]	127
48.	Stationary Case. North Level Error [Rad/140 μ rad] for Initial East Level Error [140 μ rad]	128
49.	Stationary Case. East Level Error [Rad/140 μ rad] for Initial East Level Error [140 μ rad]	129
50.	Stationary Case. North Level Error [Rad/140 μ rad] for Initial Azimuth Level Error [140 μ rad]	130
51.	Stationary Case. East Level Error [Rad/140 μ rad] for Initial Azimuth Level Error [140 μ rad]	131
52.	Stationary Case. North Level Error [Rad/(2 ft/sec)] for Initial Latitude Rate Error [0.345mrad/hour = 2 ft/sec]	132

53.	Stationary Case. Azimuth Level Error [Rad/(2 ft/sec)] for Initial Latitude Rate Error [0.345mrad/hour = 2 ft/sec]	133
54.	Stationary Case. Latitude Error [Rad/(2 ft/sec)] for Initial Latitude Rate Error [0.345mrad/hour = 2 ft/sec]	134
55.	Stationary Case. Longitude Error [Rad/(2 ft/sec)] for Initial Latitude Rate Error [0.345mrad/hour = 2 ft/sec]	135
56.	Stationary Case. Latitude Rate Error [(Rad/hour)/(2 ft/sec)] for Initial Latitude Rate Error [0.345mrad/hour = 2 ft/sec]	136
57.	Stationary Case. Longitude Rate Error [(Rad/hour)/(2 ft/sec)] for Initial Latitude Rate Error [0.345mrad/hour = 2 ft/sec]	137
58.	Stationary Case. North Level Error [Rad/(2 ft/sec)] for Initial Longitude Rate Error [0.345mrad/hour = 2 ft/sec]	138
59.	Stationary Case. East Level Error [Rad/(2 ft/sec)] for Initial Longitude Rate Error [0.345mrad/hour = 2 ft/sec]	139
60.	Stationary Case. Latitude Error [Rad/(2 ft/sec)] for Initial Longitude Rate Error [0.345mrad/hour = 2 ft/sec]	140
61.	Stationary Case. Longitude Error [Rad/(2 ft/sec)] for Initial Longitude Rate Error [0.345mrad/hour = 2 ft/sec]	141
62.	Stationary Case. Latitude Rate Error [(Rad/hour)/(2 ft/sec)] for Initial Longitude Rate Error [0.345mrad/hour = 2 ft/sec]	142
63.	Stationary Case. Longitude Rate Error [(Rad/hour)/(2 ft/sec)] for Initial Longitude Rate Error [0.345mrad/hour = 2 ft/sec]	143
64.	Theoretical I.N.S./G.P.S., 4-Hour Process. North Attitude Error [Rad]	144
65.	Theoretical I.N.S./G.P.S., 4-Hour Process. East Attitude Error [Rad]	145

66.	Theoretical I.N.S./G.P.S., 4-Hour Process. Azimuth Attitude Error [Rad]	146
67.	Theoretical I.N.S./G.P.S., 4-Hour Process. Y Position Error [Rad]	147
68.	Theoretical I.N.S./G.P.S., 4-Hour Process. X Position Error [Rad]	148
69.	Theoretical I.N.S./G.P.S., 4-Hour Process. Y Velocity Error [Rad/hour]	149
70.	Theoretical I.N.S./G.P.S., 4-Hour Process. X Velocity Error [Rad/hour]	150
71.	Normalized Input Noise Versus Time	151
72.	Normalized Measurement Noise Versus Time	152
73.	Theoretical I.N.S./G.P.S., 36-Hour Process. North Attitude Error [Rad]	153
74.	Theoretical I.N.S./G.P.S., 36-Hour Process. East Attitude Error [Rad]	154
75.	Theoretical I.N.S./G.P.S., 36-Hour Process. Azimuth Attitude Error [Rad]	155
76.	Theoretical I.N.S./G.P.S., 36-Hour Process. Y Position Error [Rad]	156
77.	Theoretical I.N.S./G.P.S., 36-Hour Process. X Position Error [Rad]	157
78.	Theoretical I.N.S./G.P.S., 36-Hour Process. Y Velocity Error [Rad/hour]	158
79.	Theoretical I.N.S./G.P.S., 36-Hour Process. X Velocity Error [Rad/hour]	159
80.	Realistic I.N.S./G.P.S., 4-Hour Process. North Attitude Error [Rad]	160
81.	Realistic I.N.S./G.P.S., 4-Hour Process. East Attitude Error [Rad]	161
82.	Realistic I.N.S./G.P.S., 4-Hour Process. Azimuth Attitude Error [Rad]	162

83.	Realistic I.N.S./G.P.S., 4-Hour Process. Y Position Error [Rad]	163
84.	Realistic I.N.S./G.P.S., 4-Hour Process. X Position Error [Rad]	164
85.	Realistic I.N.S./G.P.S., 4-Hour Process. Y Velocity Error [Rad/hour]	165
86.	Realistic I.N.S./G.P.S., 4-Hour Process. X Velocity Error [Rad/hour]	166
87.	Realistic I.N.S./G.P.S., 36-Hour Process. North Attitude Error [Rad]	167
88.	Realistic I.N.S./G.P.S., 36-Hour Process. East Attitude Error [Rad]	168
89.	Realistic I.N.S./G.P.S., 36-Hour Process. Azimuth Attitude Error [Rad]	169
90.	Realistic I.N.S./G.P.S., 36-Hour Process. Y Position Error [Rad]	170
91.	Realistic I.N.S./G.P.S., 36-Hour Process. X Position Error [Rad]	171
92.	Realistic I.N.S./G.P.S., 36-Hour Process. Y Velocity Error [Rad/hour]	172
93.	Realistic I.N.S./G.P.S., 36-Hour Process. X Velocity Error [Rad/hour]	173
94.	Realistic I.N.S./G.P.S., Exponentially Correlated Input Noise, 4-Hour Process. North Attitude Error [Rad]	174
95.	Realistic I.N.S./G.P.S., Exponentially Correlated Input Noise, 4-Hour Process. East Attitude Error [Rad]	175
96.	Realistic I.N.S./G.P.S., Exponentially Correlated Input Noise, 4-Hour Process. Azimuth Attitude Error [Rad]	176
97.	Realistic I.N.S./G.P.S., Exponentially Correlated Input Noise, 4-Hour Process. Y Position Error [Rad]	177

98.	Realistic I.N.S./G.P.S., Exponentially Correlated Input Noise, 4-Hour Process. X Position Error [Rad]	178
99.	Realistic I.N.S./G.P.S., Exponentially Correlated Input Noise, 4-Hour Process. Y Velocity Error [Rad/hour]	179
100.	Realistic I.N.S./G.P.S., Exponentially Correlated Input Noise, 4-Hour Process. X Velocity Error [Rad/hour]	180
101.	I.N.S. Aided by Position Data	183
102.	Kalman Filter Block Diagram	186
103.	Feedback Kalman Filter Configuration	190
104.	Normalized Input Noise Versus Time	200
105.	Normalized Measurement Noise Versus Time	201
106.	Case I. Kalman Filter Gain to Velocity	202
107.	Case I. Kalman Filter Gain to Acceleration	203
108.	Case I. True Position Versus Time	204
109.	Case I. Predicted Position Versus Time	205
110.	Case I. Predicted Velocity Versus Time	206
111.	Case I. I.N.S. Indicated Position Versus Time	207
112.	Case I. Radar Indicated Position Versus Time	208
113.	Case I. I.N.S. Indicated Velocity Versus Time	209
114.	Case II. Kalman Filter Gain to Velocity	210
115.	Case II. Kalman Filter Gain to Acceleration	211
116.	Case II. True Position Versus Time	212
117.	Case II. Predicted Position Versus Time	213
118.	Case II. Predicted Velocity Versus Time	214

119.	Case II. I.N.S. Indicated Position Versus Time	215
120.	Case II. Radar Indicated Position Versus Time	216
121.	Case II. I.N.S. Indicated Velocity Versus Time	217
122.	Case III. Kalman Filter Gain to Velocity	218
123.	Case III. Kalman Filter Gain to Acceleration	219
124.	Case III. True Position Versus Time	220
125.	Case III. Predicted Position Versus Time	221
126.	Case III. True Velocity Versus Time	222
127.	Case III. Predicted Velocity Versus Time	223
128.	Case III. I.N.S. Indicated Position Versus Time	224
129.	Case III. Radar Indicated Position Versus Time	225
130.	Case III. I.N.S. Indicated Velocity Versus Time	226
131.	Case IV. Kalman Filter Gain to Velocity	227
132.	Case IV. Kalman Filter Gain to Acceleration	228
133.	Case IV. True Position Versus Time	229
134.	Case IV. Predicted Position Versus Time	230
135.	Case IV. Predicted Velocity Versus Time	231
136.	Case IV. I.N.S. Indicated Position Versus Time	232
137.	Case IV. Radar Indicated Position Versus Time	233
138.	Case IV. I.N.S. Indicated Velocity Versus Time	234
139.	Case V. Kalman Filter Gain to Velocity	235

140.	Case V.	Kalman Filter Gain to Acceleration . . .	236
141.	Case V.	True Position Versus Time	237
142.	Case V.	Predicted Position Versus Time	238
143.	Case V.	Predicted Velocity Versus Time	239
144.	Case V.	I.N.S. Indicated Position Versus Time	240
145.	Case V.	Radar Indicated Position Versus Time	241
146.	Case V.	I.N.S. Indicated Velocity Versus Time	242
147.	Case VI.	Kalman Filter Gain to Velocity	243
148.	Case VI.	Kalman Filter Gain to Acceleration . . .	244
149.	Case VI.	True Position Versus Time	245
150.	Case VI.	Predicted Position Versus Time	246
151.	Case VI.	Predicted Velocity Versus Time	247
152.	Case VI.	I.N.S. Indicated Position Versus Time	248
153.	Case VI.	Radar Indicated Position Versus Time	249
154.	Case VI.	I.N.S. Indicated Velocity Versus Time	250
155.		Range Vector Definition	252
156.		Observability-Criterion Geometry	258

ACKNOWLEDGEMENT

I would like to express my sincere appreciation to both my advisors, Professor D. Collins for his instruction, guidance and support during this work and Professor H. Titus for his help and his outstanding lectures on Kalman filters which stimulated my interest on this area.

I. INTRODUCTION

A. OVERVIEW OF AN INERTIAL NAVIGATION SYSTEM (I.N.S.)

A conventional gimballed inertial measurement unit consists of a platform suspended by a gimbal structure that allows three degrees of rotational freedom [Ref. 1,2,7]. The outermost gimbal can be attached to the body of some vehicle and allow that vehicle to undergo any change in angular orientation while maintaining the platform fixed with respect to some desired coordinate frame.

Gyros mounted on the platform sense the angular rate of the platform with respect to inertial space and their outputs are sent through electronics to the torque motors on the gimballed structure, commanding them to maintain a desired platform orientation regardless of the orientation of the outermost gimbal which remains fixed to the body.

Feedback control loops that keep the gyro outputs nulled, will maintain at the same time the platform fixed with respect to the inertial space. These feedback loops are such that, in practice, the platform orientation is kept essentially stable regardless of the most violent vehicle maneuvering. Additional (computed) inputs can be added to the above feedback loops to maintain some other orientation,

such as North-East-Down, corresponding to the current location of the vehicle.

Accelerometers mounted on the platform can provide the vehicle's acceleration with respect to the known set of reference coordinates. In fact, specific force is measured by the accelerometers so that local gravity must be computed and appropriately subtracted from these sensor outputs in order to obtain a measurement of actual vehicle acceleration.

The vehicle's velocity and position are obtained by integration of the above acceleration measurement signals. Attitude information as well as translational information is provided by the I.N.S.. A typical gimballed inertial measurement unit [Ref. 2] is shown in Fig. 1.

B. OVERVIEW OF THE G.P.S.

The Global Positioning System (GPS) is a satellite navigation system currently under development. It will consist, according to today's available information, of 18 satellites placed in groups of six in each of three different circular, 12 hour orbits at an altitude of 10,900 N.M. inclined 63° to the equator and spaced 120° apart.

The satellites will broadcast pseudo-random noise codes (codes P and C/A) and ephemerides on two L-band signals to users worldwide in such a way that each satellite signal can be distinguished from the others by the user. A user will

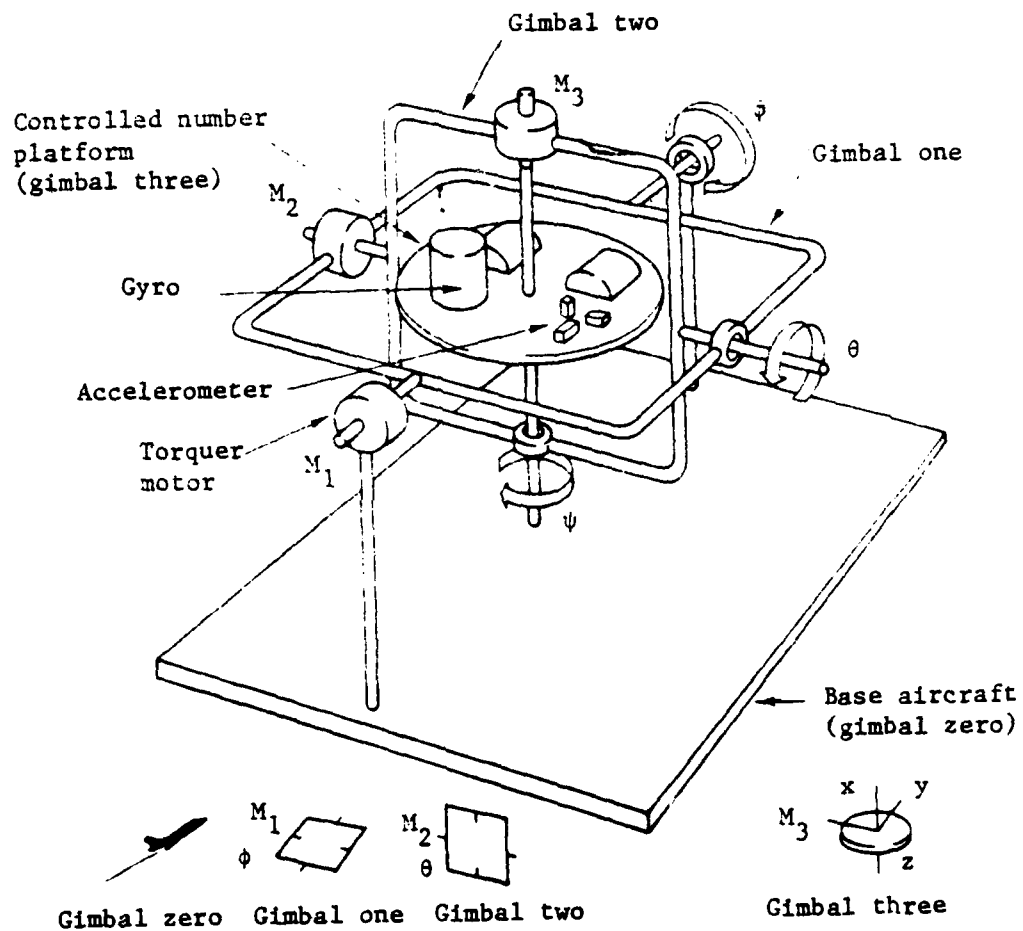


Figure 1. Typical Gimbaled Inertial Measurement Unit [Ref. 2]

be equipped with a small receiver (G.P.S. user equipment) which measures the pseudo-range and pseudo-range rate from the user to the satellite.

By means of a correlator-detector the time (phase) shift between each satellite signal and the user's unsynchronized clock will be measured in his receiver to provide an indication of the range from the satellite to the user. Typically, four satellite signals may be received simultaneously by the user equipment.

The phases of the NAVSTAR/G.P.S. system are shown in Fig. 2 [Ref. 8].

C. I.N.S. OPTIMAL AIDING

Once we have available a typical inertial measurement unit, or the inertial navigation system as a whole, the question naturally arises: why does this system requires optimal aiding by other navigational sensors? The answer to this question is given in Ref. 2 and here we present the concepts only.

Due to the tight control loops supporting the I.N.S. very good high frequency information is provided. However, because of gyro characteristics, the system drifts at a slow rate so that the long term (low frequency content) of the data is poor. It is well known that all inertial systems have position errors that grow slowly with time and these errors are unbounded.

NAVSTAR GLOBAL POSITIONING SYSTEM SCHEDULE

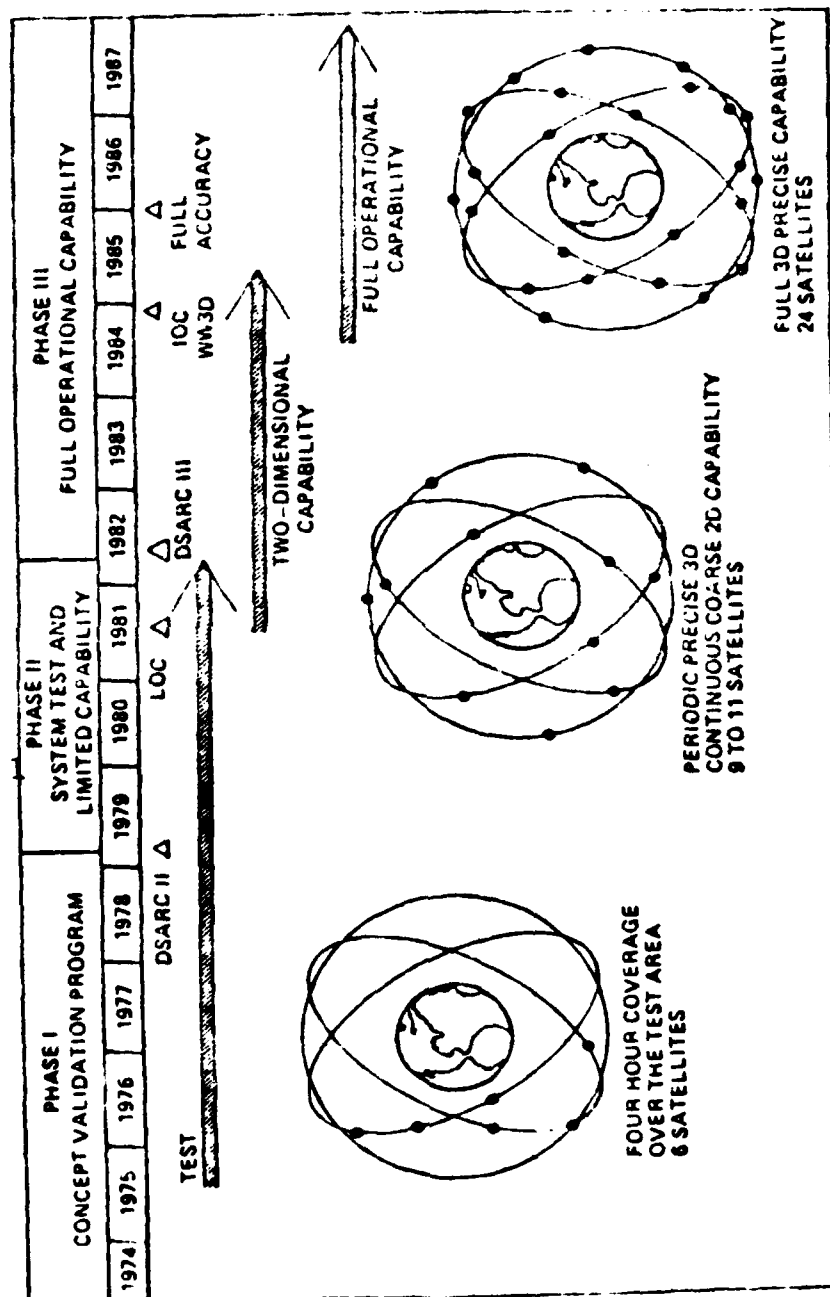


Figure 2. NAVSTAR/G.P.S. Phases [Ref. 8]

As opposed to an I.N.S. which can be classed as a "one nautical mile per hour system" due to the associated position error, most other navigation aids provide very good low frequency information but subject to considerable high frequency noise, due to instrument noise, atmospheric effects, antenna oscillation, unlevel ground effects and so forth.

One would want to combine the available information from an I.N.S. and other external sources in an optimal manner if possible so that one can obtain efficient estimates of navigation parameters that are best with respect to some well defined criterion. Such an optimal approach is provided by the Kalman filter approach which is briefly discussed next.

D. KALMAN FILTER

The Kalman filter is an optimal recursive data processing algorithm located in the on-board computer or central processor that uses sampled data with sample period on the order of 5-60 seconds, to maintain estimates of approximately 60-70 state variables. The filter combines all available measurement data with prior knowledge of the system and measuring devices to produce an estimate of the system states in such a manner as to statistically minimize the resulting errors. In more easily understood terms the filter, or computer program, uses the statistical

characteristics of the errors in both the inertial navigation components and the external information providing the best estimate possible, subject to certain modeling assumptions.

The filter will act to optimize the attitude, position, and velocity information accuracy by weighting each data source heavily in the frequency ranges where it provides more accurate information, and suppressing it in the region where it is less accurate. The inertial system provides good high frequency information but it drifts slowly and therefore exhibits poor low frequency performance. On the other hand, the external aids (such as G.P.S.) generally exhibit good low frequency information but are subject to high frequency noise. Therefore, the filter will use the good low frequency external (G.P.S.) information to damp out the slowly growing errors in the inertial system.

1. Type of Filter Implementation

There are two very important aspects of implementation of a Kalman filter in conjunction with an inertial system [Ref. 2].

a) Total state space (direct) versus error state space (indirect) formulation, and

b) Feedforward versus feedback mechanizations.

In the indirect formulation the errors in the I.N.S. indicated position and velocity are among the estimated variables and each measurement presented to the filter is

the difference between the I.N.S. and the external source (G.P.S.) data. The I.N.S. itself follows the high frequency motions of the vehicle very accurately, and there is no need to model these dynamics explicitly in the filter but the dynamics upon which the filter is based is a set of inertial system error propagation equations, which are relatively well developed, well behaved, low frequency, and very adequately represented as linear [Ref. 2, pp. 296].

The indirect feedback configuration is considered where the Kalman filter generates the estimates of the errors of the I.N.S. and feeds back these errors to the I.N.S. to correct it. By this configuration we use the two major advantages. First that the I.N.S. errors are not allowed to grow unchecked and the adequacy of a linear model is enhanced. Second is the fact that many of the predicted error states which at next time sample time are zero, need not be computed explicitly.

The indirect feedback configuration of the Kalman filter is shown in Figure 3. In Ref. 2 there is explicitly documented the discussion of the Kalman filter configurations and mechanizations with their advantages and more comments.

2. Assumptions

The Kalman filter can be shown to be the best filter of any possible form based on the following three

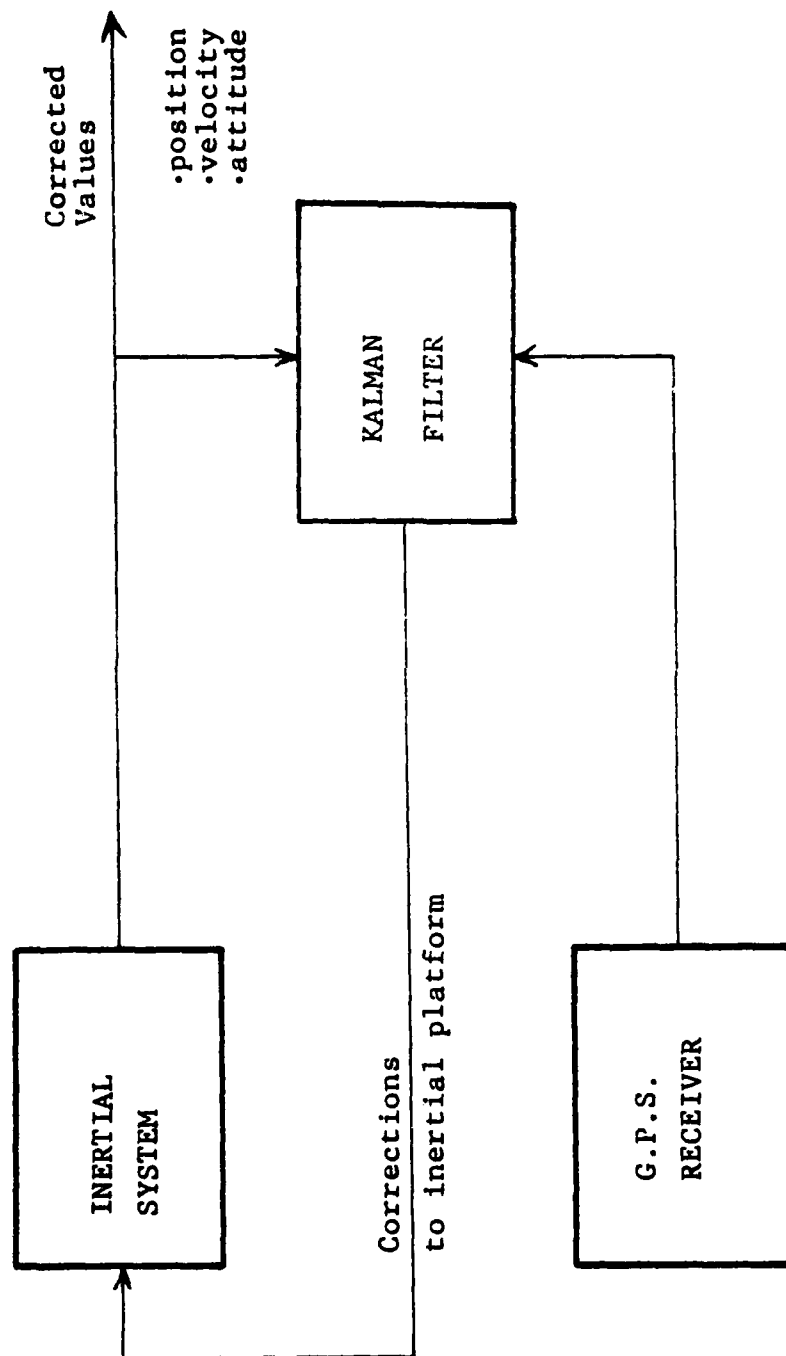


Figure 3. Indirect Feedback Kalman Filter [Ref. 2]

assumptions: a linear system, white noise drivers, and the Gaussian distribution of noise.

Although the system itself may be nonlinear, formulation of an approximate linear error state space model makes linear analysis possible. The justification for the linear model is based on two points. For the aided I.N.S. case the use of linear error state space models yields a very adequate representation. The techniques of linear system analysis are also well developed and better understood than those of nonlinear analysis.

The white noise assumption implies that the noise is not correlated in time and also has equal power at all frequencies. If, in fact, a time correlated noise is required to adequately model the system, it can be produced by passing white noise through a linear shaping filter. The system can then be modeled with an augmented state variable as a linear system driven by white noise.

Gaussianity pertains to the distribution of amplitudes of the noise and implies that at any single point in time the probability density function of the amplitude takes on the shape of a normal bell-shaped curve. The assumption of Gaussian noise amplitude is justified by the fact that the system or measurement noise is typically caused by a number of sources. It can be shown mathematically that when a number of independent random

variables are added the resultant effect is very nearly a Gaussian probability density even though the individual densities are not Gaussian [Ref. 9].

Under the above mentioned assumptions of a purely white Gaussian noise, the first two moments specify the entire shape of the density describing the noise, and the mathematics of the problem are greatly simplified.

In Appendix A, a simple example of a Kalman filter application to a radar position-aided I.N.S. is given in order to make easier the understanding of Kalman filter operation.

Finally, information about the G.P.S. satellites' geometry and their observability is given in Appendix B.

II. KALMAN FILTER EQUATIONS

A. GENERAL

The design of a Kalman filter and especially the integrated I.N.S. Kalman filter design requires extensive computer simulation. This chapter of the work is a presentation of the equations which are required not only for the mechanization of the filter but also those which are necessary to simulate the dynamics of any user (aircraft, missile).

The principal tool used for the solution of this specific and other similar problems is the very common method of covariance analysis. It is known that the covariance is a measure of the uncertainty in the knowledge of the true values of the state vector components. In this work, as the covariance matrix is concerned, the off diagonal terms are assumed to be zero initially and initial conditions on the diagonal elements are arbitrarily taken. The covariance matrix of both the system and the filter are propagated forward in time by numerical integration techniques.

The adjustment of the values of the state variables, to those of the best estimate obtained with the Kalman filter, is achieved when a control is applied to the system after

the specified update time is reached and the best estimates of the states have been determined. The square root of the individual diagonal elements of the system covariance matrix (RMS values) are plotted as a function of time to provide the performance of the filter. For this study the plots are also utilized to determine the error contribution associated with each modeled error source. Furthermore, the error statistics are propagated which means that the standard deviation of the noise value is supplied whenever a noise is required.

One attribute of covariance analysis is, that under the assumptions stated in Chapter One, i.e., the linearity and white Gaussian noise, the covariance is independent of the actual measurement values and can be computed through generating a sample sequence of measurements. And as a matter of fact this method is easier to handle and work with than the corresponding Monte Carlo type simulation.

B. SYSTEM MODEL EQUATIONS

The differential equations that describe how the inertial navigator errors propagate with time are the basic equations used in this process. These equations are formulated in a set of first order, linear differential equations, driven by white Gaussian noise for the reasons described previously in this work.

Linear measurements corrupted also by white Gaussian noise are made upon the actual system variables. It is furthermore assumed that the equations which represent a detailed model of the system are of the form:

$$\dot{\underline{x}}_s = F_s \underline{x}_s + G_s \underline{w}_s \quad (1)$$

where

\underline{x}_s is an n_1 vector denoting the true state

F_s is an $n_1 \times n_1$ matrix of system dynamics

G_s is an $n_1 \times m_1$ matrix of gains

\underline{w}_s is an m_1 vector of white noise inputs with the characteristics of zero mean and variance:

$$E[\underline{w}(i)\underline{w}(j)^T] = \begin{matrix} Q_s(i) & \text{for } i = j \\ 0 & \text{for } i \neq j \end{matrix} \quad (2)$$

where the indices i and j are instants in time.

The observations which are obtained from external references and in our case of study from the G.P.S. can be described by the following linear measurement vector equation:

$$\underline{z}_s = H_s \underline{x}_s + \underline{v}_s \quad (3)$$

where:

\underline{z}_s is a q vector of measurements

H_s is a $q \times n_1$ matrix of measurements

\underline{v}_s is a q vector of white noise inputs with the characteristics of zero mean and variance:

$$E[\underline{v}(i)\underline{v}(j)^T] = \begin{matrix} R_s(i) & \text{for } i = j \\ 0 & \text{for } i \neq j \end{matrix} \quad (4)$$

A further assumption for the study is that the system noise w and the measurement noise v are uncorrelated for all time, i.e.,

$$E[\underline{w}(i)\underline{v}(j)^T] = 0 \quad \text{for all } i, j \quad (5)$$

C. FILTER EQUATIONS

The equations discussed above are assumed to be a complete and accurate mathematical description of the G.P.S. aided inertial navigation system dynamics and measurement equations for the purpose of simulation. They also constitute a set of equations which would be utilized in the design of a fully optimal Kalman filter.

In our case of study as also in general a suboptimal or reduced order filter design is obtained by reducing the dimension of the state vector due to the computational burden of the fully optimal filter. The states that are

eliminated are those that affect the accuracy the least of the mathematical description of the aided-I.N.S. The designed suboptimal filter can be implemented with the on-board computer (aircraft or missile).

The equations which describe the suboptimal filter are of the form:

$$\dot{\underline{x}}_f = F_f \underline{x}_f + G_f \underline{w}_f$$

where

\underline{x}_f is an n_2 vector

F_f is an $n_2 \times n_2$ matrix of filter dynamics

G_f is an $n_2 \times m_2$ matrix of gains

\underline{w}_f is an m vector of white noise inputs with the characteristics of zero mean and variance:

$$E[\underline{w}_f(i)\underline{w}_f(j)^T] = \begin{matrix} Q_f(i) & \text{for } i = j \\ 0 & \text{for } i \neq j \end{matrix} \quad (6)$$

The equation for the filter measurement is:

$$\underline{z}_f = H_f \underline{x}_f + \underline{v}_f \quad (7)$$

where:

\underline{z}_f is a q vector

H_f is a $q \times q$ matrix of measurements

\underline{v}_f is a q vector of white noise inputs with the characteristics of zero mean and variance:

$$E[\underline{v}_f(i)\underline{v}_f(j)^T] = \begin{matrix} R_f(i) & \text{for } i = j \\ 0 & \text{for } i \neq j \end{matrix} \quad (8)$$

The filter propagation and update equations based on the above models are then given below.

At measurement times (update):

$$K_f = P_f^{-1} H_f^T [H_f P_f^{-1} H_f^T + R_f]^{-1} \quad (9)$$

$$P_f^+ = P_f^- - K_f H_f P_f^- \quad (10)$$

$$\hat{\underline{x}}_f^+ = \hat{\underline{x}}_f^- + K_f [\underline{z}_s - H_f \hat{\underline{x}}_f^-] \quad (11)$$

and between measurements (extrapolate):

$$\hat{\underline{x}}_f = F_f \hat{\underline{x}}_f \quad (12)$$

$$\dot{P}_f = F_f P_f + P_f F_f^T + G_f Q_f G_f^T \quad (13)$$

where:

$\hat{\underline{x}}_f$ is an n_2 vector denoting the best estimate

P_f is the covariance matrix of the filter

K_f is the matrix of Kalman gains

\underline{z}_s is a q vector of the actual values of the measurements taken

+ superscript indicates the time instant just after update

- superscript indicates the time instant just prior to update

T superscript denotes the transpose matrix or vector superscripted.

The filter subtracts from the actual taken measurement \underline{z}_s the best prediction of its value before the actual measurement is taken, i.e., the value of $H_f \hat{\underline{x}}_f^-$. This difference is then passed through an optimal weighting matrix K_f and used to correct $\hat{\underline{x}}_f^-$, the best prediction of the state at the time instant before the measurement is taken. This process gives the best estimate after update. This estimate is propagated to the time of the next measurement sample according to equations (12) and (13).

The above recursive relationships are solved based on initial conditions of an assumed Gaussian density which describe the a-priori knowledge of the state as:

$$\hat{\underline{x}}(0) = \hat{\underline{x}}_0 \quad (14)$$

and $P(0) = P_0$

The Kalman filter conditioned on the actual measurements taken, propagates the conditioned probability density of the desired states. The probability density function of a Gaussian noise amplitude takes on the shape of a normal bell-shaped curve. The assumption of Gaussian noise amplitude is well justified by the fact that a system or measurement noise is typically caused by a number of small sources and according to the Central Limit Theorem it can be shown mathematically that when a number of random variables are added together, the summation is a random variable whose density is nearly a Gaussian probability density, regardless of the shape of the densities of the individual random variables. Furthermore, the use of Gaussian densities makes the mathematics easier to handle and tractable. It is known that a Gaussian density is completely determined by its first and second order statistics, i.e., the mean and the variance. Thus, the Kalman filter, which propagates the first and second order statistics, includes all information contained in the conditional probability density mentioned above [Ref. 2: pp. 3-9].

The mean of a density function or its expectation μ , is defined as

$$E[x] = \mu = \int_{-\infty}^{\infty} xf(x)dx \quad (16)$$

and it is interpreted as the weighted average of the values of x , using the probability density function $f(x)$ as the weighted function. All the Gaussian white noise inputs in this study are assumed to have zero mean.

The variance of a density function, or the square of the standard deviation σ , is defined as:

$$\text{Var}[x] = \sigma^2 = \int_{-\infty}^{\infty} (x - \mu)^2 f(x) dx \quad (17)$$

and it is interpreted as the weighted average of the values of $(x - \mu)^2$; thus, σ^2 is a measure of the density spread and a direct measure of the uncertainty since the larger σ is, the broader the probability peak is, spreading the probability weight over a larger range of x values. For the example of Gaussian density, 68.3% of the probability weight is contained within the band of σ units to each side of the mean μ , which represents the area under the normal bell-shaped curve between the values of $-\sigma$ and $+\sigma$ and 95.4% of the probability weight is contained between the values of -2σ and $+2\sigma$. Since in this study vectors are used instead of scalars, the above equations (16) and (17) which give the first and second order statistics respectively for the scalar case, must be extended for the vector case as follows:

$$E[\underline{x}] = \underline{\mu} = \int_{-\infty}^{\infty} \dots \int_{-\infty}^{\infty} \underline{x} f(\underline{x}) dx_1 \dots dx_n \quad (18)$$

n

$$\text{Cov}[\underline{x}] = P = \int_{-\infty}^{\infty} \dots \int_{-\infty}^{\infty} (\underline{x} - \underline{\mu})(\underline{x} - \underline{\mu})^T f(\underline{x}) dx_1 \dots dx_n \quad (19)$$

n

III. I.N.S. ERROR ANALYSIS

A. GENERAL

One general approach to determine the navigation error caused by individual sources of error is to simulate the inertial-navigation-system nonlinear equations and sources of error and compare the navigation outputs with the simulated true position--the difference being the navigation error. However, this is not the approach used here.

Assuming that the position errors are small compared with earth radius, that the velocity errors are small compared with orbital velocity, and that the alignment errors are small compared with 1 radian (or 3437 arc-min) it can be demonstrated that the propagation of errors in an inertial navigation system is very accurately governed by a set of corresponding linear differential equations. Therefore, most inertial-navigation-system error analyses are conducted, working directly with a set of linear error differential equations.

Sets of error equations have been developed for various I.N.S. configurations in the context of a particular application. As a consequence, many sets of I.N.S. error equations have been developed for the various broad classes

of mechanization such as local level, space stabilized, wander azimuth, free azimuth, strapdown, etc.

The choice of navigation error variables for analysis has often followed from the coordinate system used in the navigation equations or that implied by the physical I.N.S. platform orientation. Regardless of the differences in the sets of equations the fact is that I.N.S. error propagation is to a large extent, completely independent of system mechanization. Britting [Ref. 2] has shown that the basic error differential equations for any I.N.S. may be written in standard coordinates, regardless of the physical mechanization or internal navigation variables. Furthermore, the unforced (homogeneous) portion of these differential equations is, under certain very broad assumptions, identical for any arbitrarily configured terrestrial I.N.S.

The error equations presented in this chapter follow the philosophy of [Ref. 2] including the choice of north-slaved coordinates for the error variables and the identification of the unforced (homogeneous) portion of the differential equations that is independent of system mechanization. Two of the differences that are noticeable are:

- 1) The error equations are written as a system of nine first order equations (and further on reduced to seven) rather than three second order plus three first order

equations. The first-order form is the state space representation of the error equations used in modern estimation theory.

2) The form of altitude compensation assumed in [Ref. 2] is not found in most inertial navigators. Gravity is assumed computed as a function of the inertial system indicated position.

B. GENERAL I.N.S. ASSUMPTIONS

The assumptions pertaining to the general error differential equations are broad enough to encompass all of the important I.N.S. configurations [Ref. 2].

1) Three accelerometers are available to measure the specific force vector. The equations for a two-accelerometer local level system are the same provided the inertial-altitude and vertical-velocity equations are deleted.

2) The accelerometers are mounted on a platform whose angular velocity is either controlled (as with gyro-stabilized gimballed platforms) or is measured (as with the strapdown systems).

3) The system's indicated velocity vector and three-dimensional indicated position are obtained by integration of the gravity field compensated specific force measurements, using a correct set of differential equations.

4) A model of the earth's gravity field is used to calculate the gravity vector as a function of the system-indicated position.

5) External altitude information and other navigation measurements may be used to update the inertial-navigation-system indicated position, velocity, and attitude.

6) A computer is available to process the navigation information and the computation errors are either negligible or may be treated as equivalent instrument uncertainties.

7) Both the mechanical coordinate frame (the frame tracked by the platform) and the computation frame (the frame to which the specific force measurements are transformed for velocity and position integration) are arbitrary.

C. LOCAL-LEVEL TERRESTRIAL NAVIGATOR

Many inertial navigators do use a local-level coordinate system for the velocity and position integration. The local-level terrestrial navigation system physically instruments the local geographic coordinate frame. The platform axes are commanded into alignment with the local north-east-down coordinate system.

The local-level terrestrial system is undoubtedly the most successfully of all inertial-navigation-system configurations. The class of local-level systems today constitutes the majority of operational inertial navigation systems. Since this system is described in detail in [Ref. 2] here are listed some of its advantages:

1) The computation of gravity components is greatly simplified. In fact some navigators use zero for both horizontal components of gravity.

2) Some inertial navigators have no vertical accelerometer (this is the case in the present study) and do not mechanize a vertical channel. The horizontal velocity and position equations of a local-level set are appropriate for such a navigator.

3) The well-known altitude and vertical velocity instability of a pure inertial navigator must be stabilized by means of an external altitude reference. But a local-level set of variables includes altitude and vertical velocity explicitly. The altitude stabilization equations therefore can be simplified.

4) The calculations required to provide navigation outputs and displays in geographic coordinates are simplified.

D. THE TWO ACCELEROMETER LOCAL-LEVEL SYSTEM

Many inertial navigators have only two accelerometers after the vertical accelerometer has been eliminated. The system is composed of a three axis inertial platform, two accelerometers which are nominally orthogonally mounted in the instrumented east and north directions and a computer which performs the necessary navigational computations [Ref. 2].

The north and east gyros are respectively connected with the instrumented north and east accelerometers at the signal level and the gyros are torqued at a rate proportional to the vehicle's longitude and latitude rates so that the platform can maintain its axes aligned with geographic axes since the vehicle carrying the navigation system is assumed to move freely over and above the earth. The accelerometer outputs provide these required torquing signals which must be so compensated that gyro command can be obtained as a function of only the north and east velocity rates.

Such a two-accelerometer local-level I.N.S. has seven state variables: two of position, two of velocity, and three of platform alignment.

1. Error Model Equations

The general model of local-level inertial navigation systems is given by the following matrix equations:

$$\dot{\underline{x}} = \underline{g} \quad (20)$$

where

\underline{A} = system characteristic matrix, same for all I.N.S. configurations

\underline{g} = forcing vector of inertial system errors

$$\text{or } \underline{g} = [q_1, q_2, q_3, q_4, q_5, q_6]^T \quad (21)$$

\underline{x} = error state vector of attitude, position, and velocity errors

$$\text{or } \underline{x} = [\epsilon_N, \epsilon_E, \epsilon_D, \delta L, \delta l, \delta h]^T \quad (22)$$

It is quite important to emphasize that a computer simulation program developed in accordance with the above equation (20) is valid for all possible I.N.S. configurations, space stabilized, strapdown, wander-azimuth and not only for the local-level one. Both the coordinate frame mechanized by the inertial instruments and the computation frame are completely arbitrary. It is only the forcing function, q , which depends on the system configuration through the angular velocity and orientation of the inertial instruments.

In order to rewrite this equation as a first order vector-differential equation the error state of the I.N.S. is defined as [Ref. 2]:

$$\epsilon^T(t) = [\epsilon_N, \epsilon_E, \epsilon_D, \delta L, \delta l, \delta \dot{L}, \delta \dot{l}, \delta h, \delta \dot{h}] \quad (23)$$

and for the case of this study for two-accelerometer local-level I.N.S. system this reduces to:

$$\epsilon^T(t) = [\epsilon_N, \epsilon_E, \epsilon_D, \delta L, \delta l, \delta \dot{L}, \delta \dot{l}] \quad (24)$$

where the seven basic I.N.S. errors are:

$\epsilon_N, \epsilon_E, \epsilon_D$ = north, east, down platform tilt errors

$\delta L, \delta l$ = latitude, longitude position errors

$$F_{57} = 1$$

$$F_{62} = -f_D/r$$

$$F_{63} = f_E/r$$

$$F_{64} = -\dot{i}(\dot{i} + 2\omega_{ie})\cos 2L$$

$$F_{67} = -\dot{\lambda} \sin 2L$$

$$F_{71} = f_D/r \cos L$$

$$F_{73} = -f_N/r \cos L$$

$$F_{74} = \ddot{l} \tan L + 2\dot{\lambda}\dot{L}$$

$$F_{76} = 2\dot{\lambda} \tan L$$

$$F_{77} = 2\dot{L} \tan L$$

$\underline{\epsilon} = 7 \times 1$ error vector matrix

where

$$\underline{\epsilon} = [\epsilon_N, \epsilon_E, \epsilon_D, \delta L, \delta l, \delta \dot{L}, \delta \dot{l}]^T$$

$G_e = 7 \times 5$ forcing matrix, with non-zero elements

$$G_{11} = 1$$

$$G_{22} = 1$$

$$G_{33} = 1$$

$\delta\dot{L}, \delta\dot{l}$ = latitude, longitude rate errors

The above statements allow equation (20) to be written as:

$$\dot{\underline{\epsilon}} = F_{\underline{\epsilon}} \underline{\epsilon} + G \underline{q} \quad (25)$$

where:

$F_{\underline{\epsilon}}$ = 7 x 7 error matrix with non-zero elements

$$F_{12} = -\dot{\lambda} \sin L$$

$$F_{13} = \dot{L}$$

$$F_{14} = -\dot{\lambda} \sin L$$

$$F_{17} = \cos L$$

$$F_{21} = \dot{\lambda} \sin L$$

$$F_{23} = \dot{\lambda} \cos L$$

$$F_{26} = -1$$

$$F_{31} = -\dot{L}$$

$$F_{32} = -\dot{\lambda} \cos L$$

$$F_{34} = -\dot{\lambda} \cos L$$

$$F_{37} = -\sin L$$

$$F_{46} = 1$$

$$G_{64} = 1/r$$

$$G_{75} = 1/r \cos L$$

and $\underline{q} = 5 \times 1$ forcing vector matrix

where

$$\underline{q} = [q_1, q_2, q_3, q_4, q_5]^T \quad (28)$$

and neglecting both gyro and accelerometer non-orthogonality errors the forcing functions are comprised of 10 I.N.S.

component errors as below:

$$\begin{bmatrix} q_1 \\ q_2 \\ q_3 \end{bmatrix} = C_p^n \begin{bmatrix} (u)\omega_N \\ (u)\omega_E \\ (u)\omega_D \end{bmatrix} + C_p^n \begin{bmatrix} r_N & 0 & 0 \\ 0 & r_E & 0 \\ 0 & 0 & r_D \end{bmatrix} \underline{\omega}_{ip}^p \quad (29)$$

$$\begin{bmatrix} q_4 \\ q_5 \\ 0 \end{bmatrix} = C_p^n \begin{bmatrix} (u)f_N \\ (u)f_E \\ 0 \end{bmatrix} + \begin{bmatrix} \epsilon_g \\ n_g \\ 0 \end{bmatrix}$$

where for our study of two accelerometer local-level system the platform-to-navigation transformation matrix C_p^n and the I.N.S. platform torquing rate $\underline{\omega}_{ip}^p$ are as below:

$$C_p^n = I, \quad \underline{\omega}_{ip}^p = \begin{bmatrix} \dot{\lambda} \cos L \\ -\dot{L} \\ -\dot{\lambda} \sin L \end{bmatrix} \quad (30)$$

TABLE I
I.N.S. SYSTEM MODEL MATRICES F_ϵ AND G_ϵ

$$F_\epsilon = \begin{bmatrix} 0 & F_{12} & F_{13} & F_{14} & 0 & 0 & F_{17} \\ F_{21} & 0 & F_{23} & 0 & 0 & F_{26} & 0 \\ F_{31} & F_{32} & 0 & F_{34} & 0 & 0 & F_{37} \\ 0 & 0 & 0 & 0 & 0 & F_{46} & 0 \\ 0 & 0 & 0 & 0 & 0 & 0 & F_{57} \\ 0 & F_{62} & F_{63} & F_{64} & 0 & 0 & F_{67} \\ F_{71} & 0 & F_{73} & F_{74} & 0 & F_{76} & F_{77} \end{bmatrix} \quad (26)$$

$$G_\epsilon = \begin{bmatrix} G_{11} & 0 & 0 & 0 & 0 \\ 0 & G_{22} & 0 & 0 & 0 \\ 0 & 0 & G_{33} & 0 & 0 \\ 0 & 0 & 0 & 0 & 0 \\ 0 & 0 & 0 & 0 & 0 \\ 0 & 0 & 0 & G_{64} & 0 \\ 0 & 0 & 0 & 0 & G_{75} \end{bmatrix} \quad (27)$$

Finally the forcing vector matrix is modeled for our case as:

$$\underline{q} = \begin{bmatrix} q_1 \\ q_2 \\ q_3 \\ q_4 \\ q_5 \end{bmatrix} = \begin{bmatrix} (u)\omega_N + r_N \dot{\lambda} \cos L \\ (u)\omega_N \\ (u)\omega_D - r_D \dot{\lambda} \sin L \\ (u)f_N - \xi_g \\ (u)f_E + n_g \end{bmatrix} \quad (31)$$

2. Error Equations Solution

The solution of the differential equations represented by equation (25) gives the error response for the two-accelerometer local-level navigator for arbitrary vehicle motion within the constraints implied by a "first-order" analysis. Since the coefficients of the differential equations are time varying the analytic solution of equation (25) would be quite tedious and require the user of a computer program to generate flight profiles. In our study specific cases are examined so that the coefficients of the differential equations can easily be calculated.

The specific cases which are examined are the following three:

- 1) Stationary case, where $\dot{\lambda} = \omega_{ie}$ and $\ddot{L}=\dot{L}=\ddot{l}=\dot{l}=\ddot{h}=\dot{h} = 0$
- 2) Easterly flight at 600 "ft/sec" or 355.5 "knots," where $\dot{\lambda} = 1.557 \times \omega_{ie}$

3) Westerly flight at 600 "ft/sec" or 355.5 "knots,"
 where $\dot{\lambda} = 0.442 \times \omega_{ie}$

Writing the equation (25) in terms of the error states explicitly we have the following system of differential equations which must be solved simultaneously:

$$\begin{aligned}\dot{x}(1) &= -\dot{\lambda}(\sin L)x(2) - \dot{\lambda}(\sin L)x(4) + (\cos L)x(7) + q_1 \\ \dot{x}(2) &= \dot{\lambda}(\sin L)x(1) + \dot{\lambda}(\cos L)x(3) - x(6) + q_2 \\ \dot{x}(3) &= -\dot{\lambda}(\cos L)x(2) - \dot{\lambda}(\cos L)x(4) - (\sin L)x(7) + q_3 \\ \dot{x}(4) &= x(6) \\ \dot{x}(5) &= x(7) \\ \dot{x}(6) &= \frac{g}{r} x(2) - \dot{\lambda}(\sin 2L)x(7) + q_4 \\ \dot{x}(7) &= -\frac{g}{r(\cos L)} x(1) + 2\dot{\lambda}(\tan L)x(6) + q_5\end{aligned}\tag{32}$$

The values of the parameters used for the computer simulation are given in Table II.

a. Constant Gyro Drift Errors

Letting constant gyro drift be the sole error source in the I.N.S. system where the constant gyro drift rates $(u)\omega_N$, $(u)\omega_E$, $(u)\omega_D$ are associated with the north, east, and azimuth gyros respectively, computer simulation verified the following.

TABLE II
COMPUTER SIMULATION PARAMETERS

Geographic Latitude, L	$45^\circ L$	
Terrestrial Longitude, l	0° (Greenwich)	
Earth Rate, ω_{ie}	0.2618 Rad/hour	
Constant Gyro Drift		
• North, $(u)\omega_N$	1 meru	(1)
• East, $(u)\omega_E$	1 meru	
• Azimuth, $(u)\omega_D$	1 meru	
Constant Accelerometer Bias		
• North, $(u)f_N$	200 μg	(2)
• East, $(u)f_E$	200 μg	
Initial Platform Tilt		
• North, $\epsilon_N(0)$	0.14 mrad	
• East, $\epsilon_E(0)$	0.14 mrad	
• Azimuth, $\epsilon_D(0)$	0.14 mrad	
Initial Latitude Error, $\delta L(0)$	0.17 mrad	(3)
Initial Longitude Error, $\delta l(0)$	0.17 mrad	
Initial Latitude Rate Error, $\delta \dot{L}(0)$	0.34 mrad	(4)
Initial Longitude Rate Error, $\delta \dot{l}(0)$	0.34 mrad	
Stationary Flight	$\dot{\lambda} = \omega_{ie}$	
Constant Easterly Flight at 600 ft/sec	$\dot{\lambda} = 1.557 \times \omega_{ie}$	
Constant Westerly Flight at 600 ft/sec	$\dot{\lambda} = 0.442 \times \omega_{ie}$	
Gravitational Acceleration Constant	$g = 32.2$ ft/sec	
Earth Radius	$r = 6,378.3$ Km	

-
1. The RMS gyro drift of 1 meru corresponds to $0.015^\circ/\text{hr}$ or 0.2618×10^{-3} rad/hr.
 2. The RMS accelerometer bias of 200 μg corresponds to 0.4356×10^{-3} rad/(hr)².
 3. The RMS position error of 0.17 mrad corresponds to 1085m or 0.586 arc min.
 4. The RMS velocity error of 0.34 mrad corresponds to 2 ft/sec.

For the stationary case we observe in Figures 4 through 10 that for the north and east level errors, ϵ_N and ϵ_E , the Foucault modulation is an effect of first-order in contrast with the latitude, longitude and azimuth errors δL , δl , and ϵ_D respectively where the Foucault modulation has only a second-order effect [Ref. 1]. These computer solution results suggest that it would be convenient, for design purposes, to neglect the Foucault modulation since the equations we obtain then are easily solved and give solutions with approximately the same amplitude information for latitude and longitude which are of primary importance for navigational purposes while the relatively poor information of the level errors is of secondary importance.

We further note from these computer graph solutions that the effect of the Foucault terms in the error equations system, is to modulate the Schuler oscillations at a frequency given by the local vertical projection of earth rate, namely $\omega_{ie} \times \sin L$, which corresponds to a period of 33.9 hours for the selected latitude $L = 45^\circ$.

For the case of constant easterly flight at 600 ft/sec the results are given in Figures 11 to 17. Comparison with the curves for the stationary case indicates that the lowest modulation frequency has increased from $\dot{\lambda} = \omega_{ie}$ to $\dot{\lambda} = 1.557 \times \omega_{ie}$ and the space rate period is 10.9 hours while the Foucault modulation now occurs with a period of

about 21.8 hours instead of the 33.9 hours period for the stationary case.

Another important feature revealed by the above comparison is that the azimuth and latitude errors are reduced from the corresponding for the stationary case by a factor of 1.557 which represents the ratio $\dot{\lambda}/\omega_{ie}$ for this case.

For the responses to the north and azimuth zero drift, $(u)\omega_N$ and $(u)\omega_E$, the vehicle motion appears to have little effect on the error growth in the cases that exhibit a longitude error which grows with time.

The level errors in response to level gyro drift are seen to remain unchanged while the level error response to azimuth gyro drift, $(u)\omega_D$, is seen to emerge from the computer noise having a peak value of 2.3 rad/meru (Figure 13).

The longitude error in response to azimuth gyro drift which was bounded for the stationary case is now reduced by the factor $\dot{\lambda}/\omega_{ie}$ or by 1.55 while the latitude and longitude rate error magnitudes are unaffected by the vehicle motion.

Finally for the westerly flight case it is verified that the level errors remain unchanged without the effect of Foucault modulation, but the latitude, longitude, and azimuth errors grow approximately in proportion to the

time-drift rate product. The computer solution graphs for the westerly flight case are shown in Figures 19 through 24.

Similar results are found for the cases of east and azimuth gyro drift but they are not included here due to large amount of graphs.

b. Accelerometer Bias Errors

Considering the accelerometer bias as the sole error source computer simulation of equations (25) shows the following result of the effects of the north and east accelerometer bias, $(u)f_N$ and $(u)f_E$ respectively, on the navigation and level errors.

For the stationary case the results are shown in Figures 25 through 31. We note that the Schuler mode is predominant since the accelerometer bias directly excites the relatively high gain level loops and that the Schuler oscillations are modulated at the Foucault mode frequency of 33.9 hours per cycle. The maximum values for the navigation errors proved to be in the range of 20×10^{-7} rad/200 μ g for the latitude error and 1.4×10^{-6} rad/200 μ g for the longitude error.

We notice as for the constant gyro drift case that we can neglect the effects of Foucault modulations as first-order ones and proceed in the solution of the resulting equations more easily obtaining almost the same approximate amplitude information of the navigation and level errors.

For the case of constant easterly flight at 600 ft/sec the computer simulation graphs are shown in Figures 32 through 38. We observe here that again the Foucault modulating frequency has increased by a factor of 1.55 which corresponds to the ratio $\dot{\lambda}/\omega_{ie}$. Nevertheless we see that the error sensitivities remain unchanged with the previously explained stationary case.

Figures 39-45 show computer solutions of the navigation and level errors for the case of westerly flight at 600 ft/sec.

We see now that the Foucault modulating frequency has decreased by a factor 0.442 corresponding to the ratio $\dot{\lambda}/\omega_{ie}$ in this case and once again we can proceed to the solution of the equations without considering the Foucault terms, especially for design purposes. An easy extension of the above observations is that for the limiting case when the terrestrial longitude rate, $\dot{\lambda}$, in a western direction is equal to the earth rate, ω_{ie} , then the Foucault modulation disappears completely leaving a pure Schuler oscillation.

c. Initial Condition Errors

The results on the navigation and level errors due to effects of the initial conditions are now presented accompanied by only the most important graphs of the

computer simulation since the total amount of graphs is too large to be included in this study.

For the stationary case selected graphs representing the level errors for an initial north, east and azimuth level error of 0.14 mrad or 0.438 arc-min are shown in Figures 46-47, 48-49, and 50-51 respectively.

Figures 52 through 57 present the level and navigation errors for an initial latitude rate error of 2 ft/sec corresponding to 0.34 mrad/hour while figures 58 through 63 show the associated errors with an initial longitude rate error of the same amount.

There is no need to include any graphs for the resulting errors due to initial longitude error since by inspection of the error differential equations we can see that longitude is uncoupled from the other computation loops so that an initial longitude error holds constant and no other error becomes non-zero.

We discussed up to now the errors of a pure I.N.S. system. In the next chapter we proceed with the consideration of the combined I.N.S./G.P.S. system and the results we achieved after computer simulation.

IV. I.N.S./G.P.S. SYSTEM MODEL AND EQUATIONS SOLUTION

In order to apply the Kalman filter equations discussed in Chapter II a reference system model which is a good approximation to the real world dynamics is needed.

In this chapter we outline the reference I.N.S./G.P.S. system equations selected for this study. First we are defining the error states incorporated in the system model along with their assumed initial conditions values. Next we discuss the modeling of the I.N.S. plant error states and finally we present the equations for the integrated I.N.S./G.P.S. system together with their simulated computer results.

A. SYSTEM MODEL

1. State Variable Definition and Initial Conditions

In Table III we present a listing of the state variables utilized in the reference system model. The initial conditions on the I.N.S. error states are highly arbitrary and the selected values are similar to those used in other unclassified studies [Refs. 4,5].

For the initial conditions on the gyro error states and the accelerometer, the values are selected for a typical inertial navigation system of one nautical mile per hour class.

After the above definition of the initial conditions we have by the same time specified in a complete way the initial covariance matrix $P(0)$, since its diagonal elements are the squared values of the given RMS initial conditions. The remaining off-diagonal elements of the initial covariance matrix are assumed to be zero initially.

Furthermore the propagation of the linear variance equation (13) requires an additional knowledge of the two matrices F and Q^* where:

$$Q^* = GQG^T \quad (33)$$

where

G is the forcing input matrix

Q is the input noise covariance matrix

and the F matrix is the same as in Equation (25) and which has been used in the previous chapter for the inertial navigation system error equations solution and computer simulation.

For the Q^* matrix the only non-zero elements are all diagonal and we will denote these from now on as Q_i where the subscript i denotes the row and column of the value. For example, Q_3 indicates that this is the value which belongs to the intersection of the 3rd row and the 3rd

column in the Q^* matrix and corresponds to a white noise input on state variable number 3.

These non-zero elements in the reference system Q^* matrix are five, corresponding to state numbers 1, 2, 3, 6 and 7 according to the notation of Table III.

2. Plant Error States

The following seven states, North, East, and Azimuth level errors, X and Y position errors, X and Y velocity errors, constitute the plant error states. The differential equations of these states describe the natural unforced dynamic response of the errors in the inertial navigation system.

There are various models for the implementation of these error states. As we did in the previous chapter we will use again the Pinson error model described by the matrix F given in equation (25) for our specific case of the local-level two-accelerometer inertial navigation system configuration.

B. EQUATIONS SOLUTION AND COMPUTER SIMULATION

Using the definitions described in previous pages we can write the following equations for the error states:

$$\dot{\underline{x}}(t) = \underline{F} \underline{x}(t) + \underline{G} \underline{w}(t) \quad (34)$$

$$\underline{z}(t) = \underline{H} \underline{x}(t) + \underline{v}(t)$$

TABLE III
I.N.S./G.P.S. SYSTEM STATE VECTOR DEFINITION

Error State	Symbol	Definition	RMS Initial Condition	
<u>I.N.S. PLANT ERROR STATES</u>				
1.	ϵ_N	North attitude error	0.14×10^{-3} Rad	
2.	ϵ_E	East attitude error	0.14×10^{-3} Rad	
3.	ϵ_D	Azimuth attitude error	0.14×10^{-3} Rad	(1)
4.	δL	Y position error	0.17×10^{-3} Rad	
5.	δl	X position error	0.17×10^{-3} Rad	
6.	$\delta \dot{L}$	Y velocity error	0.34×10^{-3} Rad/hour	(2)
7.	$\delta \dot{l}$	X velocity error	0.34×10^{-3} Rad/hour	
<u>I.N.S. ERROR SOURCES</u>				
8.	$(u)\omega_N$	North Gyro Drift	1 meru	(3)
9.	$(u)\omega_E$	East Gyro Drift	1 meru	
10.	$(u)\omega_D$	Azimuth Gyro Drift	1 meru	
11.	$(u)f_N$	North Accelerometer Bias	$200 \times 10^{-6}g$	(4)
12.	$(u)f_E$	East Accelerometer Bias	$200 \times 10^{-6}g$	

-
1. The RMS position error of 0.17 milliradians corresponds to 1085m or 0.586 arc min.
 2. The RMS velocity error of 0.34 millirad/hour corresponds to 2 ft/sec.
 3. The RMS gyro drift of 1 meru corresponds to $0.015^\circ/\text{hr}$ or 261.8×10^{-6} rad/hour.
 4. The RMS accelerometer bias of $200 \times 10^{-6}g$ corresponds to 0.4356×10^{-3} rad/(hr)².

where

$$\begin{aligned}\underline{x}(t) &= 7 \times 1 \text{ error state vector} \\ &= [\epsilon_N, \epsilon_E, \epsilon_D, \delta L, \delta l, \delta \dot{L}, \delta \dot{l}]^T\end{aligned}$$

$$\begin{aligned}\underline{F} &= 7 \times 7 \text{ Pinson error model matrix} \\ &\text{as described in equation (25)}\end{aligned}$$

$$\begin{aligned}\underline{G} &= 7 \times 5 \text{ input forcing matrix as described} \\ &\text{in equation (25)}\end{aligned}$$

$$\underline{z}(t) = 2 \times 1 \text{ vector of measured states}$$

$$\underline{H} = 2 \times 7 \text{ measurement matrix where}$$

$$\underline{H} = \begin{bmatrix} 0 & 0 & 0 & 1 & 0 & 0 & 0 \\ 0 & 0 & 0 & 0 & 1 & 0 & 0 \end{bmatrix}$$

denoting that we have available measured information for the X and Y position error.

$$\begin{aligned}\underline{w}(t) &= 5 \times 1 \text{ forcing vector assumed to be white} \\ &\text{Gaussian noise}\end{aligned}$$

and

$$\begin{aligned}\underline{v}(t) &= 2 \times 1 \text{ vector of measurements noise assumed to} \\ &\text{be white Gaussian.}\end{aligned}$$

Using the feedback configuration of the Kalman filter we can write the following equations:

$$\dot{\hat{x}}(t) = \underline{F} \hat{x}(t) + \underline{G} \underline{w}(t) + \underline{K}[\underline{z} - \underline{H} \hat{x}(t)] \quad (35)$$

and

$$\dot{P}(t) = \underline{F} \underline{P} + \underline{P} \underline{F}^T + \underline{G} \underline{Q} \underline{G}^T - \underline{P} \underline{H}^T \underline{R}^{-1} \underline{H} \underline{P} \quad (36)$$

where

$\underline{P}(t)$ = the covariance matrix

$\underline{K} = \underline{P} \underline{H}^T \underline{R}^{-1}$ the Kalman filter gains matrix

\underline{R} = the measurement noise covariance matrix

In order to achieve numerical results via computer simulation we write the predicted error states of our system in explicit form as below with the help of Table IV in which the system states and their corresponding symbols are defined:

$$\begin{aligned} \dot{\hat{x}}(1) = & -\dot{\lambda}(\sin L)\hat{x}(2) - \dot{\lambda}(\sin L)\hat{x}(4) + (\cos L)\hat{x}(7) + AA + \\ & + K_{11}[\hat{x}(8) - \hat{x}(4)] + K_{12}[\hat{x}(9) - \hat{x}(5)] \end{aligned} \quad (35-a)$$

$$\begin{aligned} \dot{\hat{x}}(2) = & \dot{\lambda}(\sin L)\hat{x}(1) + \dot{\lambda}(\cos L)\hat{x}(3) - \hat{x}(6) + BB + \\ & + K_{21}[\hat{x}(8) - \hat{x}(4)] + K_{22}[\hat{x}(9) - \hat{x}(5)] \end{aligned} \quad (35-b)$$

$$\begin{aligned} \dot{\hat{x}}(3) = & -\dot{\lambda}(\cos L)\hat{x}(2) - \dot{\lambda}(\cos L)\hat{x}(4) - (\sin L)\hat{x}(7) + SS + \\ & + K_{31}[\hat{x}(8) - \hat{x}(4)] + K_{32}[\hat{x}(9) - \hat{x}(5)] \end{aligned} \quad (35-c)$$

$$\dot{\hat{x}}(4) = \hat{x}(6) + K_{41}[\hat{x}(8) - \hat{x}(4)] + K_{42}[\hat{x}(9) - \hat{x}(5)] \quad (35-d)$$

TABLE IV
COMPUTER SIMULATION VARIABLES AND CONSTANTS

x(1)	= ϵ_N	= North attitude error
x(2)	= ϵ_E	= East attitude error
x(3)	= ϵ_D	= Azimuth attitude error
x(4)	= δL	= Y position error
x(5)	= δl	= X position error
x(6)	= $\delta \dot{L}$	= Y velocity error
x(7)	= $\delta \dot{l}$	= X velocity error
x(8)	= δL_g	= G.P.S. Y position error measurement
x(9)	= δl_g	= G.P.S. X position error measurement
x(10)	= δL_t	= True Y position error
x(11)	= δl_t	= True X position error
x(12)	= w	= Input white Gaussian noise
x(13)	= v	= Measurement white Gaussian noise
A	= $[(u)\omega_N]^2$	= North Gyro Drift Variance
B	= $[(u)\omega_E]^2$	= East Gyro Drift Variance
S	= $[(u)\omega_D]^2$	= Azimuth Gyro Drift Variance
D	= $[(u)f_N]^2$	= North Accelerometer Bias Variance
E	= $[(u)f_E]^2$	= East Accelerometer Bias Variance
F	= R_{11}	= Measured Y position error variance
G	= R_{22}	= Measured X position error variance
AA	= $x(12) \cdot A$	= White noise like North Gyro Drift strength
BB	= $x(12) \cdot B$	= White noise like East Gyro Drift strength

TABLE IV (CONTINUED)

SS	= $x(12) \cdot S$	= White noise like Azimuth Gyro Drift strength
DD	= $x(12) \cdot D$	= White noise like North Accelerometer bias strength
EE	= $x(12) \cdot E$	= White noise Like East Accelerometer bias strength
FF	= $x(13) \cdot F$	= White noise like Y-position error strength
GG	= $x(13) \cdot G$	= White noise like X-position error strength
k	= g/r	= constant

$$\hat{\dot{x}}(5) = \hat{x}(7) + K_{51}[\hat{x}(8) - \hat{x}(4)] + K_{52}[\hat{x}(9) - \hat{x}(5)] \quad (35-e)$$

$$\begin{aligned} \hat{\dot{x}}(6) = & k\hat{x}(2) - \dot{\lambda}(\sin 2L)\hat{x}(7) + DD + \\ & + K_{61}[\hat{x}(8) - \hat{x}(4)] + K_{62}[\hat{x}(9) - \hat{x}(5)] \end{aligned} \quad (35-f)$$

$$\begin{aligned} \hat{\dot{x}}(7) = & -\frac{k}{\cos L} \hat{x}(1) + 2\dot{\lambda}(\tan L)\hat{x}(6) + EE + \\ & + K_{71}[\hat{x}(8) - \hat{x}(4)] + K_{72}[\hat{x}(9) - \hat{x}(5)] \end{aligned} \quad (35-g)$$

Assuming the input forcing vector as white Gaussian noise whose strength is related to the value of the variance of each input error source (the corresponding one) computer simulation was proceeded in the following way.

First with the help of the RICATI FILTER computer program available at the NPS W.R. Church Computer Center we solved the corresponding for our study Riccati equation of covariance propagation obtaining the Kalman filter gain matrix. The data we used to run the above program are provided in Tables III and V. A listing of the data formulation for the RICATI FILTER program is given in Appendix D.

The calculated from the above program values of the Kalman filter gains for a processing period of four hours are given in the following Table VI.

Additional runs of the above program have been contacted for processing periods up to 36 hours and it has been observed that the Kalman filter gains reach a steady state

TABLE V
NUMERICAL VALUES FOR RICATI PROGRAM¹

F Matrix (7 x 7)

$F_{12} = -0.1851$	$F_{14} = -0.1851$	$F_{17} = 0.707$
$F_{21} = 0.1851$	$F_{23} = 0.1851$	$F_{26} = -1.0$
$F_{32} = -0.1851$	$F_{34} = -0.1851$	$F_{37} = -0.707$
$F_{46} = 1.0$		
$F_{57} = 1.0$		
$F_{62} = 19.92$	$F_{67} = -0.2618$	
$F_{71} = -28.175$	$F_{76} = 0.5235$	

All other elements are zero.

G^T Matrix (5 x 7)

$G_{11} = G_{22} = G_{33} = 1.0$
 $G_{46} = 0.0915$
 $G_{57} = 0.1294$

All other elements are zero.

H Matrix (2 x 7)

$H_{14} = H_{25} = 1.0$

All other elements are zero.

¹For the used values of elements in the matrices the results will be given having units the appropriate for each case combination of radians and hours.

TABLE V (CONTINUED)

Q Matrix (5 x 5)

$$Q_{11} = Q_{22} = Q_{33} = [0.0002618 \text{ rad/hr}]^2 = 0.7 \times 10^{-7} [\text{rad/hr}]^2$$

$$Q_{44} = Q_{55} = [0.0004356 \text{ rad}/(\text{hr})^2]^2 = 0.19 \times 10^{-6} [\text{rad}/(\text{hr})^2]^2$$

All other elements are zero.

R Matrix (2 x 2)

$$R_{11} = R_{22} = 0.52 \times 10^{-6} [\text{rad}]^2$$

$$R_{12} = R_{21} = 0.0$$

P(0) Matrix (7 x 7)

$$P_{11}(0) = P_{22}(0) = P_{33}(0) = [0.00014 \text{ rad}]^2 = 0.1 \times 10^{-7} [\text{rad}]^2$$

$$P_{44}(0) = P_{55}(0) = [0.00017 \text{ rad/hr}]^2 = 0.3 \times 10^{-7} [\text{rad/hr}]^2$$

$$P_{66}(0) = P_{77}(0) = [0.00034 \text{ rad}/(\text{hr})^2]^2 = 0.115 \times 10^{-6} [\text{rad}/(\text{hr})^2]^2$$

All other off-diagonal elements are zero.

TABLE VI
KALMAN FILTER CASE FOR A 4 HOUR PROCESS

$$K_{11} = 0.034756672$$

$$K_{12} = 1.17201123$$

$$K_{21} = -1.36921265$$

$$K_{22} = -0.0401669175$$

$$K_{31} = 1.56555360$$

$$K_{32} = -2.86193609$$

$$K_{41} = 3.44020611$$

$$K_{42} = 0.090728150$$

$$K_{51} = 0.0907281520$$

$$K_{52} = 4.31037639$$

$$K_{61} = 5.92162434$$

$$K_{62} = -0.339257459$$

$$K_{71} = 1.04245351$$

$$K_{72} = 9.29378811$$

condition for which their values are not very much different from those achieved for a 4 hour processing period.

So in the following calculations and computer simulation we have used the values of the Kalman filter gains resulted for a 4 hour simulation period.

Having available the values of Kalman filter gain matrix elements which are used to multiply the residuals in the appropriate equations in order to achieve the predicted error states of the integrated I.N.S./G.P.S. system, the appropriate program has been formulated in order to solve the error differential equations (32) described above, with the use of the available routine INTEG2S slightly modified for accurate evaluation and plot of the error state variables.

The simulation results for the I.N.S./G.P.S. system operation for a period of four (4) hours are presented below in Figures 64 through 93. We can easily observe that all the state error variables of the combined I.N.S./G.P.S. system are damped out and the resulting value of the errors after a period of one (1) hour is small enough so that the operation of our system model can be characterized as successful.

Specifically in Figure 64 we observe that the north level error of our system is dropped down to 0.025 milliradians after one (1) hour even if the starting initial

condition value was 0.14 milliradians. Furthermore at the end of a 4 hour period the error has been diminished to the value of 0.005 milliradians which is subject to error reduction by a factor of 28.

In Figures 65 and 66 the East and Azimuth attitude errors are presented respectively where similar as with the north attitude error observations occur.

The Y position error behavior is presented in Figure 67. There we can see that even if we started from an initial condition error of 0.17 milliradians (or 3256 ft) after one hour processing the error has been diminished to only 0.028 milliradians (or 536 ft) and furthermore after a four hour period this error drops down to 0.01 milliradians (or 191.5 ft).

The X position error damping out seems to be more attractive since from Figure 68 we can see that after one hour the error drops down to 0.020 milliradians (or 383 ft) and at the end of a four hour period the error is diminished to 0.0002 milliradians (or 3.83 ft) which is very small considering also that we started with an initial condition value of the X position error of 0.17 milliradians (or 3256 ft).

Figure 69 presents the propagation of Y velocity error. It is easily observed that this error drops down to the very small value of 0.040 milliradians/hour (or 68×10^{-4} ft/sec)

after one hour and to the negligible error of 0.002 milliradians/hour (or 34×10^{-5} ft/sec) which provides the advantage of very accurate evaluation and tracking of the Y velocity state variable.

Similar with the above considerations and even better results occur for the case of the X velocity error of the integrated I.N.S./G.P.S. system. We see from Figure 70 that this error starting from an initial condition value of 0.34 milliradians/hour (or 2 ft/sec) drops down to 0.1 milliradians/hour (or 17×10^{-3} ft/sec) after one hour operation and furthermore down to 0.002 milliradians/hour (or 34×10^{-5} ft/sec) after a period of four hours which again denotes a very accurate tracking of the X velocity error state variable.

In Figures 71 and 72 the normalized inserted and measurement noise of the combined I.N.S./G.P.S. systems are presented respectively.

Thinking of the operation of our system in the long term, results of the computer simulation are presented in Figures 73 through 79. Using the same input data for our I.N.S./G.P.S. system model and running the program for a 36 hour process we see that the behavior of the feedback configuration of the Kalman filter in our system continues to be attractive throughout the long term period of interest without diverging at any moment.

In addition to the above considerations, in order to make our system more realistic and compatible to the real world's conditions we put some noise in the two error state equations of X and Y position which did not include any noise from our theoretical design of the system. So we replace the two equations (35-d) and (35-e) in our system of equations with the following two equations:

$$\dot{\hat{x}}(4) = \hat{x}(6) + AA + K_{41}[\hat{x}(8) - \hat{x}(4)] + K_{42}[\hat{x}(9) - \hat{x}(5)] \quad (35-d')$$

and

$$\dot{\hat{x}}(5) = \hat{x}(7) + AA + K_{51}[\hat{x}(8) - \hat{x}(4)] + K_{52}[\hat{x}(9) - \hat{x}(5)] \quad (35-e')$$

Assigning to the strength of this intentionally inserted noise a value similar to that of the strength of the gyro drift (that is a value of $0.0685 \times 10^{-6} \text{ [rad]}^2$) we ran the same program and we achieved results proving that the combined I.N.S./G.P.S. system reacted in a way exactly the same as it had reacted without the inserted noise in the X and Y position error equations. So we make the conclusion that the intentionally inserted noise did not affect the operation of our system model neither from the accuracy point of view nor from the time point of view.

The above considerations and results can be seen in Figures 80 through 86 for the four (4) hours short term process and in Figures 87 through 93 for the 36 hours long term operation.

In Table VII on the next page we summarized the state errors of the combined I.N.S./G.P.S. system after a period of two and four hours operation. In the same table we included the starting initial condition for each error state in order to make our comparisons easier and handy. The results included in Table VII are those achieved from the computer simulation without any noise corrupting the two error states of Y and X position. But since the addition of noise with strength similar to that of the gyro drift ($0.0685 \times 10^{-6} \text{ [rad]}^2$) did not affect the system model operation as mentioned before, the same Table VII represents also the summary of state errors for the real world's system model of the I.N.S./G.P.S. system.

Up to now we considered our system to be corrupted by white Gaussian input noise. Since in the real world in many cases the presence of colored noise is apparent we must consider the operation of our I.N.S./G.P.S. system under the presence of such noise and compare the results with those achieved when the system was driven by white noise.

In the following section a realistic modeling of the I.N.S. component errors is discussed and the results of the computer simulation are presented together with the comparison conclusions of the system's operation under colored noise versus white noise corruption.

TABLE VII

SUMMARY OF STATE ERRORS FOR THE I.N.S./G.P.S. SYSTEM MODEL

<u>State Error</u>	<u>Initial Condition</u>	<u>Error in 2 hours</u>	<u>Error in 4 hours</u>
ϵ_N	0.14 mrad	0.025 mrad	0.005 mrad
ϵ_E	0.14 mrad	0.021 mrad	0.001 mrad
ϵ_D	0.14 mrad	0.04 mrad	0.02 mrad
δL	0.17 mrad (3256 ft)	0.028 mrad (536 ft)	0.01 mrad (191.5 ft)
δl	0.17 mrad (3256 ft)	0.020 mrad (383 fft)	0.0002 mrad (3.8 ft)
$\delta \dot{L}$	0.34 mrad/hr (2 ft/sec)	0.040 mrad/hr (0.0068 ft/sec)	0.002 mrad/hr (0.00034 ft/sec)
$\delta \dot{l}$	0.34 mrad/hr (2 ft/sec)	0.1 mrad/hr (0.017 ft/sec)	0.002 mrad/hr (0.00034 ft/sec)

C. I.N.S. COMPONENT ERROR MODELS

In Chapter III equation (31) indicates that the I.N.S. component errors consist of three gyro drift uncertainties, two accelerometer measurement uncertainties, two gyro torquer scale factor errors and two geodetic uncertainties. Realistic modeling of the two major error components, the gyro drift and the accelerometer measurement is described below.

1. Gyro Drift Uncertainties

The three gyro drift uncertainties, $(u)_{\omega_N}$, $(u)_{\omega_E}$, $(u)_{\omega_D}$ are each modeled as an exponentially-correlated (colored) noise plus an additive random (white) noise:

$$(u)_{\omega_i} = \delta_i + w_{g_i} ; \quad i = N, E, D \quad (37)$$

where the colored noise δ_i is determined by:

$$\dot{\delta}_i = -\frac{1}{t_{g_i}} \delta_i + v_{g_i} \quad (38)$$

The t_{g_i} represents the correlation time of the colored noise and the v_{g_i} the strength of the driving white noise obtained using the specified variance $\sigma_{\delta_i}^2$ of the colored noise and the formula

$$Q_{v_{g_i}} = 2\sigma_{\delta_i}^2 / t_{g_i} \quad (39)$$

The quantity w_{g_i} is a white noise of specified strength.

2. Accelerometer Measurement Uncertainties

The accelerometer measurement uncertainties $(u)f_N$ and $(u)f_E$ are modeled in the same way as the gyro drift uncertainties, as colored noise plus white noise:

$$(u)f_i = a_i + w_{a_i} ; \quad i = N, E \quad (40)$$

where again w_{a_i} is the white noise of specified strength and the colored noise is given by:

$$\dot{a}_i = -\frac{1}{t_{a_i}} a_i + v_{a_i} \quad (41)$$

where t_{a_i} is the correlation time of the colored noise with variance $\sigma_{a_i}^2$, and the strength of the driving white noise v_{a_i} is given by:

$$Q_{v_{a_i}} = 2 \sigma_{a_i}^2 / t_{a_i} \quad (42)$$

3. Computer Simulation Results

Using the same set of equations (35-a) through (35-g) but introducing the appropriate state augmentation in order to incorporate the exponentially correlated noise for the gyro drift and the accelerometer measurement, we simulated the operation of the combined I.N.S./G.P.S. system and achieved the following result.

The operation of the system proved to be excellent for all the used correlation times from 60 seconds up to 3600 seconds (1 hour). The attitude and navigation errors were found to behave in the same way being minimized after a period of one hour. Furthermore, the variation of the attitude and navigation errors is similar with the case of the white noise driven I.N.S./G.P.S. combined system which again is similar, if not exactly the same, with the ideal I.N.S./G.P.S. system.

In Figures 94 through 100 we present the I.N.S./G.P.S. system operation for an exponentially correlated input noise with a correlation time of 1 hour (3600 sec). We can easily see in these figures that the behavior of the combined I.N.S./G.P.S. system is the same with that when white noise drives the input except for a very small and negligible increase of the attitude and navigation errors after the first hour of operation.

V. CONCLUSIONS AND RECOMMENDATIONS

A. CONCLUSIONS

From knowledge gained throughout this work and based on the material presented in our study, the following conclusions are drawn:

As far as the I.N.S. errors are concerned we saw that

1. The effects of constant gyro drift errors for the stationary case are related to Foucault modulation which has only a second-order effect on the longitude and latitude error states and permit us to neglect it in cheap systems designed for navigational purposes.

2. For the case of easterly flight, latitude errors were reduced by a factor of 1.557 which corresponds to the ratio $\dot{\lambda}/\omega_{ie}$ and Foucault modulation period reduced analogously from 33.9 hours to 21.8 hours.

3. For the westerly flight, case longitude and latitude errors grow in approximate proportion to the time-drift rate product.

4. The accelerometer bias errors have the same effects for the stationary case as the gyro drift errors.

5. The Foucault modulation period increased by the same as above factor of 1.557 for the easterly flight case, while for the westerly flight decreased by a factor of 0.442

corresponding again to the ration $\dot{\lambda}/\omega_{ie}$ for the specific case.

6. The error sensitivities remain unchanged for the easterly and westerly flight and again we may neglect Foucault modulation as producing only second-order effects on the navigation states.

For the combined I.N.S./G.P.S. system the results achieved by this study proved that the errors of the system's state variables are damped out in less than one hour, denoting effective and successful operation of the G.P.S. aiding to the I.N.S. Specifically:

7. Using suboptimal Kalman filter gains for one hour process, the Y-position error reduced from its initial value by a factor of 6 in one hour and by a factor of 17 in four hours.

8. With the same suboptimal Kalman filter gains of one hour process, the X-position error proved the system more attractive since the error reduced by a factor of 8.5 after one hour and by a factor of 856 after four hours.

9. Both the X and Y-velocity errors damped out very quickly so that after one hour the Y-velocity error reduced by a factor of 312.5 and the X-velocity error by a factor of 117.6, while for a four-hour process both velocity errors reduced by a factor of 571 from its initial value.

10. The consideration of long term filter's operation proved no divergence at all for a process of 36 whole hours. The errors remained at the same attractive levels as for the four-hour process, fact which enables us to conclude that the combined I.N.S./G.P.S. system works with excellent results for both short and long term periods.

11. Finally the operation of the combined I.N.S./G.P.S. system under exponentially correlated input noise proved to be excellent for all different correlation times from 60 sec up to 3600 sec, with a negligible increase in the attitude and navigation error magnitudes after the first hour of operation.

B. RECOMMENDATIONS

Continued study of this work can be based on the following recommendations:

1. A Kalman filter design study where the primary emphasis will be placed upon determination of the "best" filter state variable vector. A general covariance analysis program for the analysis, evaluation and design of Kalman filters, which will help this study, has been tape recorded from the Wright Patterson Air Force Base, Air Force Avionics Laboratory and modified by the author for use in N.P.S. campus computer.

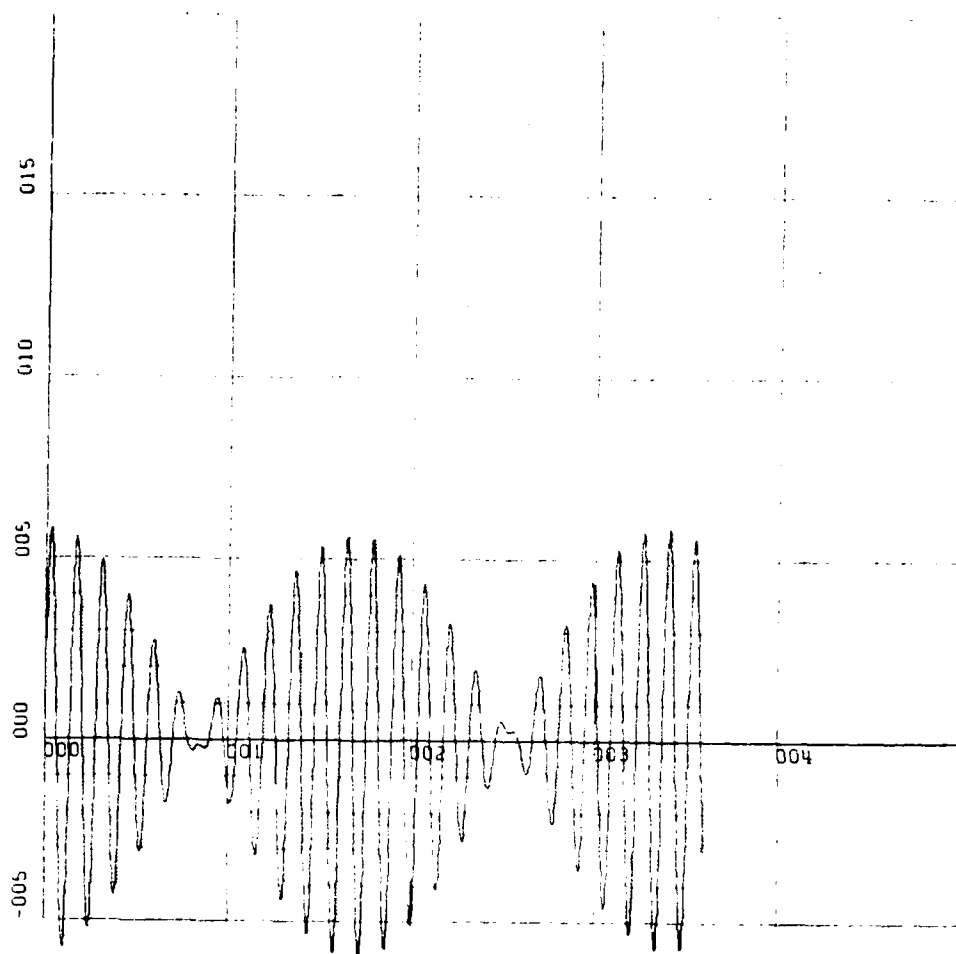
2. Investigation of various measurement rates using the external range measurements from a set of satellites in view

among the 18 of the G.P.S. and Kalman filter's performance for these rates.

3. Possible use of a flight profile generator program, which will generate simulated flight patterns instead of considering specific only cases for stationary, easterly, and westerly flights, together with a satellite motion generator required to provide necessary information regarding the satellites' orbital elements. This recommendation applies only to U.S. citizens since such programs already exist but they are classified.

4. Investigation and results evaluation for the effects upon filter performance when range-rate measurements are available. Then a comparison with the usage of only range measurements could be extracted. Another aspect for investigation could be the satellite bearing measurements to declare best observable satellites and to provide better accuracy.

5. Finally a comparison of sequential versus simultaneous measurement would be another area of interest. The performance of a filter working with sequential measurements is of interest primarily, because of the increased cost of equipment required to perform simultaneous measurements and computations as compared to the sequential ones.



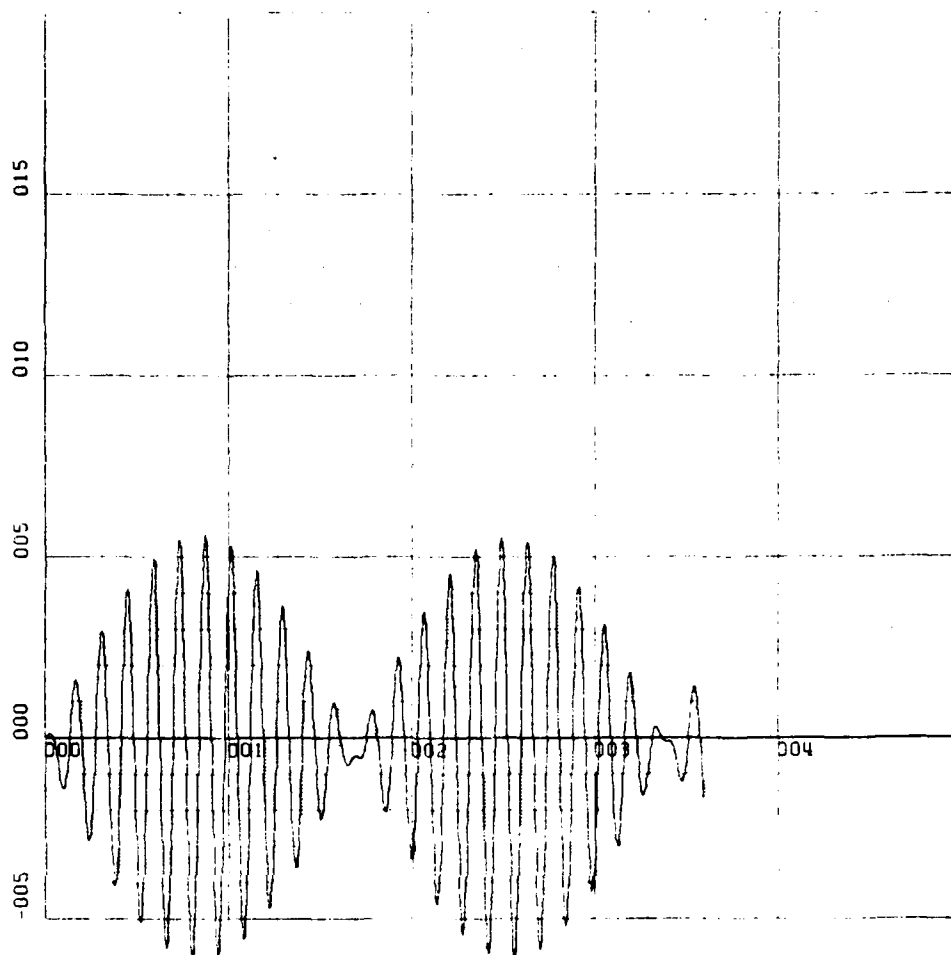
X-SCALE=1.00E+01 UNITS INCH. [hours]
 Y-SCALE=5.00E-05 UNITS INCH. [rad/meru]

KWSTAS

RUN 1

E 'N' VS TIME

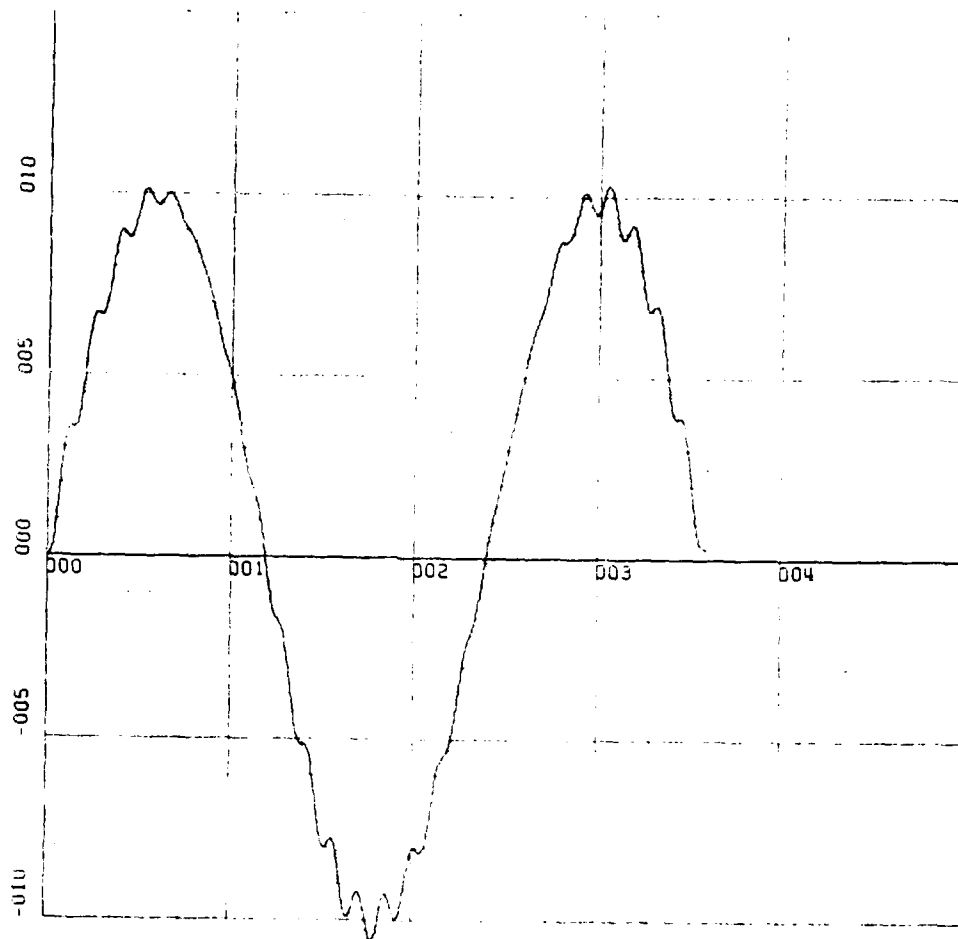
Figure 4. Stationary Case. North Level Error [rad/meru]
 for Constant North Gyro Drift [1 meru].



X-SCALE=1.00E+01 UNITS INCH. [hours]
 Y-SCALE=5.00E-05 UNITS INCH. [rad/meru]
 KWSTAS
 RUN 1

E'E' VS TIME

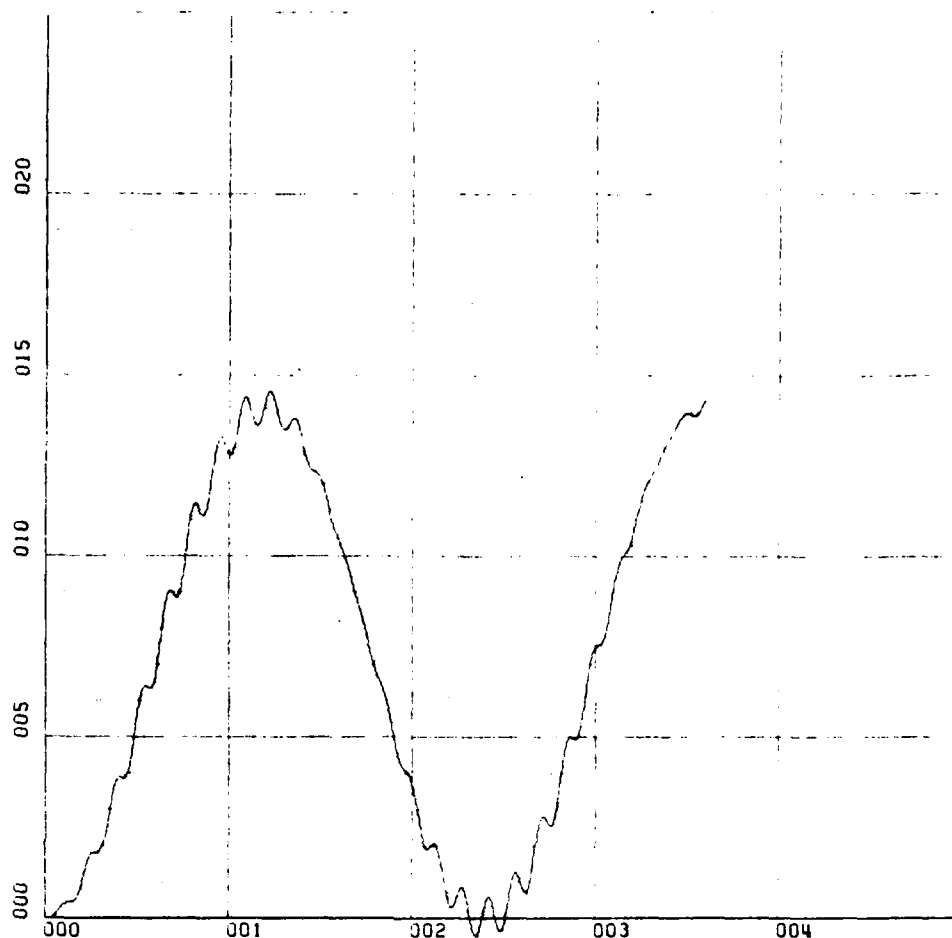
Figure 5. Stationary Case. East Level Error [Rad/meru] for
 Constant North Gyro Drift [1 meru].



X-SCALE=1.00E+01 UNITS INCH. [hours]
 Y-SCALE=5.00E-04 UNITS INCH. [Rad/meru]
 KWSTAS
 RUN 1

E'D' VS TIME

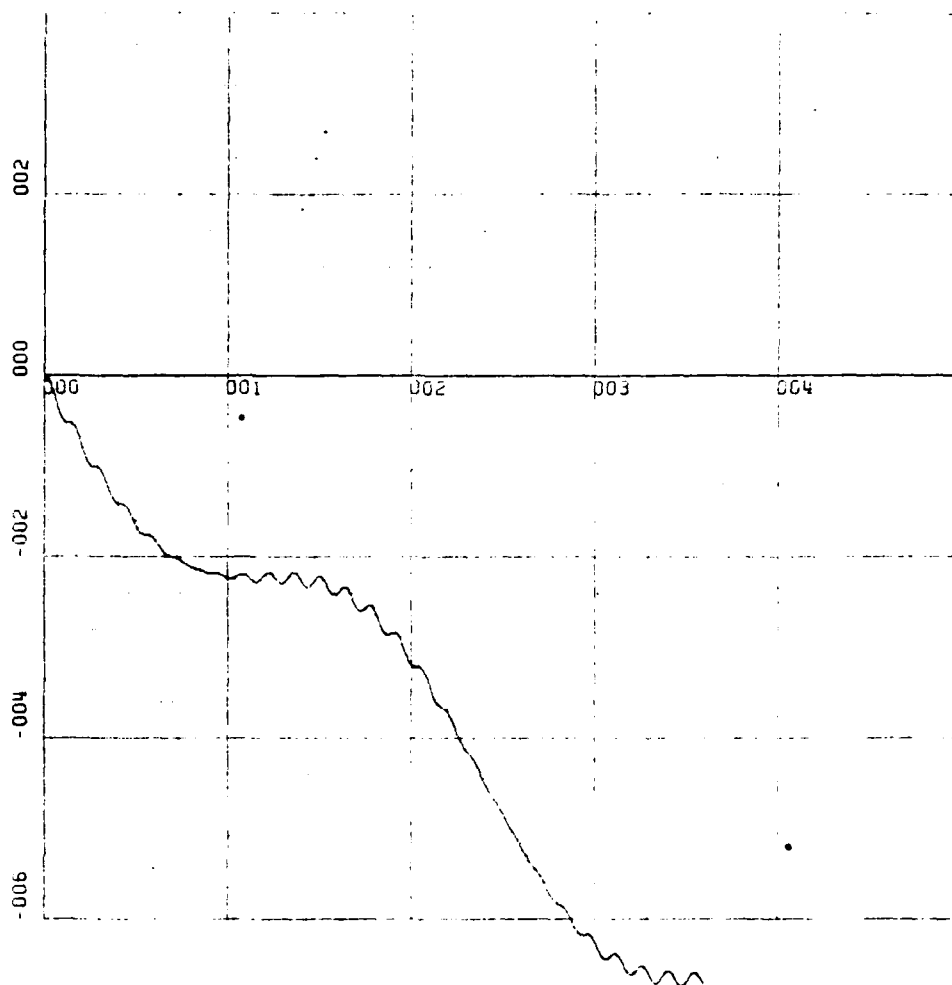
Figure 6. Stationary Case. Azimuth Level Error [Rad/meru]
 for Constant North Gyro Drift [1 meru].



X-SCALE=1.00E+01 UNITS INCH. [hours]
 Y-SCALE=5.00E-04 UNITS INCH. [Rad/meru]
 KWSTAS
 RUN 1

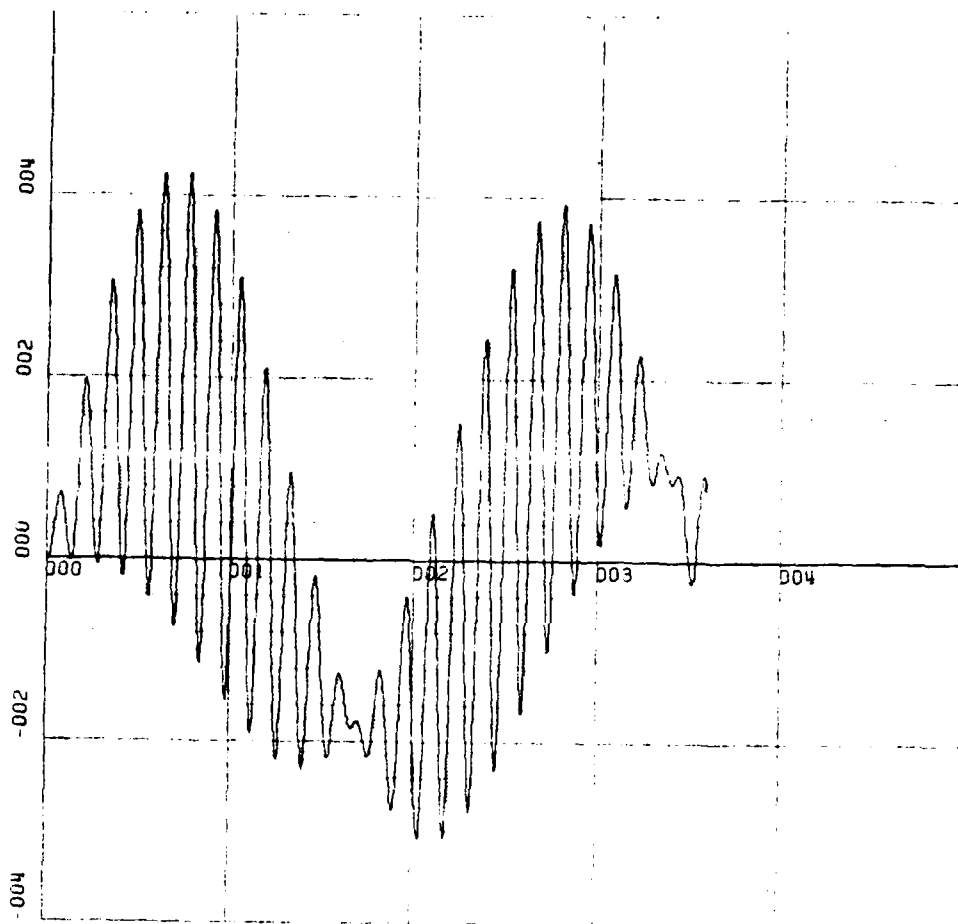
DLA VS TIME

Figure 7. Stationary Case. Latitude Error [Rad/meru] for
 Constant North Gyro Drift [1 meru].



X-SCALE=1.00E+01 UNITS INCH. [hours]
 Y-SCALE=2.00E-03 UNITS INCH. [Rad/meru]
 KWSTAS
 RUN 2 DLO VS TIME

Figure 8. Stationary Case. Longitude Error [Rad/meru] for
 Constant North Gyro Drift [1 meru].



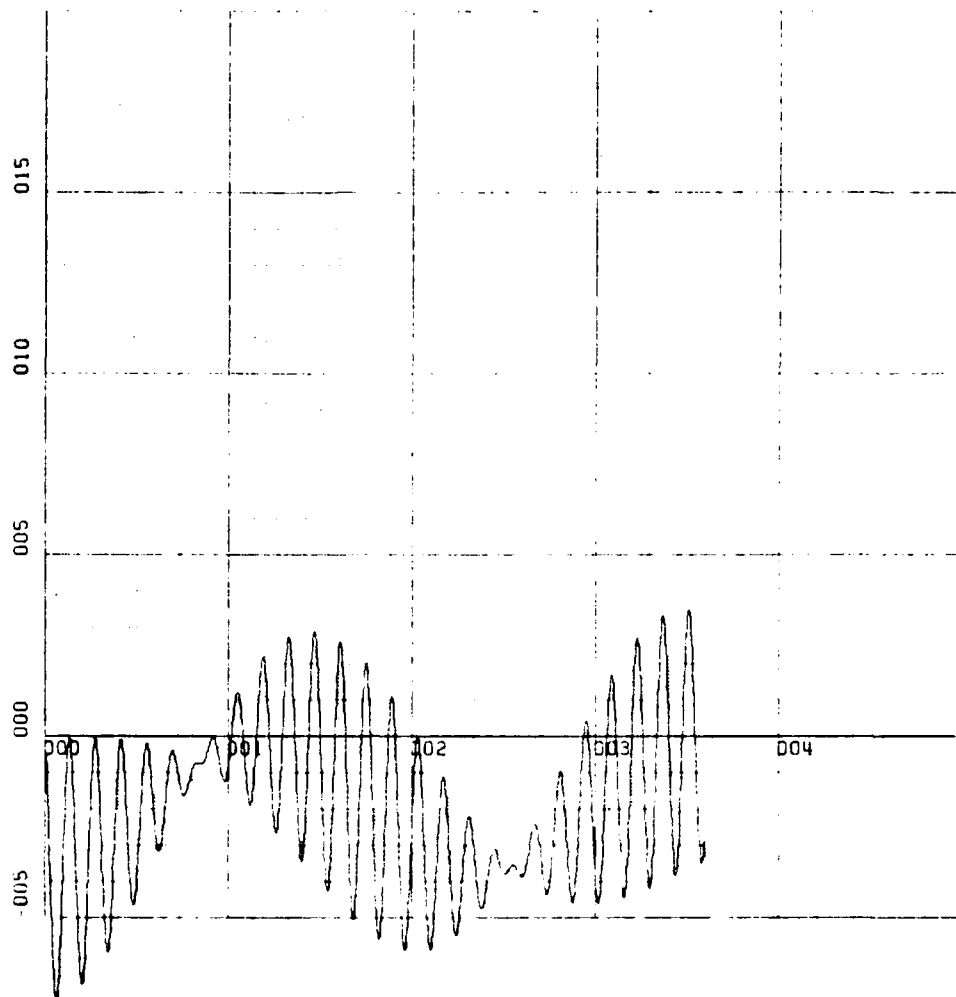
X-SCALE=1.00E+01 UNITS INCH. [hours]
 Y-SCALE=2.00E-04 UNITS INCH. [Rad/hours·meru]

KWSTAS

RUN 2

DLAD VS TIME

Figure 9. Stationary Case. Latitude Rate Error
 [Rad/hours·meru] for Constant North Gyro Drift
 [1 meru].



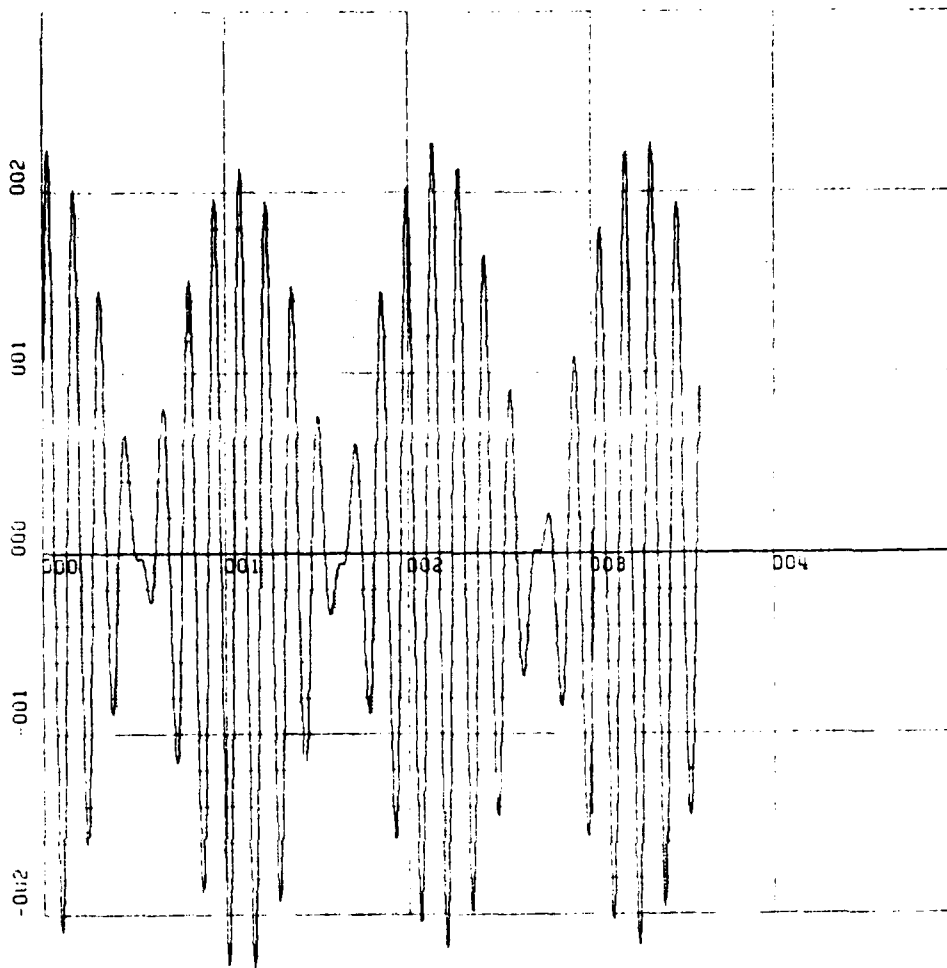
X-SCALE=1.00E+01 UNITS INCH. [hours]
Y-SCALE=5.00E-04 UNITS INCH. [Rad/hour·meru]

KWSTAS

RUN 2

DL0D VS TIME

Figure 10. Stationary Case. Longitude Rate Error
[Rad/hour·meru] for Constant North Gyro Drift
[1 meru].



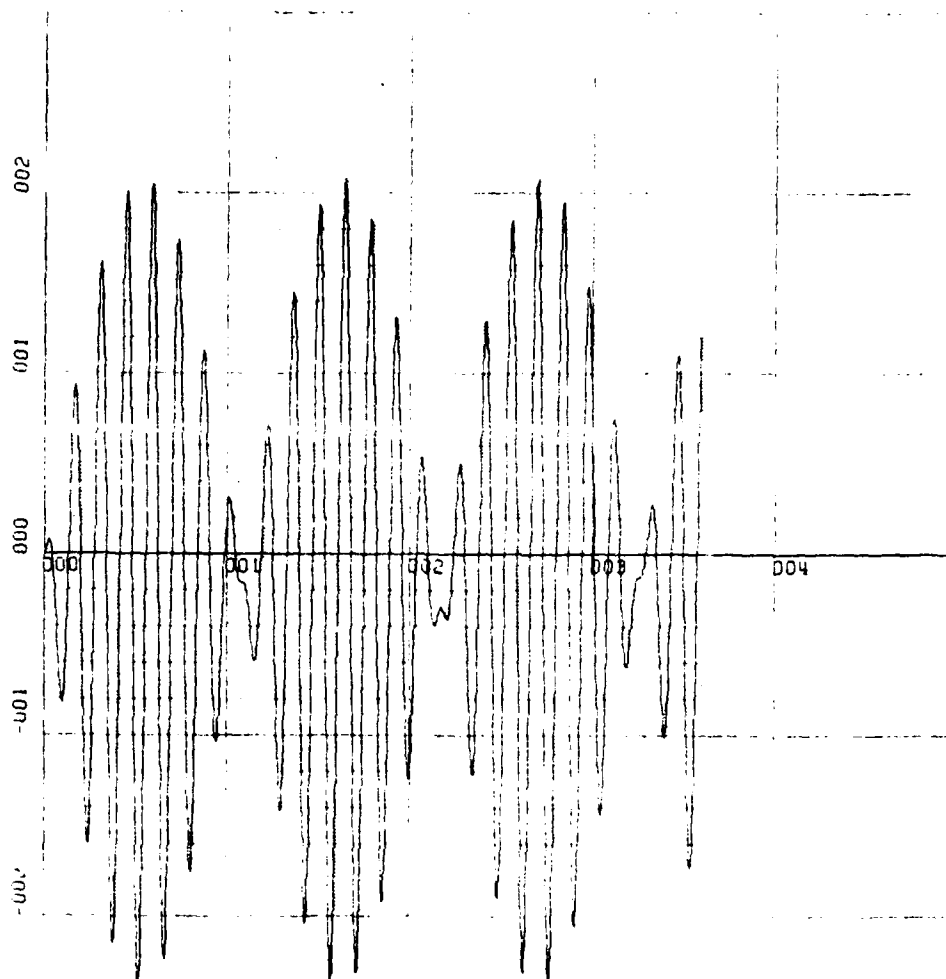
X-SCALE=1.00E+01 UNITS INCH. [hours]
 Y-SCALE=1.00E-01 UNITS INCH. [Rad/meru]

KWSTAS

RUN 1

E 'N' VS TIME

Figure 11. Easterly Flight at 600 ft/sec.
 North Level Error [Rad/meru] for Constant
 North Gyro Drift [1 meru].



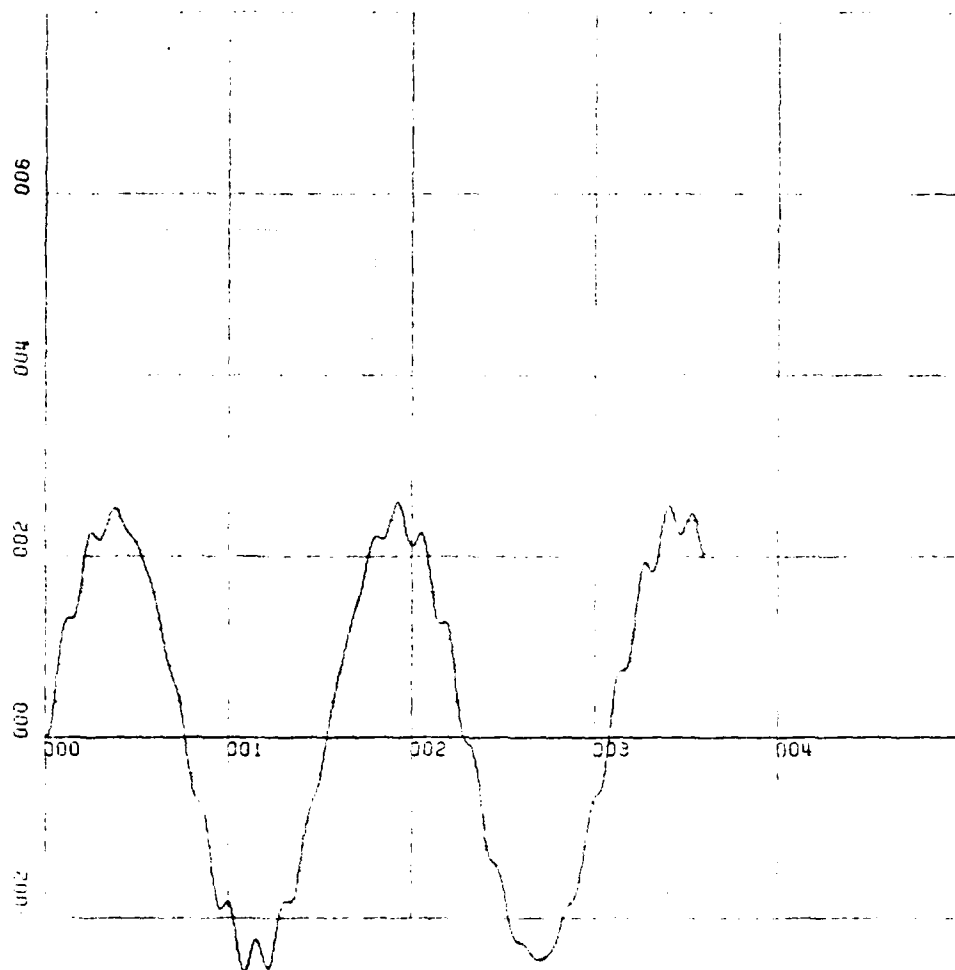
X-SCALE=1.00E+01 UNITS INCH. [hours]
 Y-SCALE=1.00E-01 UNITS INCH. [Rad/meru]

KWSTAS

RUN 1

E'E' VS TIME

Figure 12. Easterly Flight at 600 ft/sec
 East Level Error [Rad/meru] for Constant North
 Gyro Drift [1 meru].



X-SCALE=1.00E+01 UNITS INCH. [hours]

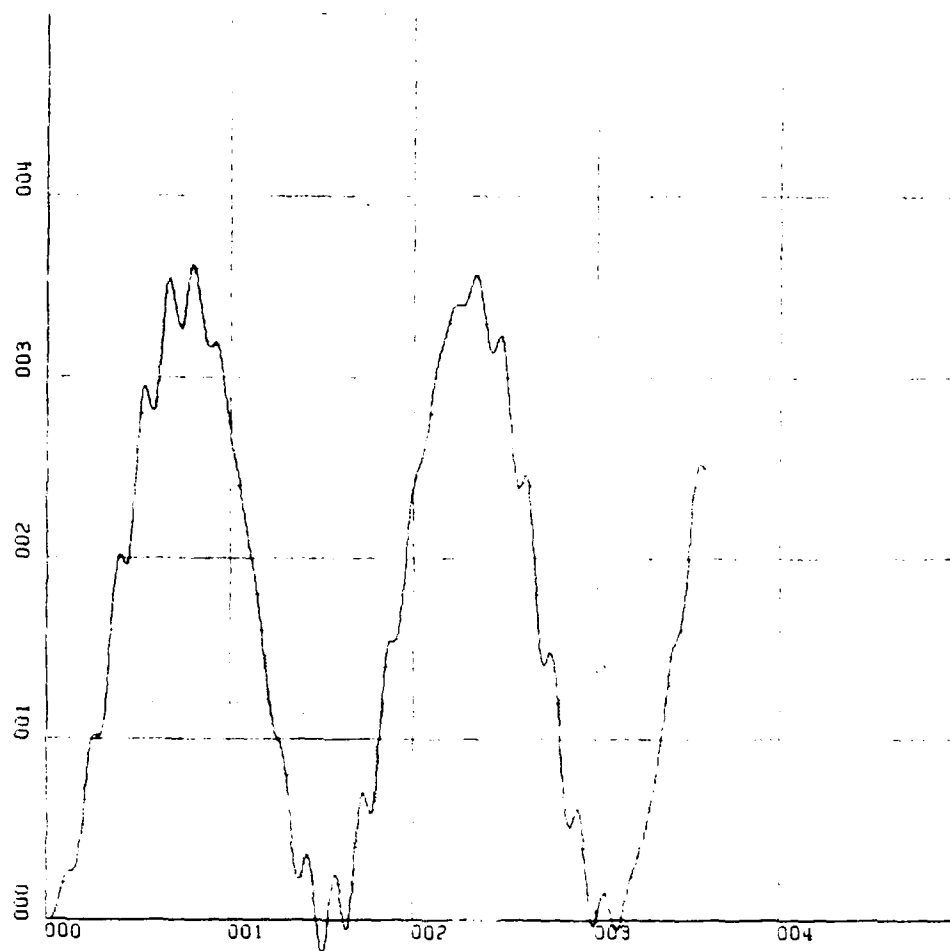
Y-SCALE=2.00E+00 UNITS INCH. [Rad/meru]

KWSTAS

RUN 1

E'D' VS TIME

Figure 13. Easterly Flight at 600 ft/sec.
Azimuth Level Error [Rad/meru] for Constant
North Gyro Drift [1 meru].



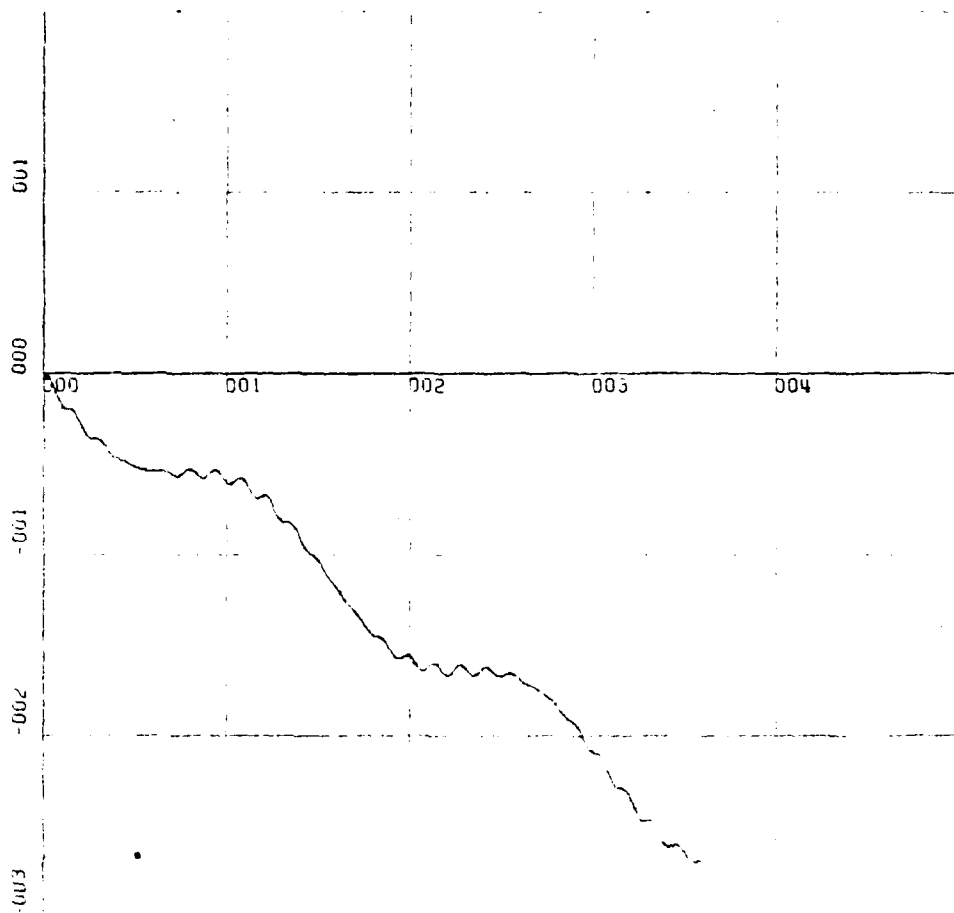
X-SCALE=1.00E+01 UNITS INCH. [hours]
 Y-SCALE=1.00E+00 UNITS INCH. [Rad/meru]

KWSTAS

RUN 1

DLA VS TIME

Figure 14. Easterly Flight at 600 ft/sec.
 Latitude Error [Rad/meru] for Constant North
 Gyro Drift [1 meru].



X-SCALE=1.00E+01 UNITS INCH. [hours]
Y-SCALE=1.00E+01 UNITS INCH. [Rad/meru]

KWSTAS

RUN 2

DLO VS TIME

Figure 15. Easterly Flight at 600 ft/sec.
Longitude Error [Rad/meru] for Constant North
Gyro Drift [1 meru].

AD-A126 689

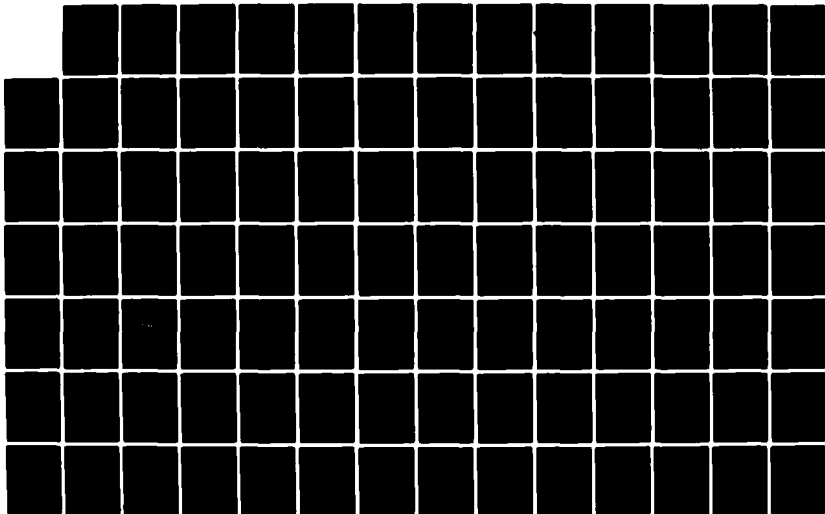
INERTIAL NAVIGATION SYSTEMS AIDED BY GPS(U) NAVAL
POSTGRADUATE SCHOOL MONTEREY CA C C SAFLIANIS DEC 82

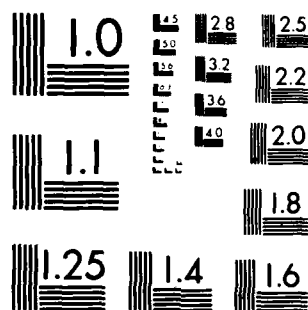
2/4

UNCLASSIFIED

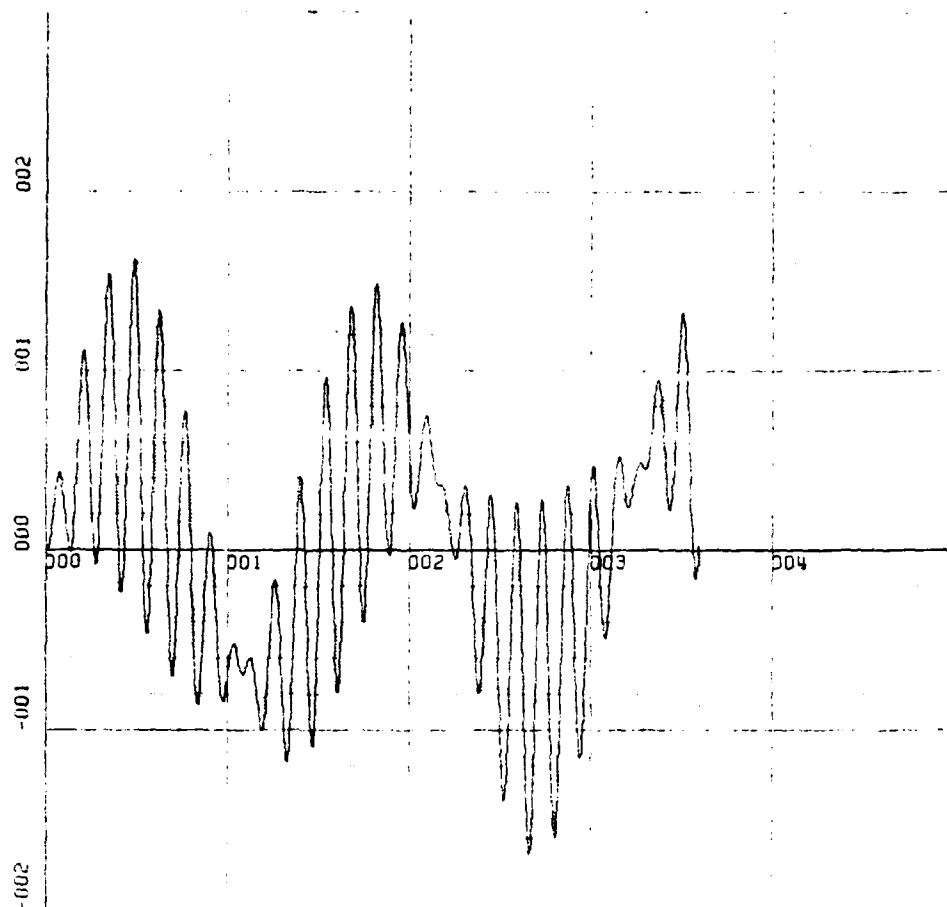
F/G 17/7

NL





MICROCOPY RESOLUTION TEST CHART
NATIONAL BUREAU OF STANDARDS-1963-A

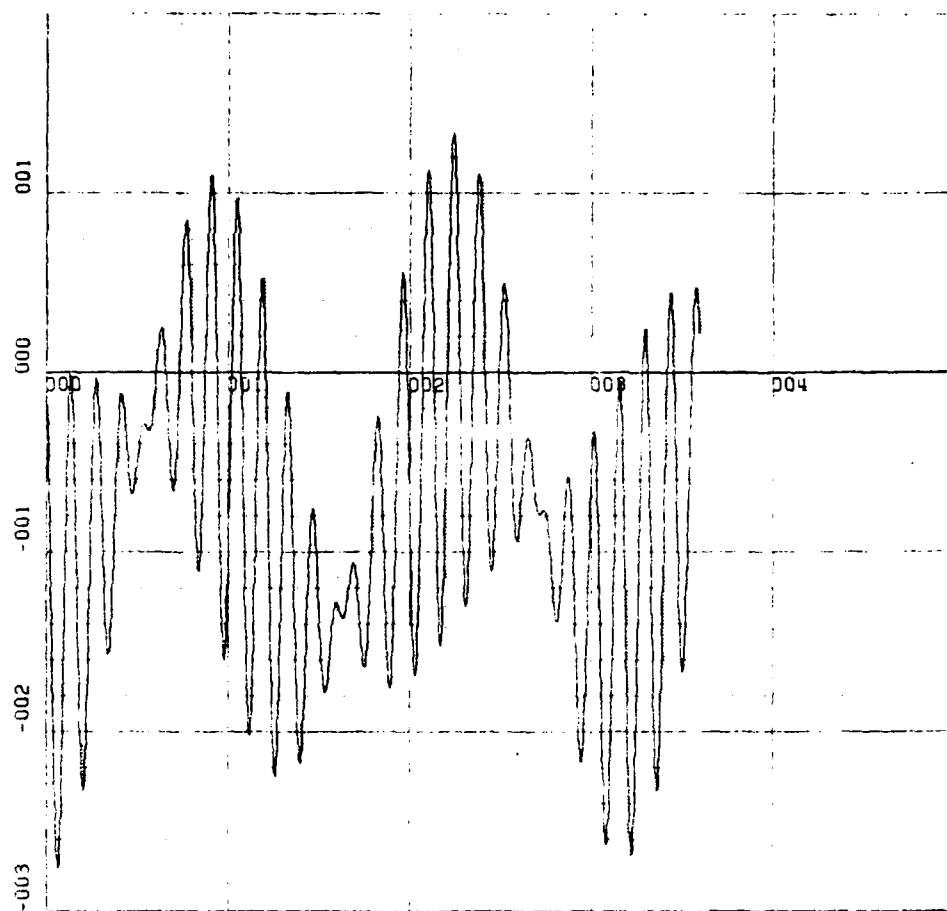


X-SCALE=1.00E+01 UNITS INCH. [hours]
Y-SCALE=1.00E+00 UNITS INCH. [Rad/hour·meru]

KWSTAS
RUN 2

DLAD VS TIME

Figure 16. Easterly Flight at 600 ft/sec.
Latitude Rate Error [Rad/hour·meru] for Constant
North Gyro Drift [1 meru].



X-SCALE=1.00E+01 UNITS INCH.[hours]

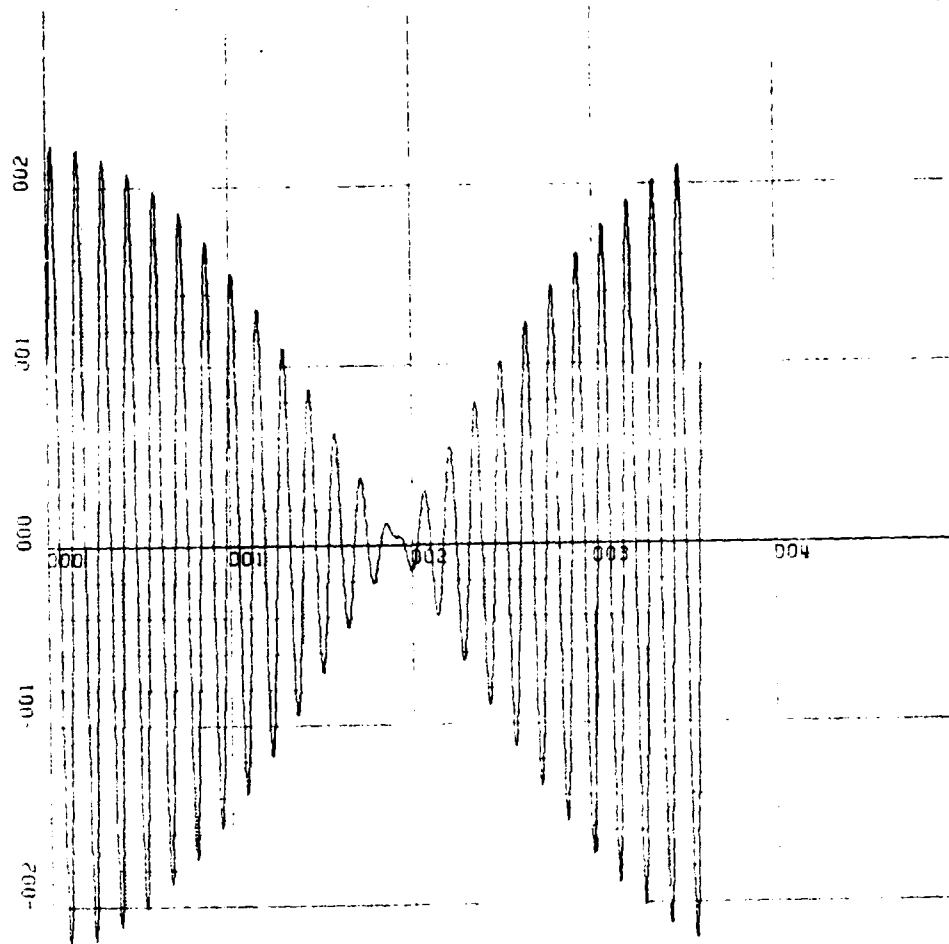
Y-SCALE=1.00E+00 UNITS INCH.[Rad/hour·meru]

KWSTAS

RUN 2

DL0D VS TIME

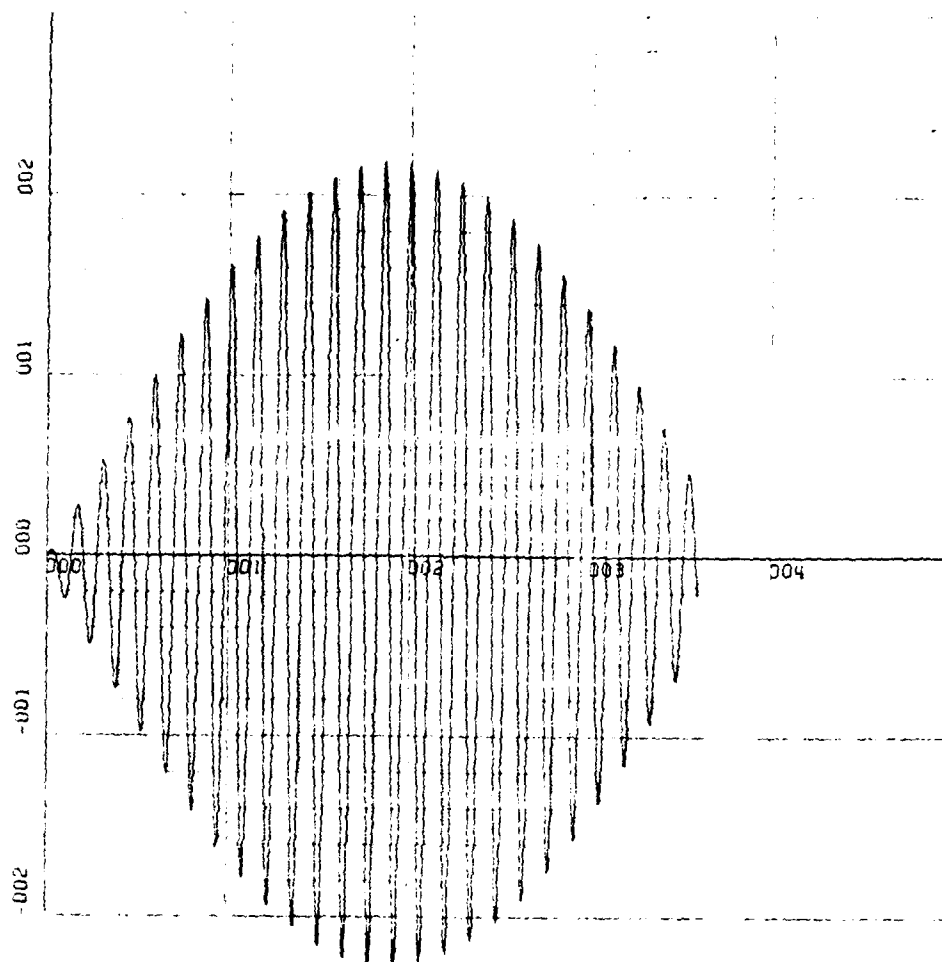
Figure 17. Easterly Flight at 600 ft/sec.
Longitude rate error [Rad/hour·meru] for Constant
North Gyro Drift [1 meru].



X-SCALE=1.00E+01 UNITS INCH. [hours]
 Y-SCALE=1.00E-01 UNITS INCH. [Rad/meru]
 KWSTAS
 RUN 1

E 'N' VS TIME

Figure 18. Westerly Flight at 600 ft/sec.
 North Level Error [Rad/meru] for Constant
 North Gyro Drift [1 meru].



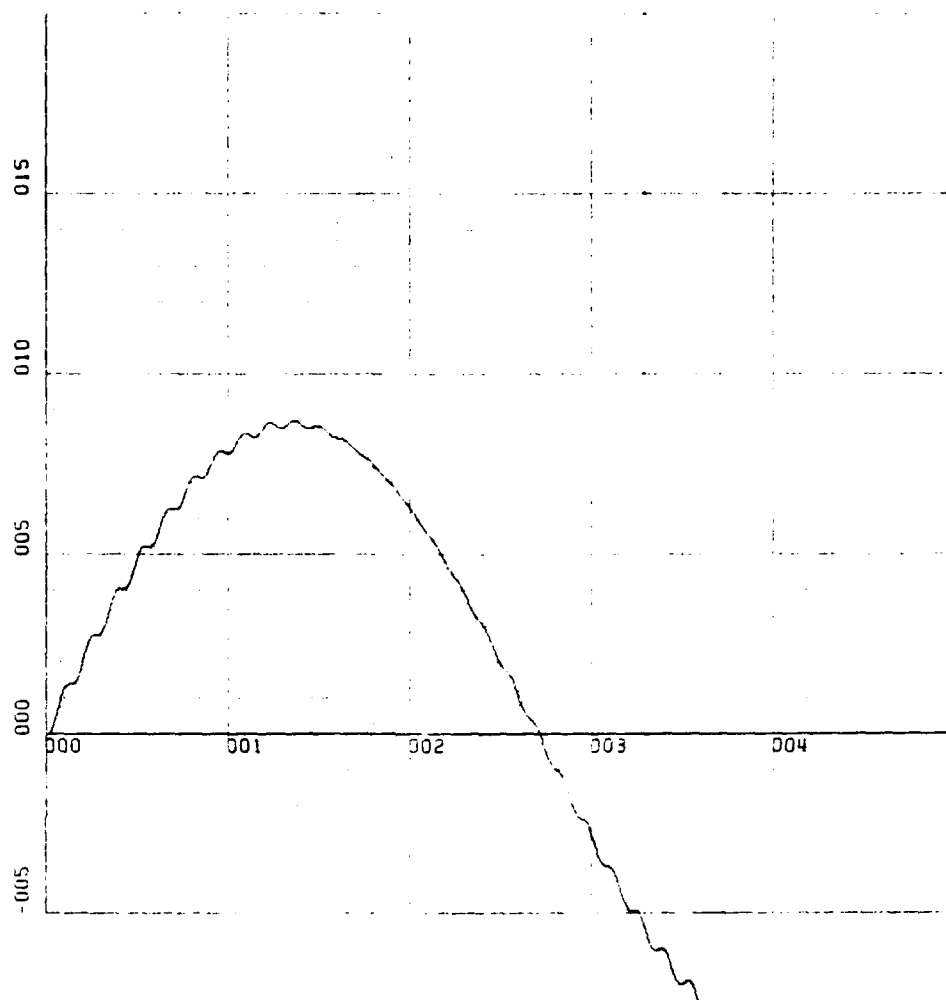
X-SCALE=1.00E+01 UNITS INCH. [hours]
 Y-SCALE=1.00E-01 UNITS INCH. [Rad/meru]

KWSTAS

RUN 1

E'E' VS TIME

Figure 19. Westerly Flight at 600 ft/sec.
 East Level Error [Rad/meru] for Constant North
 Gyro Drift [1 meru].



X-SCALE=1.00E+01 UNITS INCH. [hours]

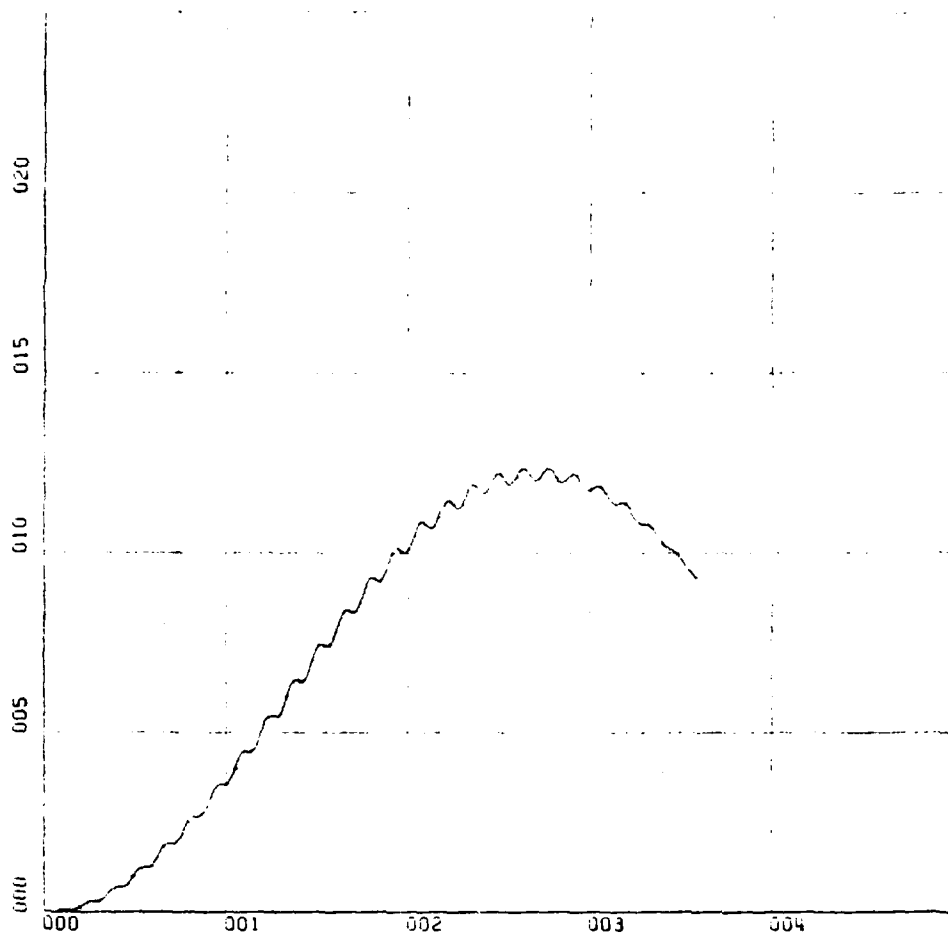
Y-SCALE=5.00E+00 UNITS INCH. [Rad/meru]

KWSTAS

RUN 1

E'D' VS TIME

Figure 20. Westerly Flight at 600 ft/sec.
Azimuth Level Error [Rad/meru] for Constant
North Gyro Drift [1 meru].



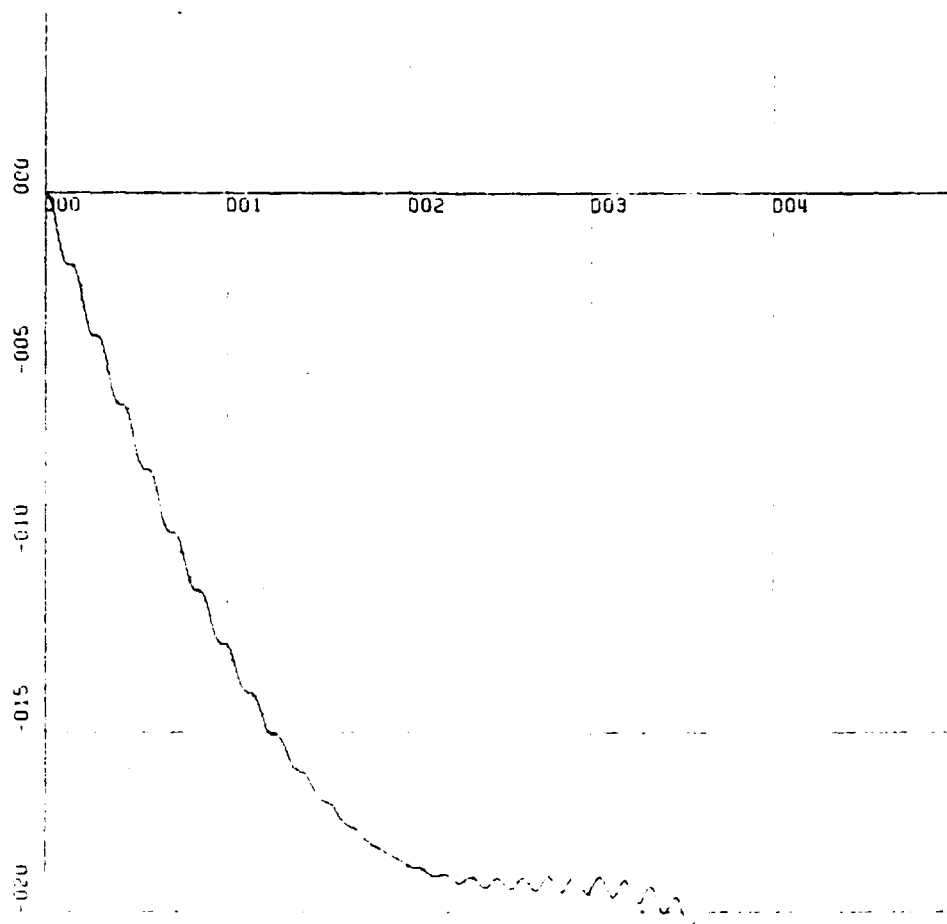
X-SCALE=1.00E+01 UNITS INCH. [hours]
 Y-SCALE=5.00E+00 UNITS INCH. [Rad/meru]

KWSTAS

RUN 1

DIA VS TIME

Figure 21. Westerly Flight at 600 ft/sec.
 Latitude Error [Rad/meru] for Constant North
 Gyro Drift [1 meru].



X-SCALE=1.00E+01 UNITS INCH. [hours]

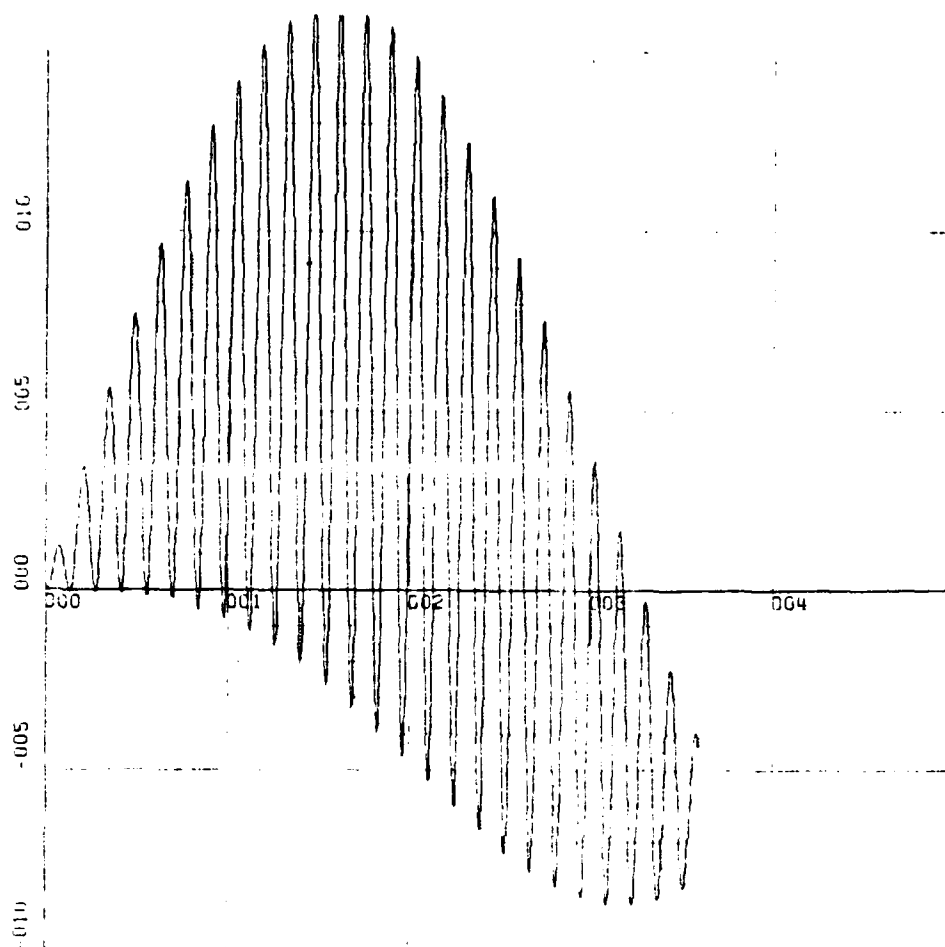
Y-SCALE=5.00E+00 UNITS INCH. [Rad/meru]

KWSTAS

RUN 2

DLO VS TIME

Figure 22. Westerly Flight at 600 ft/sec.
Longitude Error [Rad/meru] for Constant North
Gyro Drift [1 meru].



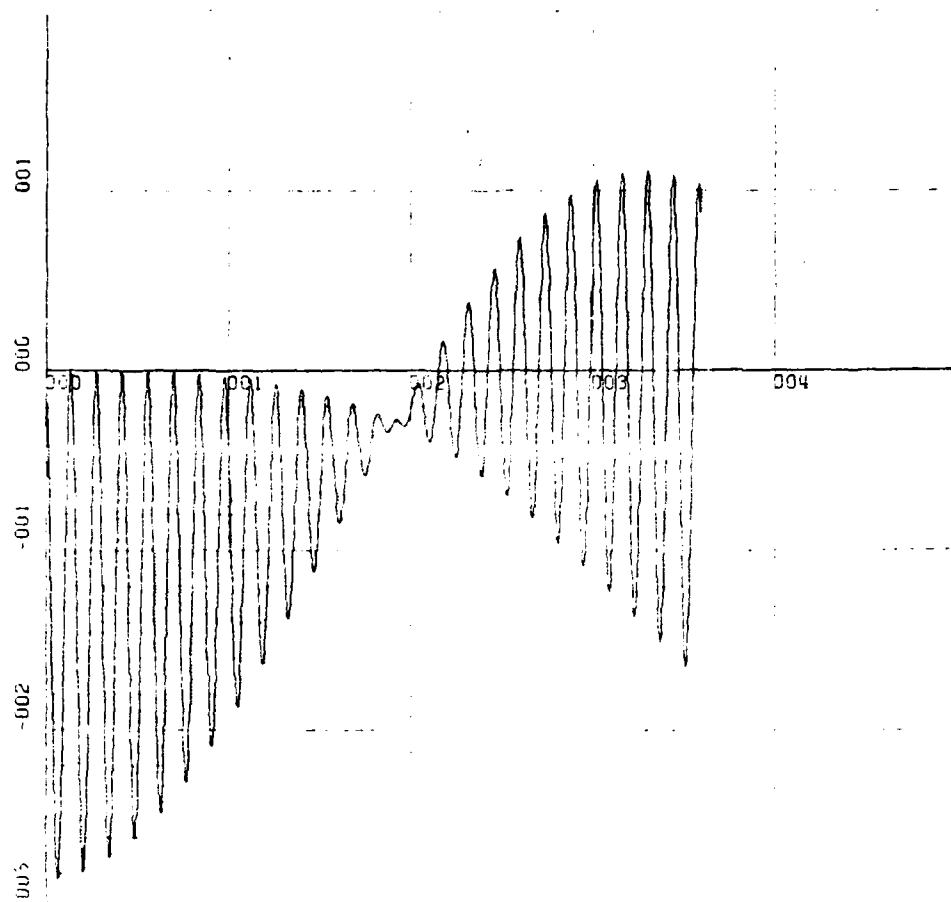
X-SCALE=1.00E+01 UNITS INCH. [hours]
 Y-SCALE=5.00E-01 UNITS INCH. [Rad/hour·meru]

KWSTAS

RUN 2

DLAD VS TIME

Figure 23. Westerly Flight at 600 ft/sec.
 Latitude Rate Error [Rad/hour·meru] for Constant
 North Gyro Drift [1 meru].



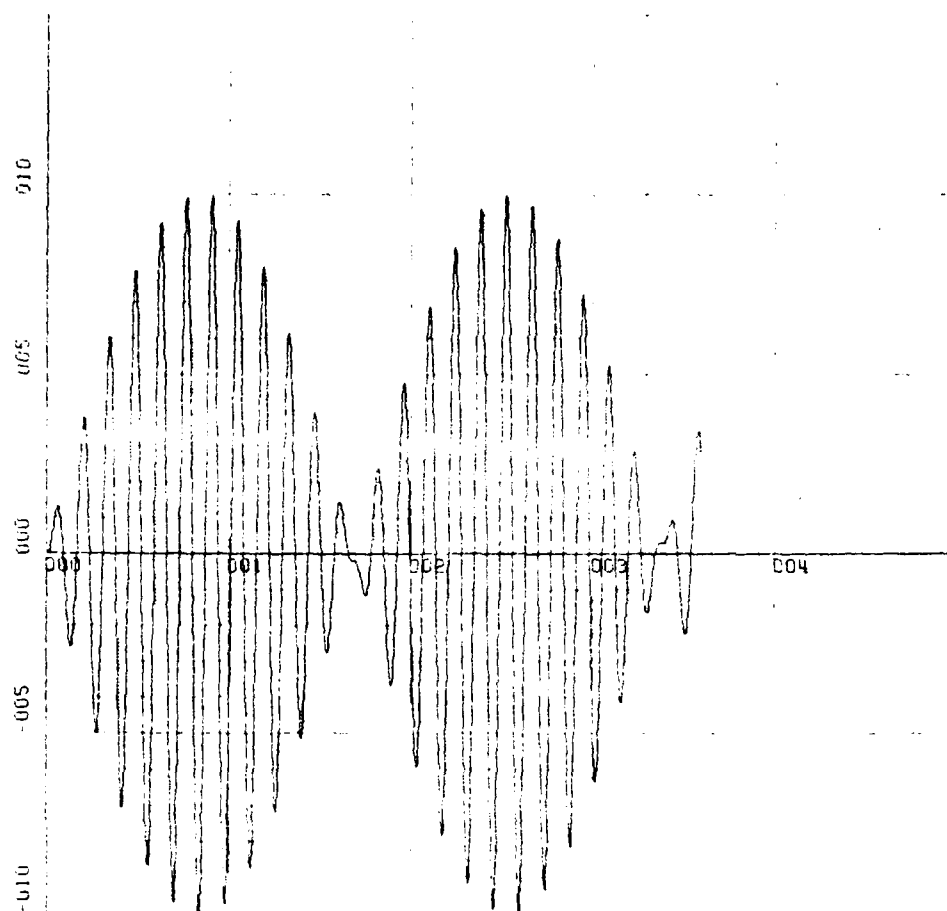
X-SCALE=1.00E+01 UNITS INCH. [hours]
 Y-SCALE=1.00E+00 UNITS INCH. [Rad/hour·meru]

KWSTAS

RUN 2

DL0D VS TIME

Figure 24. Westerly Flight at 600 ft/sec.
 Longitude Rate Error [Rad/hour·meru] for Constant
 North Gyro Drift [1 meru].

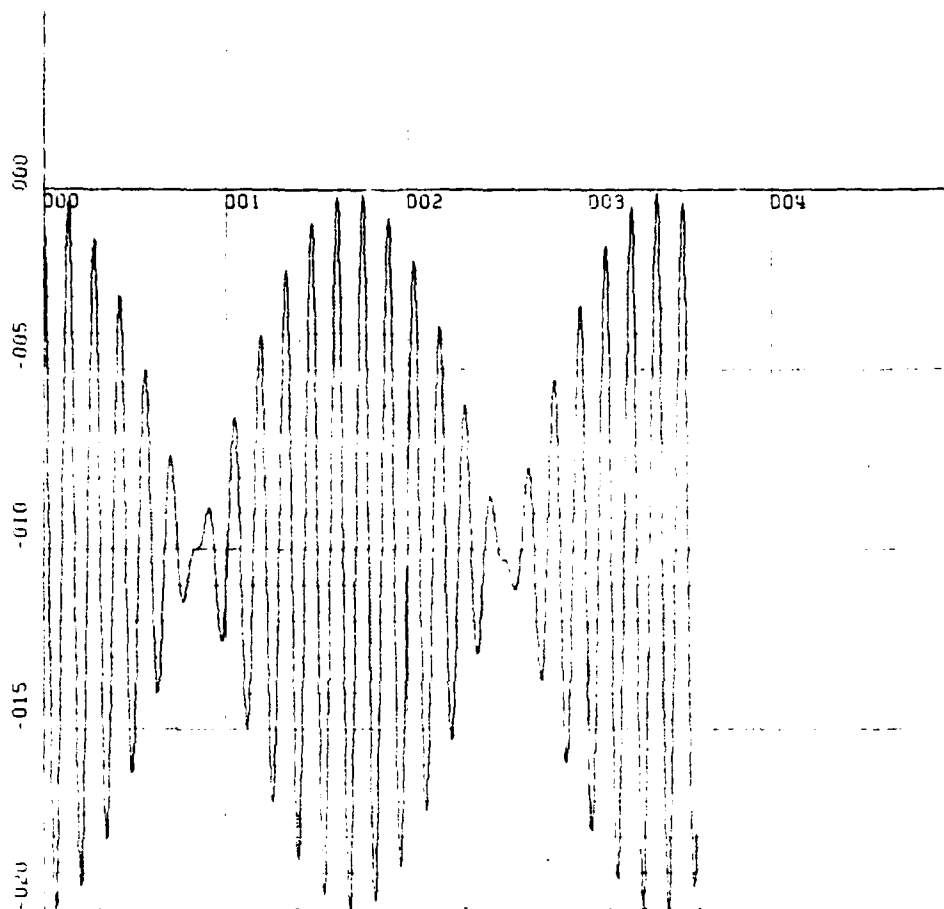


X-SCALE=1.00E+01 UNITS INCH. [hours]
 Y-SCALE=5.00E-07 UNITS INCH. [Rad/200 μ g]
 KWSTAS

RUN 1

E'N' VS TIME

Figure 25. Stationary Case. North Level Error [Rad/200 μ g]
 for Constant North Accelerometer Bias [200 μ g].



X-SCALE=1.00E+01 UNITS INCH. [hours]

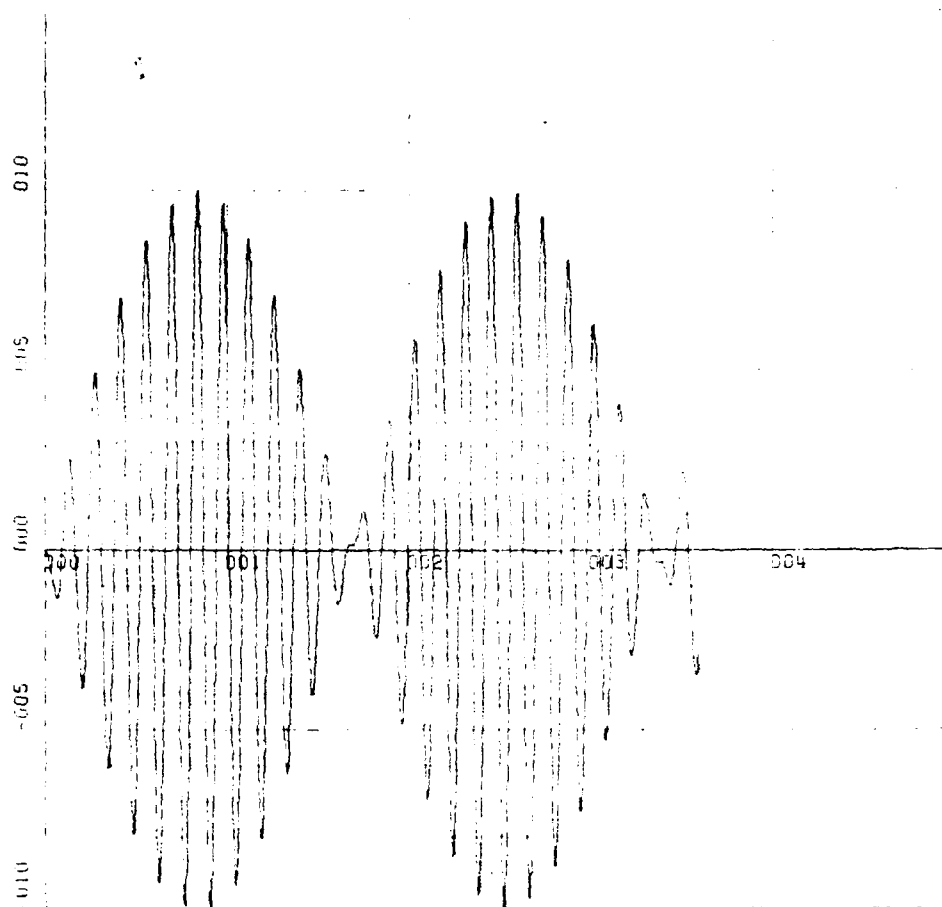
Y-SCALE=5.00E-07 UNITS INCH. [Rad/200ug]

KWSTAS

RUN 1

E'E' VS TIME

Figure 26. Stationary Case. East Level Error [Rad/200ug]
for Constant North Accelerometer Bias [200ug].



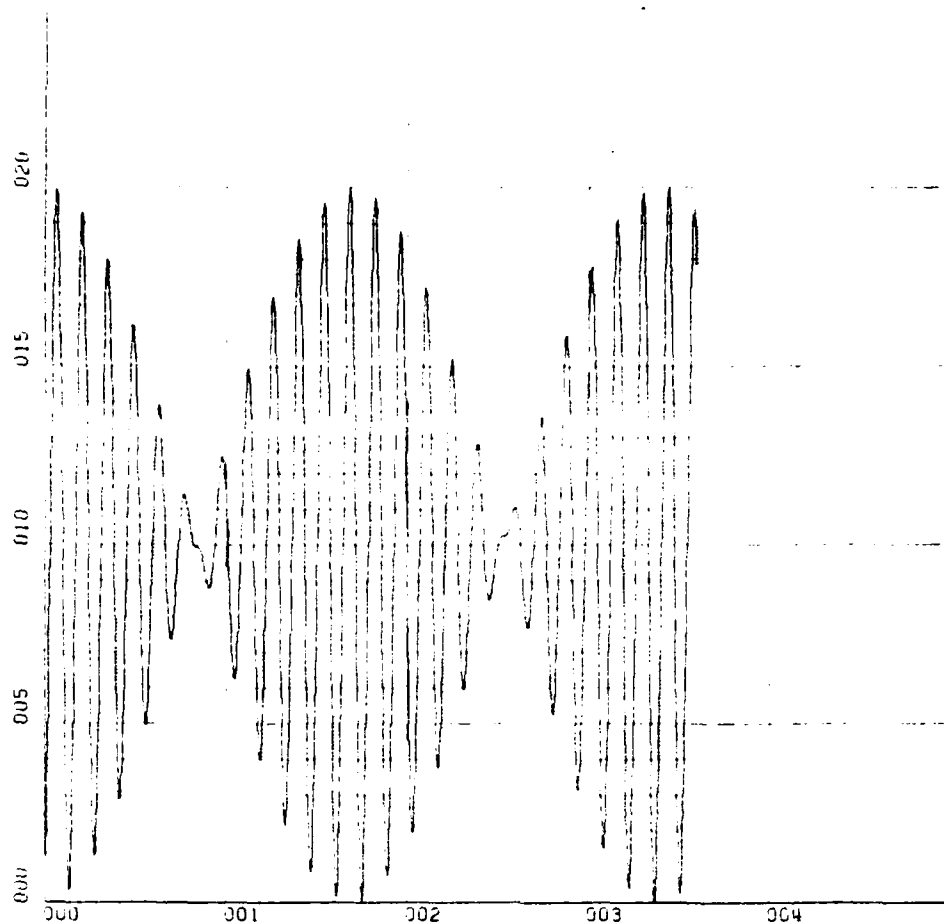
X-SCALE=1.00E+01 UNITS INCH. [hours]
 Y-SCALE=5.00E-07 UNITS INCH. [Rad/200 μ g]

KWSTAS

RUN 1

E'D' VS TIME

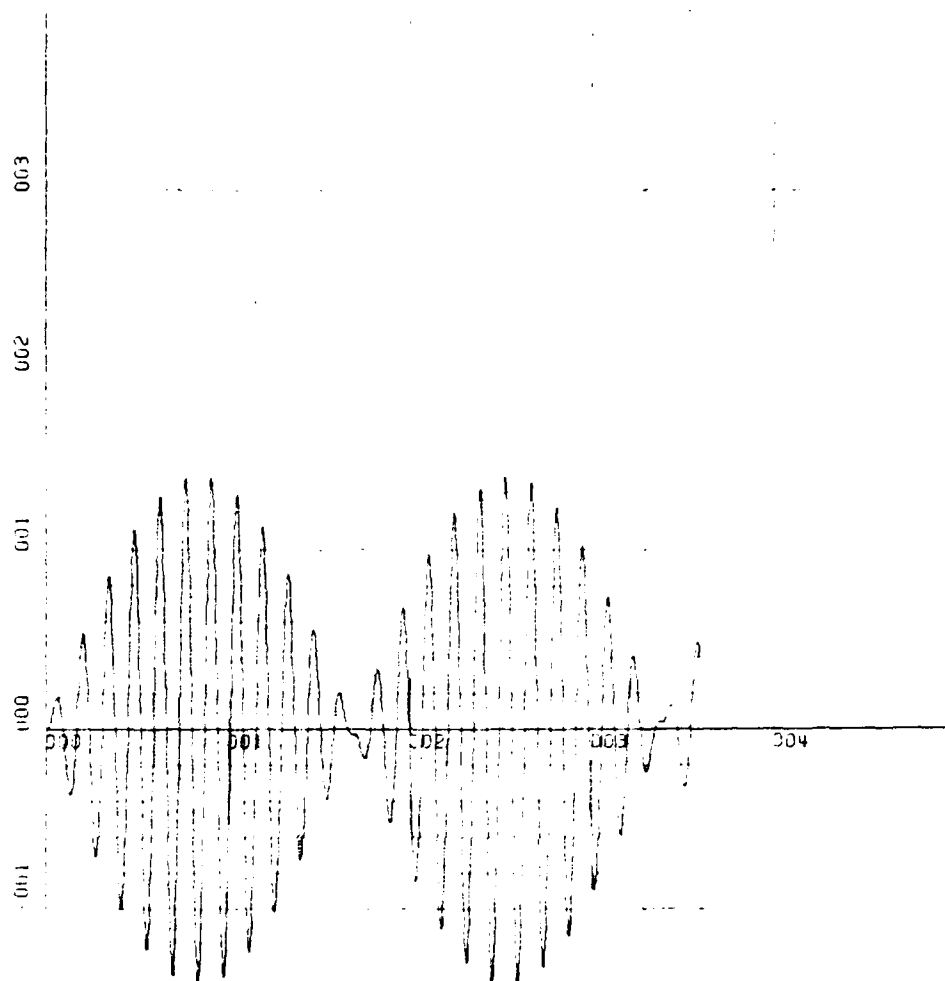
Figure 27. Stationary Case. Azimuth Level Error
 [Rad/200 μ g] for Constant North Accelerometer
 Bias [200 μ g].



X-SCALE=1.00E+01 UNITS INCH. [hours]
 Y-SCALE=5.00E-07 UNITS INCH. [Rad/200µg]
 KWSTAS
 RUN 1

DLA VS TIME

Figure 28. Stationary Case. Latitude Error [Rad/200µg] for
 Constant North Accelerometer Bias [200µg].



X-SCALE=1.00E+01 UNITS INCH. [hours]

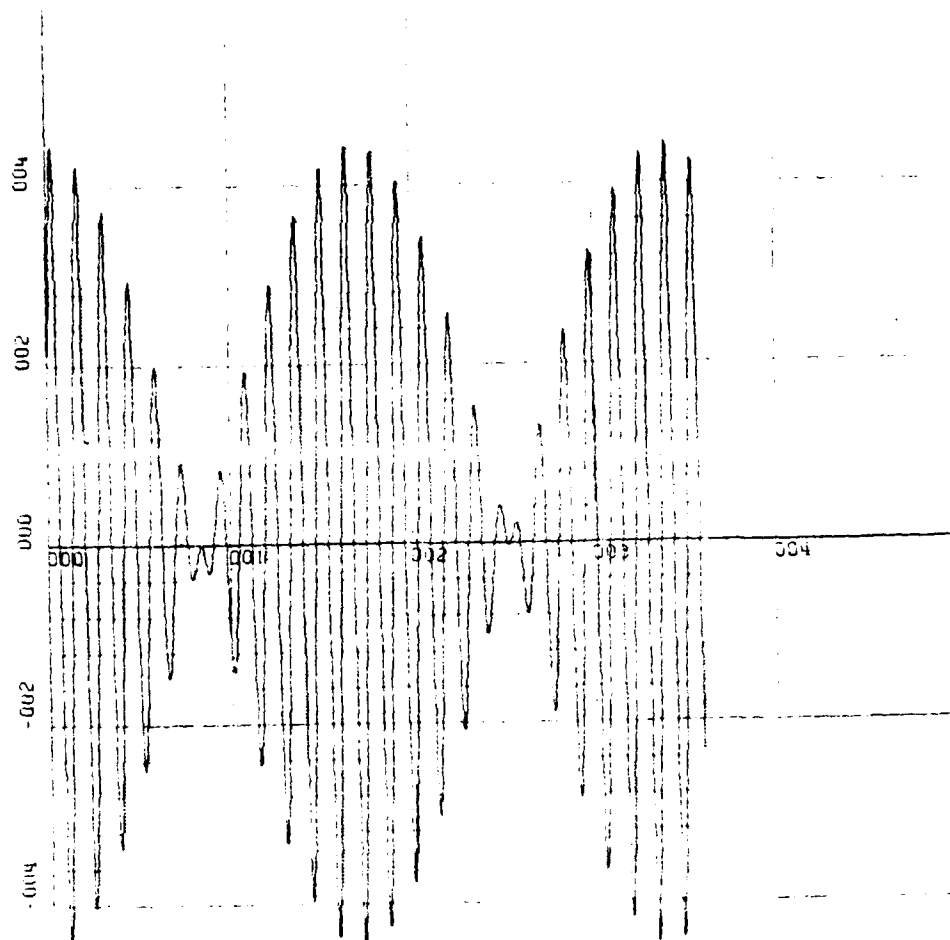
Y-SCALE=1.00E-06 UNITS INCH. [Rad/200 μ g]

KWSTAS

RUN 2

DLO VS TIME

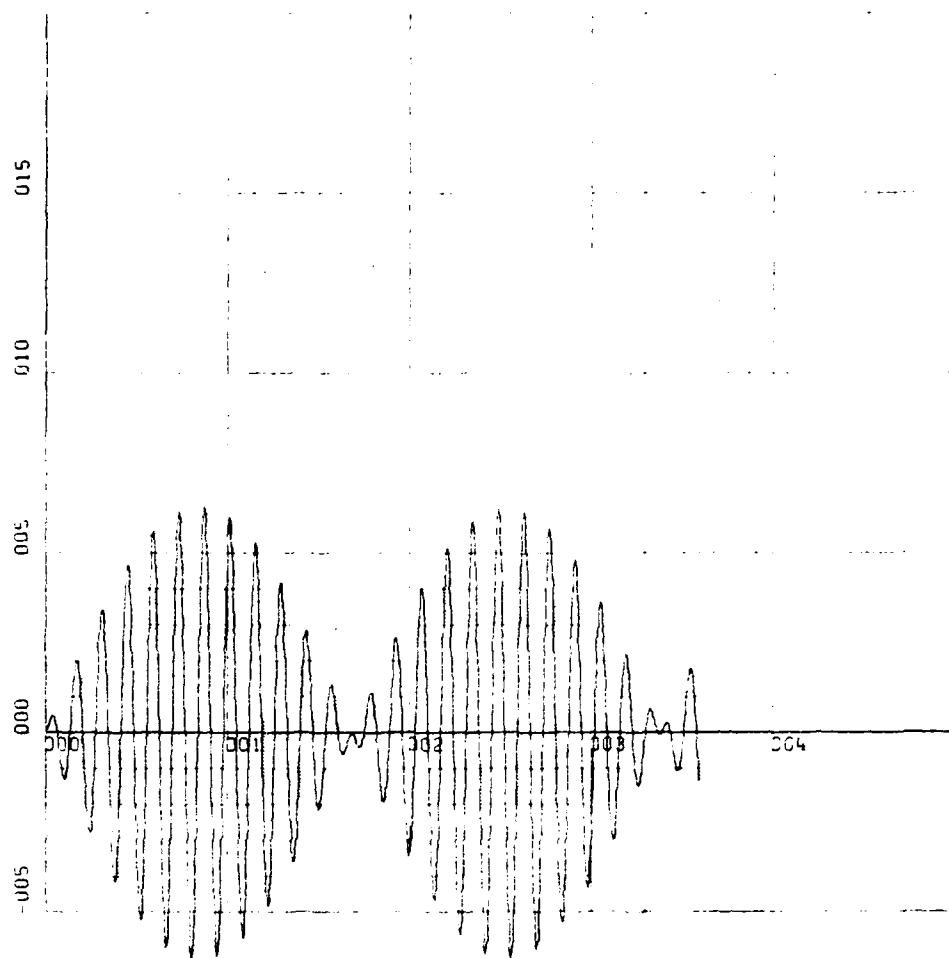
Figure 29. Stationary Case. Longitude Error [Rad/200 μ g]
for Constant North Accelerometer Bias [200 μ g].



X-SCALE=1.00E+01 UNITS INCH.[hours]
 Y-SCALE=2.00E-06 UNITS INCH.[Rad/hour·200μg]
 KWSTAS
 RUN 2

DLAD VS TIME

Figure 30. Stationary Case. Latitude Rate Error
 [Rad/hour·200μg] for Constant North Accelerometer
 Bias [200μg].



X-SCALE=1.00E+01 UNITS INCH.[hours]

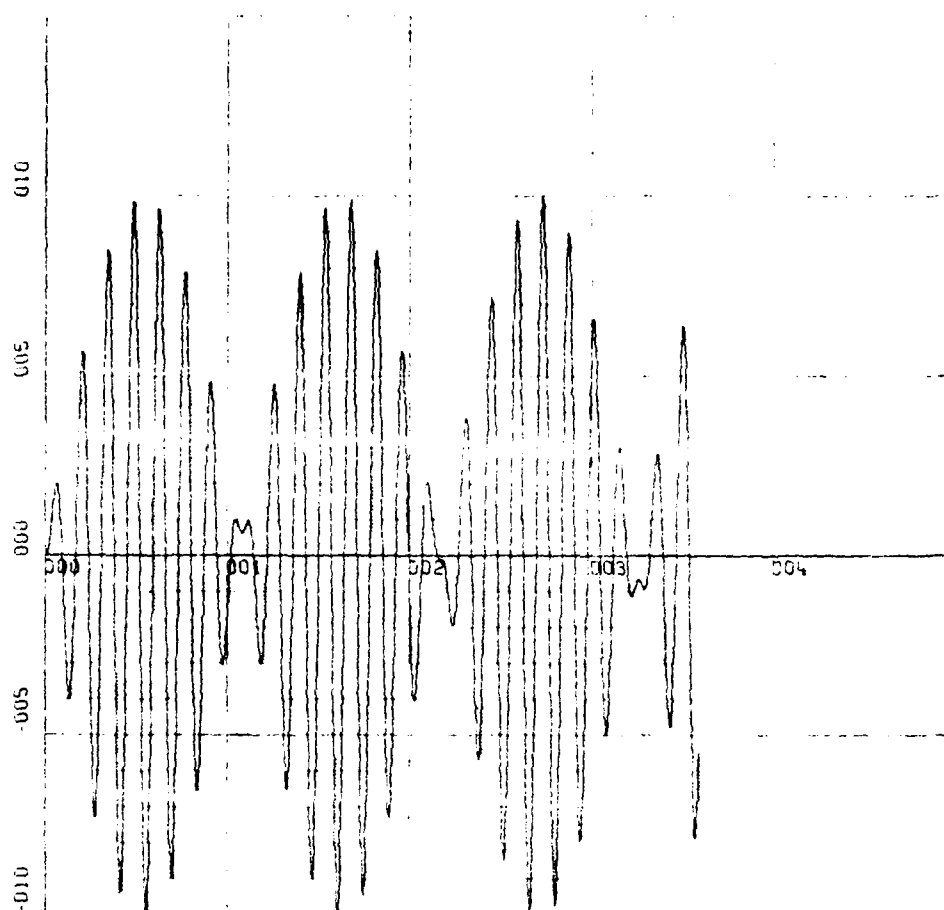
Y-SCALE=5.00E-06 UNITS INCH.[Rad/hour·200 μ g]

KWSTAS

RUN 2

DL0D VS TIME

Figure 31. Stationary Case. Longitude Rate Error
[Rad/hour·200 μ g] for Constant North Accelerometer
Bias [200 μ g].



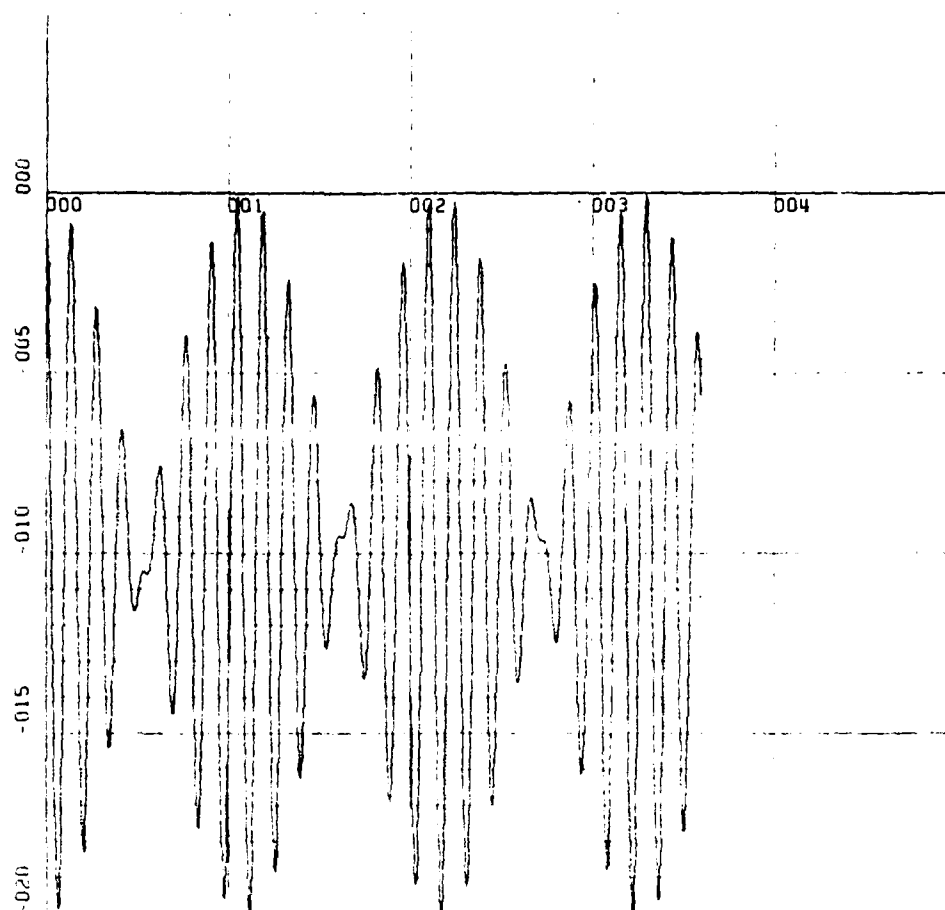
X-SCALE=1.00E+01 UNITS INCH. [hours]
 Y-SCALE=5.00E-07 UNITS INCH. [Rad/200 μ g]

KWSTAS

RUN 1

E'N' VS TIME

Figure 32. Easterly Flight at 600 ft/sec.
 North Level Error [Rad/200 μ g] for Constant
 North Accelerometer Bias [200 μ g].



X-SCALE=1.00E+01 UNITS INCH. [hours]

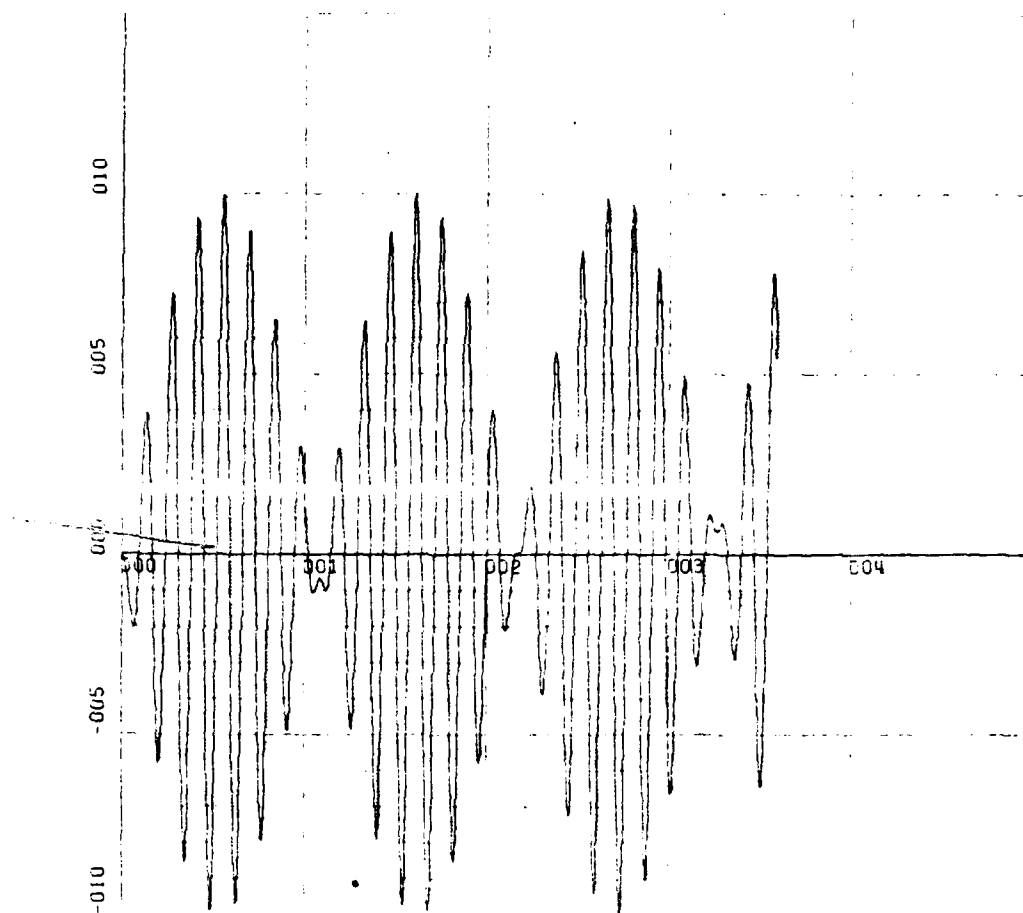
Y-SCALE=5.00E-07 UNITS INCH. [Rad/200 μ g]

KWSTAS

RUN 1

E'E' VS TIME

Figure 33. Easterly Flight at 600 ft/sec.
East Level Error [Rad/200 μ g] for Constant North
Accelerometer Bias [200 μ g].



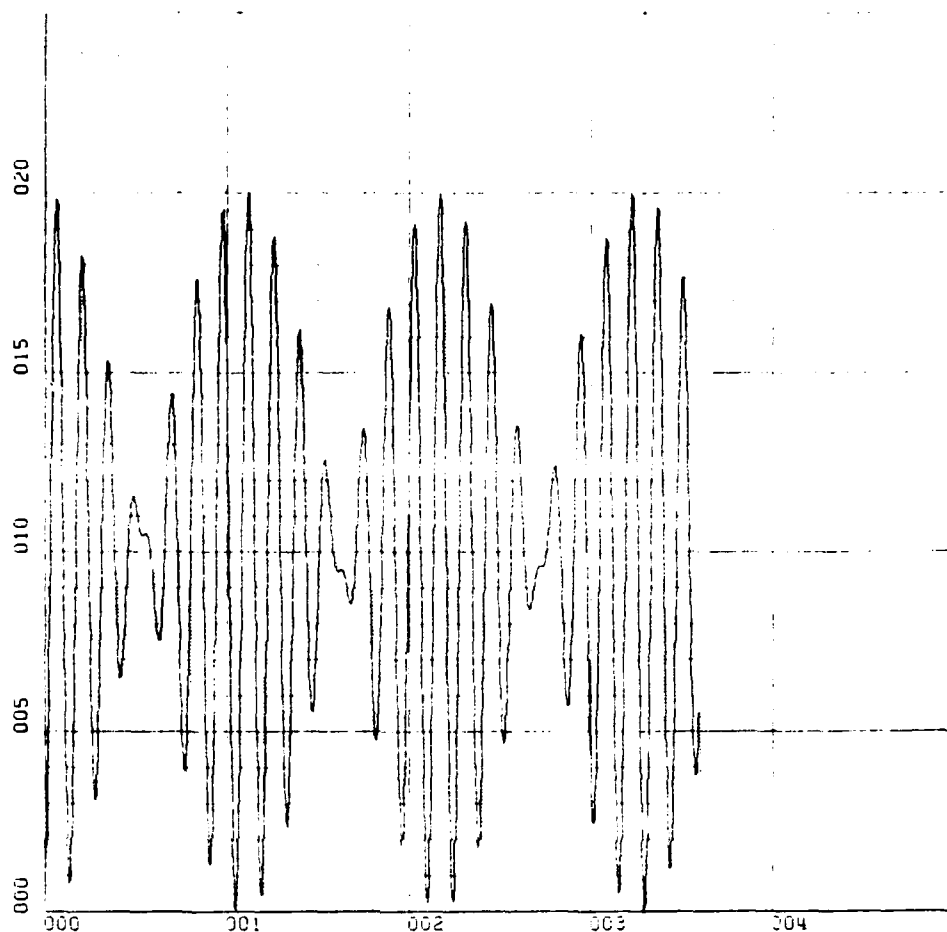
X-SCALE=1.00E+01 UNITS INCH. [hours]
 Y-SCALE=5.00E-07 UNITS INCH. [Rad/200 μ g]

KWSTAS

RUN 1

E'D' VS TIME

Figure 34. Easterly Flight at 600 ft/sec.
 Azimuth Level Error [Rad/200 μ g] for Constant North
 Accelerometer Bias [200 μ g].



X-SCALE=1.00E+01 UNITS INCH. [hours]

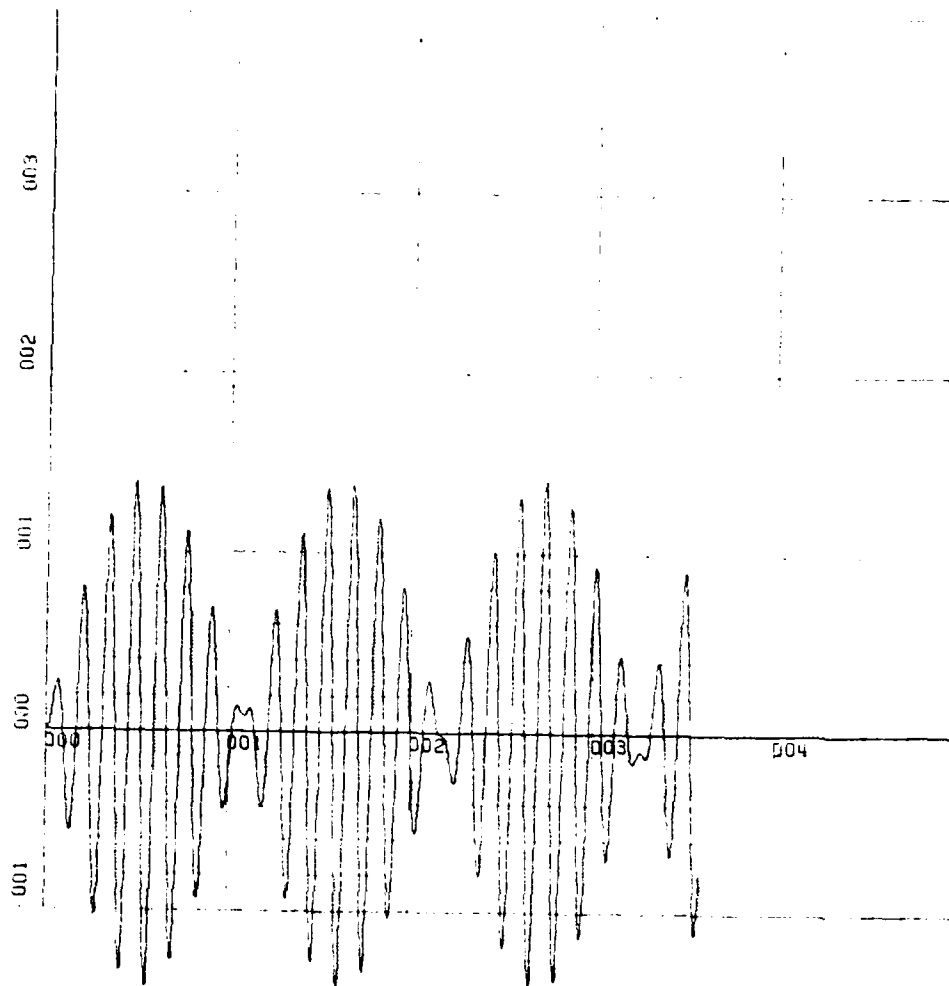
Y-SCALE=5.00E-07 UNITS INCH. [Rad/200 μ g]

KWSTAS

RUN 1

DLA VS TIME

Figure 35. Easterly Flight at 600 ft/sec.
Latitude Error [Rad/200 μ g] for Constant
North Accelerometer Bias [200 μ g].



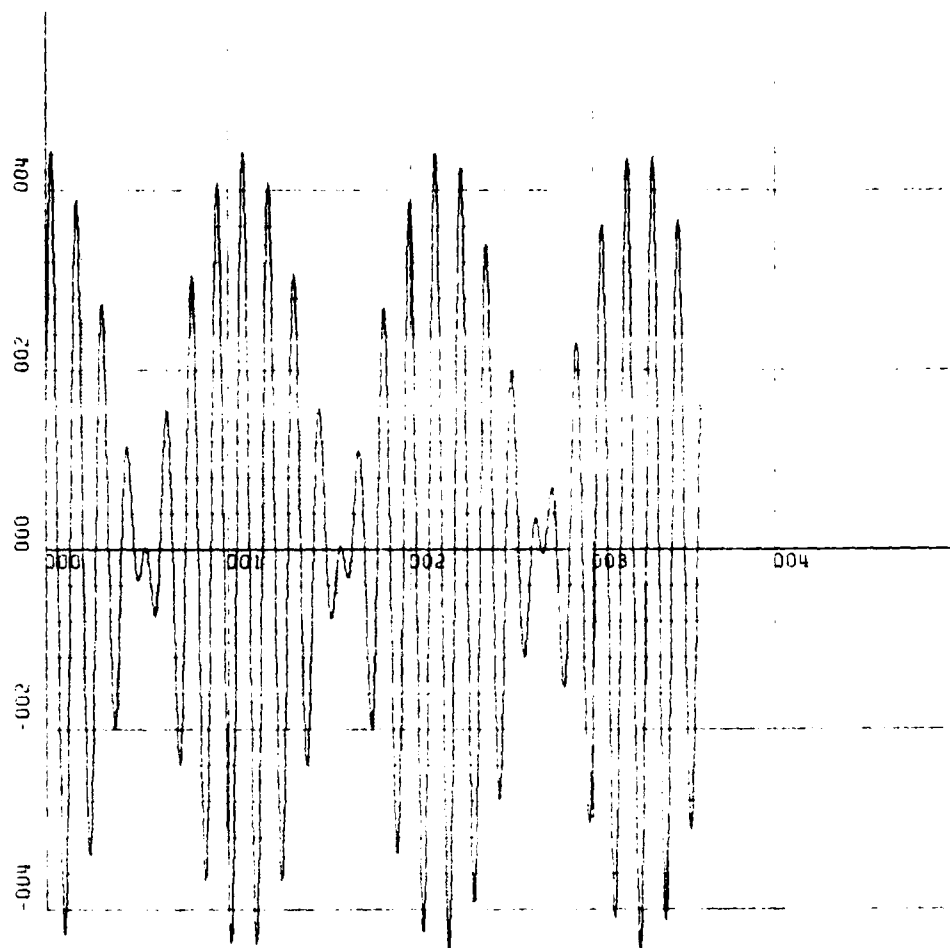
X-SCALE=1.00E+01 UNITS INCH. [hours]
 Y-SCALE=1.00E-06 UNITS INCH. [Rad/200 μ g]

KWSTAS

RUN 2

DLO VS TIME

Figure 36. Easterly Flight at 600 ft/sec.
 Longitude Error [Rad/200 μ g] for Constant North
 Accelerometer Bias [200 μ g].



X-SCALE=1.00E+01 UNITS INCH. [hours]

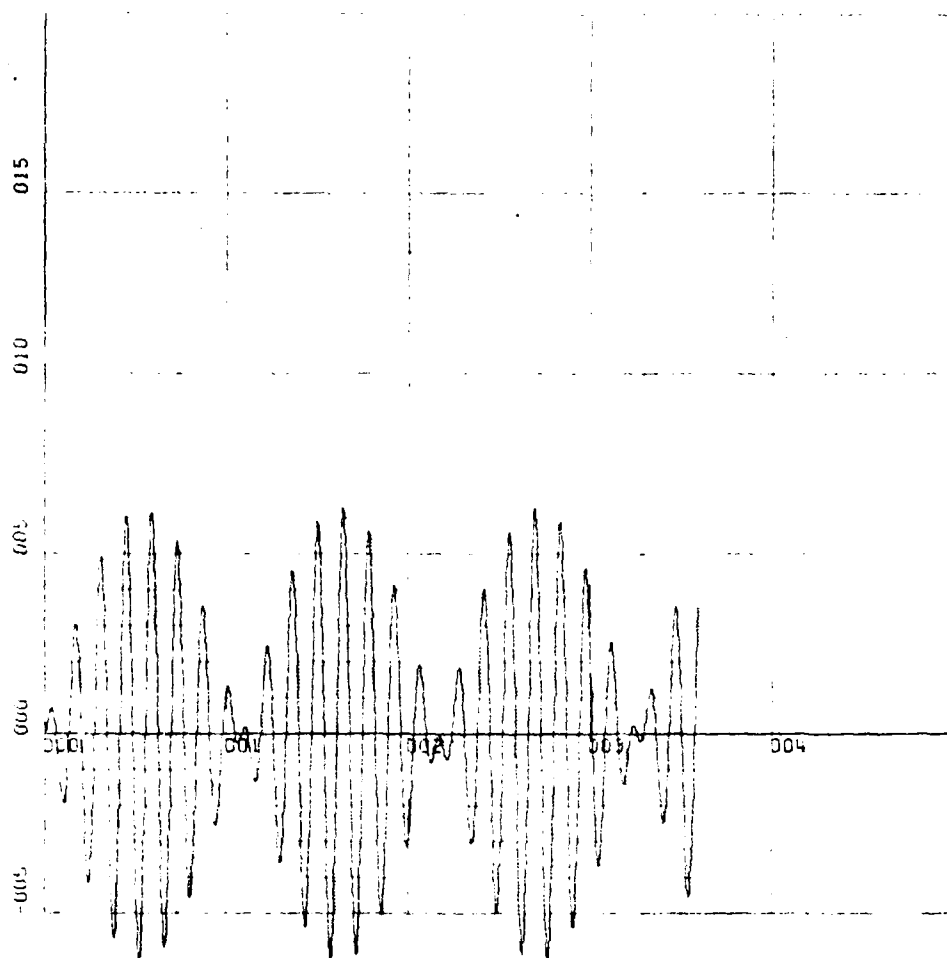
Y-SCALE=2.00E-06 UNITS INCH. [Rad/hour·200 μ g]

KWSTAS

RUN 2

DLAD VE TIME

Figure 37. Easterly Flight at 600 ft/sec.
Latitude Rate Error [Rad/hour·200 μ g] for Constant
North Accelerometer Bias [200 μ g].



X-SCALE=1.00E+01 UNITS INCH. [hours]

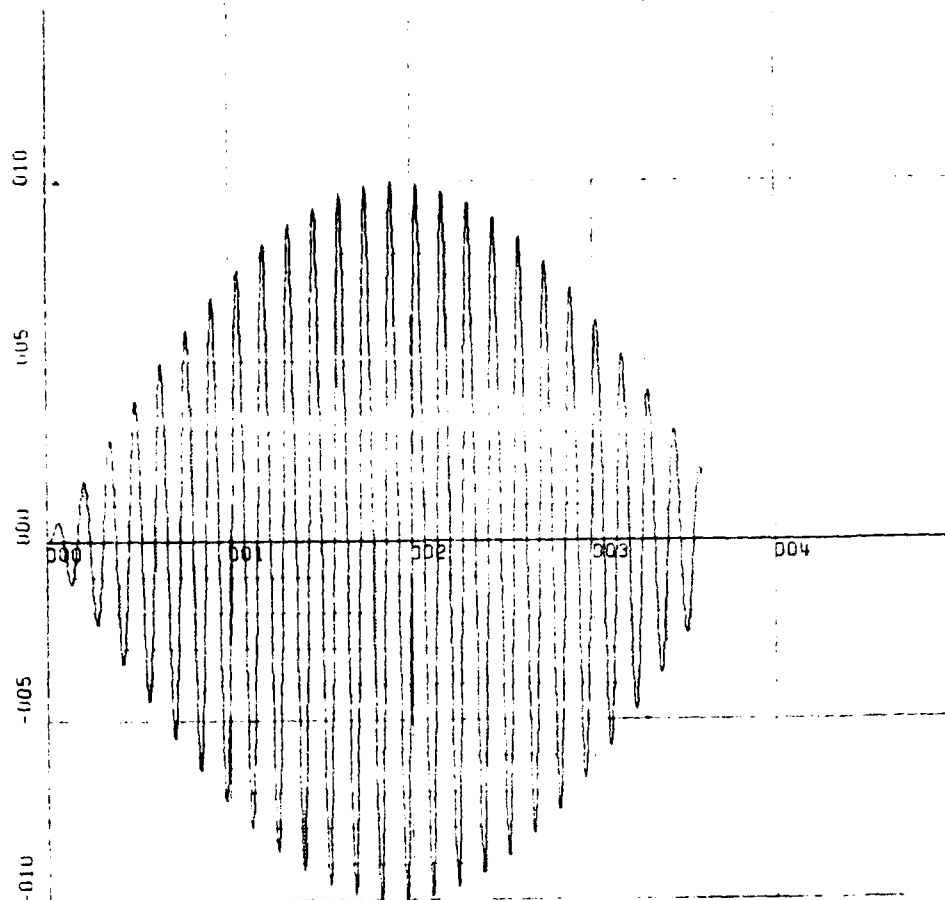
Y-SCALE=5.00E-06 UNITS INCH. [Rad/hour·200 μ g]

KWSTAS

RUN 2

DL0D VS TIME

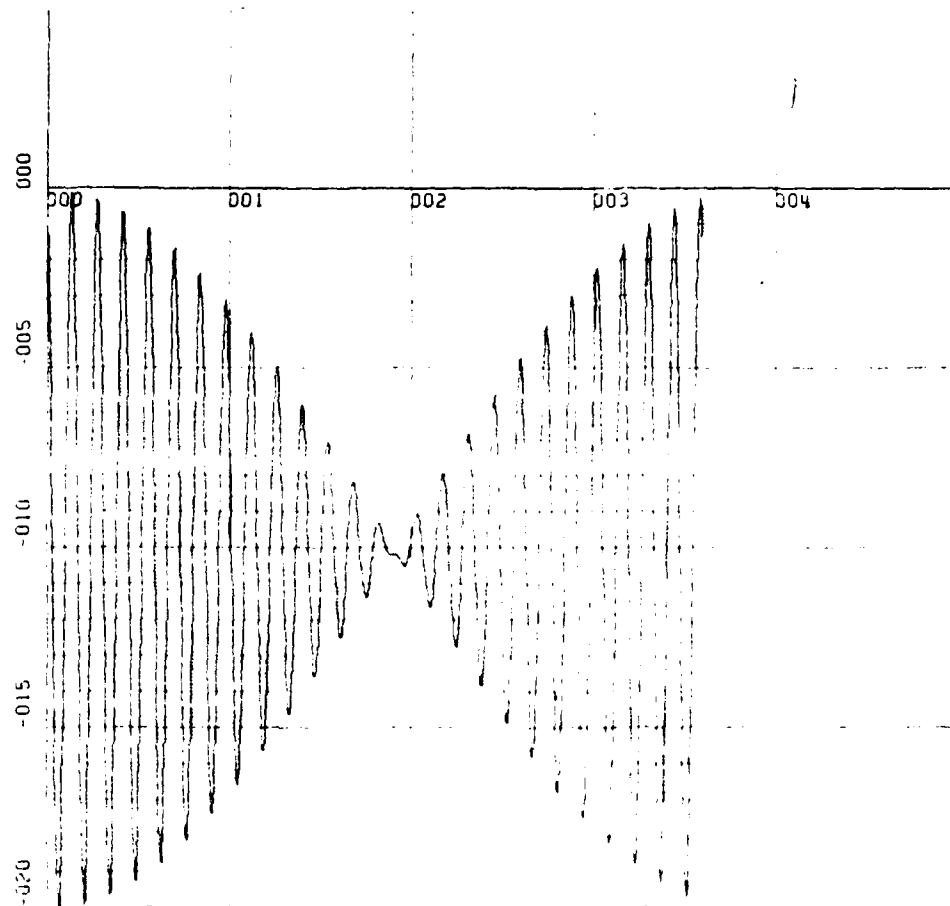
Figure 38. Easterly Flight at 600 ft/sec.
Longitude Rate Error [Rad/hour·200 μ g] for Constant
North Accelerometer Bias [200 μ g].



X-SCALE=1.00E+01 UNITS INCH. [hours]
 Y-SCALE=5.00E-07 UNITS INCH. [Rad/200 μ g]
 KWSTAS
 RUN 1

E'N' VS TIME

Figure 39. Westerly Flight at 600 ft/sec.
 North Level Error [Rad/200 μ g] for Constant
 North Accelerometer Bias [200 μ g].



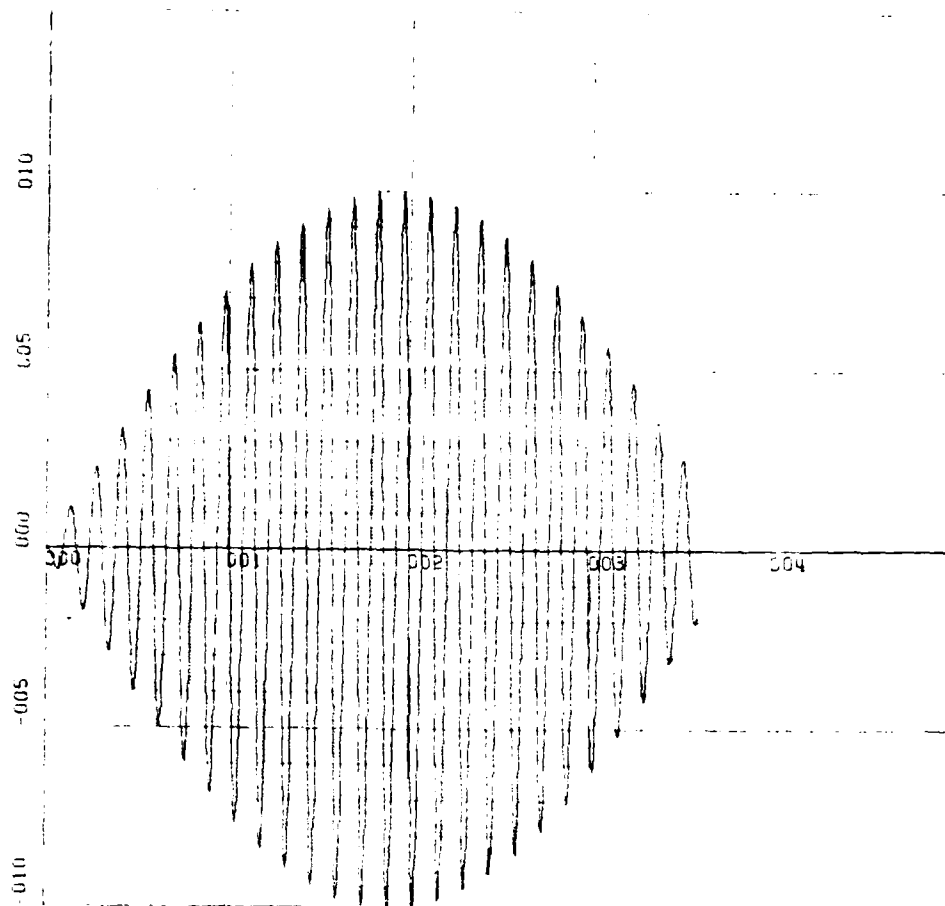
X-SCALE=1.00E+01 UNITS INCH. [hours]
 Y-SCALE=5.00E-07 UNITS INCH. [Rad/200μg]

KWSTAS

RUN 1

E'E' VS TIME

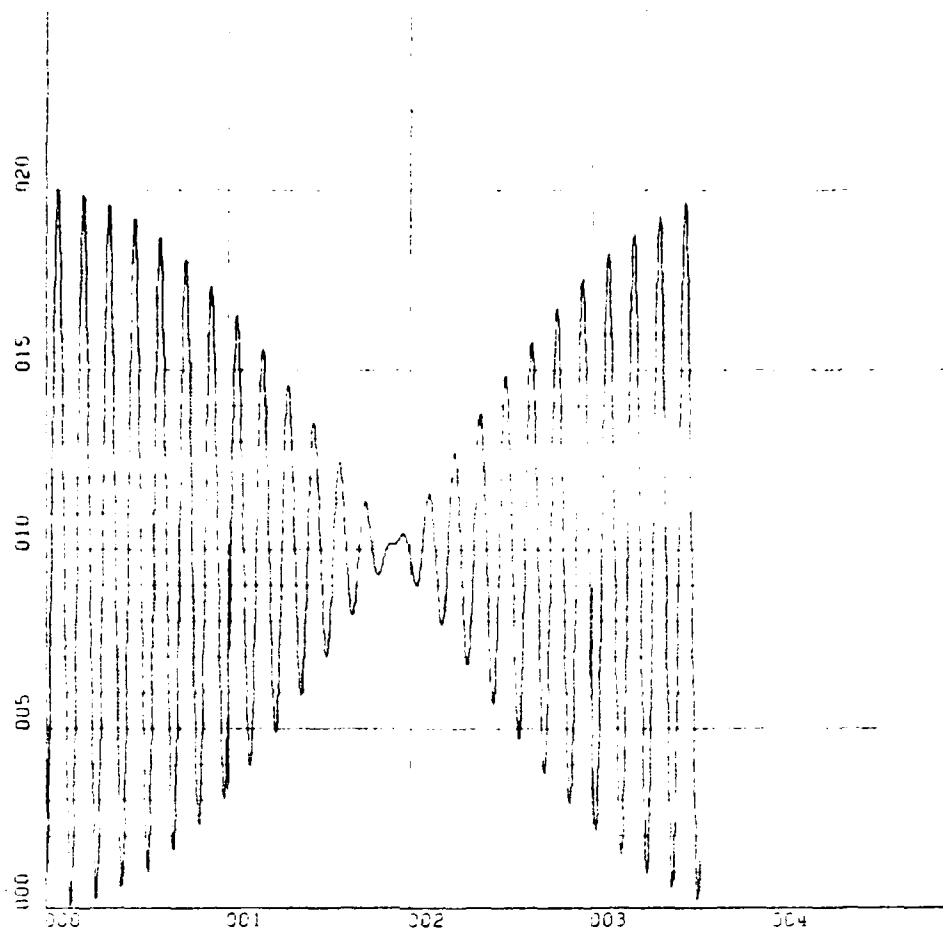
Figure 40. Westerly Flight at 600 ft/sec.
 East Level Error [Rad/200μg] for Constant North
 Accelerometer Bias [200μg].



X-SCALE=1.00E+01 UNITS INCH. [hours]
 Y-SCALE=5.00E-07 UNITS INCH. [Rad/200 μ g]
 KWSTAS
 RUN 1

E'D' VS TIME

Figure 41. Westerly Flight at 600 ft/sec.
 Azimuth Level Error [Rad/200 μ g] for Constant
 North Accelerometer Bias [200 μ g].



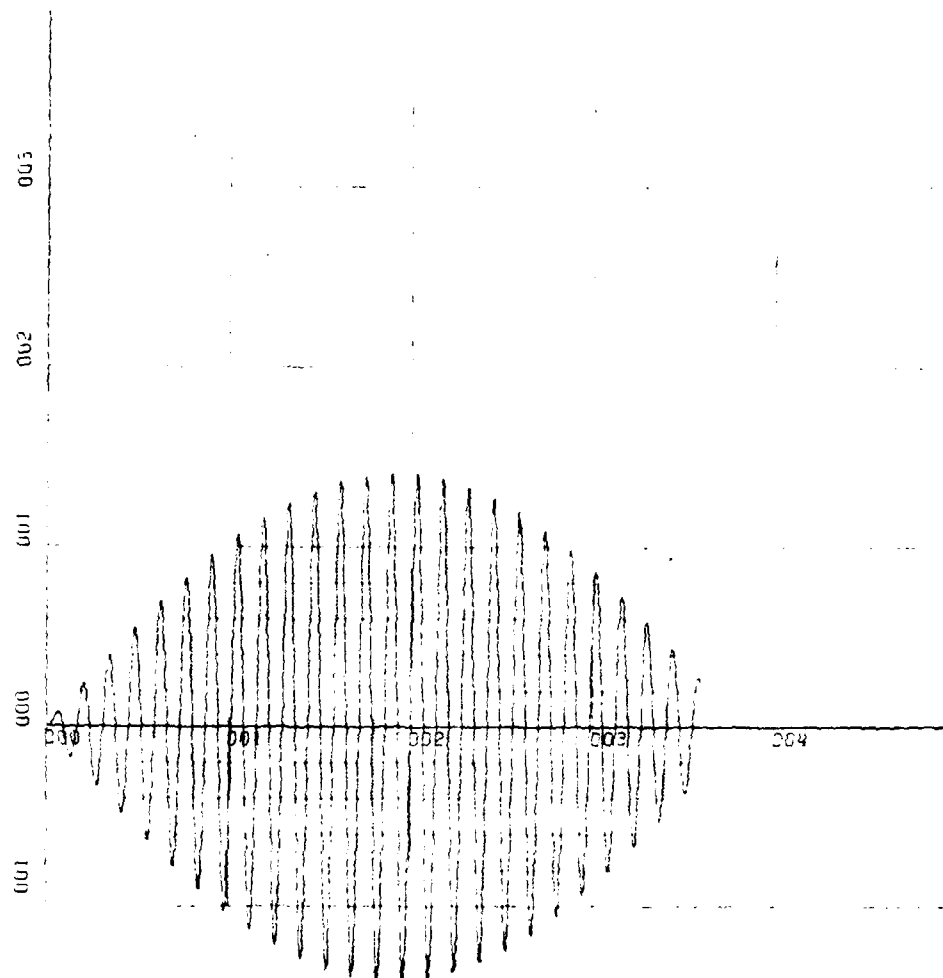
X-SCALE=1.00E+01 UNITS INCH. [hours]
Y-SCALE=5.00E-07 UNITS INCH. [Rad/200 μ g]

KWSTAS

RUN 1

DLA VS TIME

Figure 42. Westerly Flight at 600 ft/sec.
Latitude Error [Rad/200 μ g] for Constant North
Accelerometer Bias [200 μ g].



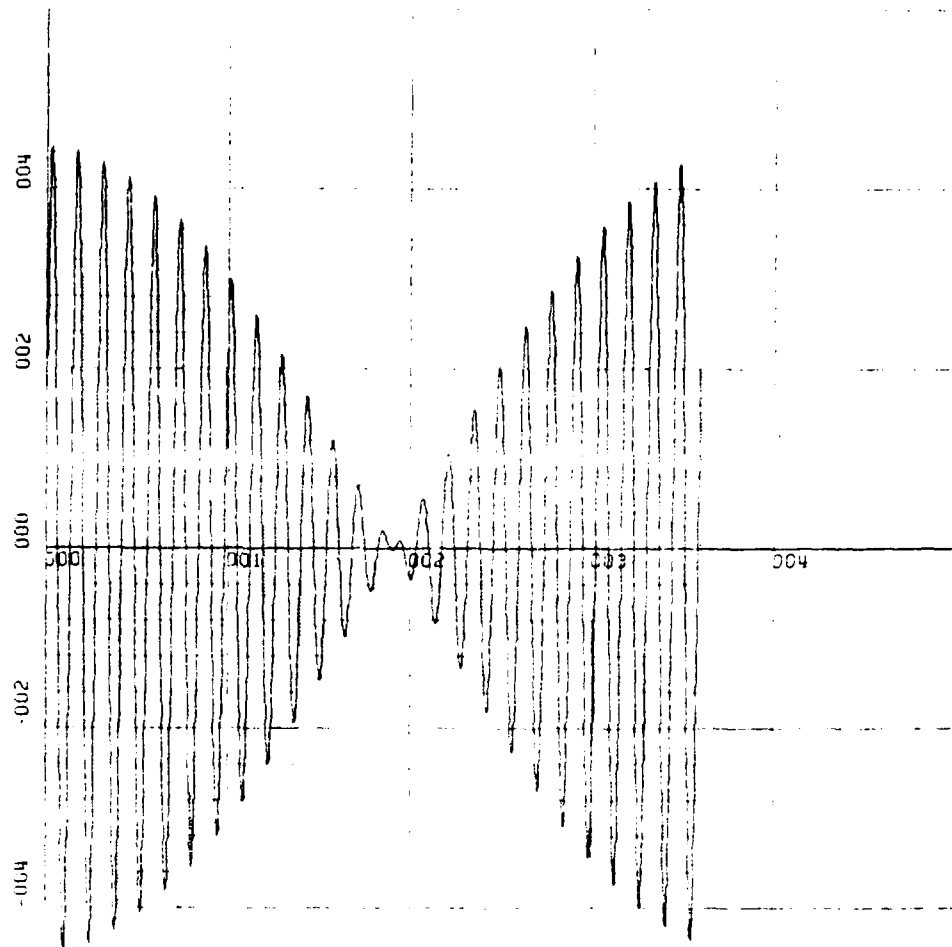
X-SCALE=1.00E+01 UNITS INCH. [hours]
 Y-SCALE=1.00E-06 UNITS INCH. [Rad/200 μ g]

KWSTAS

RUN 2

DLO VS TIME

Figure 43. Westerly Flight at 600 ft/sec.
 Longitude Error [Rad/200 μ g] for Constant North
 Accelerometer Bias [200 μ g].



X-SCALE=1.00E+01 UNITS INCH.[hours]

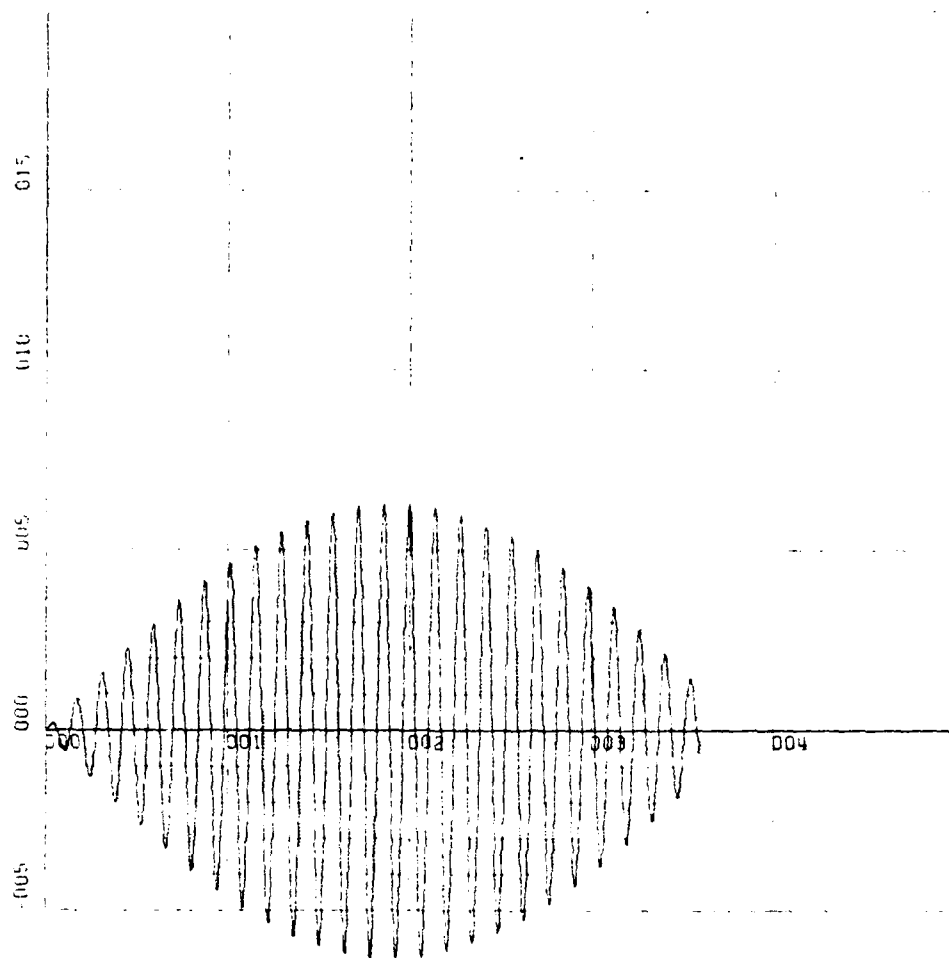
Y-SCALE=2.00E-06 UNITS INCH.[Rad/hour•200 μ g]

KWSTAS

RUN 2

DLAD VS TIME

Figure 44. Westerly Flight at 600 ft/sec.
Latitude Rate Error [Rad/hour•200 μ g] for Constant
North Accelerometer Bias [200 μ g].



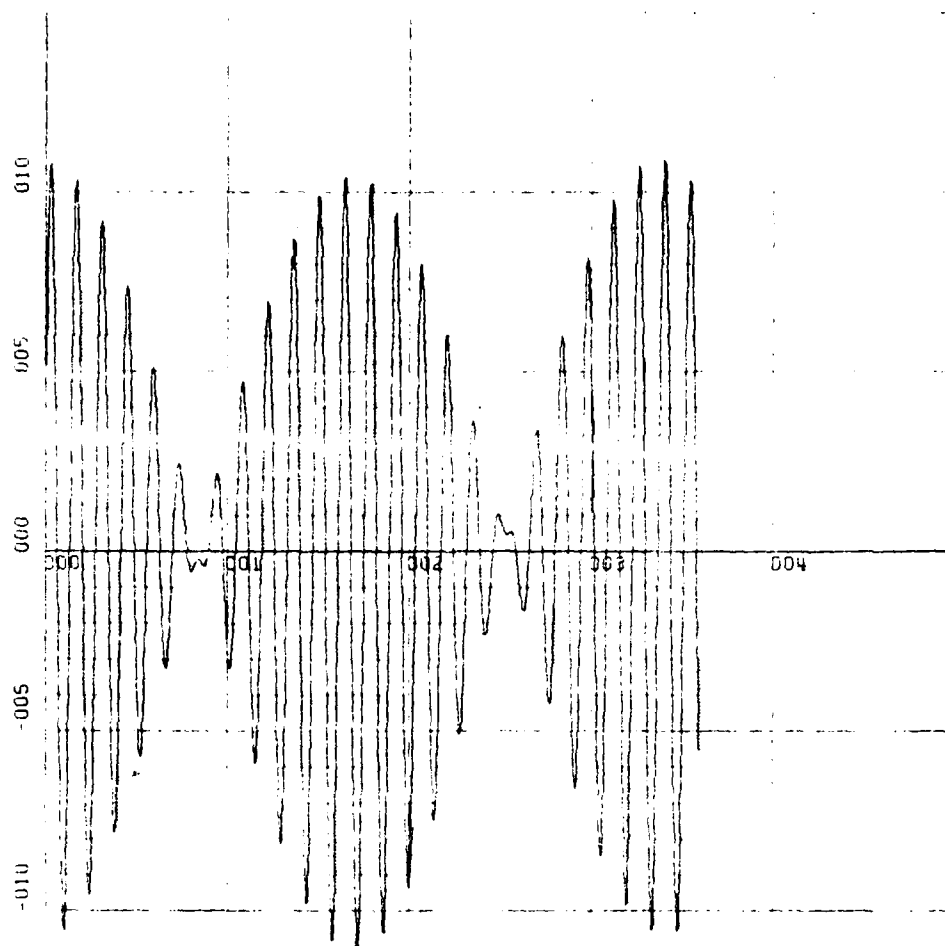
X-SCALE=1.00E+01 UNITS INCH. [hours]
 Y-SCALE=5.00E-06 UNITS INCH. [Rad/hour·200 μ g]

KWSTAS

RUN 2

DL0D VS TIME

Figure 45. Westerly Flight at 600 ft/sec.
 Longitude Rate Error [Rad/hour·200 μ g] for Constant
 North Accelerometer Bias [200 μ g].



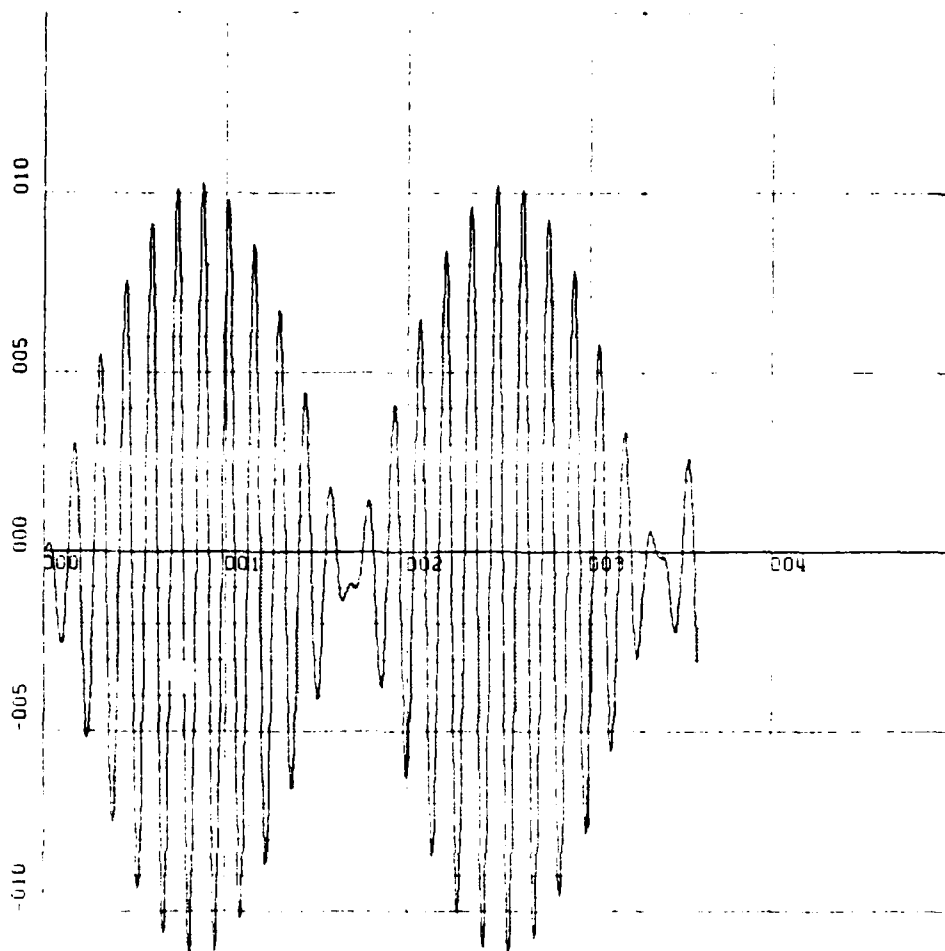
X-SCALE=1.00E+01 UNITS INCH.[hours]
Y-SCALE=5.00E-02 UNITS INCH.[Rad/140 μ rad]

KWSTAS

RUN 1

E'N' VS TIME

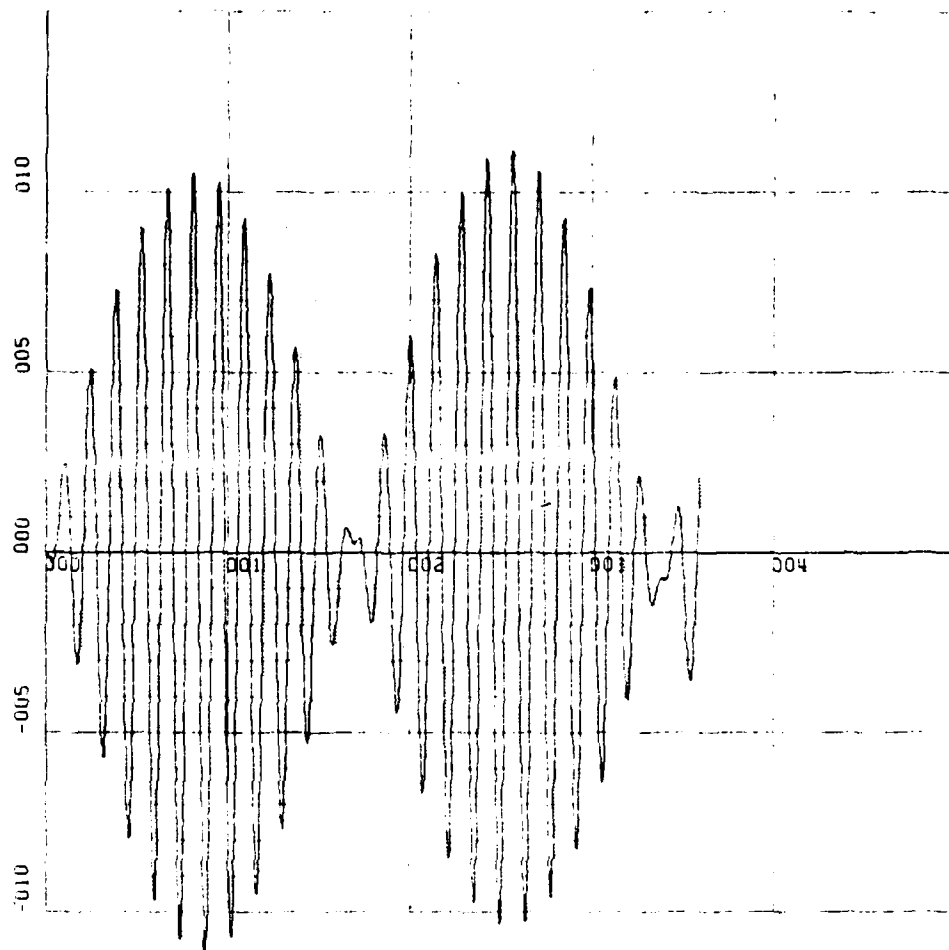
Figure 46. Stationary Case. North Level Error
[Rad/140 μ rad] for Initial North Level Error
[140 μ rad].



X-SCALE=1.00E+01 UNITS INCH.[hours]
 Y-SCALE=5.00E-02 UNITS INCH.[Rad/140 μ rad]
 KWSTAS
 RUN 1

E'E' VS TIME

Figure 47. Stationary Case. East Level Error [Rad/140 μ rad]
 for Initial North Level Error [140 μ rad].



X-SCALE=1.00E+01 UNITS INCH. [hours]

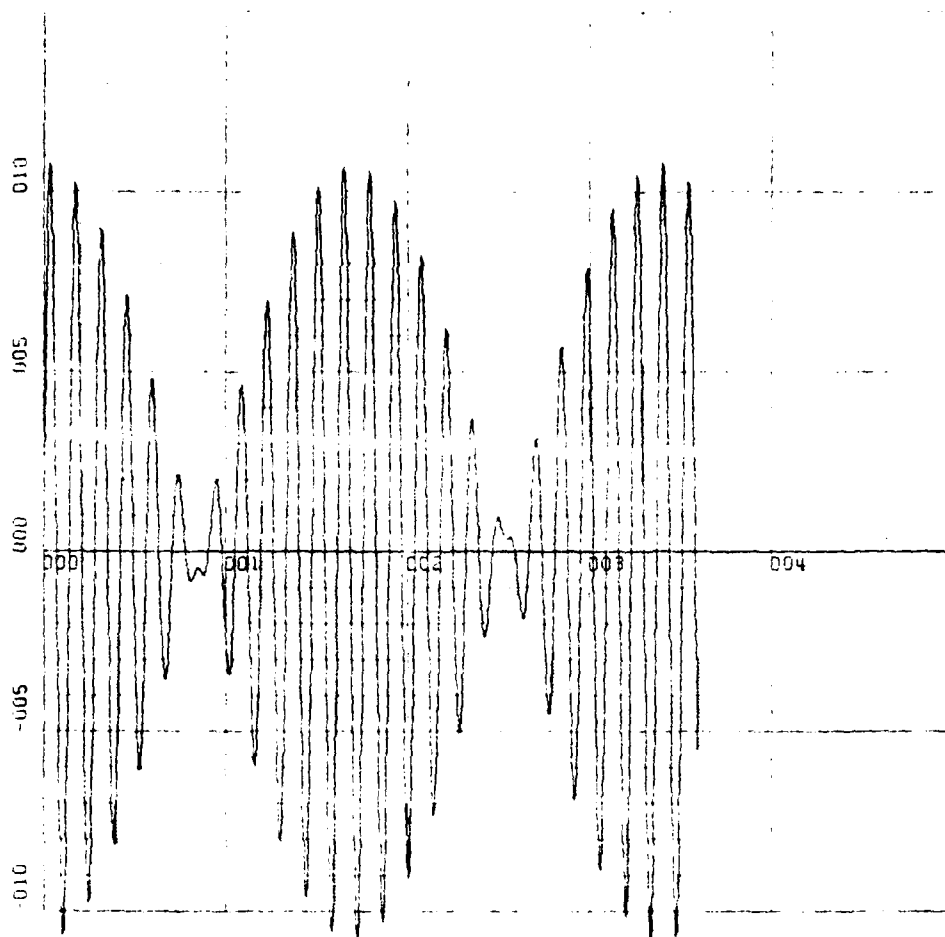
Y-SCALE=5.00E-02 UNITS INCH. [Rad/140 μ rad]

KWSTAS

RUN 3

E'N' VS TIME

Figure 48. Stationary Case. North Level Error [Rad/140 μ rad]
for Initial East Level Error [140 μ rad].



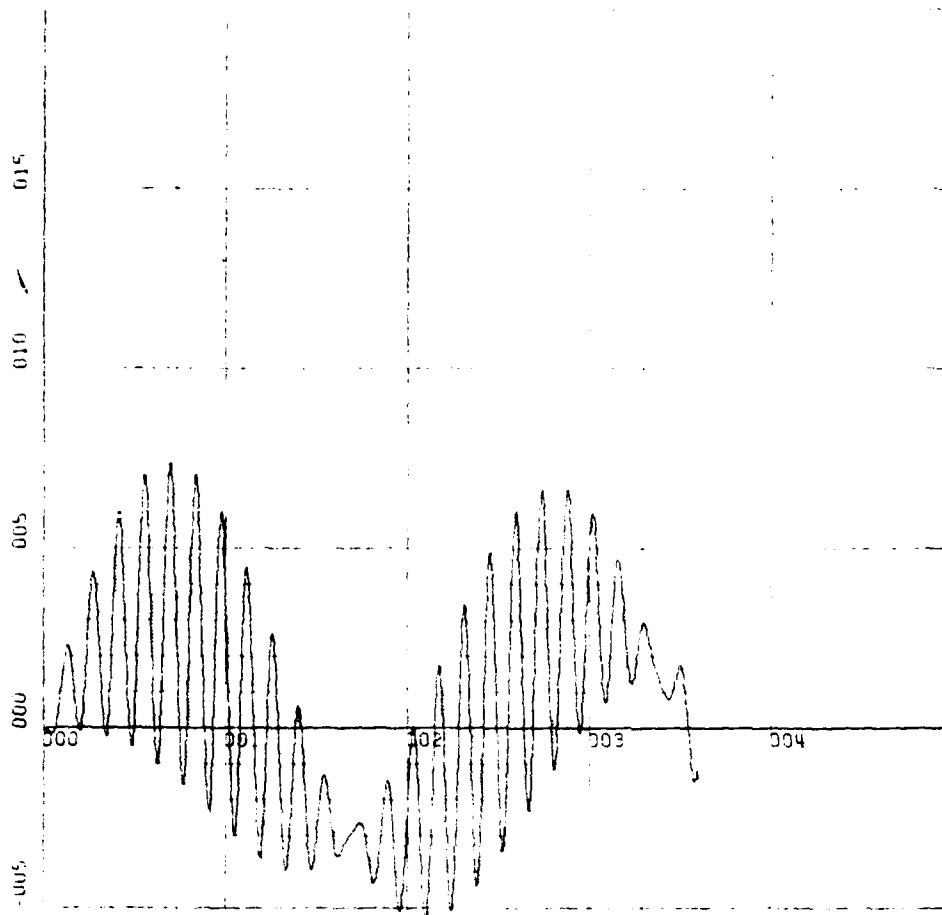
X-SCALE=1.00E+01 UNITS INCH. [hours]
 Y-SCALE=5.00E-02 UNITS INCH. [Rad/140 μ rad]

KWSTAS

RUN 3

E'E' VS TIME

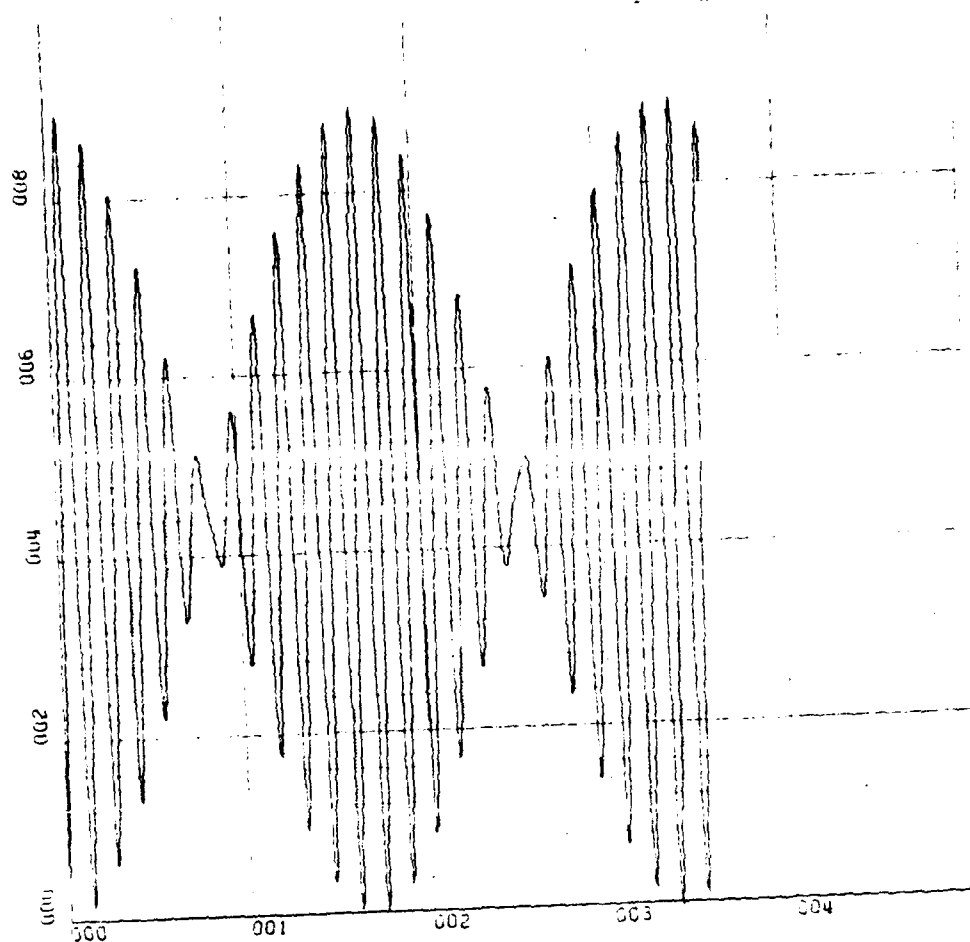
Figure 49. Stationary Case. East Level Error [Rad/140 μ rad]
 for Initial East Level Error [140 μ rad].



X-SCALE=1.00E+01 UNITS INCH. [hours]
 Y-SCALE=5.00E-03 UNITS INCH. [Rad/140μrad]
 KWSTAS
 RUN 5

E'N' VS TIME

Figure 50. Stationary Case. North Level Error [Rad/140μrad]
 for Initial Azimuth Level Error [140μrad].

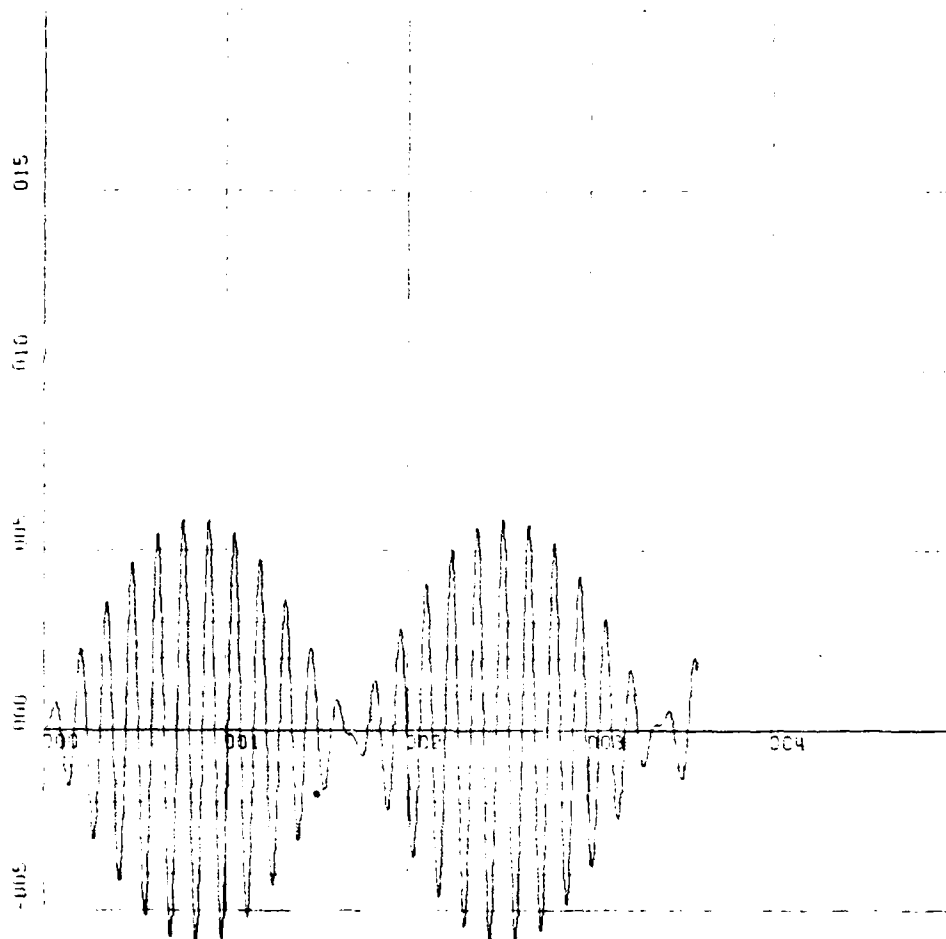


X-SCALE=1.00E+01 UNITS INCH. [hours]
 Y-SCALE=2.00E-03 UNITS INCH. [Rad/140 μ rad]

KWSTAS
 RUN 5

E'E' VS TIME

Figure 51. Stationary Case. East Level Error [Rad/140 μ rad]
 for Initial Azimuth Level Error [140 μ rad].



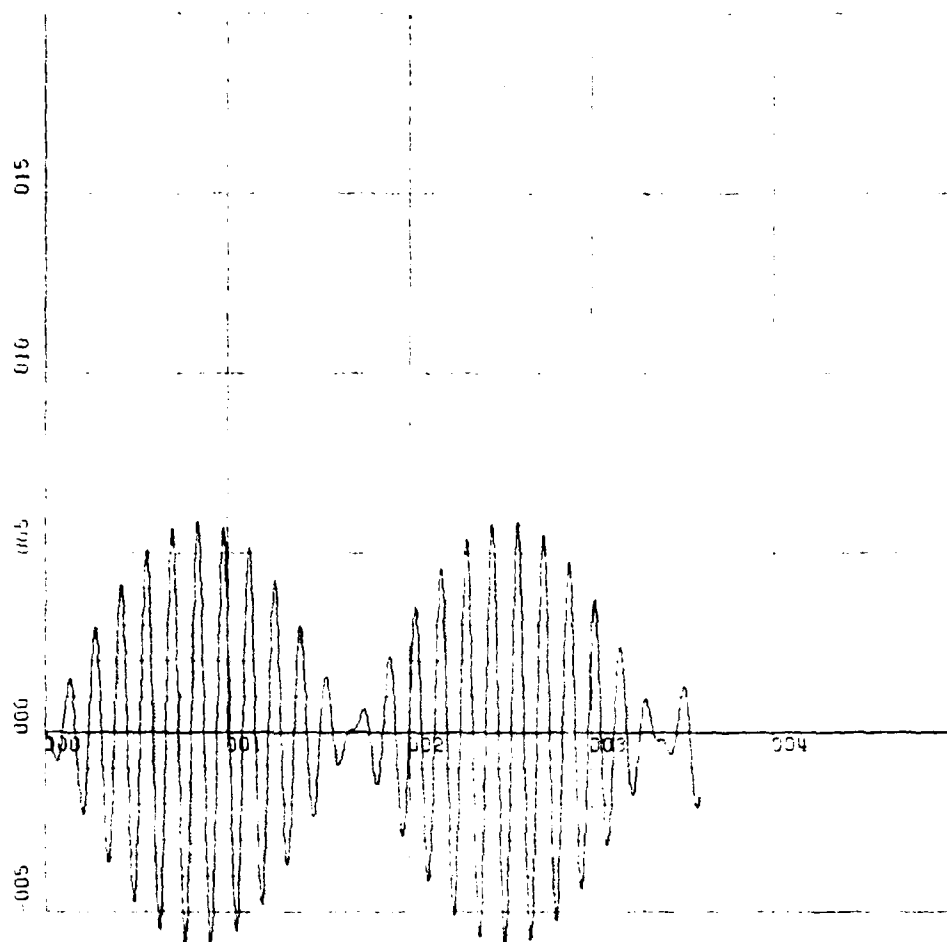
X-SCALE=1.00E+01 UNITS INCH. [hours]
 Y-SCALE=5.00E-02 UNITS INCH. [Rad/(2 ft/sec)]

KWSTAS

RUN 1

E'N' VS TIME

Figure 52. Stationary Case. North Level Error
 [Rad/(2 ft/sec)] for Initial Latitude Rate Error
 [0.345mrad/hour = 2 ft/sec].



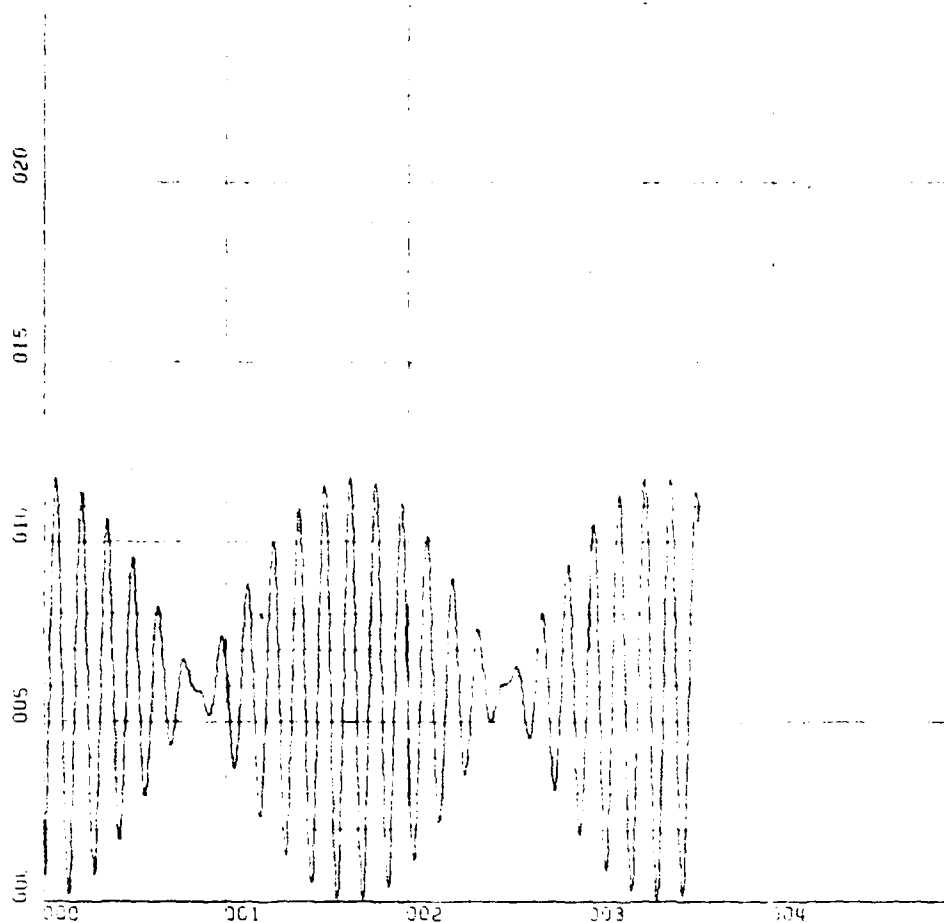
X-SCALE=1.00E+01 UNITS INCH. [hours]
 Y-SCALE=5.00E-02 UNITS INCH. [Rad/(2 ft/sec)]

KWSTAS

RUN 1

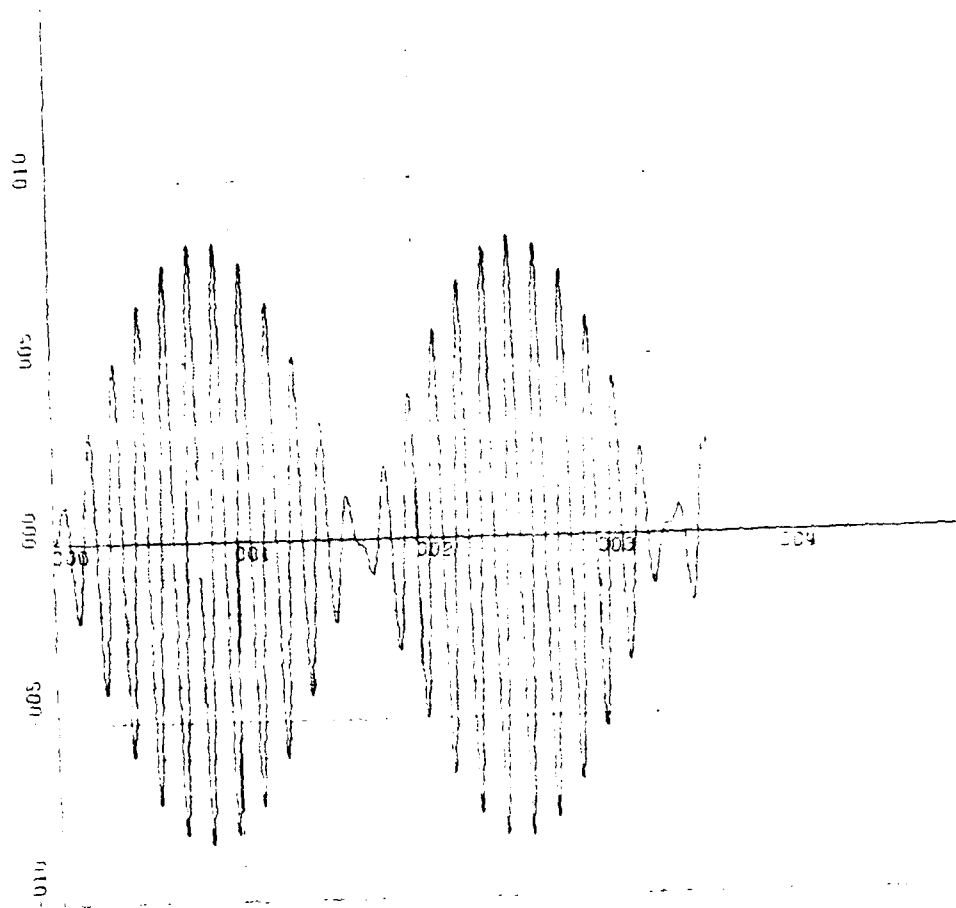
E'D' VS TIME

Figure 53. Stationary Case. Azimuth Level Error
 [Rad/(2 ft/sec)] for Initial Latitude Rate Error
 [0.345 mrad/hour = 2 ft/sec].



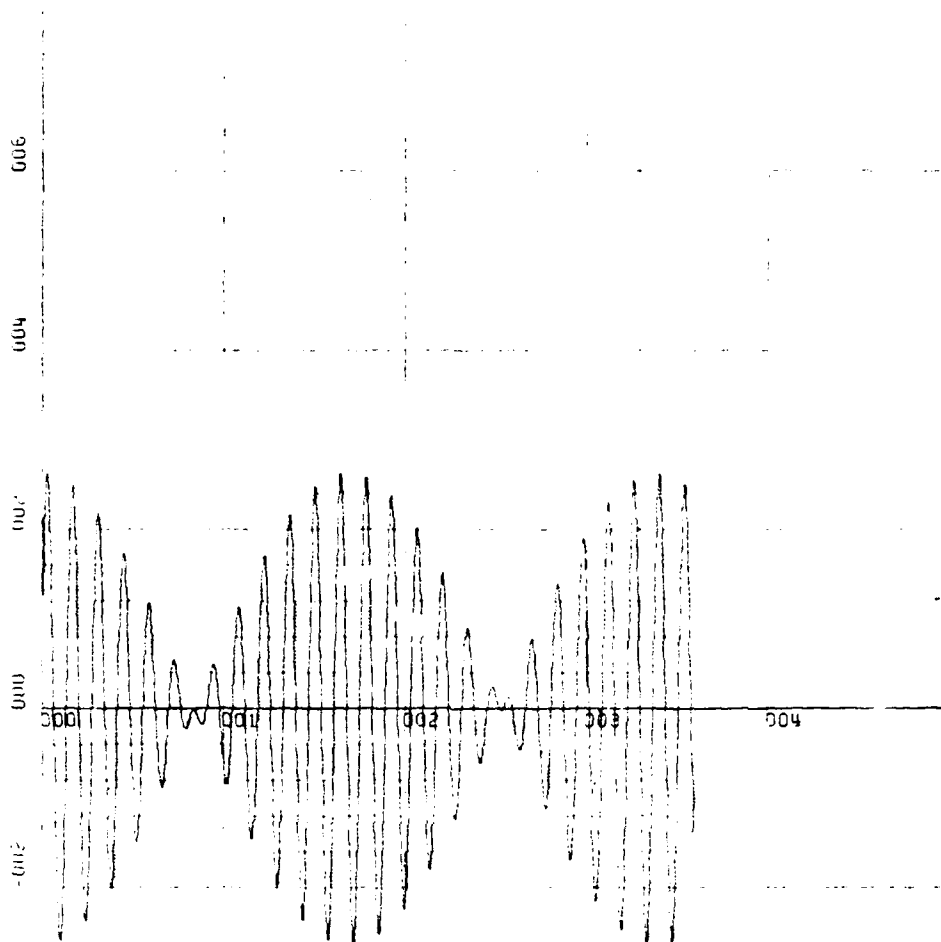
X-SCALE=1.00E+01 UNITS INCH. [hours]
 Y-SCALE=5.00E-02 UNITS INCH. [Rad/(2 ft/sec)]
 KWSTAS
 RUN 1 DLA VS TIME

Figure 54. Stationary Case. Latitude Error
 [Rad/(2 ft/sec)] for Initial Latitude Rate Error
 [0.345mrad/hour = 2 ft/sec].



X-SCALE=1.00E+01 UNITS INCH. [hours]
 Y-SCALE=5.00E-02 UNITS INCH. [Rad/(2 ft/sec)]
 KWSTAS
 RUN 2
 DLO VS TIME

Figure 55. Stationary Case. Longitude Error
 [Rad/(2 ft/sec)] for Initial Latitude Rate Error
 [0.345mrad/hour = 2 ft/sec].



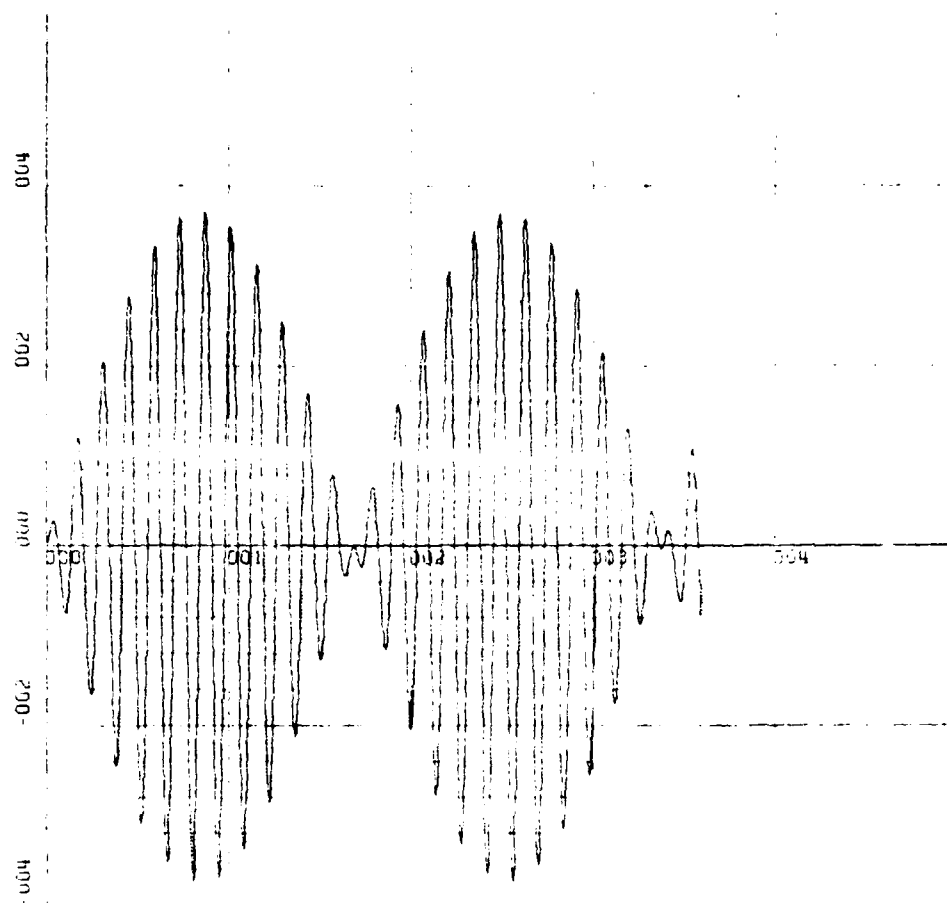
X-SCALE=1.00E+01 UNITS INCH. [hours]
 Y-SCALE=2.00E-01 UNITS INCH. $\left[\frac{(\text{Rad/hour})}{2 \text{ ft/sec}}\right]$

KWSTAS

RUN 2

DLAD VS TIME

Figure 56. Stationary Case. Latitude Rate Error
 $\left[\frac{(\text{Rad/hour})}{(2 \text{ ft/sec})}\right]$ for Initial Latitude
 Rate Error $[0.345 \text{ mrad/hour} = 2 \text{ ft/sec}]$.



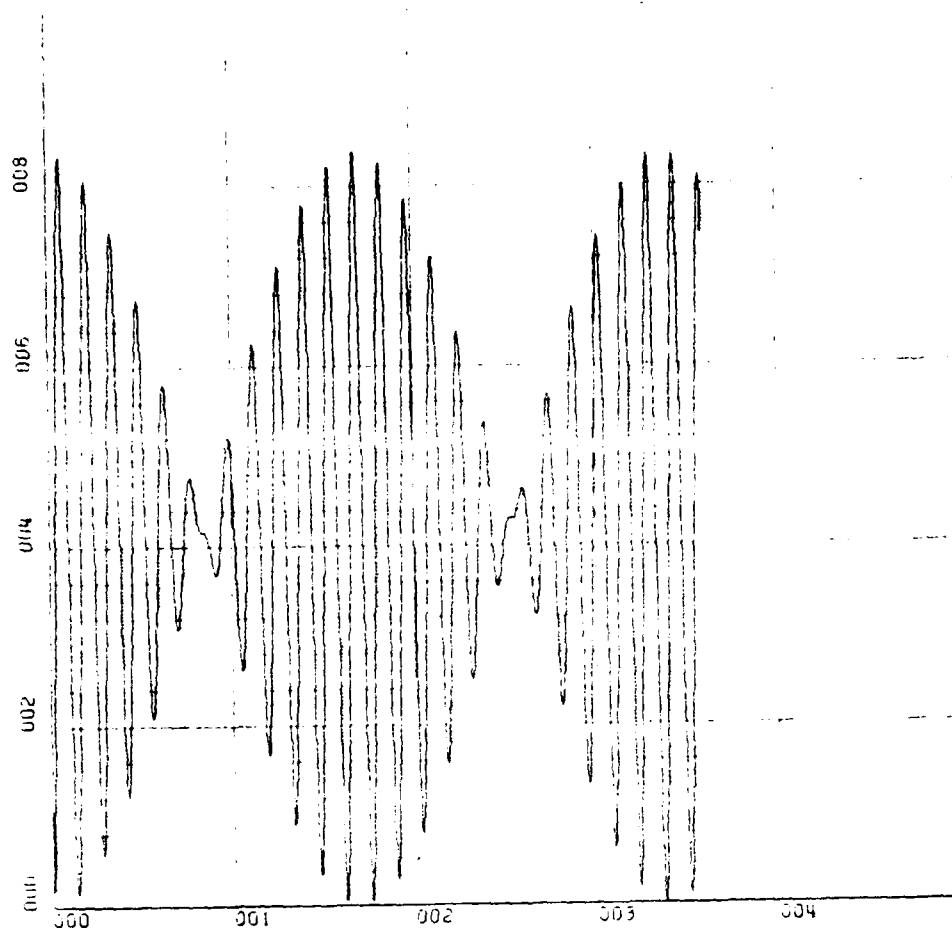
X-SCALE=1.00E+01 UNITS INCH. [hours]
 Y-SCALE=2.00E-01 UNITS INCH. [(Rad/hour)/
 2 ft/hour)]

KWSTAS

RUN 2

DL0D VS TIME

Figure 57. Stationary Case. Longitude Rate Error
 [(Rad/hour)/(2 ft/sec)] for Initial Latitude
 Rate Error [0.345mrad/hour = 2 ft/sec].

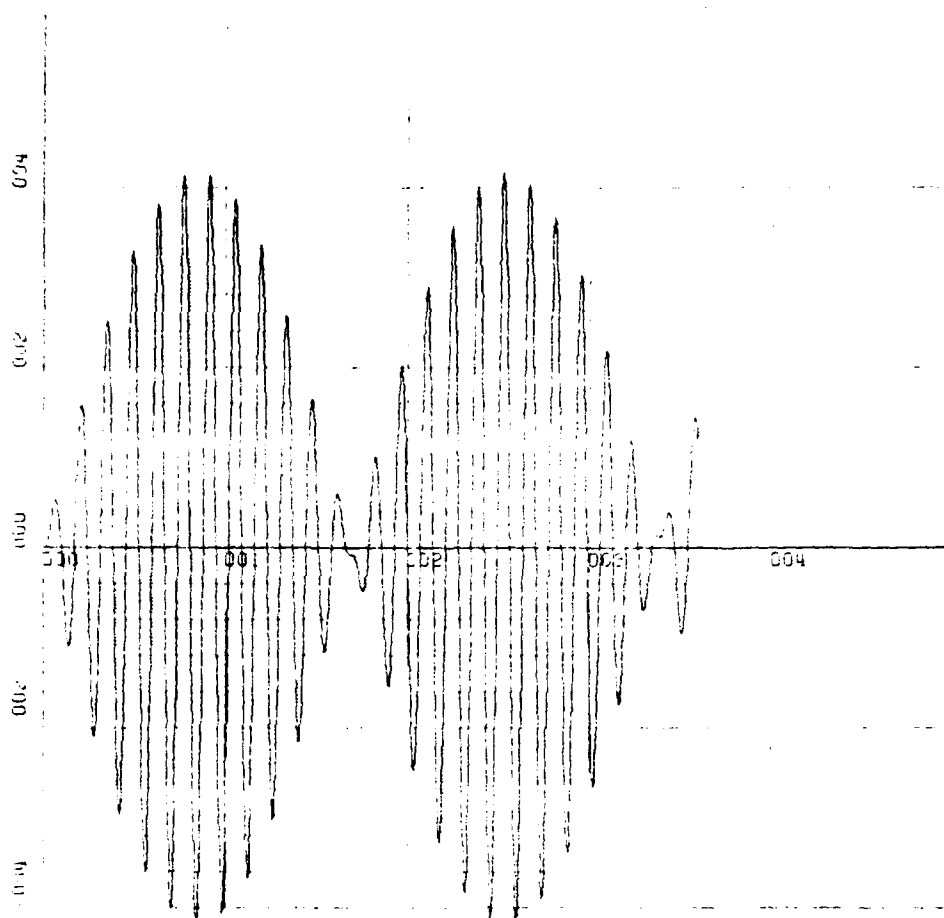


X-SCALE=1.00E+01 UNITS INCH.[hours]
 Y-SCALE=2.00E-02 UNITS INCH.[Rad/(2 ft/sec)]

KWSTAS
 RUN 3

E'N' VS TIME

Figure 58. Stationary Case. North Level Error
 [Rad/(2 ft/sec)] for Initial Longitude Rate Error
 [0.345mrad/hour = 2 ft/sec].



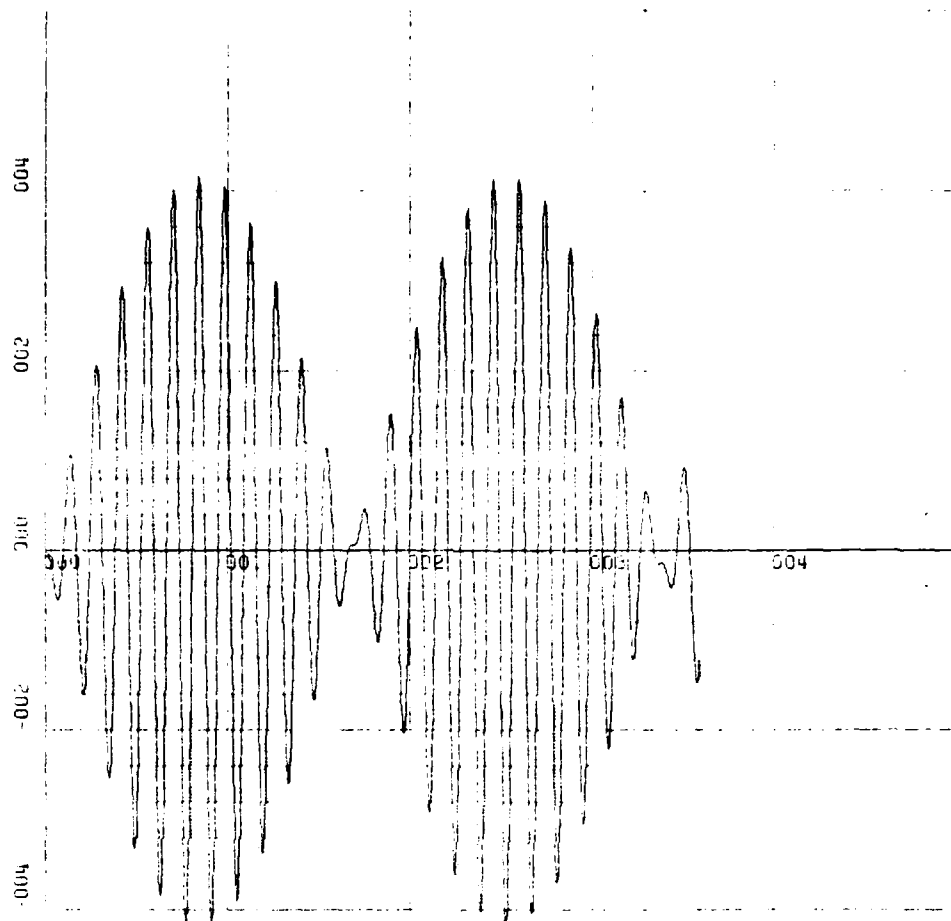
X-SCALE=1.00E+01 UNITS INCH. [hours]
 Y-SCALE=2.00E-02 UNITS INCH. [Rad/(2 ft/sec)]

KWSTAS

RUN 3

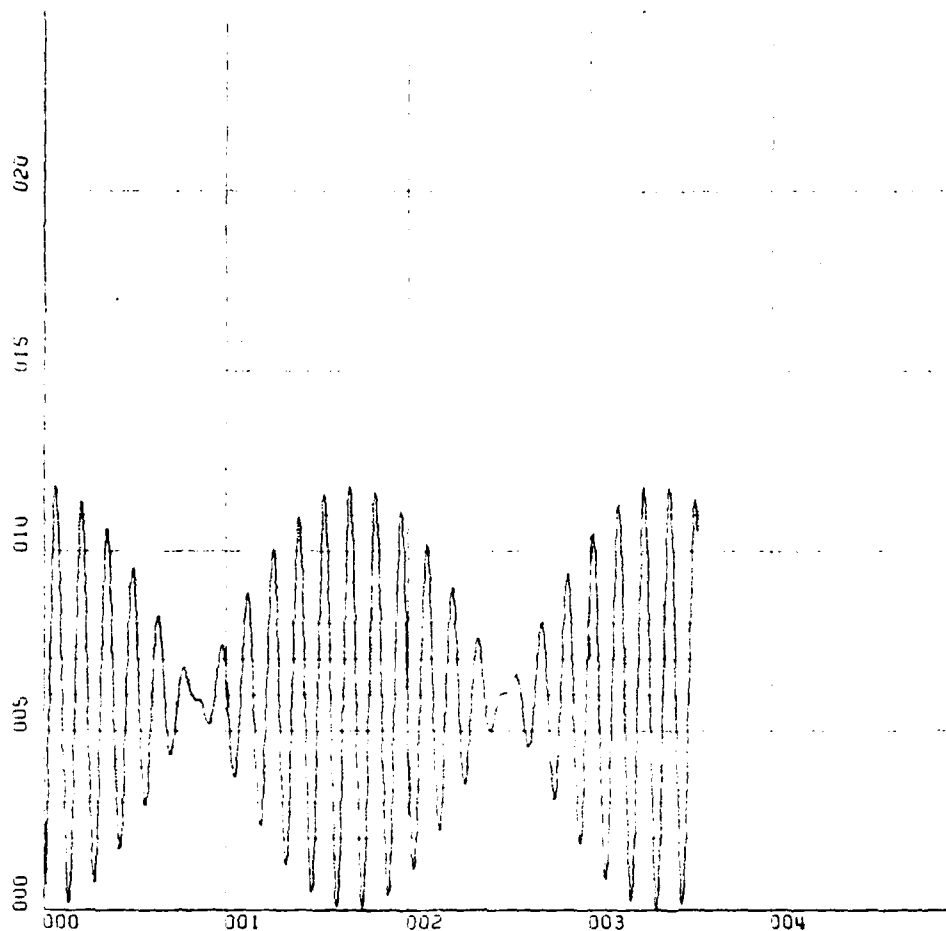
E'E' VS TIME

Figure 59. Stationary Case. East Level Error
 [Rad/(2 ft/sec)] for Initial Longitude Rate
 Error [0.345mrad/hour = 2 ft/sec].



X-SCALE=1.00E+01 UNITS INCH. [hours]
 Y-SCALE=2.00E-02 UNITS INCH. [Rad/(2 ft/sec)]
 KWSTAS
 RUN 3 DLA VS TIME

Figure 60. Stationary Case. Latitude Error [Rad/(2 ft/sec)]
 for Initial Longitude Rate Error
 [0.345mrad/hour = 2 ft/sec].



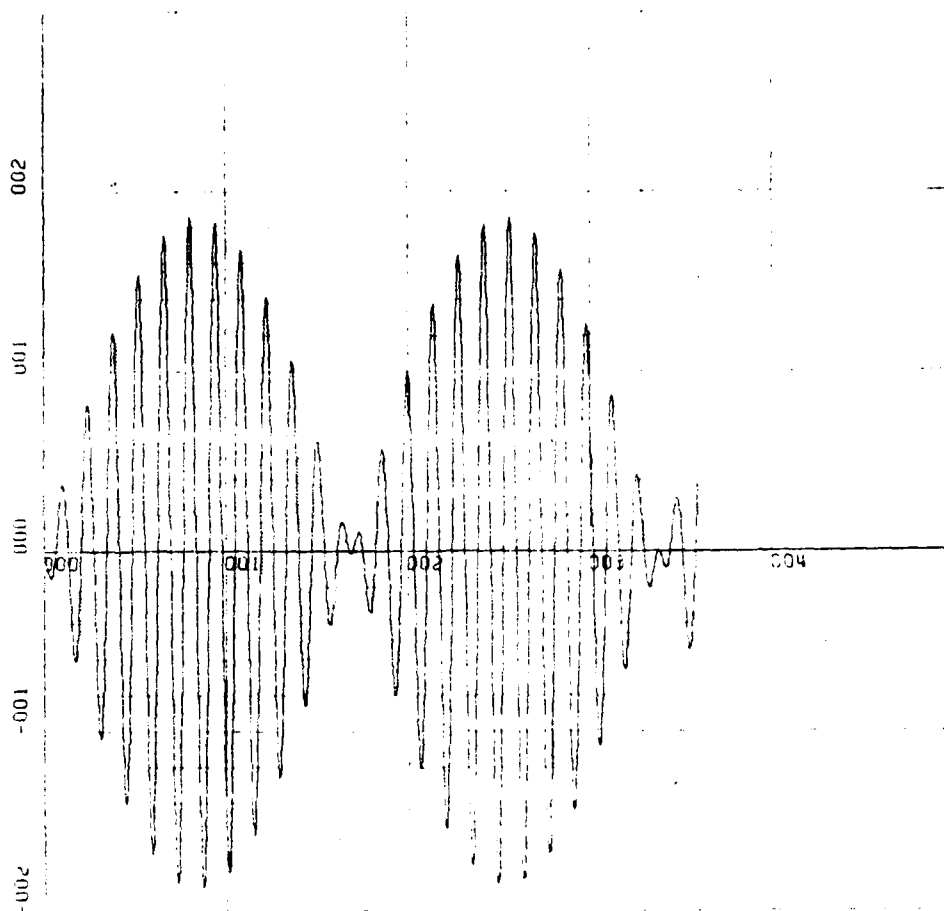
X-SCALE=1.00E+01 UNITS INCH. [hours]
 Y-SCALE=5.00E-02 UNITS INCH. [Rad/(2 ft/sec)]

KWSTAS

RUN 4

DLO VS TIME

Figure 61. Stationary Case. Longitude error [Rad/(2 ft/sec)]
 for Initial Longitude Rate Error
 [0.345mrad/hour = 2 ft/sec].



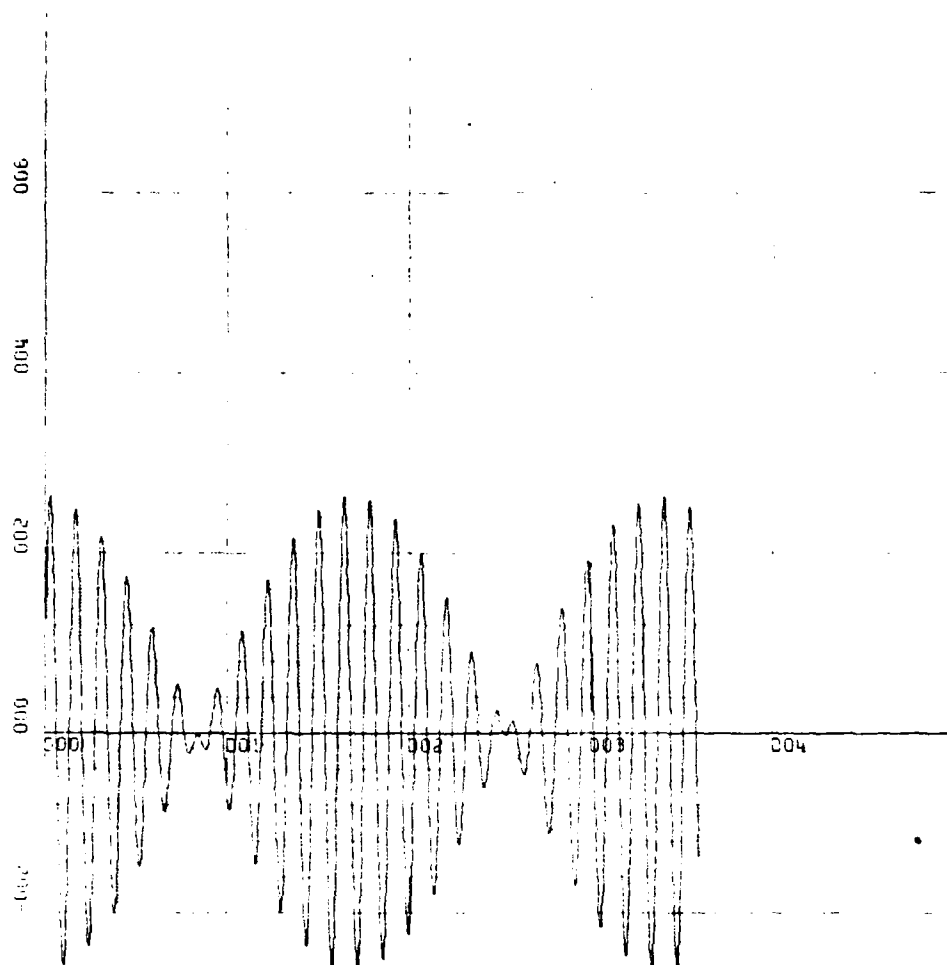
X-SCALE=1.00E+01 UNITS INCH. [hours]
 Y-SCALE=1.00E-01 UNITS INCH. [(Rad/hour)/
 (2 ft/sec)]

KWSTAS

RUN 4

DLAD VS TIME

Figure 62. Stationary Case. Latitude Rate Error
 [(Rad/hour)/(2 ft/sec)] for Initial Longitude
 Rate Error [0.345mrad/hour = 2 ft/sec].

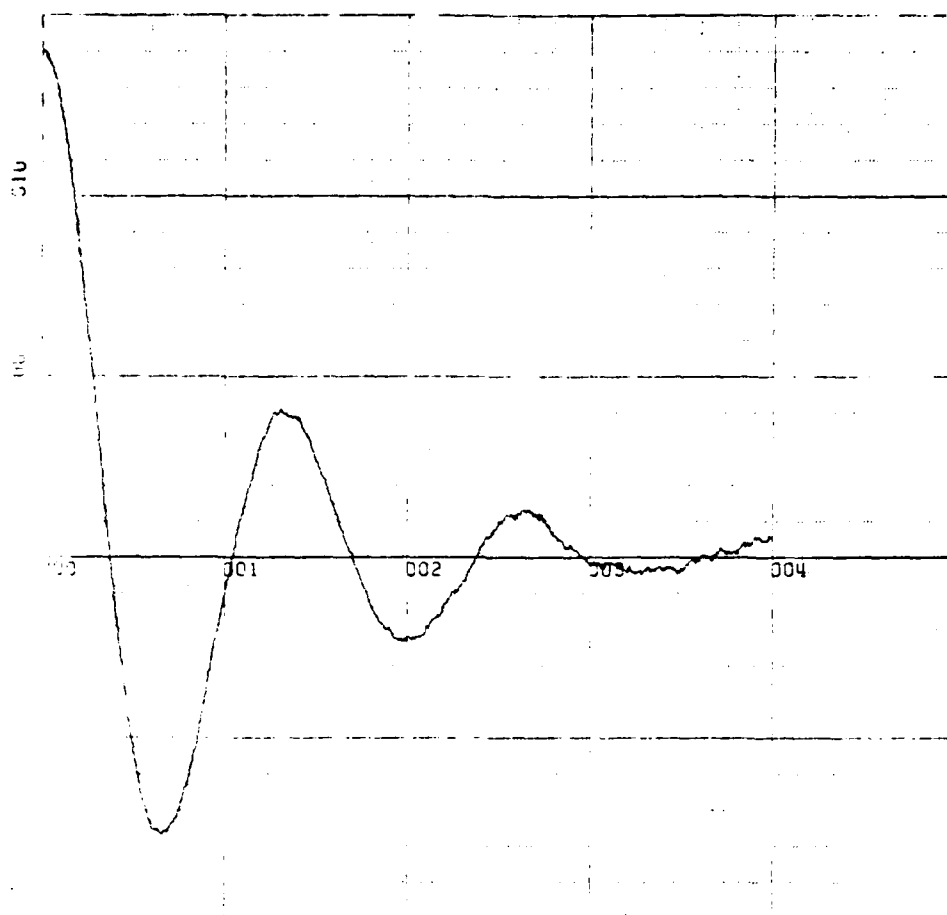


X-SCALE=1.00E+01 UNITS INCH. [hours]
 Y-SCALE=2.00E-01 UNITS INCH. [(Rad/hour)/
 KWSTAS (2 ft/sec)]

RUN 4

DL0D VS TIME

Figure 63. Stationary Case. Longitude Rate Error
 [(Rad/hour)/(2 ft/sec)] for Initial Longitude
 Rate Error [0.345mrad/hour = 2 ft/sec].



X-SCALE=1.00E+00 UNITS INCH. [hours]

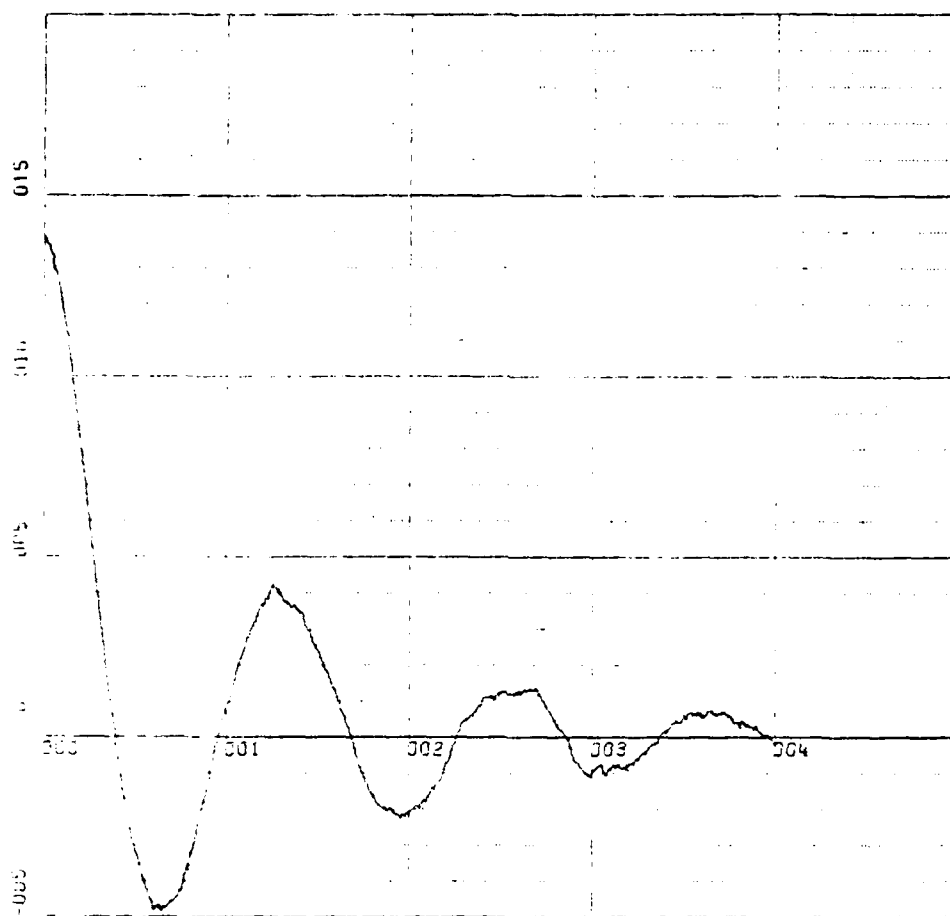
Y-SCALE=5.00E-05 UNITS INCH. [Rad]

KWSTAS

RUN 1

E<N> VS TIME

Figure 64. Theoretical I.N.S./G.P.S., 4-Hour Process.
North Attitude Error [Rad].



X-SCALE=1.00E+00 UNITS INCH. [hours]

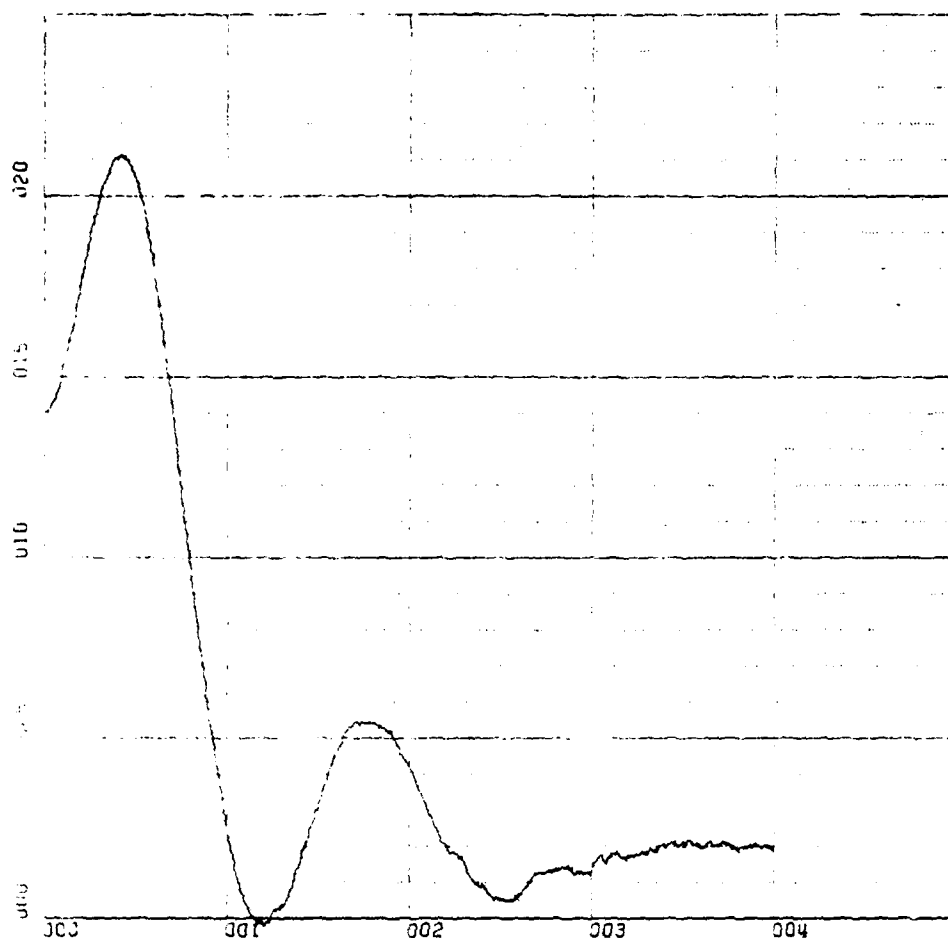
Y-SCALE=5.00E-05 UNITS INCH. [Rad]

KWSTAS

RUN 1

E<E> VS TIME

Figure 65. Theoretical I.N.S./G.P.S., 4-Hour Process.
Fast Attitude Error [Rad].



X-SCALE=1.00E-00 UNITS INCH. [hours]

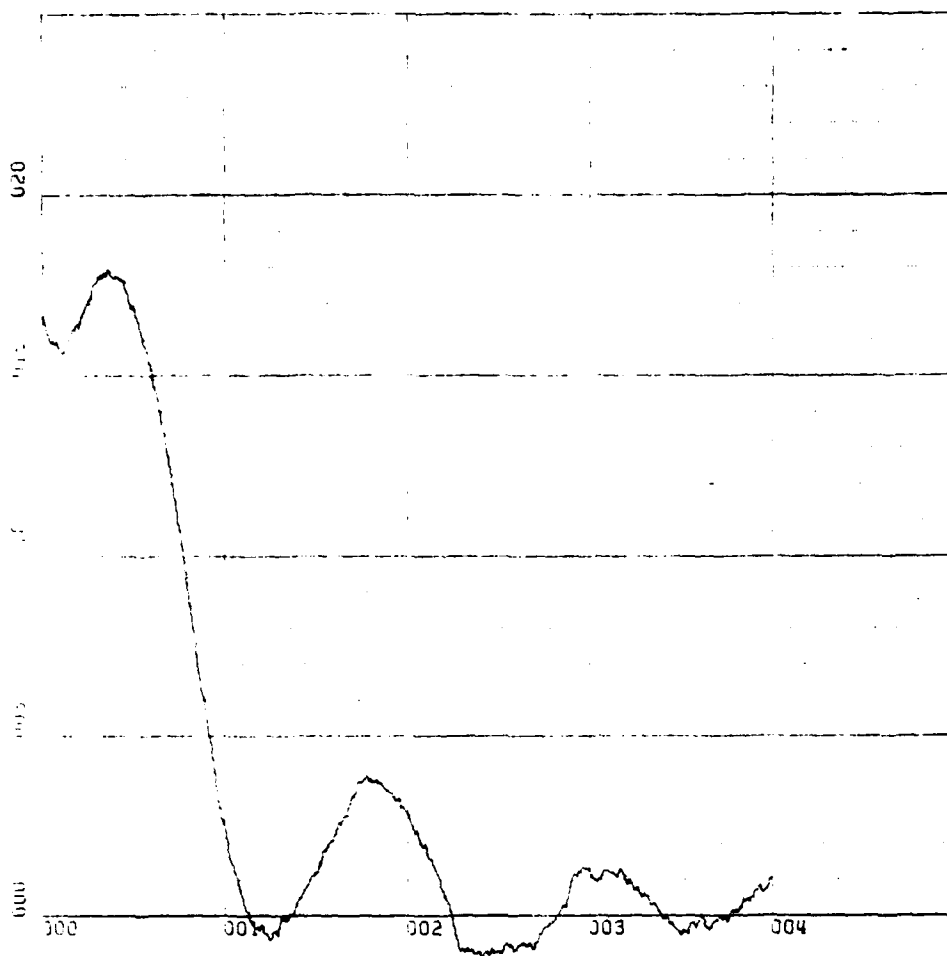
Y-SCALE=5.00E-03 UNITS INCH. [Rad]

KWSTAS

RUN 1

E<D> VS TIME

Figure 66. Theoretical I.N.S./G.P.S., 4-Hour Process
Azimuth Attitude Error [Rad].



X-SCALE=1.00E+00 UNITS INCH. [hours]

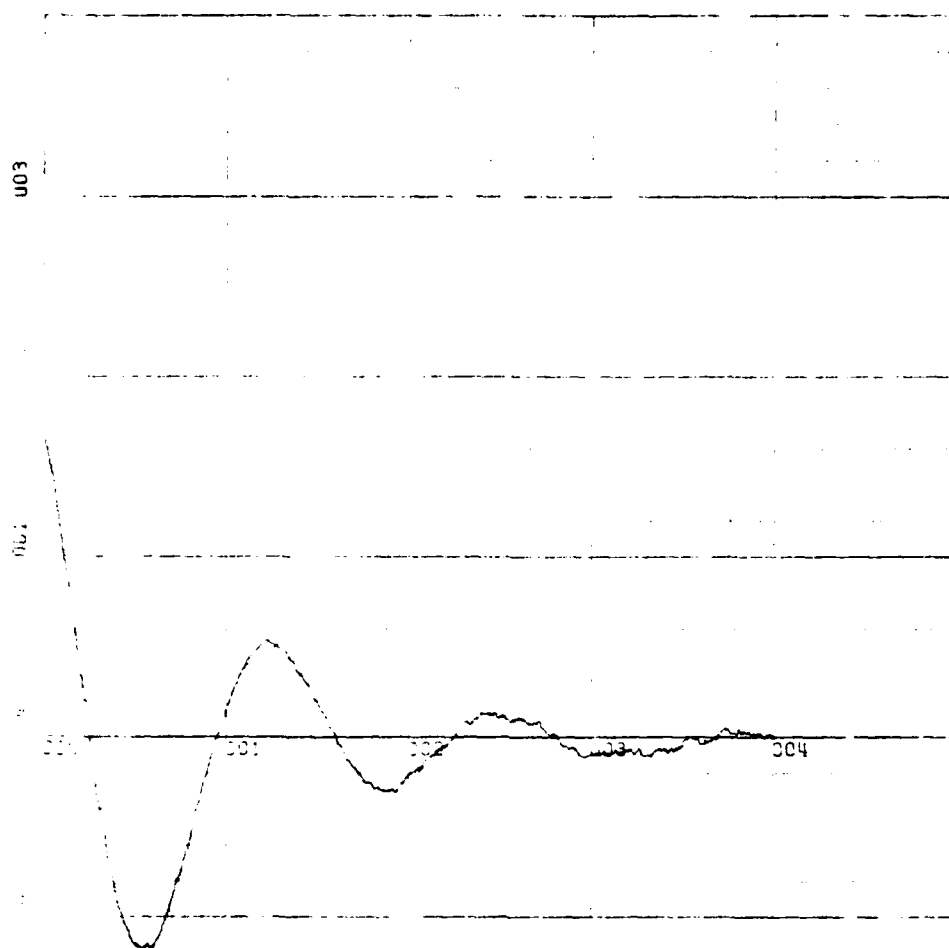
Y-SCALE=5.00E-05 UNITS INCH. [Rad]

KWSTAS

RUN 1

DLAT VS TIME

Figure 67. Theoretical I.N.S./G.P.S., 4-Hour Process.
Y Position Error [Rad].



SCALE=1.00E-03 UNITS INCH.[hours]

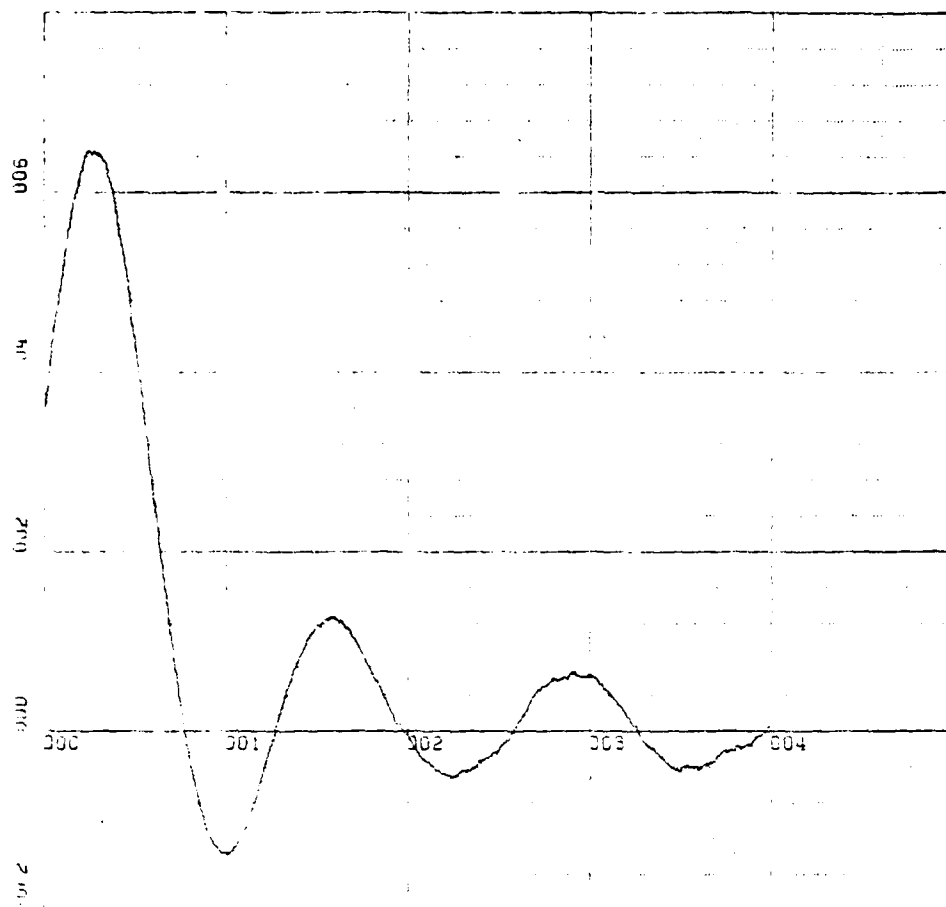
SCALE=1.00E-04 UNITS INCH.[Rad]

WASTAS

PUN 2

DLONG VS TIME

Figure 68. Theoretical I.N.S./G.P.S., 4-Hour Process.
X Position Error [Rad].



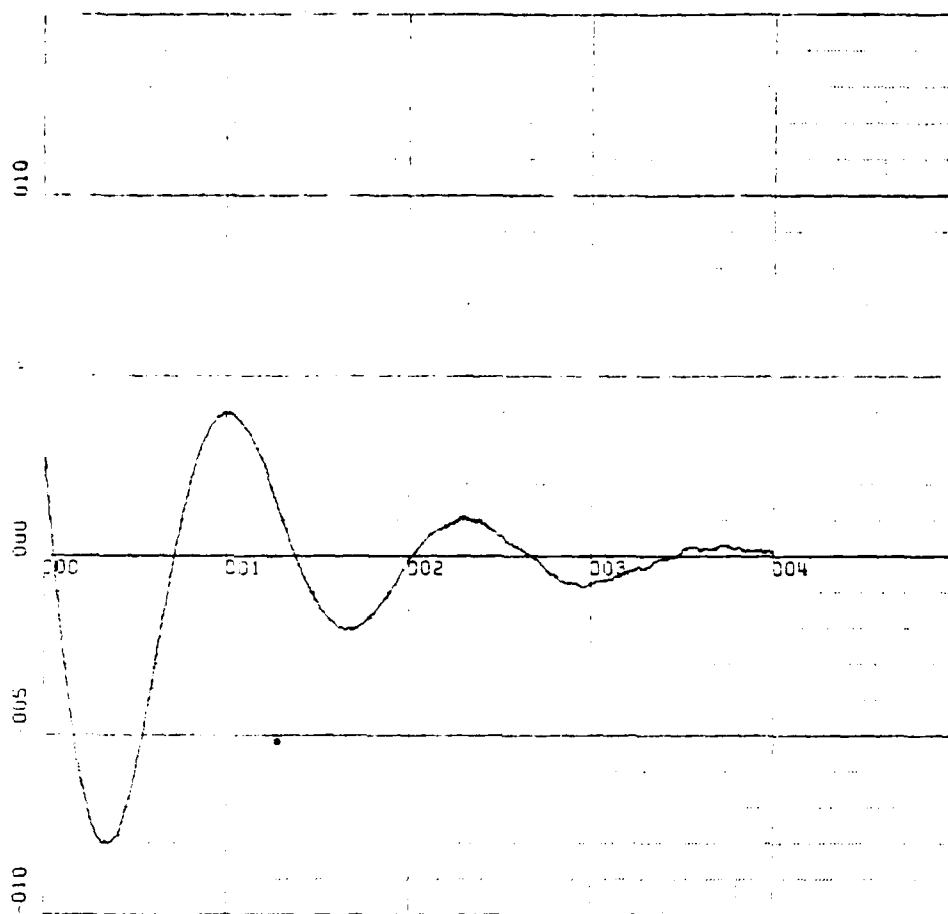
X-SCALE=1.00E+00 UNITS INCH. [hours]
 Y-SCALE=2.00E-04 UNITS INCH. [Rad/hour]

KWSTAS

RUN 2

DLADOT VS TIME

Figure 69. Theoretical I.N.S./G.P.S., 4-Hour Process.
 Y Velocity Error [Rad/hour].



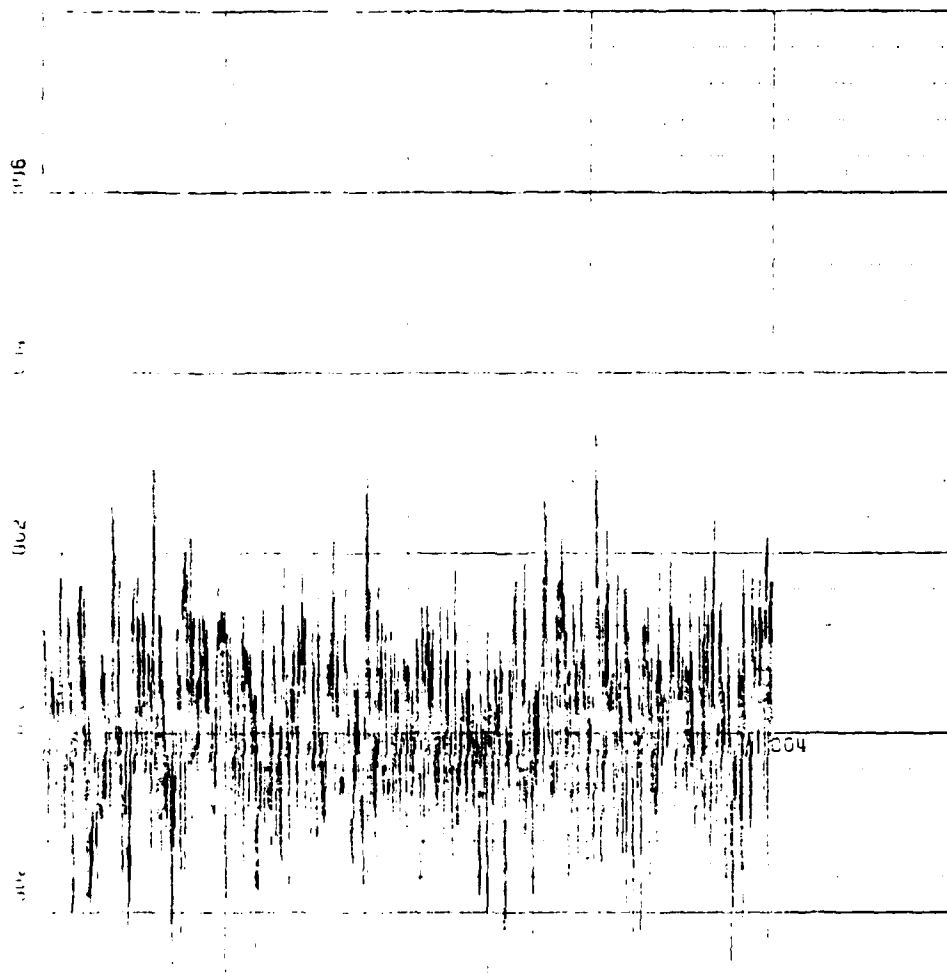
X-SCALE=1.00E+00 UNITS INCH. [hours]
 Y-SCALE=5.00E-04 UNITS INCH. [Rad/hour]

KWSTAS

RUN 2

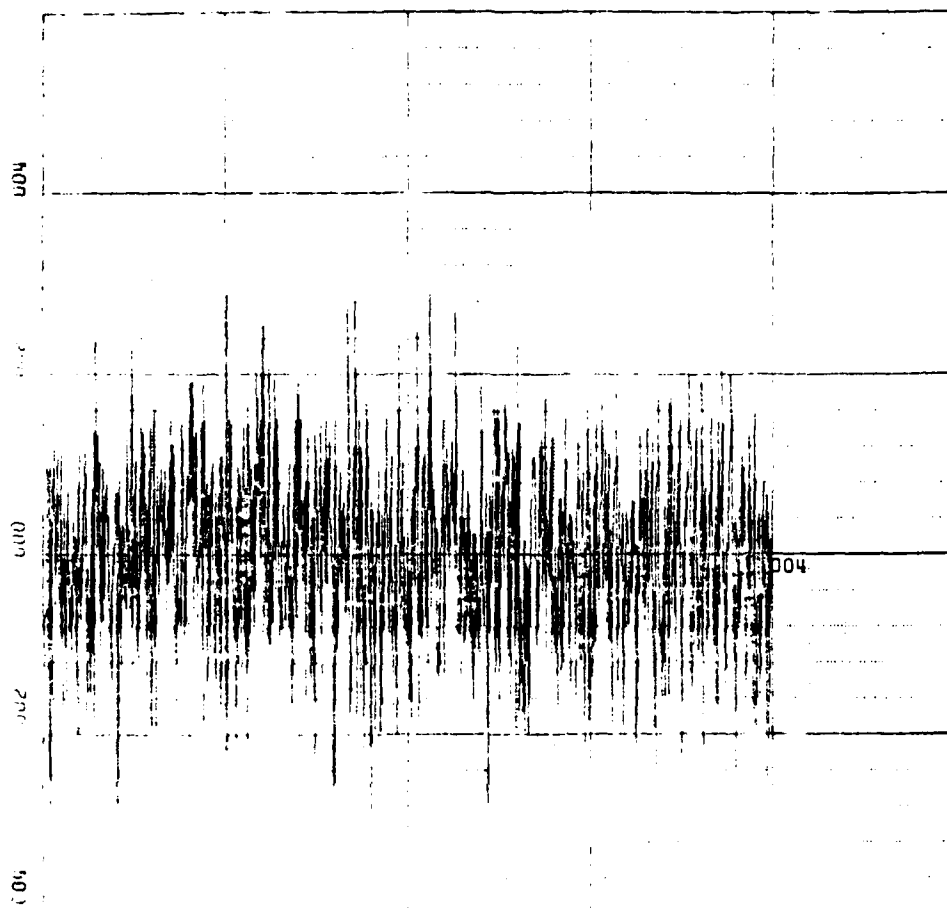
DL0ND0T VS TIME

Figure 70. Theoretical I.N.S./G.P.S., 4-Hour Process.
 X Velocity Error [Rad/hour].



X-SCALE=1.00E+00 UNITS INCH. [hours]
 Y-SCALE=2.00E+00 UNITS INCH. $\left[\left(\frac{\text{Rad}}{\text{hour}} \right)^2 \right]$ or $\left[\left(\frac{\text{Rad}}{\text{hour}} \right)^2 \right]$
 WASTAS
 RUN 3 NOISE W VS TIME

Figure 71. Normalized Input Noise Versus Time.



X-SCALE=1.00E+00 UNITS INCH. [hours]

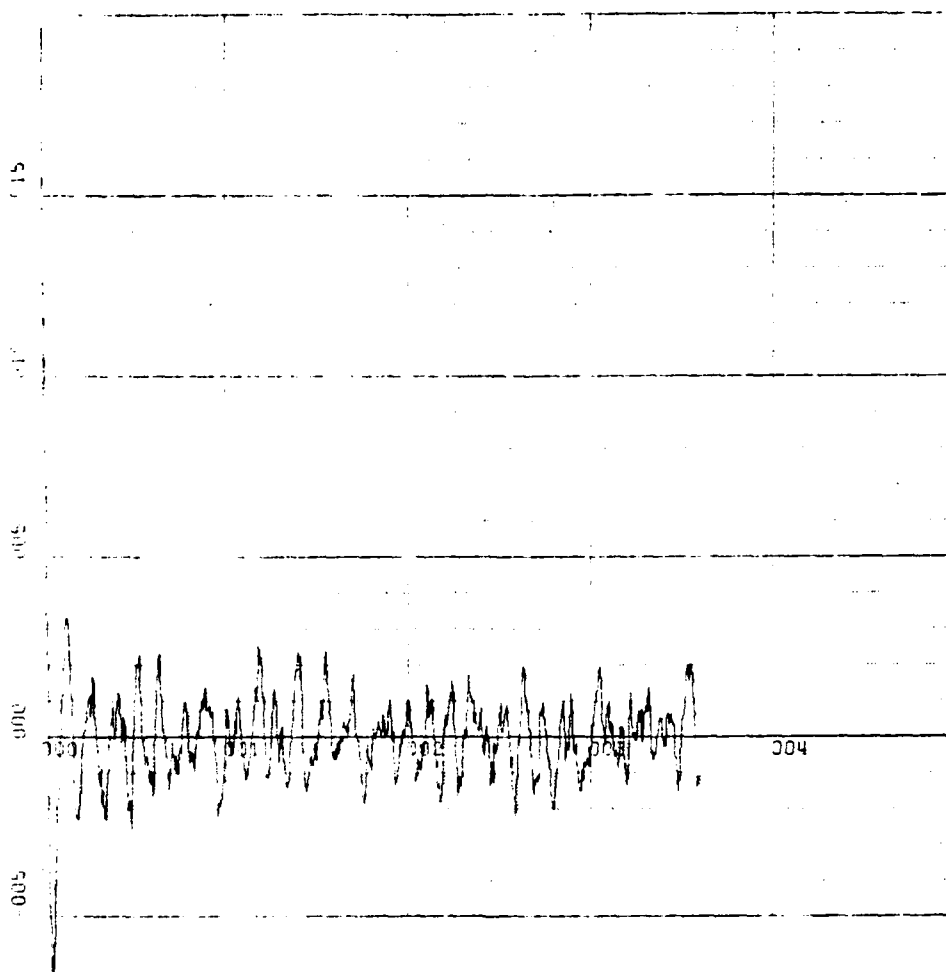
Y-SCALE=2.00E+00 UNITS INCH. [(Rad)²]

KWSTAS

RUN 3

NOISE V VS TIME

Figure 72. Normalized Measurement Noise versus Time.



X-SCALE=1.00E+01 UNITS INCH. [hours]

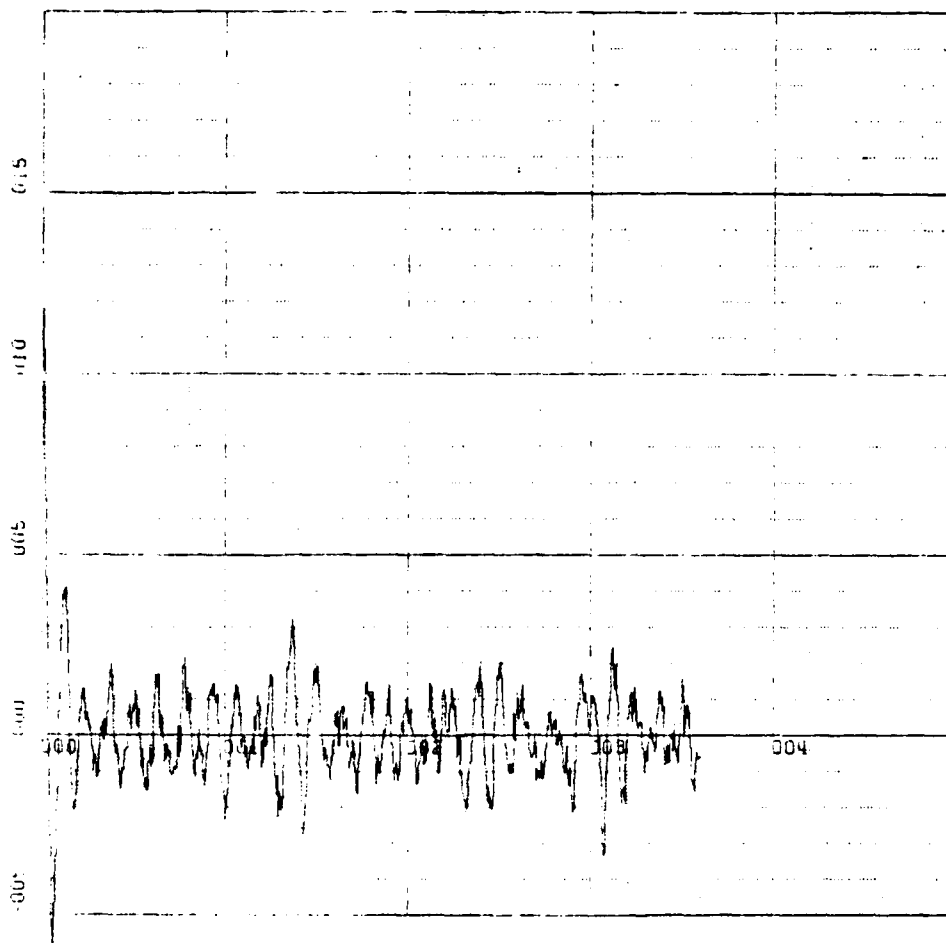
-SCALE=5.00E-05 UNITS INCH. [Rad]

<N> STAS

RUN 1

<N> VS TIME

Figure 73. Theoretical I.N.S./G.P.S., 36-Hour Process.
North Attitude Error [Rad].



X-SCALE=1.00E+01 UNITS INCH. [hours]

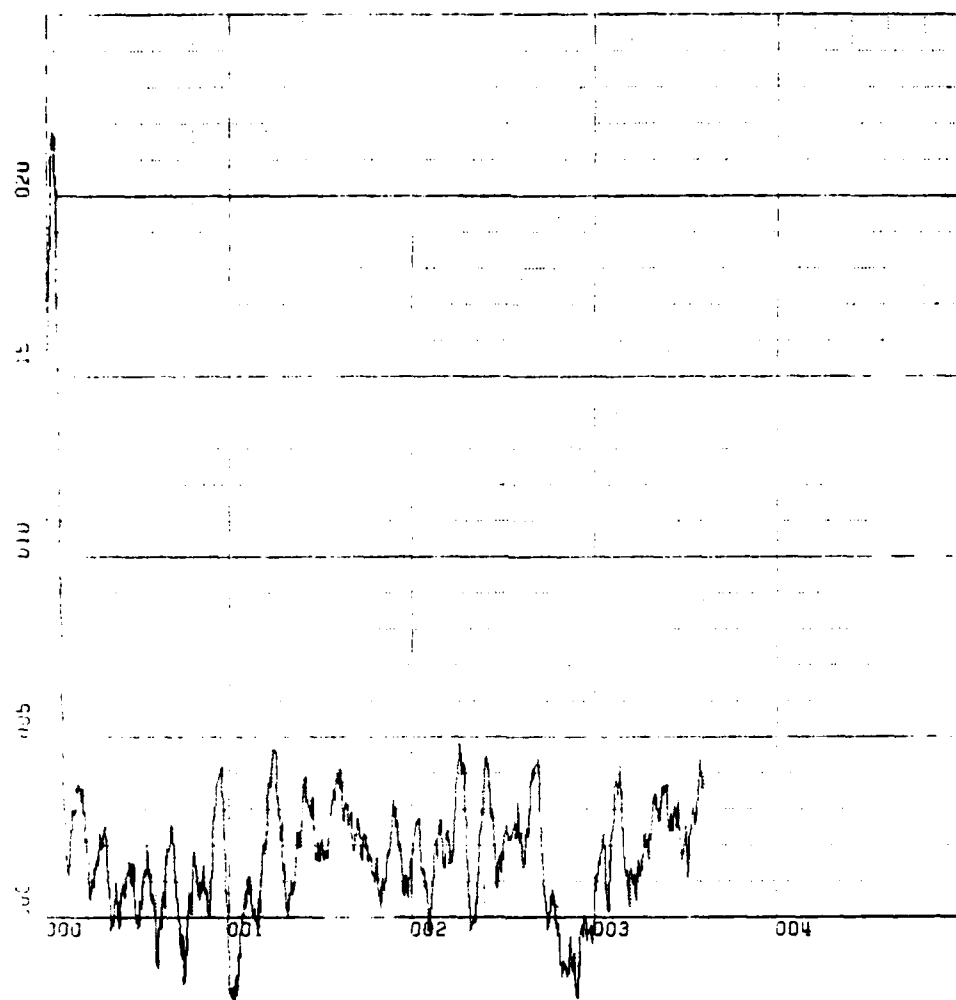
Y-SCALE=5.00E-05 UNITS INCH. [Rad]

KWSTAS

RUN 1

E<E> VS TIME

Figure 74. Theoretical I.N.S./G.P.S., 36-Hour Process.
East Attitude Error [Rad].



X-SCALE=1.00E+01 UNITS INCH. [hours]

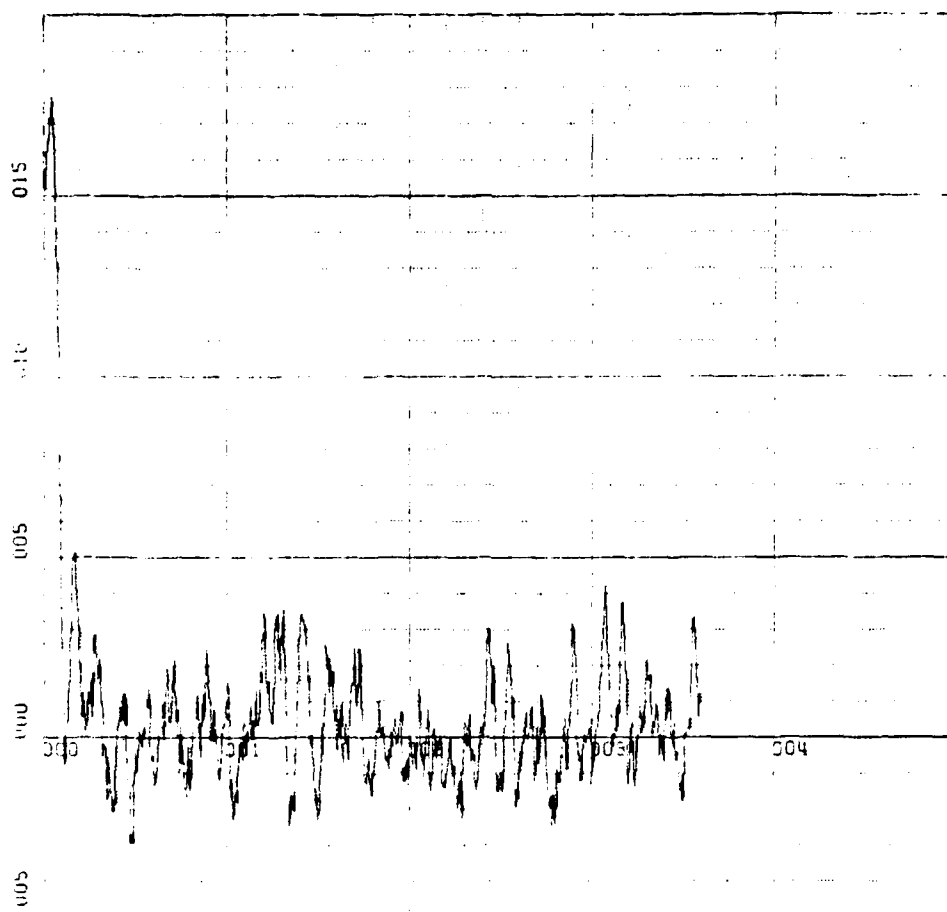
Y-SCALE=5.00E-05 UNITS INCH. [Rad]

KWSTAS

RUN 1

E<D> VS TIME

Figure 75. Theoretical I.N.S./G.P.S., 36-Hour Process.
Azimuth Attitude Error [Rad].



X-SCALE=1.00E+01 UNITS INCH. [hours]

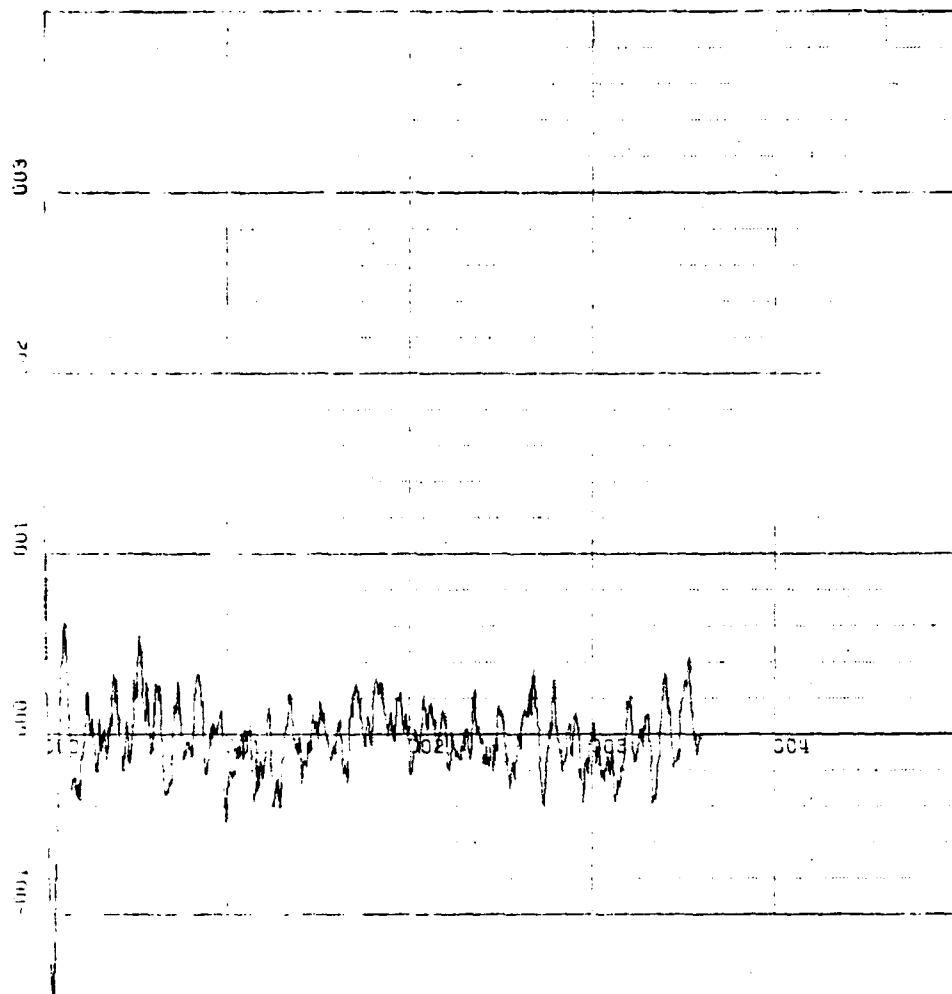
Y-SCALE=5.00E-05 UNITS INCH. [Rad]

KWSTAS

RUN 1

DLAT VS TIME

Figure 76. Theoretical I.N.S./G.P.S., 36-Hour Process.
Y Position Error [Rad].



Y-SCALE=1.00E+01 UNITS INCH. [hours]

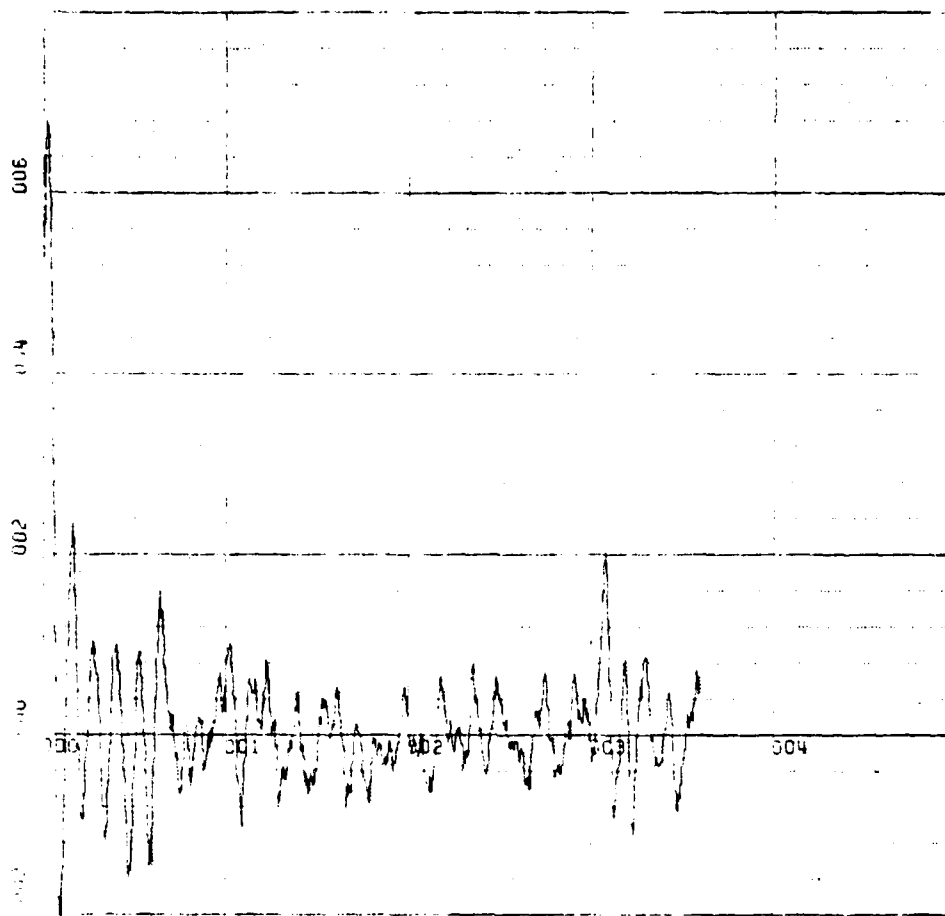
X-SCALE=1.00E-04 UNITS INCH. [Rad]

KWSTPS

RUN 2

DLONG VS TIME

Figure 77. Theoretical I.N.S./G.P.S., 36-Hour Process.
X Position Error [Rad].



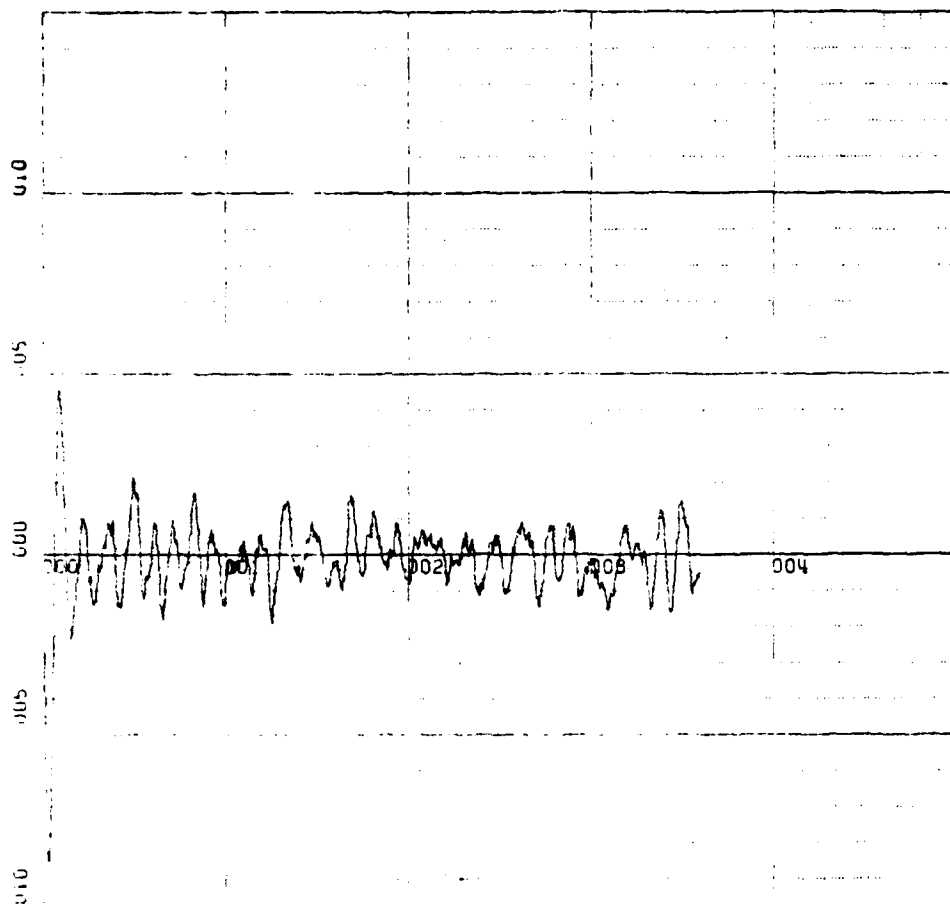
X-SCALE=1.00E+01 UNITS INCH. [hours]
 Y-SCALE=2.00E-04 UNITS INCH. [Rad/hour]

KWSTAS

RUN 2

DILADCT VS TIME

Figure 78. Theoretical I.N.S./G.P.S., 36-Hour Process.
 Y Velocity Error [Rad/hour].



X-SCALE=1.00E+01 UNITS INCH. [hours]

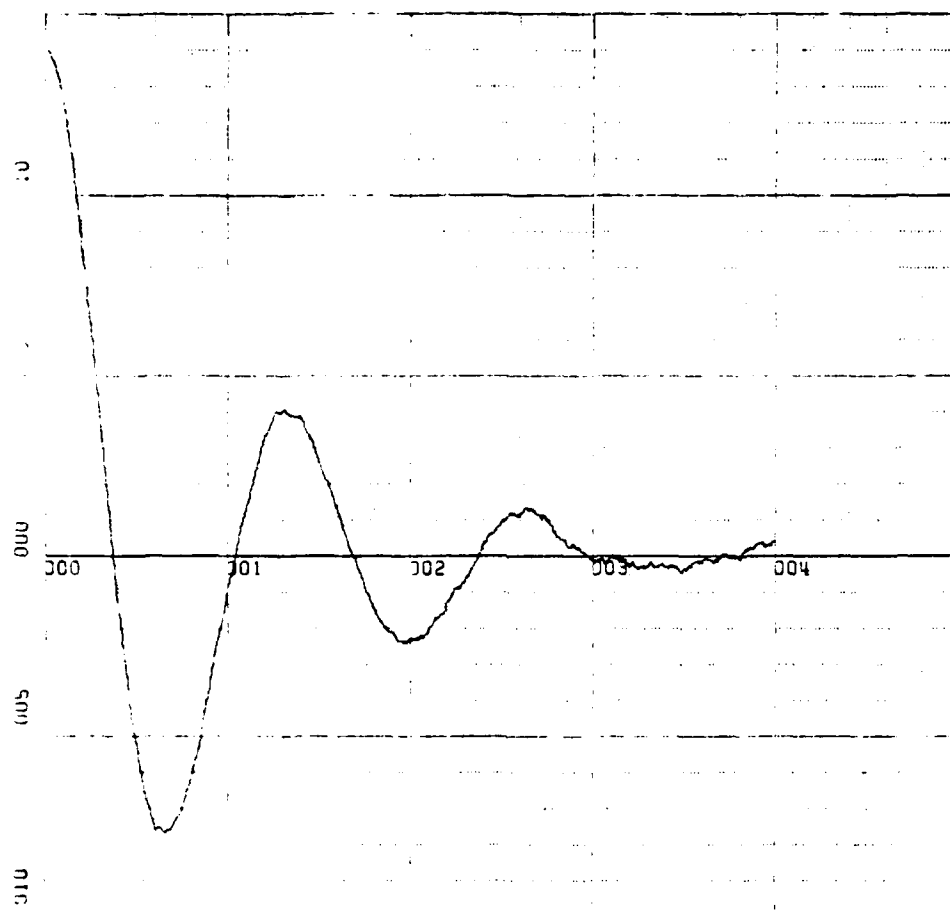
Y-SCALE=5.00E-04 UNITS INCH. [Rad/hour]

KWSTAS

RUN 2

DLONDOT VS TIME

Figure 79. Theoretical I.N.S./G.P.S., 36-Hour Process.
X Velocity Error [Rad/hour].



X-SCALE=1.00E+00 UNITS INCH. [hours]

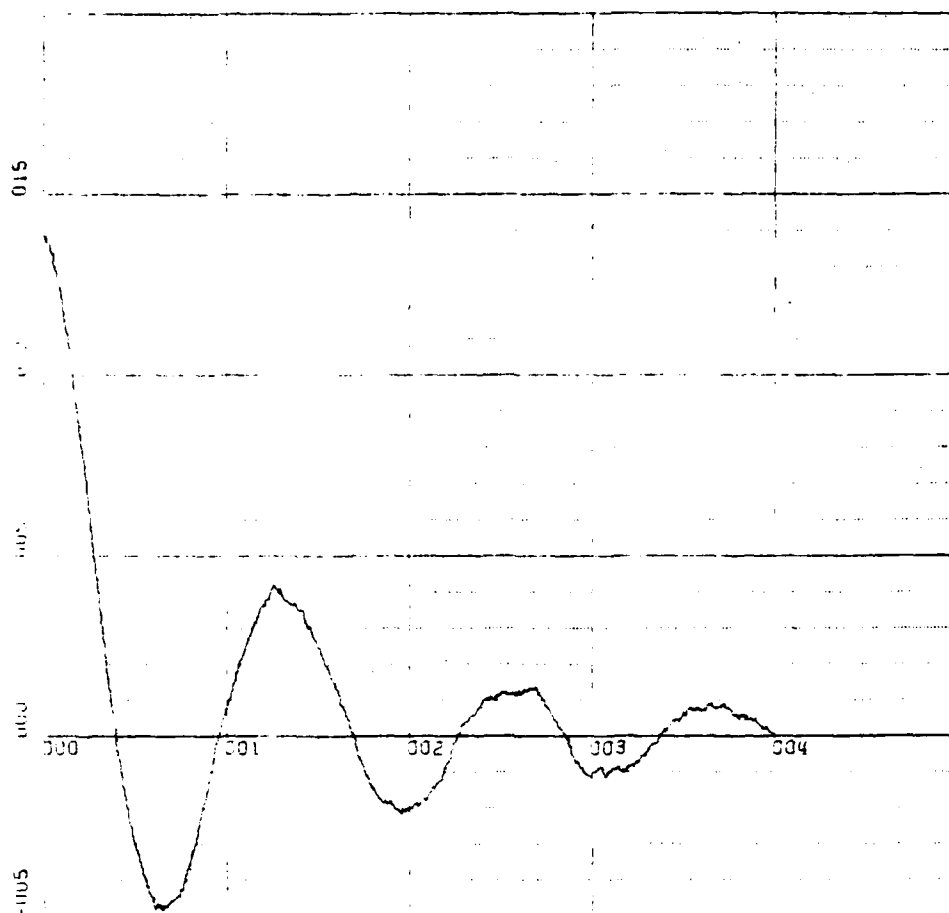
Y-SCALE=5.00E-05 UNITS INCH. [Rad]

KWSTAS

RUN 1

E<N> VS TIME

Figure 80. Realistic I.N.S./G.P.S., 4-Hour Process.
North Attitude Error [Rad].



X-SCALE=1.00E+00 UNITS INCH. [hours]

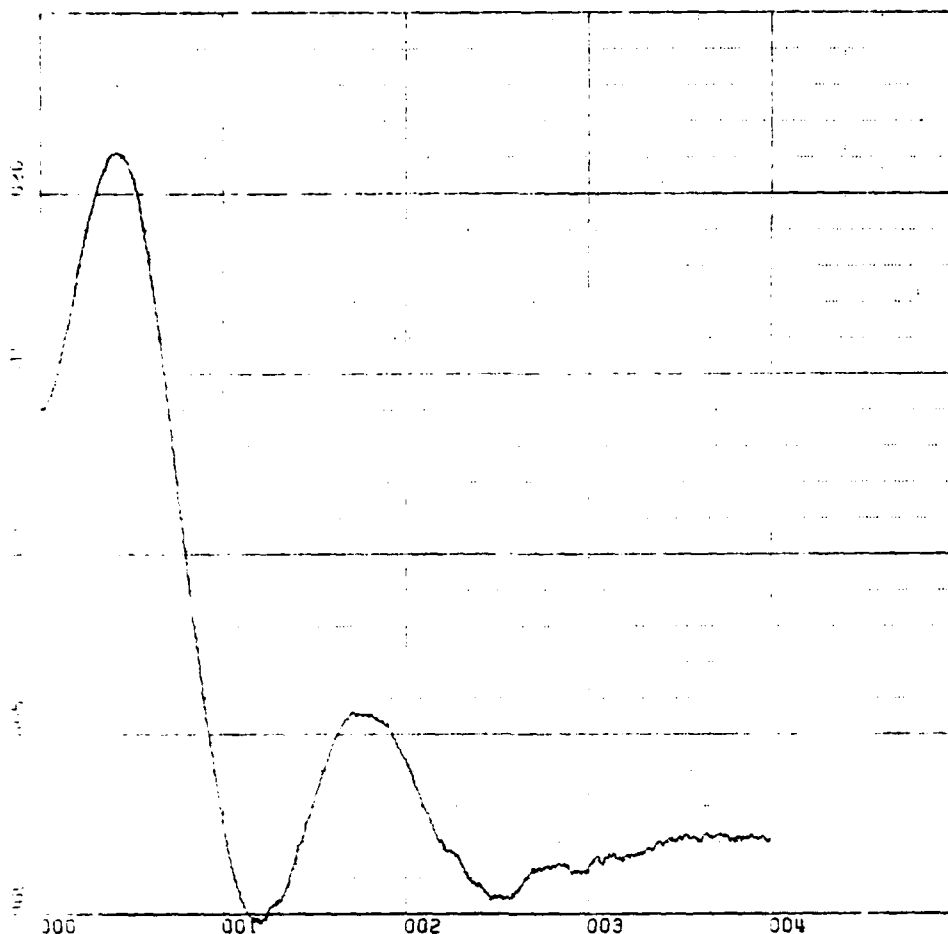
Y-SCALE=5.00E-05 UNITS INCH. [Rad]

KWSTAS

RUN 1

E<E> VS TIME

Figure 81. Realistic I.N.S./G.P.S., 4-Hour Process.
East Attitude Error [Rad].



X-SCALE=1.00E+00 UNITS INCH. [hours]

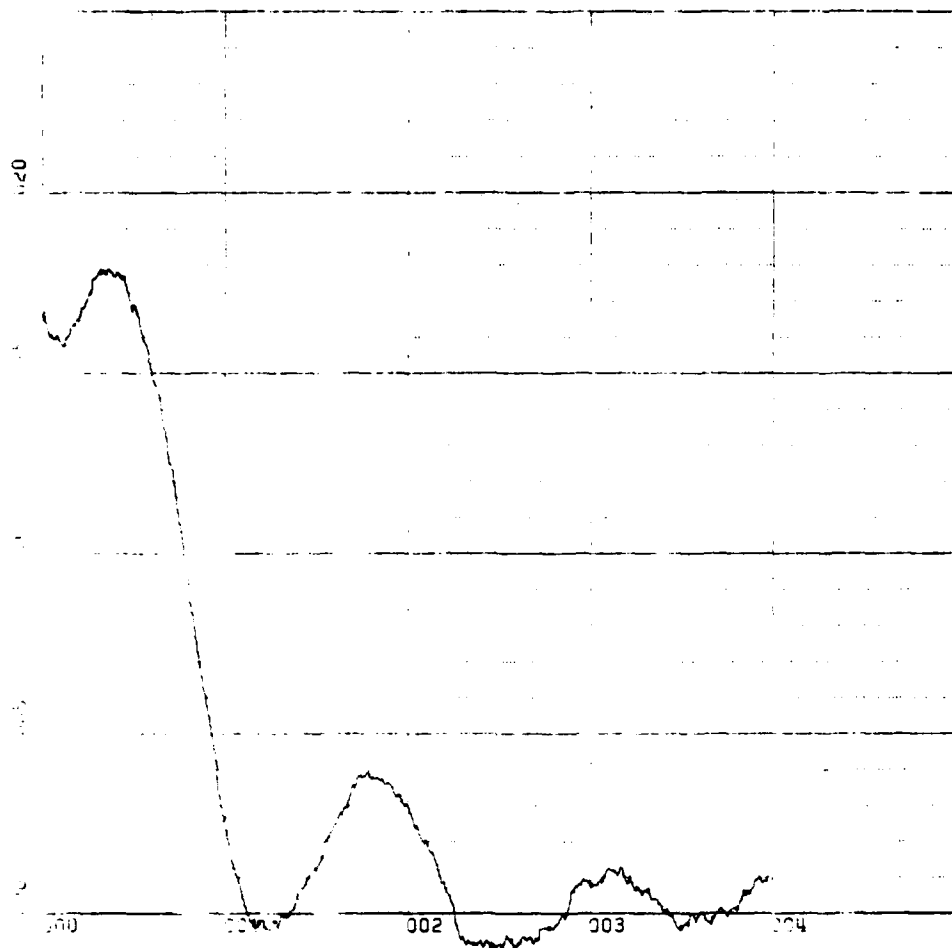
Y-SCALE=5.00E-05 UNITS INCH. [Rad]

KWSTAS

RUN 1

E<D> VS TIME

Figure 82. Realistic I.N.S./G.P.S., 4-Hour Process.
Azimuth Attitude Error [Rad].



SCALE=1.00E+00 UNITS INCH. [hours]

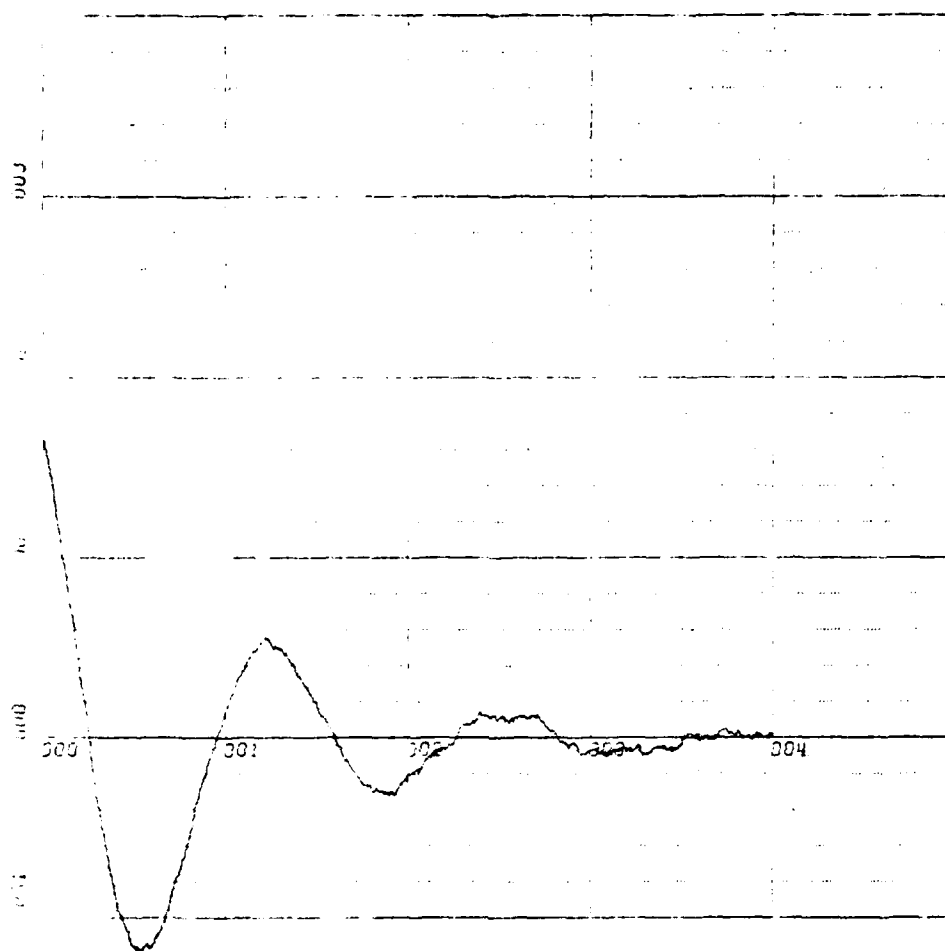
SCALE=5.00E-05 UNITS INCH. [Rad]

KW3TOS

RUN 1

DLAT VS TIME

Figure 83. Realistic I.N.S./G.P.S., 4-Hour Process.
Y Position Error [Rad].



SCALE=1.00E+00 UNITS INCH. [hours]

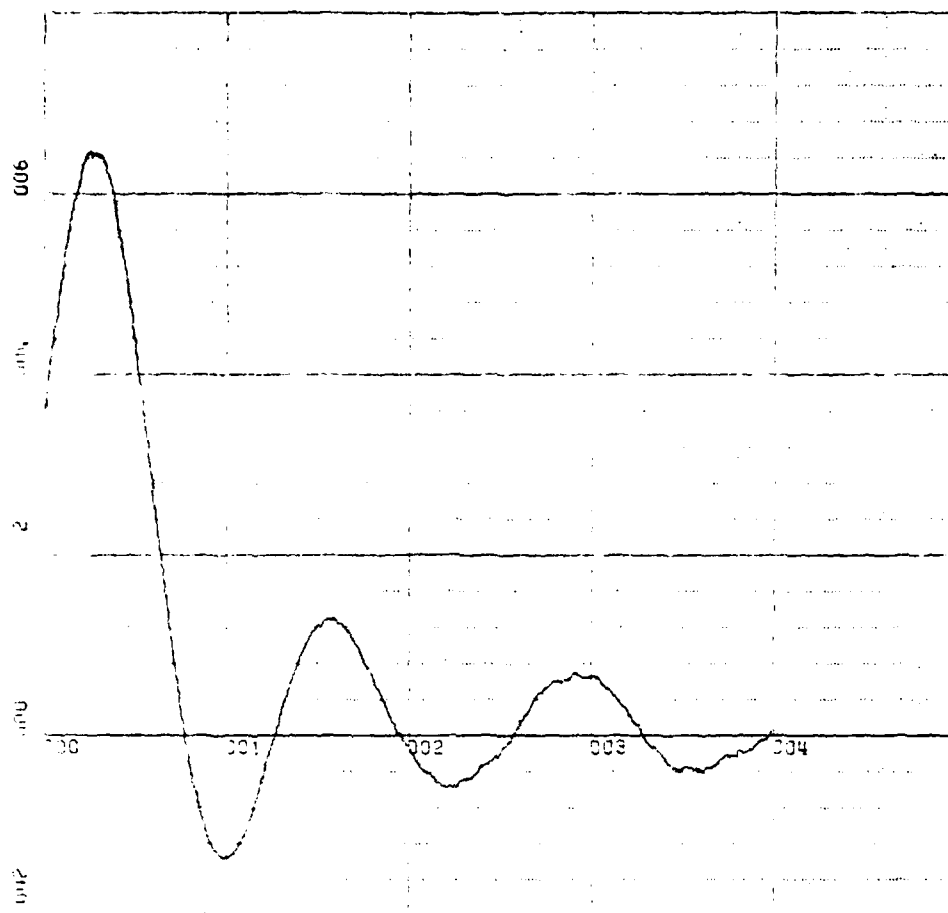
SCALE=1.00E-02 UNITS INCH. [Rad]

ASTAS

RUN 2

DLONG VS TIME

Figure 84. Realistic I.N.S./G.P.S., 4-Hour Process.
X Position Error [Rad].



X-SCALE=1.00E+00 UNITS INCH. [hours]

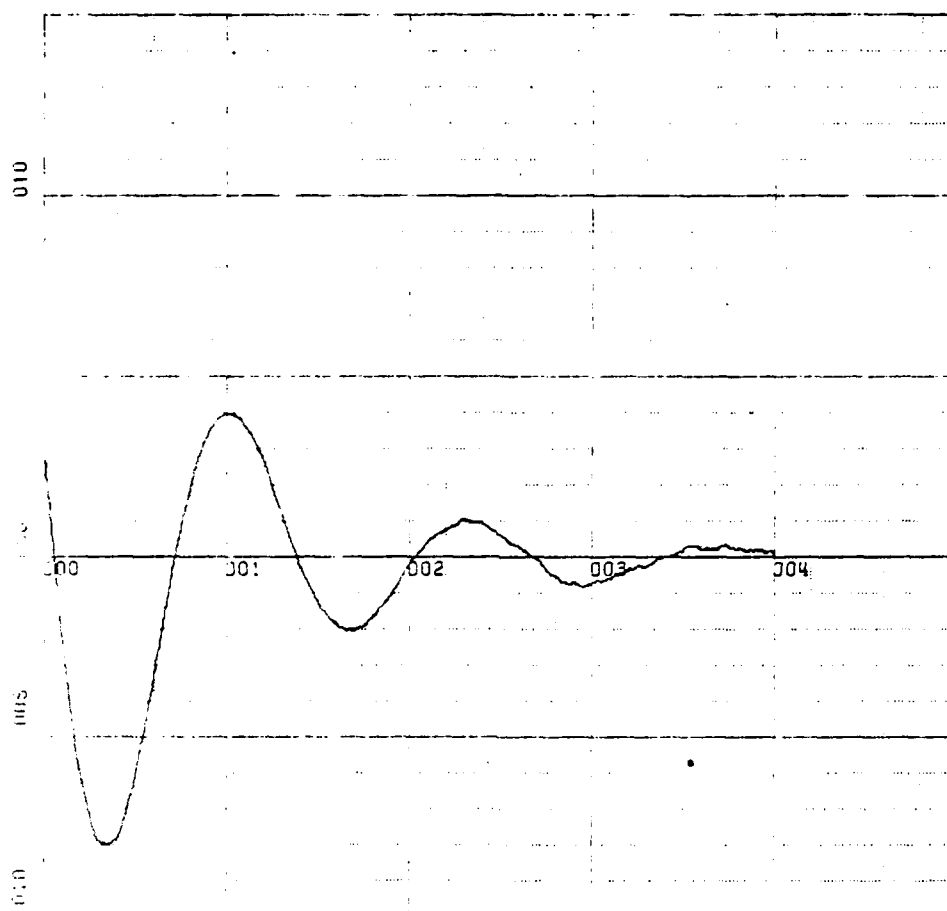
Y-SCALE=2.00E-04 UNITS INCH. [Rad/hour]

KWSTAS

RUN 2

DL=DOT VS TIME

Figure 85. Realistic I.N.S./G.P.S., 4-Hour Process.
Y Velocity Error [Rad/hour].



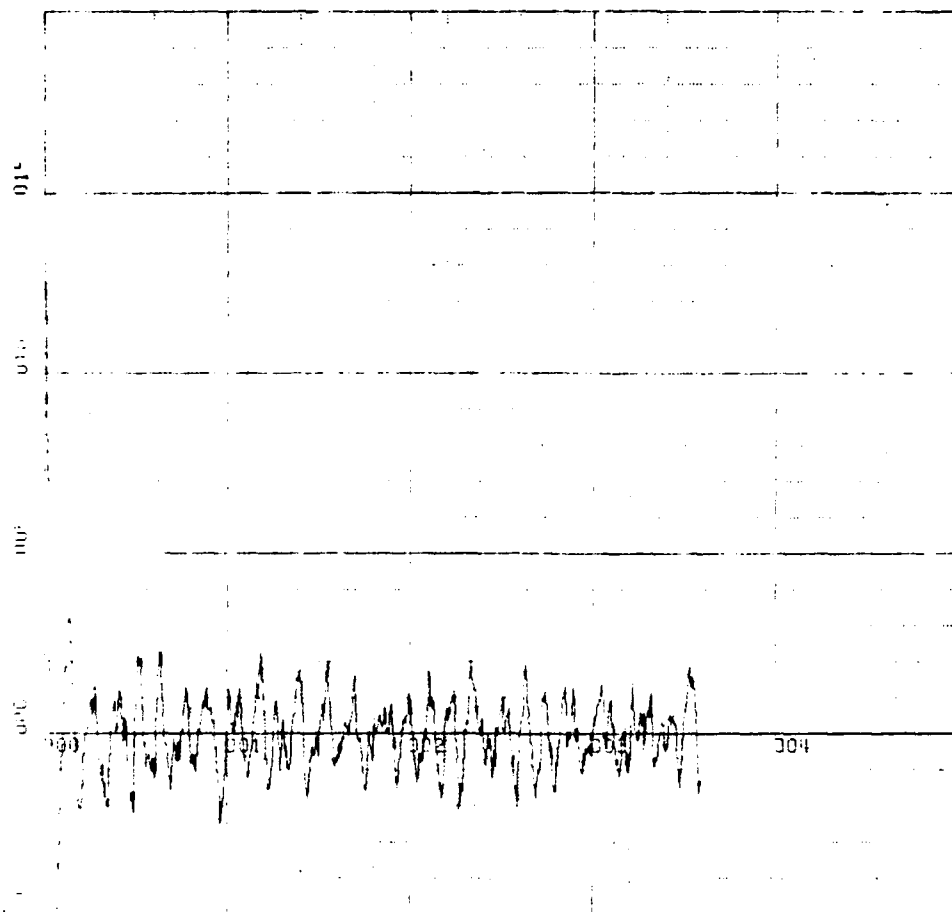
X-SCALE=1.00E+00 UNITS INCH. [hours]
 Y-SCALE=5.00E-04 UNITS INCH. [Rad/hour]

KWSTAS

RUN 2

DLONDOT VS TIME

Figure 86. Realistic I.N.S./G.P.S., 4-Hour Process.
 X Velocity Error [Rad/hour].



X-SCALE=1.00E+01 UNITS INCH. [hours]

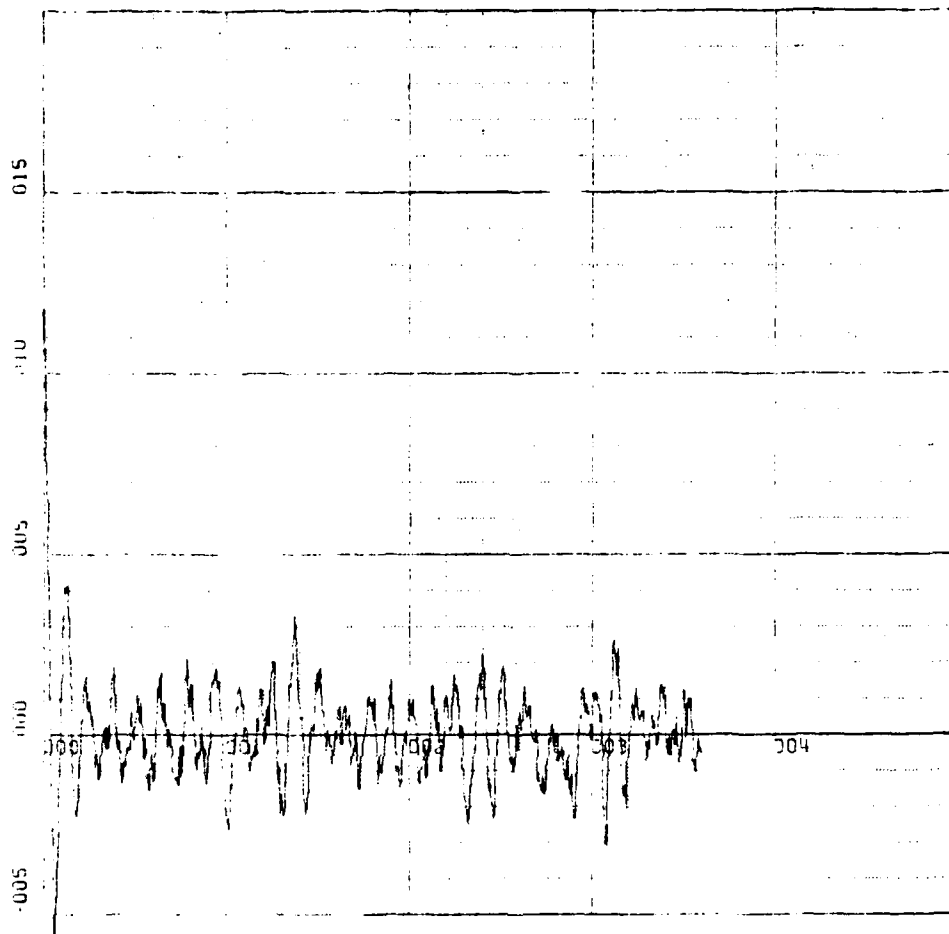
Y-SCALE=5.00E-05 UNITS INCH. [Rad]

WSTAS

RUN 1

E<N> VS TIME

Figure 87. Realistic I.N.S./G.P.S., 36-Hour Process.
North Attitude Error [Rad].



X-SCALE=1.00E+01 UNITS INCH. [hours]

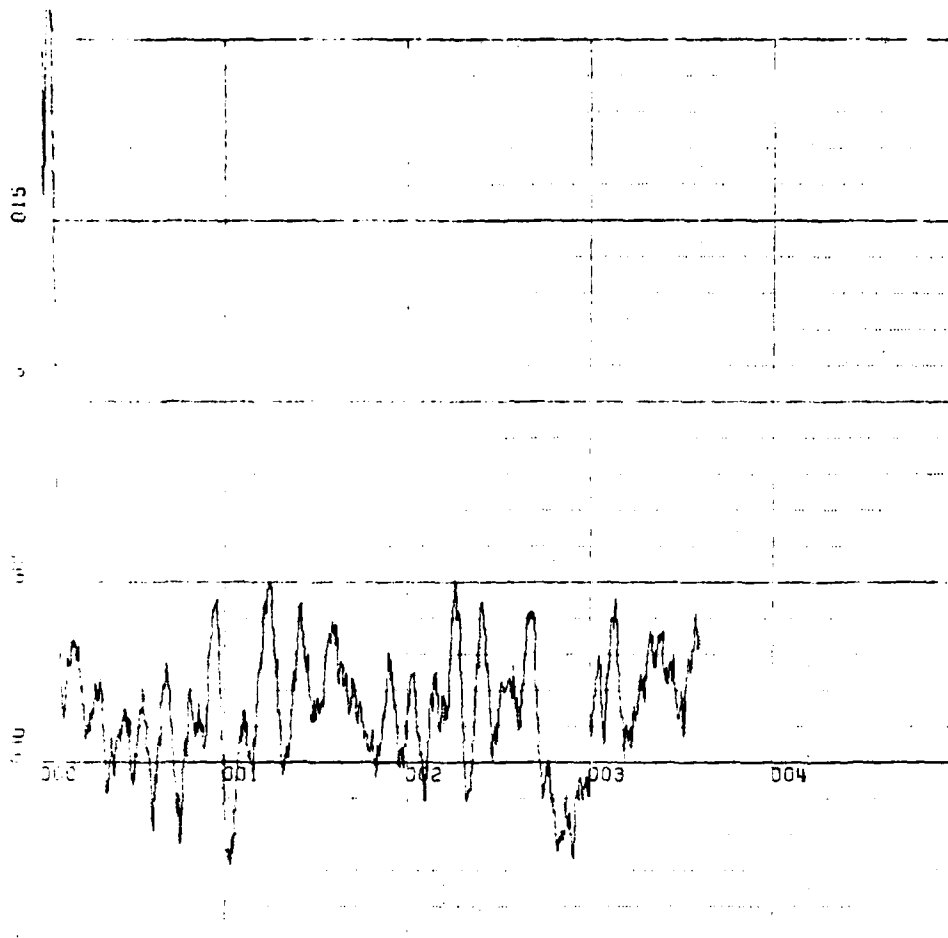
Y-SCALE=5.00E-05 UNITS INCH. [Rad]

KWSTPS

RUN 1

E<E> VS TIME

Figure 88. Realistic I.N.S./G.P.S., 36-Hour Process.
East Attitude Error [Rad].



SCALE=1.00E+01 UNITS INCH. [hours]

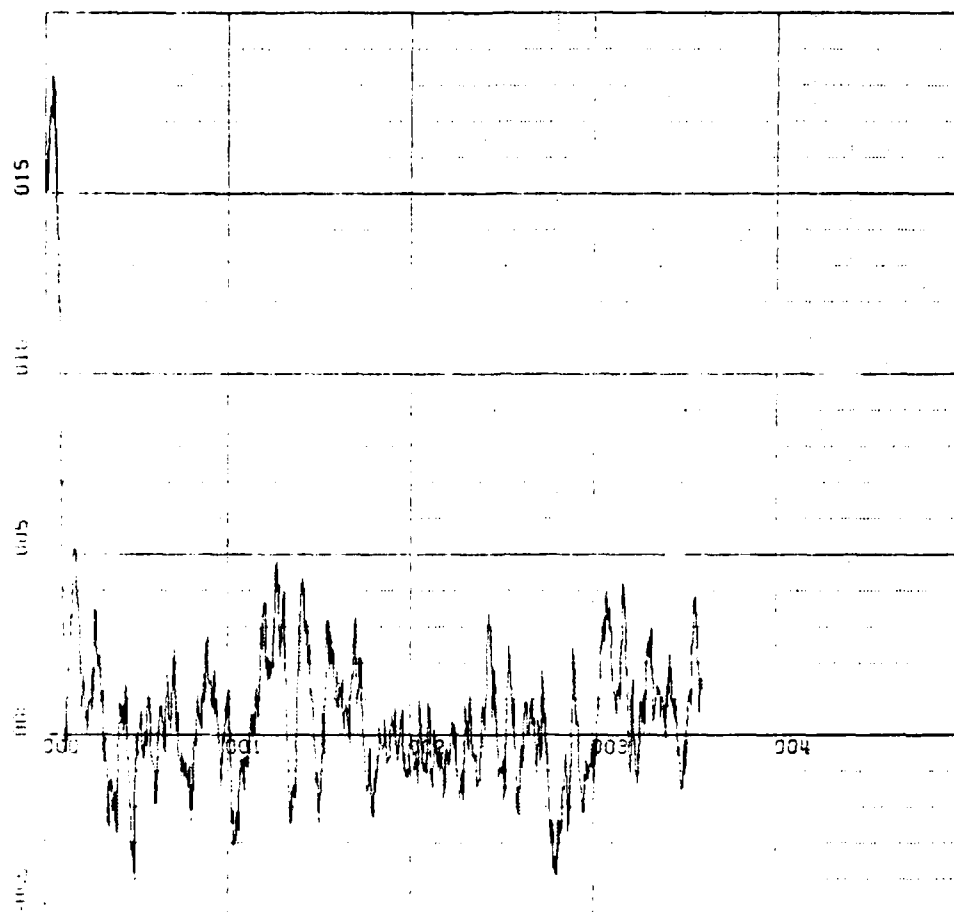
SCALE=5.00E-05 UNITS INCH. [Rad]

AKSTAR

RUN 1

E<L> VS TIME

Figure 89. Realistic I.N.S./G.P.S., 36-Hour Process.
Azimuth Attitude Error [Rad].



X-SCALE=1.00E+01 UNITS INCH. [hours]

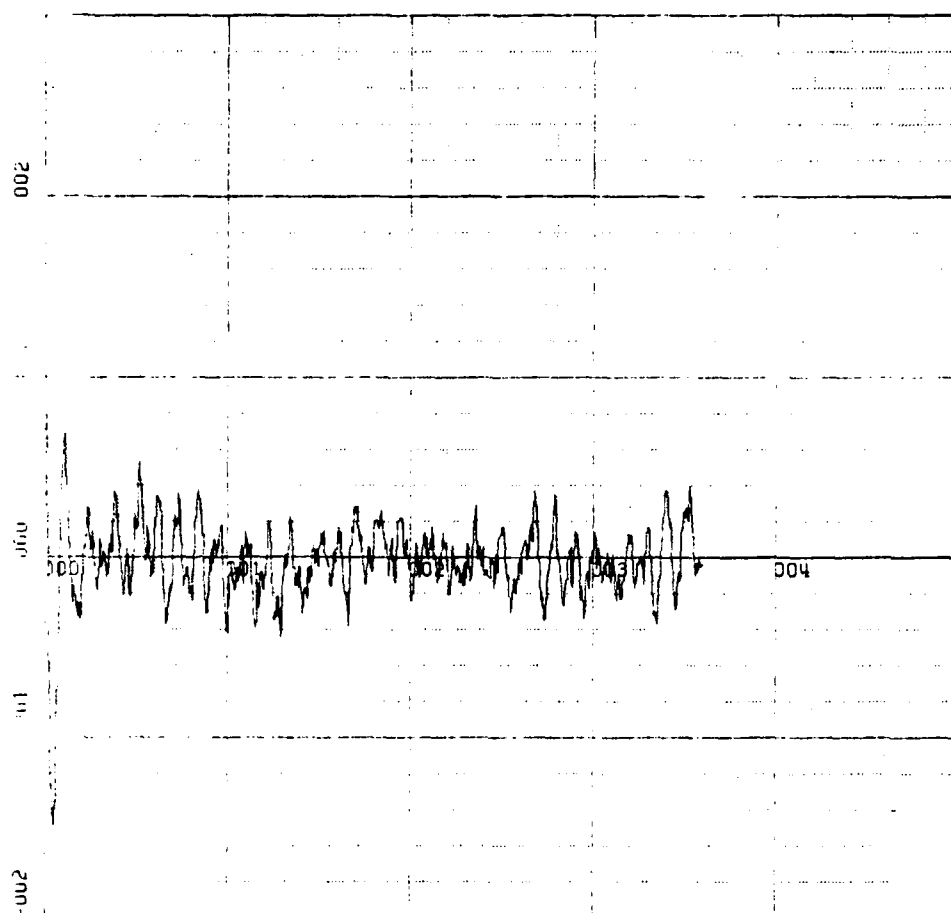
Y-SCALE=5.00E-05 UNITS INCH. [Rad]

KWSTAS

RUN 1

DLAT VS TIME

Figure 90. Realistic I.N.S./G.P.S., 36-Hour Process.
Y Position Error [Rad].



SCALE=1.00E+01 UNITS INCH. [hours]

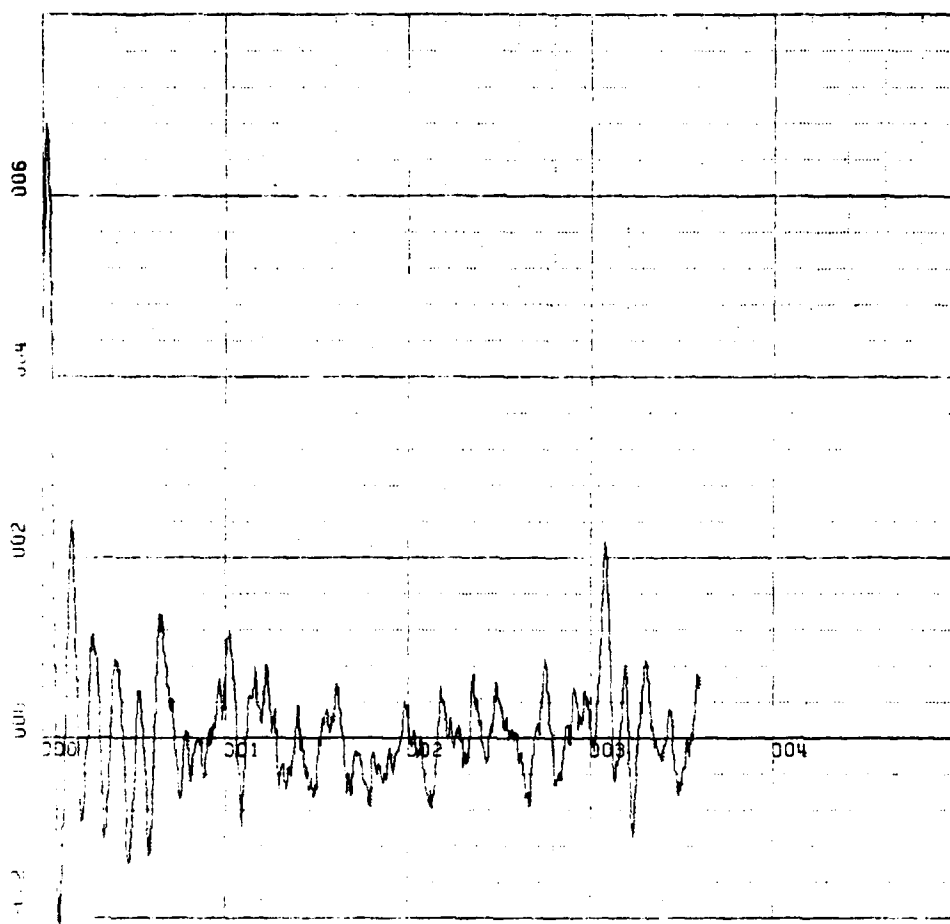
SCALE=1.00E-04 UNITS INCH. [Rad]

KWSTAS

RUN 2

DLONG VS TIME

Figure 91. Realistic I.N.S./G.P.S., 36-Hour Process.
X Position Error [Rad].



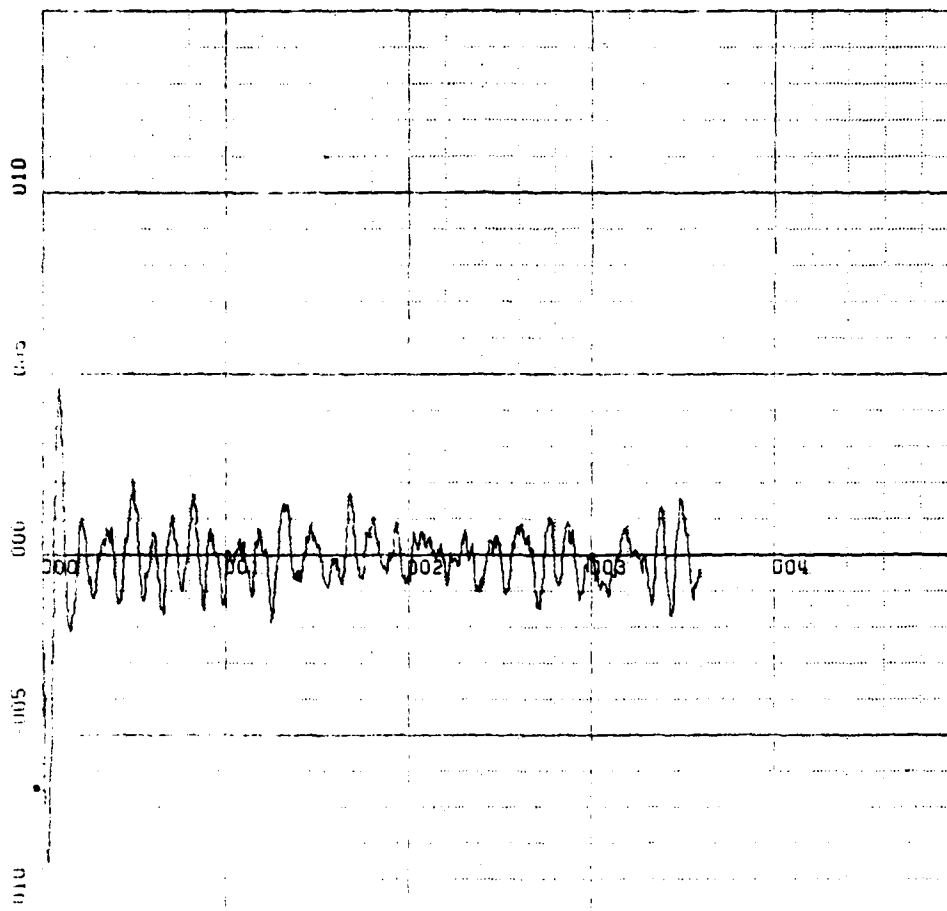
X-SCALE=1.00E+01 UNITS INCH. [hours]
Y-SCALE=2.00E-04 UNITS INCH. [Rad/hour]

KWSTAS

RUN 2

DLADOT VS TIME

Figure 92. Realistic I.N.S./G.P.S., 36-Hour Process.
Y Velocity Error [Rad/hour].

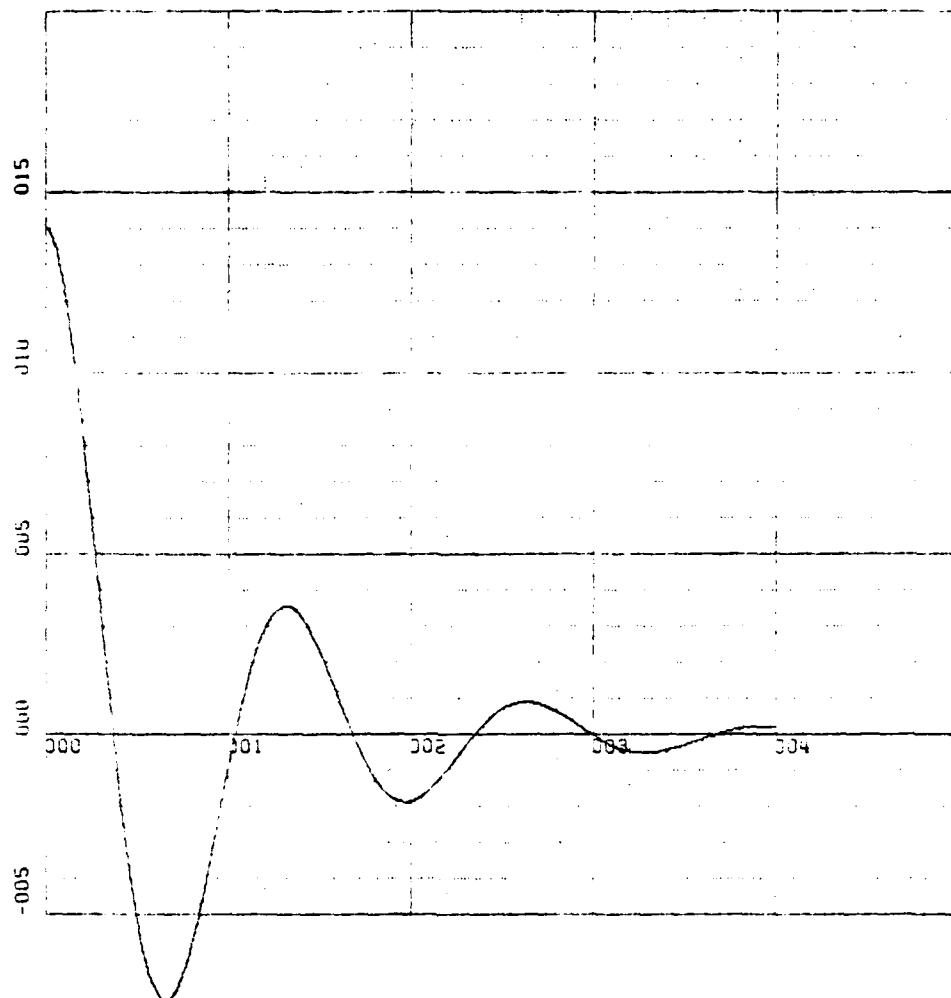


X-SCALE=1.00E+01 UNITS INCH. [hours]
 Y-SCALE=5.00E-04 UNITS INCH. [Rad/hour]

KWSTAS
 RUN 2

DLONDOT VS TIME

Figure 93. Realistic I.N.S./G.P.S., 36-Hour Process.
 X Velocity Error [Rad/hour].



X-SCALE=1.00E+00 UNITS INCH. [hours]

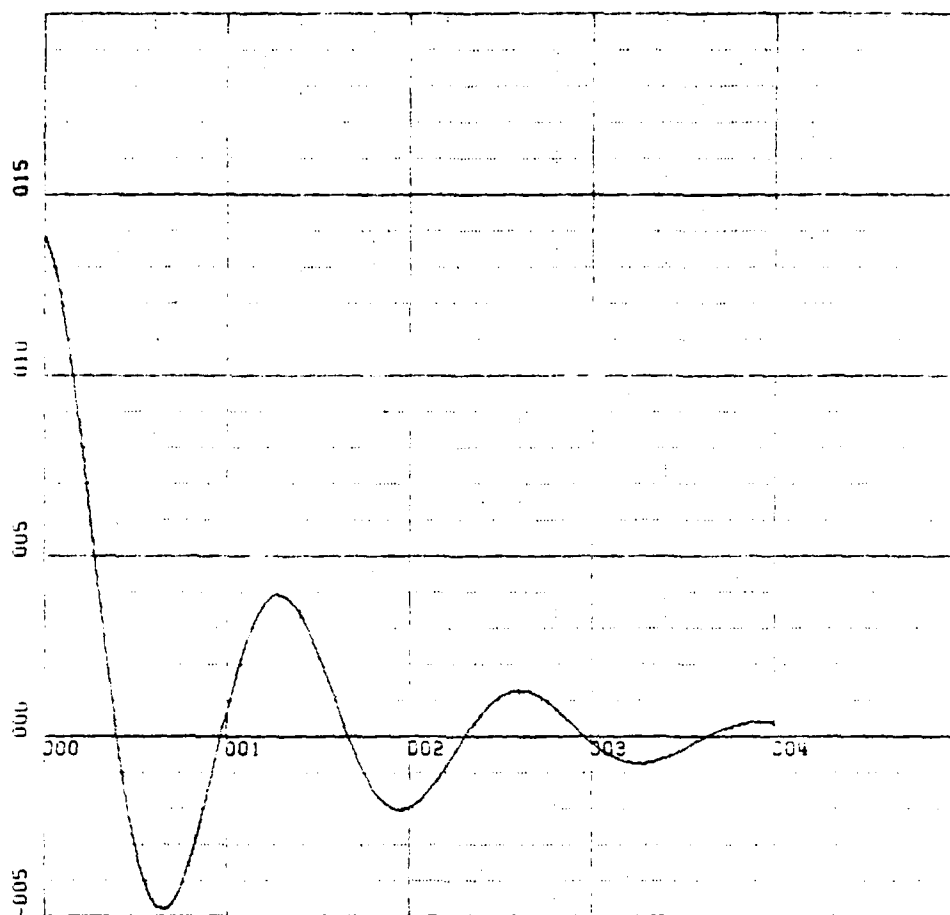
Y-SCALE=5.00E-05 UNITS INCH. [Rad]

KWSTAS

RUN 1

E<N> VS TIME

Figure 94. Realistic I.N.S./G.P.S., Exponentially Correlated Input Noise. 4-Hour Process. North Attitude Error [Rad].



X-SCALE=1.00E+00 UNITS INCH. [hours]

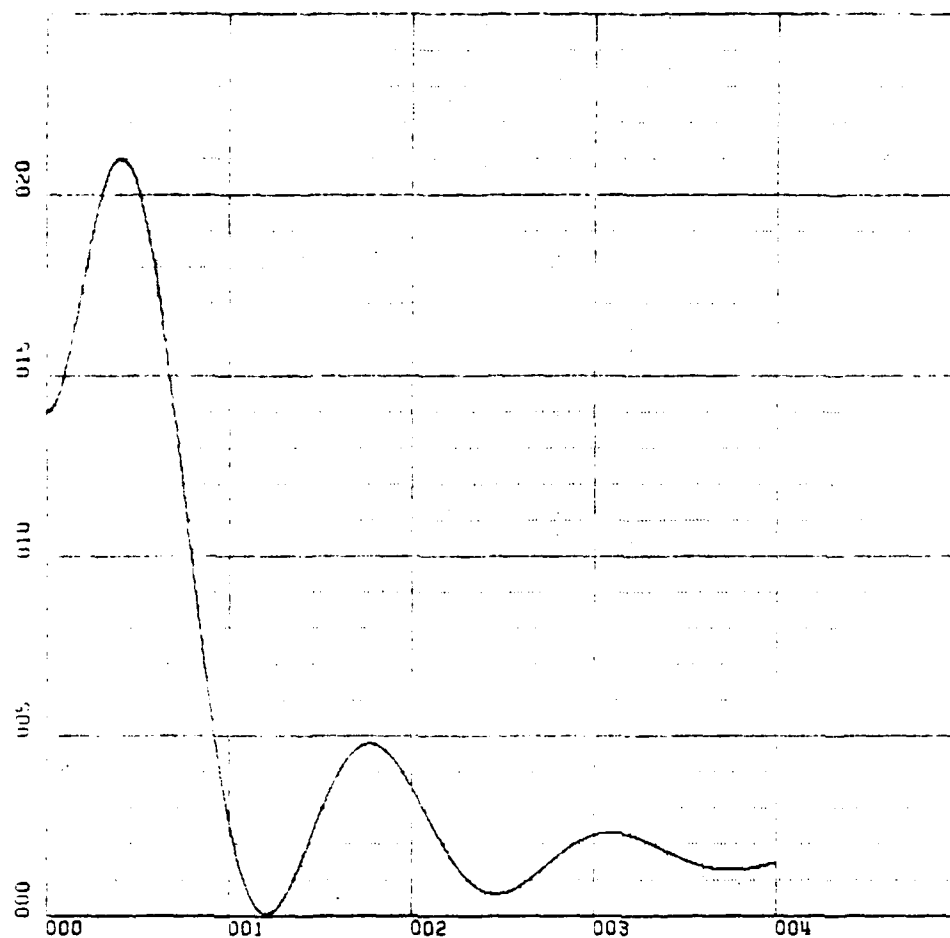
Y-SCALE=5.00E-05 UNITS INCH. [Rad]

KWSTAS

RUN 1

E<E> VS TIME

Figure 95. Realistic I.N.S./G.P.S., Exponentially Correlated
Input Noise. 4-Hour Process. East Attitude
Error [Rad]



X-SCALE=1.00E+00 UNITS INCH. [hours]

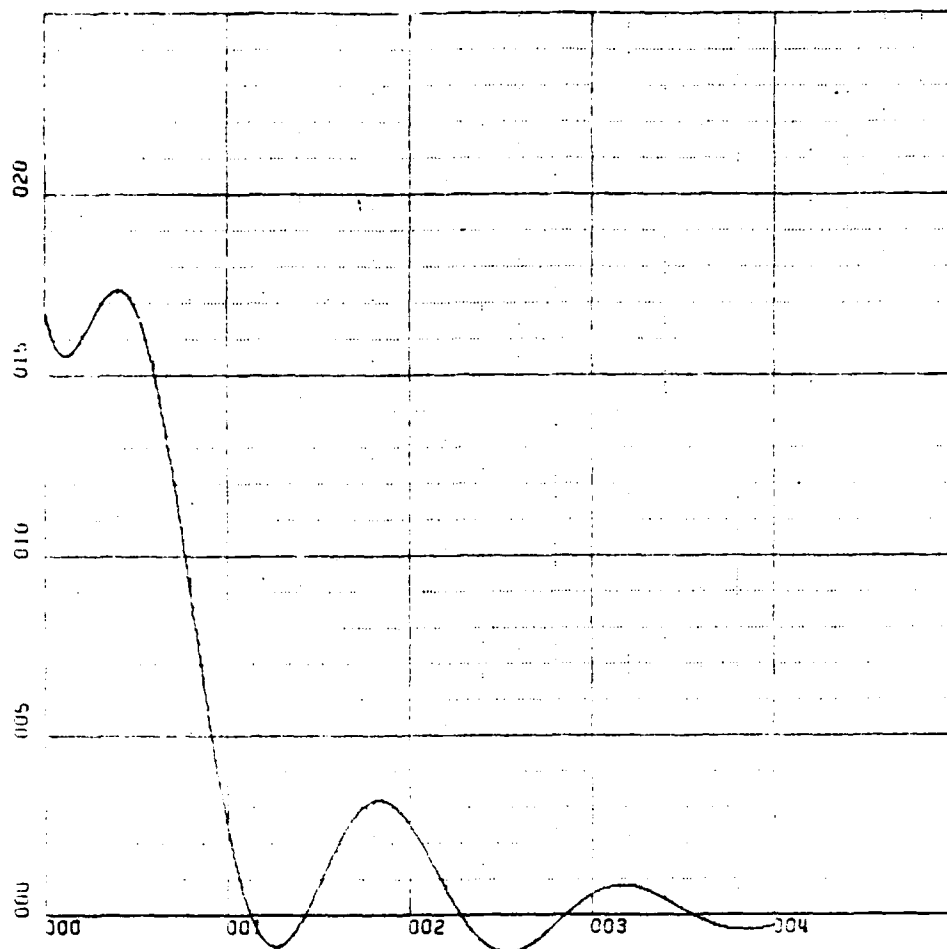
Y-SCALE=5.00E-05 UNITS INCH. [Rad]

KWSTAS

RUN 1

E<D> VS TIME

Figure 96. Realistic I.N.S./G.P.S., Exponentially Correlated Input Noise. 4-Hour Process. Azimuth Attitude Error [Rad].



X-SCALE=1.00E+00 UNITS INCH. [hours]

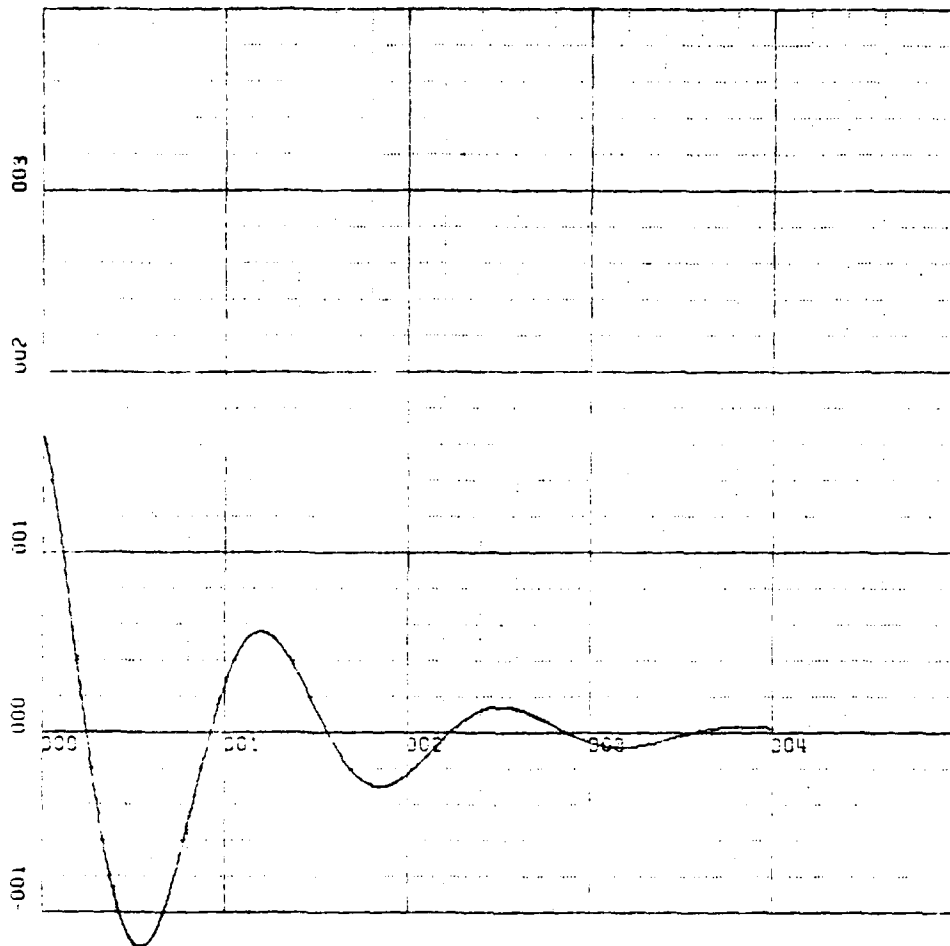
Y-SCALE=5.00E-05 UNITS INCH. [Rad]

KWSTAS

RUN 1

DLAT VS TIME

Figure 97. Realistic I.N.S./G.P.S., Exponentially Correlated Input Noise. 4-Hour Process. Y-Position Error [Rad].



X-SCALE=1.00E+00 UNITS INCH. [hours]

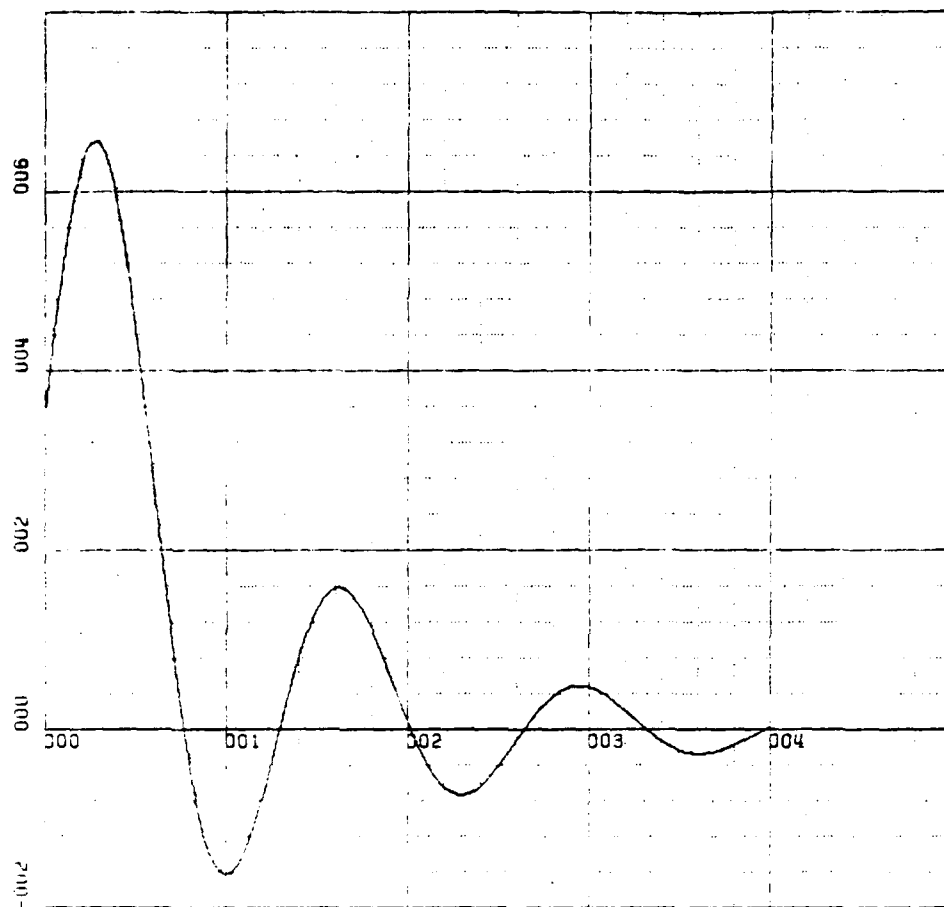
Y-SCALE=1.00E-04 UNITS INCH. [Rad]

KWSTAS

RUN 2

DLONG VS TIME

Figure 98. Realistic I.N.S./G.P.S., Exponentially Correlated
Input Noise. 4-Hour Process. X-Position Error
[Rad].



X-SCALE=1.00E+00 UNITS INCH. [hours]

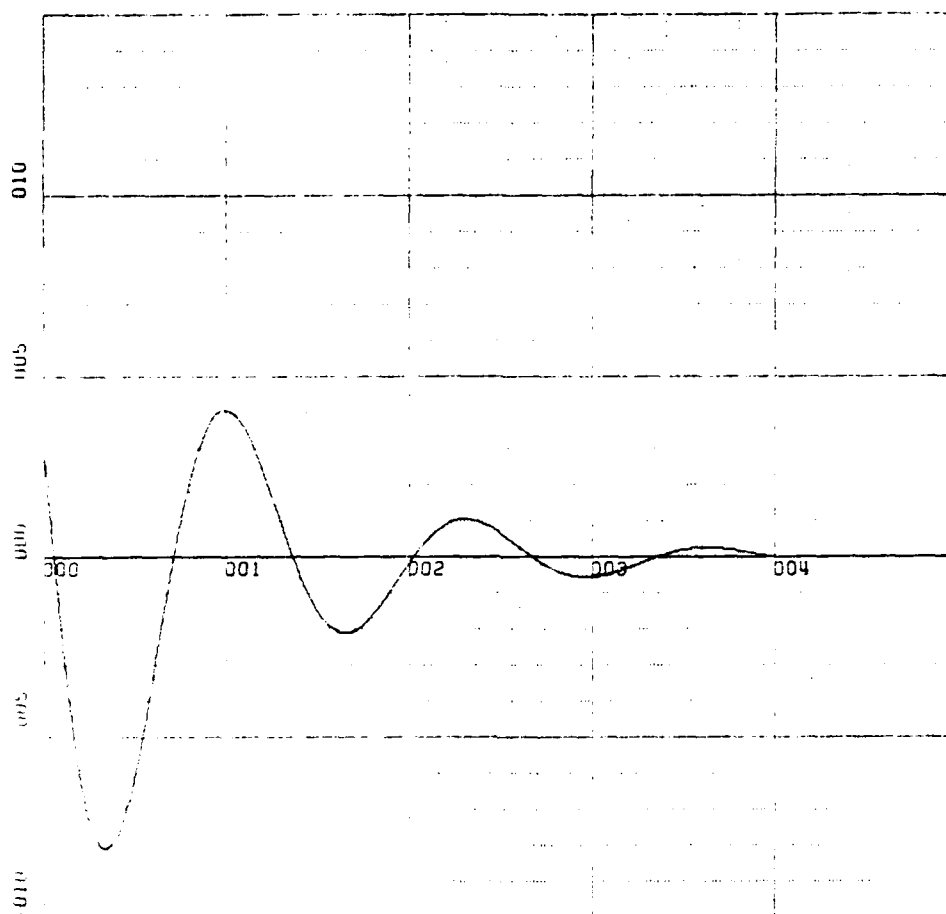
Y-SCALE=2.00E-04 UNITS INCH. [Rad/hour]

KWSTAS

RUN 2

DLADOT VS TIME

Figure 99. Realistic I.N.S./G.P.S., Exponentially Correlated Input Noise. 4-Hour Process. Y-Velocity Error [Rad/hour].



X-SCALE=1.00E+00 UNITS INCH. [hours]

Y-SCALE=5.00E-04 UNITS INCH. [Rad/hour]

KWSTAS

RUN 2

DLONDOT VS TIME

Figure 100. Realistic I.N.S./G.P.S., Exponentially Correlated Input Noise. 4-Hour Process. X-Velocity Error [Rad/hour].

APPENDIX A

A SIMPLE EXAMPLE:

KALMAN FILTER APPLICATION TO A RADAR POSITION AIDED INERTIAL NAVIGATION SYSTEM

I. INTRODUCTION

The application of a Kalman filter to a simplified radar position aided inertial navigation system was investigated as a first step of our study. Since the case appears to be easy to understand difficult concepts and the results prove the design expectations we present hereafter this simple case formulated according to the concepts and the outline of Ref. 2.

The I.N.S. system was modeled as white noise driving a $1/s^2$ plant. Radar measurements were assumed to be available and were similarly corrupted by white noise.

The differential equations describing the system and the Kalman filter were numerically integrated to yield the response for a wide range of input conditions and system noise statistics. Particular attention was paid to conditions in which the noise statistics employed in the filter were different from the statistics of the noise actually driving the system dynamics and measurements.

For all cases considered, including those for which intentional mismatches in the noise statistics were

introduced, the filter was found to perform in an entirely satisfactory manner. This is the filter reliably and quite accurately tracked the system's dynamics even at the presence of at times rather severe levels of noise.

In the section to follow, the theoretical development of the Kalman filter equations will be presented. This development is based on that given in Chapter 6 of Maybeck [Ref.2] and according to explanations given in class notes from Prof. Collins [Ref. 12].

Next, a discussion of simulation results will be given, in which the various cases considered are outlined, and the performance of the filter in each case is described. Finally an overall summary and conclusions regarding the observed performance of the filter over a wide range of test conditions, is presented.

II. I.N.S. AIDED BY POSITION DATA

For this problem, the model of the I.N.S. is simply a double integration of noise-corrupted acceleration information, as depicted in Fig. 101. The noise w is a white Gaussian noise of zero mean and variance Kernel

$$E[w(t)w(t+\tau)] = Q\delta(\tau)$$

entering at the acceleration level, and it is meant to model the errors corrupting the I.N.S. accelerometer outputs (accelerometer biases and noise, platform misalignment,

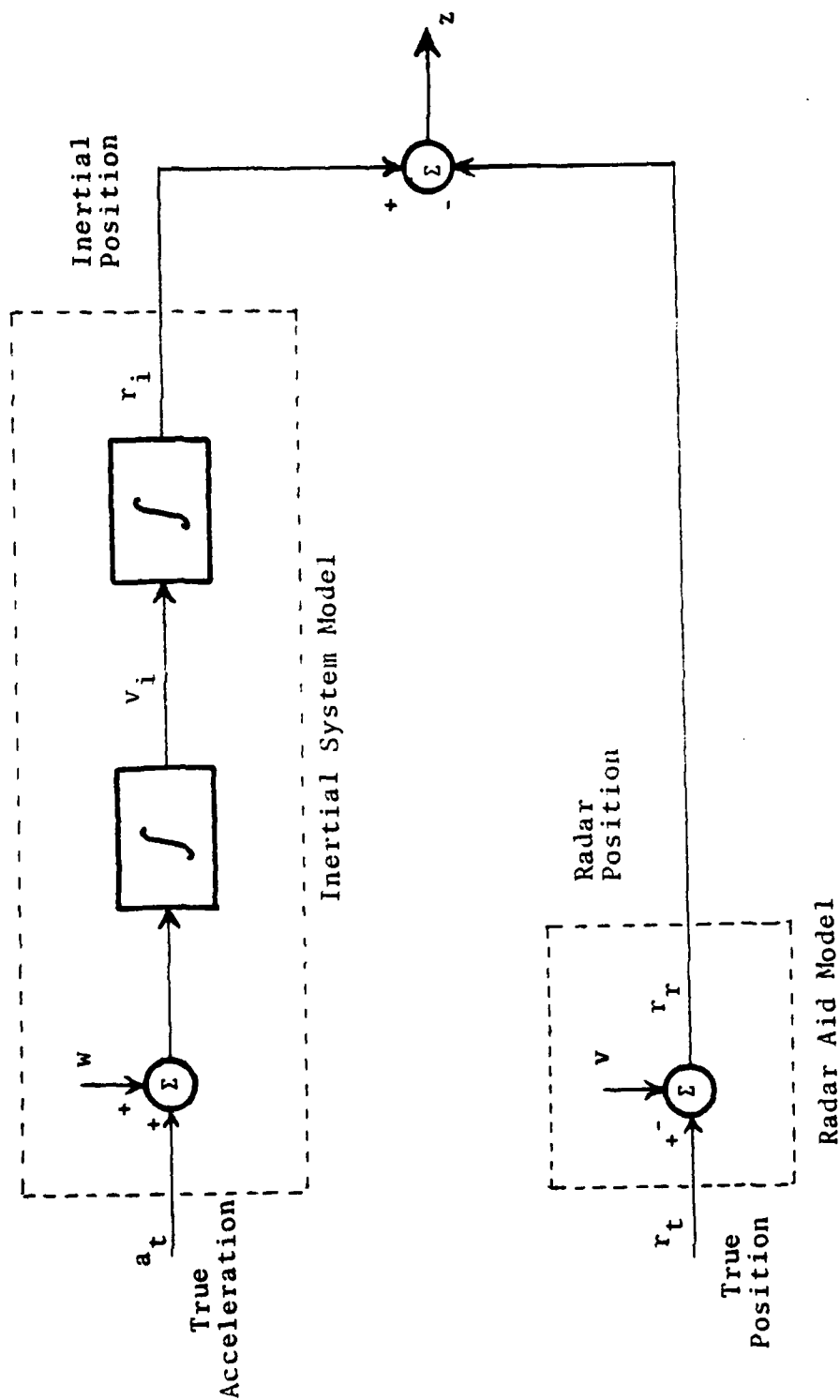


Figure 101. I.N.S. Aided by Position Data.

etc.). The noise-corrupted acceleration is integrated once to yield I.N.S.-indicated velocity (v_i), and a second time to obtain inertially-indicated position (r_i).

Similarly a simple model for the radar or radio navigation aid is the true position (r_t) corrupted by noise u , which is again white Gaussian with zero mean.

The two error state variables for this case are:

$$\delta r(t) = r_i(t) - r_t(t) \quad (A-1)$$

$$\delta v(t) = v_i(t) - v_t(t)$$

The measurement to be presented to the filter is the difference between the inertially indicated position and that measured by the radar or radio navigation aid.

From Figure 96 we have:

$$\begin{aligned} z(t) &= r_i(t) - r_r(t) \\ &= [r_t(t) + \delta r(t)] - [r_t(t) - u(t)] = \quad (A-2) \\ &= \delta r(t) + u(t) \end{aligned}$$

This is a measurement of the error $\delta r(t)$ corrupted by noise $u(t)$.

To establish the state dynamics model for the error states, first let us consider the total states r_i and v_i .

$$\begin{bmatrix} \dot{r}_i \\ \dot{v}_i \end{bmatrix} = \begin{bmatrix} 0 & 1 \\ 0 & 0 \end{bmatrix} \begin{bmatrix} r_i \\ v_i \end{bmatrix} + \begin{bmatrix} 0 \\ 1 \end{bmatrix} [a_t + w] \quad (A-3)$$

The true position velocity and acceleration are related by:

$$\begin{bmatrix} \dot{r}_t \\ \dot{v}_t \end{bmatrix} = \begin{bmatrix} 0 & 1 \\ 0 & 0 \end{bmatrix} \begin{bmatrix} r_t \\ v_t \end{bmatrix} + \begin{bmatrix} 0 \\ 1 \end{bmatrix} a_t \quad (A-4)$$

Subtracting (A-4) from (A-3) and using the error state definitions of (A-1) we find the desired relation as:

$$\begin{bmatrix} \dot{\delta r} \\ \dot{\delta v} \end{bmatrix} = \begin{bmatrix} 0 & 1 \\ 0 & 0 \end{bmatrix} \begin{bmatrix} \delta r \\ \delta v \end{bmatrix} + \begin{bmatrix} 0 \\ 1 \end{bmatrix} w \quad (A-5)$$

The measurement model z can be expressed in terms of errors as:

$$z(t) = [1 \quad 0] \begin{bmatrix} \delta r \\ \delta v \end{bmatrix} + u(t) = \underline{H} \underline{x} + u(t)$$

Since we would like to design a Kalman filter for this situation we need to solve the RICATI equation as below:

$$\dot{P} = FP + PF^T + GQG^T - PH^T R^{-1} HP \quad (A-6)$$

where

$$P = \begin{bmatrix} P_{11} & P_{12} \\ P_{21} & P_{22} \end{bmatrix} \quad \text{and} \quad P_{12} = P_{21}$$

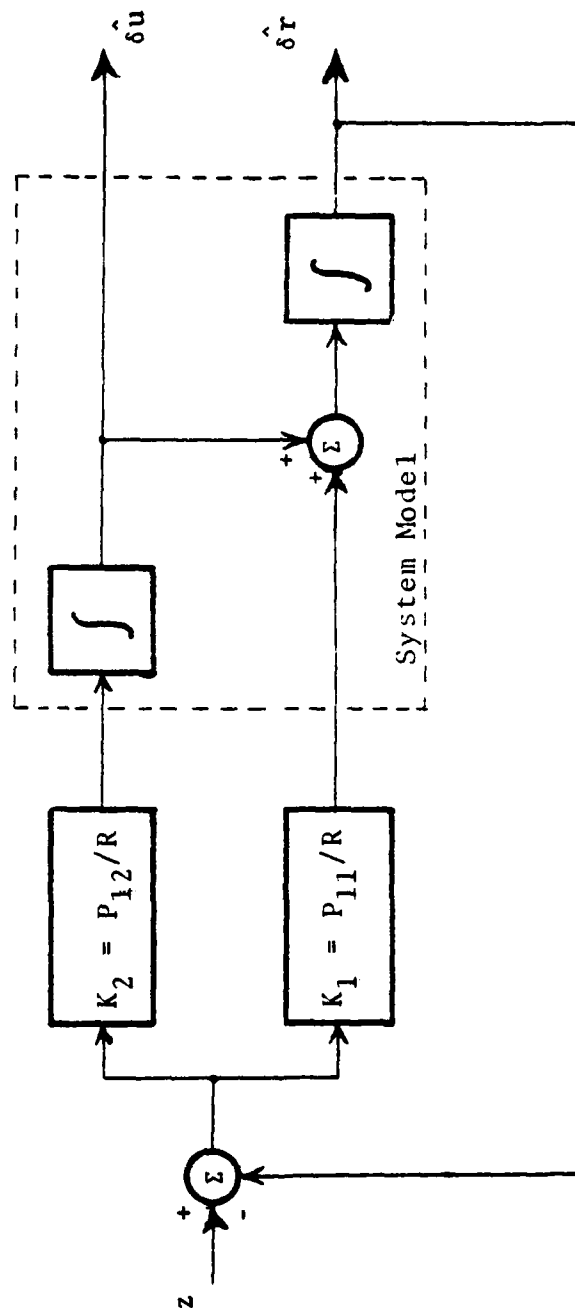


Figure 102. Kalman Filter Block Diagram

$$E[w(t)w(t+\tau)] = Q\delta(\tau)$$

$$E[u(t)u(t+\tau)] = R\delta(\tau)$$

Solving for RICATI equation for our case we get:

$$\begin{bmatrix} \dot{P}_{11} & \dot{P}_{12} \\ \dot{P}_{21} & \dot{P}_{22} \end{bmatrix} = \begin{bmatrix} 2P_{12} - (P_{11})^2/R & P_{22} - P_{11}P_{12}/R \\ P_{22} - P_{11}P_{12}/R & Q - (P_{12})^2/R \end{bmatrix} \quad (A-6a)$$

For the steady state case where $\dot{P} = 0$ we get the elements of covariance matrix in terms of Q , R and the ratio $(Q/R)^{1/4}$ which represents the natural frequency of the system:

$$\begin{aligned} P_{11} &= 2 Q^{1/4} R^{3/4} \\ P_{12} &= Q^{1/2} R^{1/2} = P_{21} \\ P_{22} &= 2 Q^{3/4} R^{1/4} \end{aligned} \quad (A-7)$$

The Kalman filter equation is

$$\dot{\hat{x}} = F\hat{x} + Gu + K(t) [z - H\hat{x}] \quad (A-8)$$

which in terms of error quantities becomes:

$$\begin{bmatrix} \dot{\delta\hat{r}} \\ \dot{\delta\hat{v}} \end{bmatrix} = \begin{bmatrix} 0 & 1 \\ 0 & 0 \end{bmatrix} \begin{bmatrix} \delta\hat{r} \\ \delta\hat{v} \end{bmatrix} + K [z - \delta\hat{r}] \quad (A-9)$$

where $K = PH^T R^{-1} =$

$$= \begin{bmatrix} P_{11} & P_{12} \\ R_{21} & R_{22} \end{bmatrix} \begin{bmatrix} 1 \\ 0 \end{bmatrix} \frac{1}{R}$$

$$= \begin{bmatrix} P_{11}/R \\ P_{12}/R \end{bmatrix} \quad (A-10)$$

and using the results of the RICATI equation solution we can write

$$K = \begin{bmatrix} K_1 \\ K_2 \end{bmatrix} = \begin{bmatrix} 2 \omega_n \\ (\omega_n)^2 \end{bmatrix} \quad \text{where } \omega_n = \left(\frac{Q}{R}\right)^{1/4} [\text{rad/sec}] \quad (A-11)$$

From the above information we can draw the block diagram of the Kalman filter for this system as shown in Figure 102.

The initial transient behavior of the filter gains K_1 and K_2 depends on P_0 , but they are within a few percent of their steady state values (independent of P_0) after $\omega_n t = 2$, so a prediction of time to reach steady state would be approximately $2/\omega_n$ seconds [Ref. 2].

The filter can be put into either feedforward configuration or feedback configuration. Since for our study we use the feedback configuration we present here the outline and the results for this configuration. A block diagram of the system is presented in Figure 103 as depicted in Maybeck's work [Ref. 2]. This block diagram allows us to write the

system's equations which we will simulate numerically to achieve the system's performance.

We define the outputs of the I.N.S. system corrected by feedback from the filter as follows:

$$\begin{aligned}\hat{r}(t) &= r_i(t) - \delta \hat{r}(t) \\ \hat{v}(t) &= v_i(t) - \delta \hat{v}(t)\end{aligned}\tag{A-12}$$

which will be a very helpful mathematical tool since the most straightforward means of generating feedback implementations is to write the system and filter equations in terms of corrected system states. (For our case corrected I.N.S. states.)

Then using the equations (A-3) and (A-9) together with equation (A-8) we can write the matrix form of the system equations as:

$$\begin{bmatrix} \dot{\hat{r}}_t(t) - \delta \dot{\hat{r}}(t) \\ \dot{\hat{v}}_i(t) - \delta \dot{\hat{v}}(t) \end{bmatrix} = \begin{bmatrix} 0 & 1 \\ 0 & 0 \end{bmatrix} \begin{bmatrix} r_i(t) - \delta \hat{r}(t) \\ v_i(t) - \delta \hat{v}(t) \end{bmatrix} + \begin{bmatrix} 0 \\ 1 \end{bmatrix} [a_t(t) + w(t)] - \begin{bmatrix} K_1(t) \\ K_2(t) \end{bmatrix} [z(t) - \delta \hat{r}(t)]\tag{A-13}$$

and finally we get the simple form:

$$\begin{bmatrix} \dot{\hat{r}}(t) \\ \dot{\hat{v}}(t) \end{bmatrix} = \begin{bmatrix} 0 & 1 \\ 0 & 0 \end{bmatrix} \begin{bmatrix} \hat{r}(t) \\ \hat{v}(t) \end{bmatrix} + \begin{bmatrix} 0 \\ 1 \end{bmatrix} [a_t(t) + w(t)] + \begin{bmatrix} K_1(t) \\ K_2(t) \end{bmatrix} [r_r(t) - \hat{r}(t)]\tag{A-14}$$

In the next section the programming and simulation results of the system is presented.

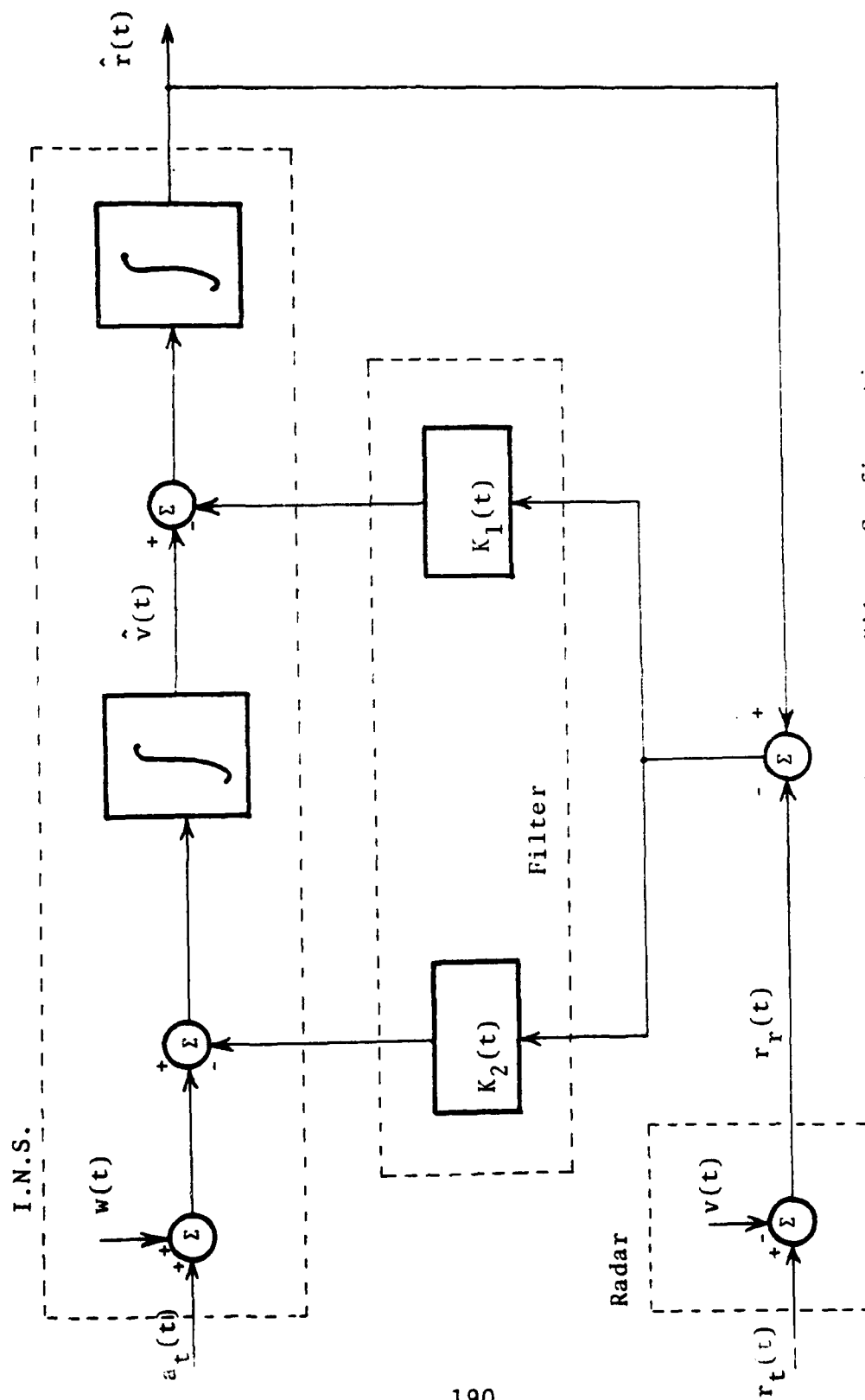


Figure 103. Feedback Kalman Filter Configuration

III. COMPUTER SIMULATION AND RESULTS

We simulated the system for different input signals, different noise characteristics (zero mean Gaussian noise with different variances) to see the effect of the filter for error estimation.

From the block diagram of the system in Figure 103 we can write the following set of equations which we will use to get results by numerical computer simulation.

$$\dot{x}(1) = \dot{r}_t = v_t$$

$$\dot{x}(2) = \dot{v}_t = a_t$$

$$\dot{x}(3) = \dot{r}_i = v_i$$

$$\dot{x}(4) = \dot{v}_i = a_t + w$$

$$\dot{x}(5) = \dot{P}_{11} = 2P_{12} - (P_{11})^2/R$$

$$\dot{x}(6) = \dot{P}_{12} = P_{22} - P_{11}P_{22}/R \quad (A-15)$$

$$\dot{x}(7) = \dot{P}_{22} = Q - (P_{12})^2/R$$

$$\dot{x}(8) = \dot{\delta \hat{r}} = \delta \hat{v} + K_1(z - \delta \hat{r})$$

$$\dot{x}(9) = \dot{\delta \hat{v}} = K_2(z - \delta \hat{r})$$

$$x(15) = r_r = r_t - u$$

$$x(16) = \hat{v} = v_i - \delta \hat{v}$$

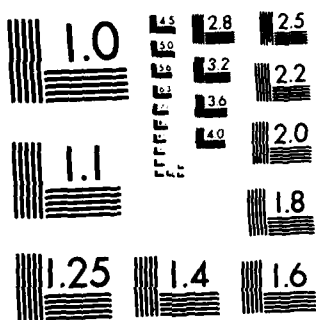
INERTIAL NAVIGATION SYSTEMS AIDED BY GPS(U) NAVAL
POSTGRADUATE SCHOOL MONTEREY CA C C SAFLIANIS DEC 82

3/4

F/G 17/7

NL

[illegible]



MICROCOPY RESOLUTION TEST CHART
NATIONAL BUREAU OF STANDARDS-1963-A

$$x(17) = \hat{r} = r_i - \delta \hat{r}$$

$$x(18) = K_2 = P_{12}/R$$

$$x(19) = K_1 = P_{11}/R$$

$$x(20) = z = r_i - r_t + u$$

$$x(21) = w$$

$$x(22) = u$$

The above set of differential equations of the I.N.S. system and feedback Kalman filter were numerically integrated using INTEG2 computer routine in conjunction with a routine (LNORM) for generating Gaussian distributed random numbers to represent the noise into the system. Typical simulation runs used an integration step size of 0.01 seconds and a total run time of 36 seconds by which point the filter had easily achieved steady-state operation in most cases.

Shown on the next page is a run summary representing the various conditions that were tested. For each of six cases, the covariances of the measurement noise (R) and process noise (Q) are indicated. Note that in a number of cases, the noise statistics used in the filter were chosen to be different from those characterizing the input noise entered into the system. This intentional "mismatch" was done to

investigate filter performance under conditions where the true "real world" noise statistics are inadequately or poorly known.

In particular it was desired to determine whether any instances of filter "divergence" could be observed as a result of the mismatch in system noise statistics. It is noteworthy that for all conditions tested, the filter performed in an entirely satisfactory manner with no evidence of divergence.

It should be noted here that in Table XI the noise covariances Q and R actually represent the statistics of Discrete Noise entering the system at the integration interval $\Delta t = 0.01$ seconds. That is:

$$Q = E[w_k w_k^T] \quad \text{where } t_k = k\Delta t$$

$$R = E[u_k u_k^T]$$

As it is pointed out by Bryson and Ho [Ref. 13] the numerical integration is a discrete approximation to a continuous system whose noise processes have spectral densities given by

$$E[w(t)w(\tau+t)] = Q'\delta(\tau)$$

$$E[u(t)u(\tau+t)] = R'\delta(\tau)$$

The relation between Q and Q' and R and R' is according to Bryson:

$$Q' = Q \cdot \Delta t$$

$$R' = R \cdot \Delta t$$

Also shown in Table XI for each case, are the filter natural frequency and the steady-state values of the Kalman gains.

A brief discussion will now be given of the results for each of the six cases. Detailed plots of the variables of interest for each case are attached and will be referred to in the subsequent discussion.

1. Case I

For this case we used $R = 10,000$ and $Q = 1$ for the filter. The actual noise however is mismatched with $R_t = 100$ and $Q_t = 1$ and thus the filter assumes the measurement noise of the radar position data considerably higher than the case is actually. Shown in the attached plots on Figures 104 and 105 is the type of noise actually entered into the system using a Gaussian random number generator. Also shown are the histories of the Kalman filter gains K_1 and K_2 versus time. The performance of the filter for this case is outstanding as evidenced by the two plots for Case I in Figures 108 and 109. Here the estimated position out of the filter coincides with the true position

denoting that the filter tracks the system extremely well. Among the other attached plots, Figure 112 presents the noise corrupted radar position in a very imposing way.

2. Case II

This case represents one in which the filter and external noise are "tuned" so that the same noise statistics are employed with $R = 100$ and $Q = 25$. Again the Kalman gains are plotted indicating the time of steady-state condition in Figure 114 and 115. As it is depicted from Figures 116, 117 and 118 the Kalman filter rapidly "locks-on" to the true position and velocity and accurately tracks the system thereafter.

3. Case III

In this case the filter and external noise are "tuned" with $R = 100$ and $Q = 1$. The system's initial conditions now include a 10 ft/sec^2 constant acceleration and it was desired to see how well the Kalman filter kept up with the changing input. Once again the performance of the filter in accurately tracking the system is excellent. This can be verified looking at Figures 124 and 125 and 126 and 127 respectively where we can see the coincidence of the true and estimated position and velocity.

4. Case IV

For this run the filter and external noise are again "tuned" but with increased statistics of $R = 400$ and $Q = 50$.

The attached set of plots in figures 131 through 138 present the system and the filter operation proving the accurate and satisfactory tracking of the system

5. Case V

Now the filter perceives the radar measurement noise to be higher than it actually is. The statistics used for this case were $R = 400$ and $Q = 50$ for the filter while for the external noise we used $R_t = 50$ and $Q_t = 50$. The reliability and the accuracy of the system is again depicted in the attached plots for Case V in Figures 139 through 146.

6. Case VI

In the last case considered the statistics of the random process noise exciting the I.N.S. accelerometers was mismatched with that assumed in the filter. Here we used $Q_t = 50$ and $Q = 10$. The radar measurement noise $R_t = R = 400$ was assumed the same. The set of plots in Figures 147 through 154 indicate very good performance of the filter despite the intentional mismatch introduced for the system driving noise.

IV. CONCLUSIONS

Following the development of Reference 2, simplified equations characterizing the Kalman filter were derived and numerically integrated to yield the filter response to a wide range of input conditions and system noise statistics. Particular attention was paid to conditions in which the

noise statistics employed in the filter differed from the statistics of the noise records actually driving the system dynamics and measurements.

For all cases considered including those for which intentional mismatches in the noise statistics were introduced, the filter was found to perform in an entirely satisfactory and reliable manner. By that is meant that the filter very accurately tracked the system dynamics even in the presence of at times rather severe levels of noise.

Examination of typical time histories for the variables of interest, showed that the filter Kalman gains K_1 and K_2 rapidly settled to their theoretical steady state values within a time short compared to the average run time. This was accompanied by the filter range and velocity estimates rapidly locking on to the true system position and velocity and accurately tracking it thereafter.

It is concluded then that the Kalman filter configuration discussed here above performed extremely well over the range of conditions considered.

TABLE VIII
COMPUTER RUNS SUMMARY

CASE	R [ft] ²	Filter	R _t [ft] ²	True	ω_n rad/sec	(K ₁) _{ss}	(K ₂) _{ss}
		Q [$\frac{\text{ft}}{\text{sec}^2}$] ²		Q _t [$\frac{\text{ft}}{\text{sec}^2}$] ²			
I	10,000	1	100	1	0.100	0.141	0.010
II	100	25	100	25	0.707	1	0.500
III ¹	100	1	100	1	0.316	0.447	0.100
IV	400	50	400	50	0.595	0.841	0.354
V	400	50	50	50	0.595	0.841	0.354
VI	400	10	400	50	0.398	0.562	0.158

Initial Conditions:

Position = 200 ft

Velocity = 50 ft/sec

Acceleration = 0

$P_{11} = P_{22} = 10^4$, $P_{12} = P_{21} = 0$

ω_n = Natural frequency = $[Q/R]^{1/4}$

R = Measurement noise covariance used in filter

Q = Process noise covariance used in filter

R_t = True measurement noise covariance

Q_t = True process noise covariance

(K₁)_{ss} = Steady state gain $K_1 = 2 \omega_n$

(K₂)_{ss} = Steady state gain $K_2 = [\omega_n]^2$

¹For this case system assumed to have constant acceleration 10 ft/sec².

```

C CC CC CC CC CC CC
//K$ST$S JCB (2211,1116), 'KWSTAS', CLASS=A
//*MAIN ORG=NPVMI, 2211P, LINES=(10)
//*FORMAT PR, DDNAME=K$ST$, DEST=LOCAL
//*FORMAT PR, DDNAME=PLOT, SYSVECTR, DEST=LOCAL
// EXEC FTXCLGP
//FORT, SY$IN DD *
DIMENSION X(30), XDOT(30), C(15)

```

```

IX=6758756

```

```

C(10) = 1.

```

```

1 CALL LNORM(IX,W,1,16807,0)
CALL LNORM(IX,V,1,16807,0)
CALL INTEG2(T,X,XDOT,C)

```

```

EQUATIONS

```

```

XDOT(1) = X(2)
XDOT(2) = C(5)
XDOT(3) = X(4)
XDOT(4) = 2.*X(6) + X(21)
XDOT(5) = C(5) - (X(5)*X(6)/C(1))
XDOT(6) = X(7) - (X(5)*X(6)/C(1))
XDOT(7) = C(2) - (X(6)*X(2)/C(1))
XDOT(8) = X(9) + X(19)*X(20) - X(8)
XDOT(9) = X(18)*X(22)
X(15) = X(1) - X(9)
X(16) = X(4) - X(8)
X(17) = X(3)/C(1)
X(18) = X(6)/C(1)
X(19) = X(5) - X(3)
X(20) = W * SQRT(C(3))
X(21) = X(1) + X(22)
X(22) = W * SQRT(C(3))

```

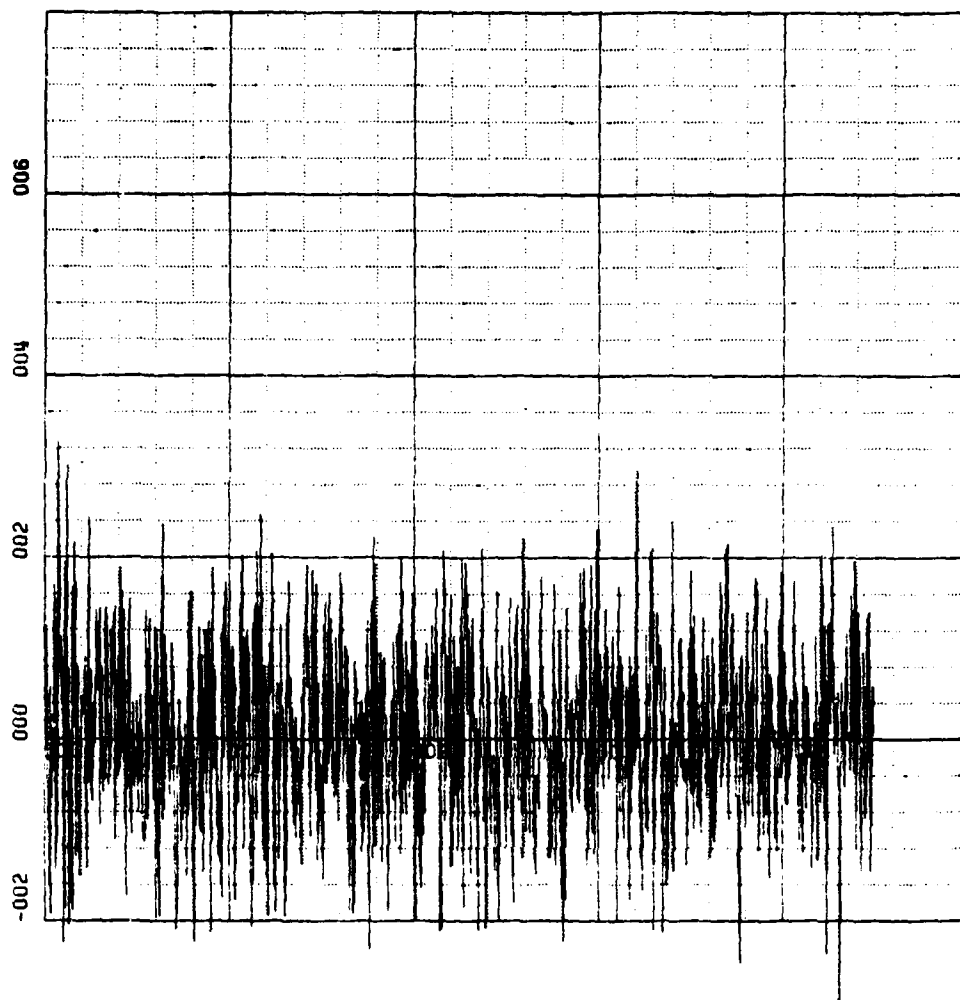
```

GO TO 1
END

```

CC

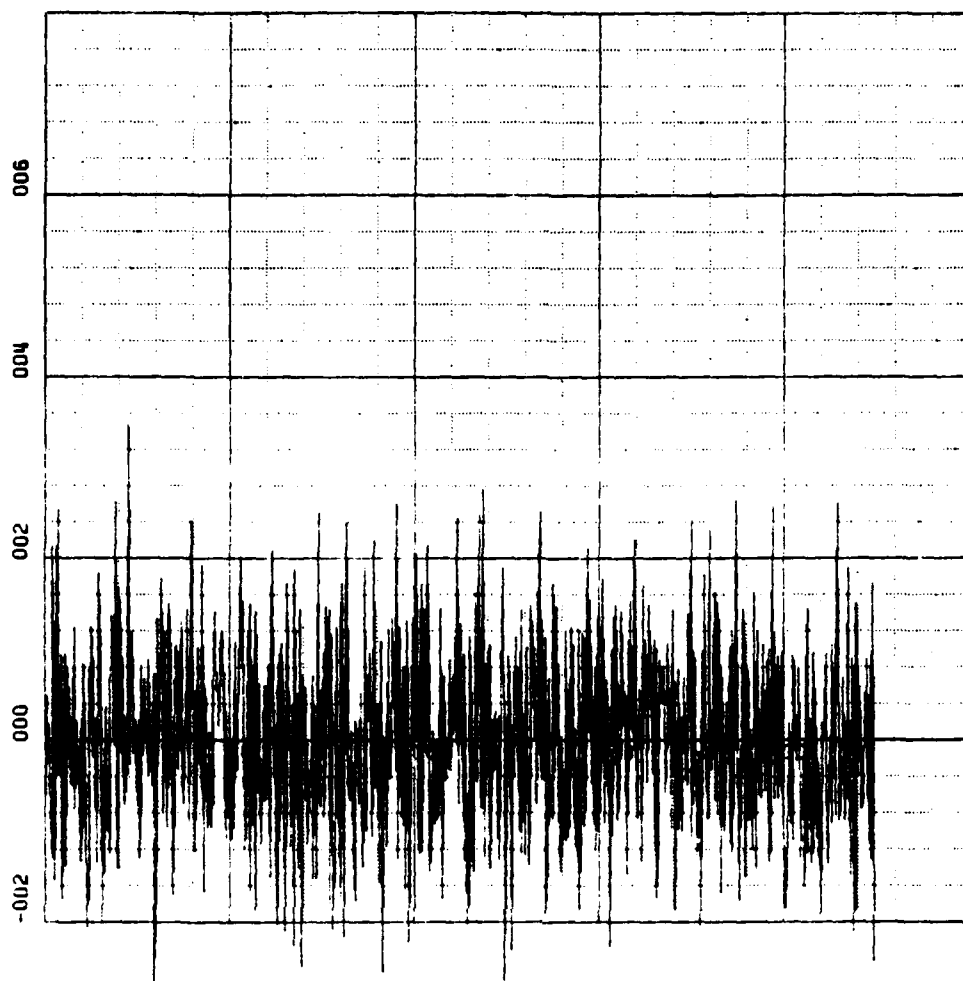
KWS00040
 KWS00050
 KWS00060
 KWS00070
 KWS00080
 KWS00090
 KWS00100
 KWS00110
 KWS00120
 KWS00130
 KWS00140
 KWS00150
 KWS00160
 KWS00170
 KWS00180
 KWS00190
 KWS00200
 KWS00210
 KWS00220
 KWS00230
 KWS00240
 KWS00250
 KWS00260
 KWS00270
 KWS00280
 KWS00290
 KWS00300
 KWS00310
 KWS00320
 KWS00330
 KWS00340
 KWS00350
 KWS00360
 KWS00370
 KWS00380
 KWS00390
 KWS00400
 KWS00410
 KWS00420
 KWS00430
 KWS00440
 KWS00450



X-SCALE=1.00E+01 UNITS INCH. [hours]
Y-SCALE=2.00E+01 UNITS INCH. [ft/(sec)²]
KWSTAS
RUN 1

NOISE-W VS TIME

Figure 104. Normalized Input Noise Versus Time.



X-SCALE=1.00E+01 UNITS INCH. [hours]

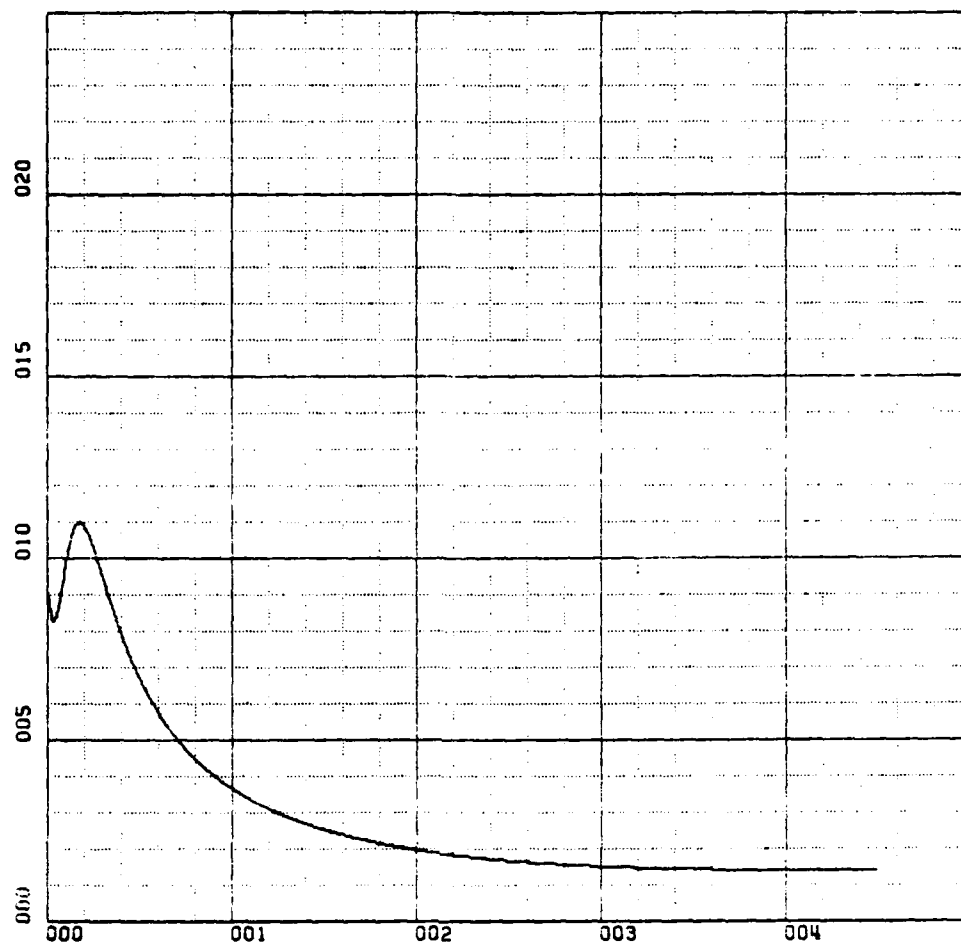
Y-SCALE=2.00E+01 UNITS INCH. [(ft)²]

KWSTAS

RUN 1

NOISE-V VS TIME

Figure 105. Normalized Measurement Noise Versus Time.



X-SCALE=1.00E+01 UNITS INCH. [hours]

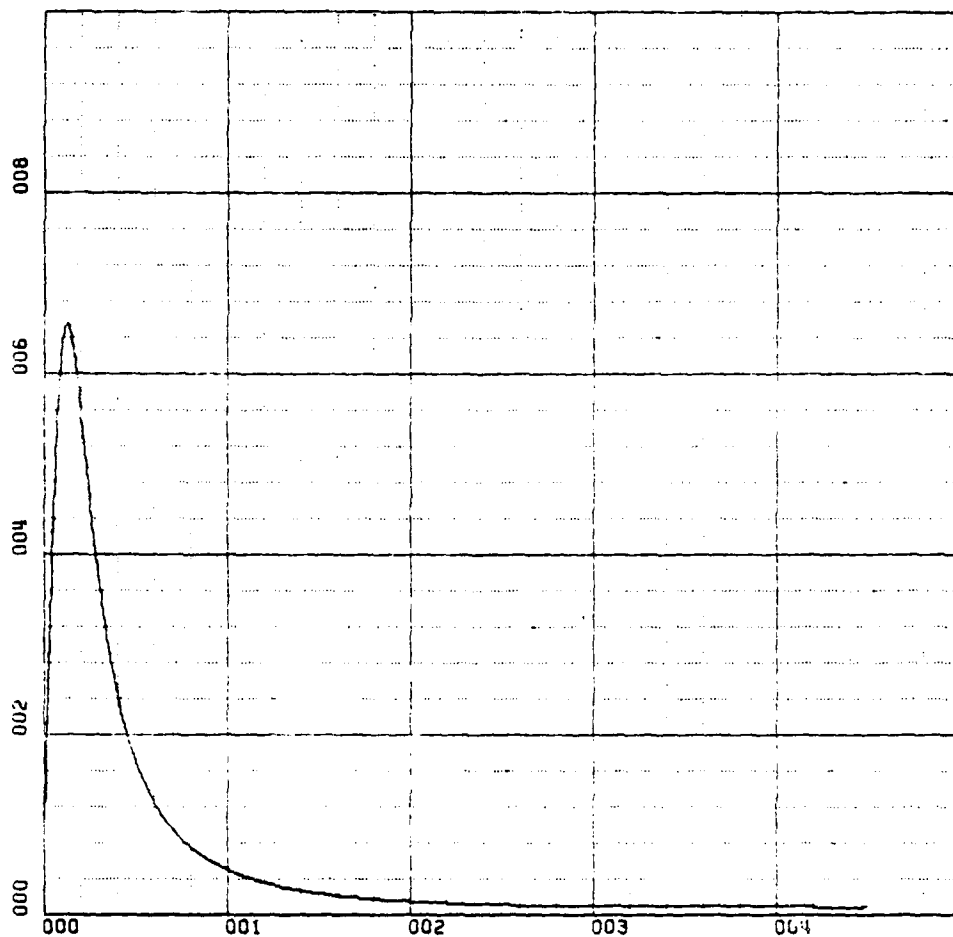
Y-SCALE=5.00E-01 UNITS INCH. [ft/sec]

KWSTAS

RUN 1

K1 VS TIME

Figure 106. Case I. Kalman Filter Gain to Velocity.



X-SCALE=1.00E+01 UNITS INCH. [hours]

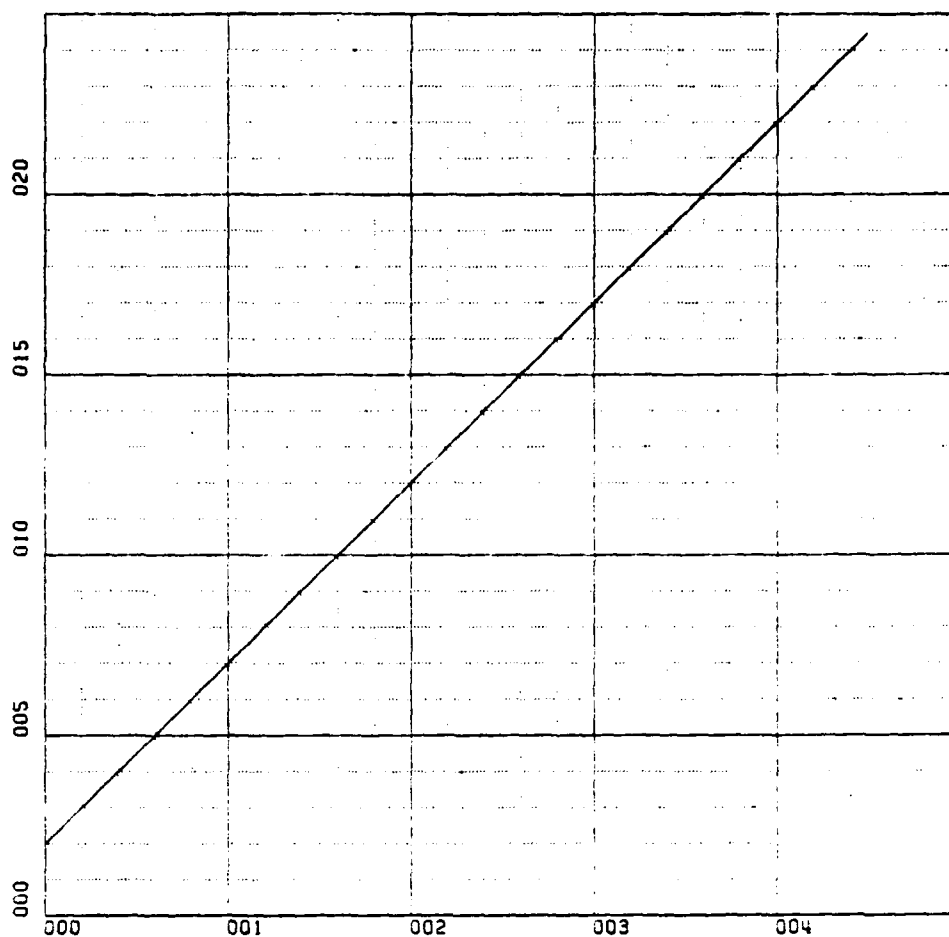
Y-SCALE=2.00E-01 UNITS INCH. [ft/(sec)²]

KWSTAS

RUN 1

K2 VS TIME

Figure 107. Case I. Kalman filter gain to Acceleration.



X-SCALE=1.00E+01 UNITS INCH. [hours]

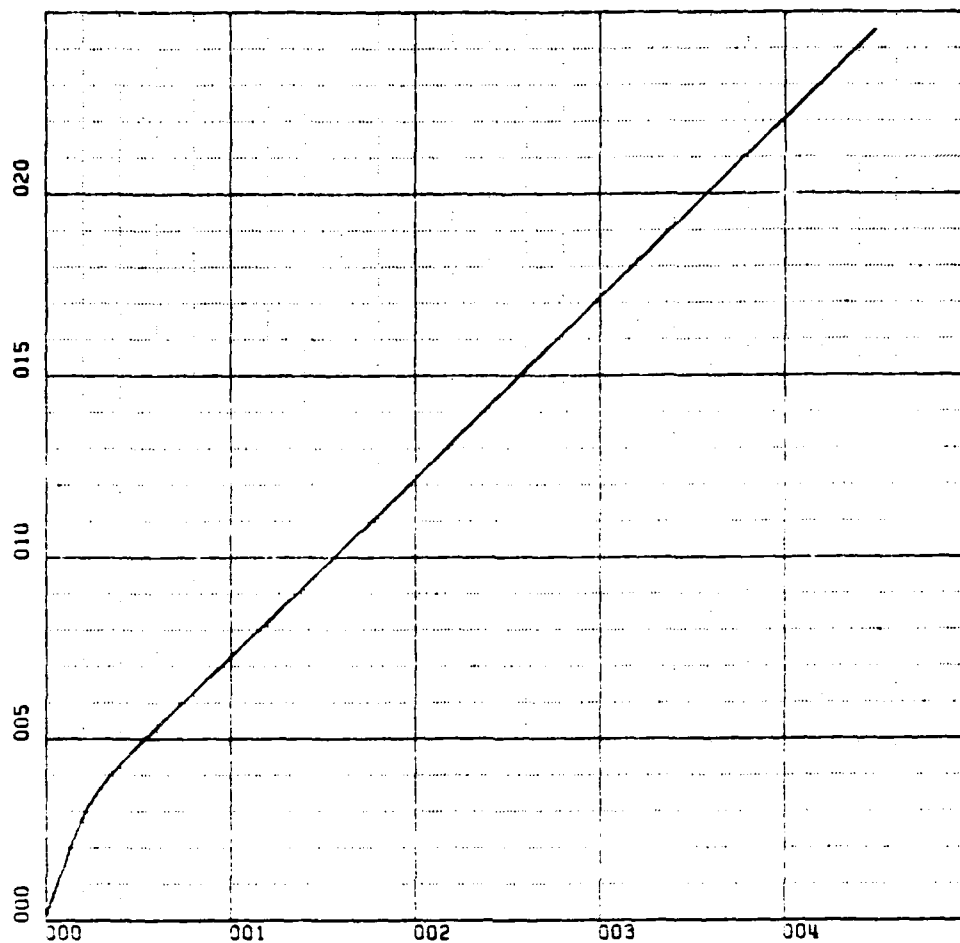
Y-SCALE=5.00E+02 UNITS INCH. [ft]

KWSTAS

RUN 2

R-TRUE VS TIME

Figure 108. Case I. True Position Versus Time.



X-SCALE=1.00E+01 UNITS INCH. [hours]

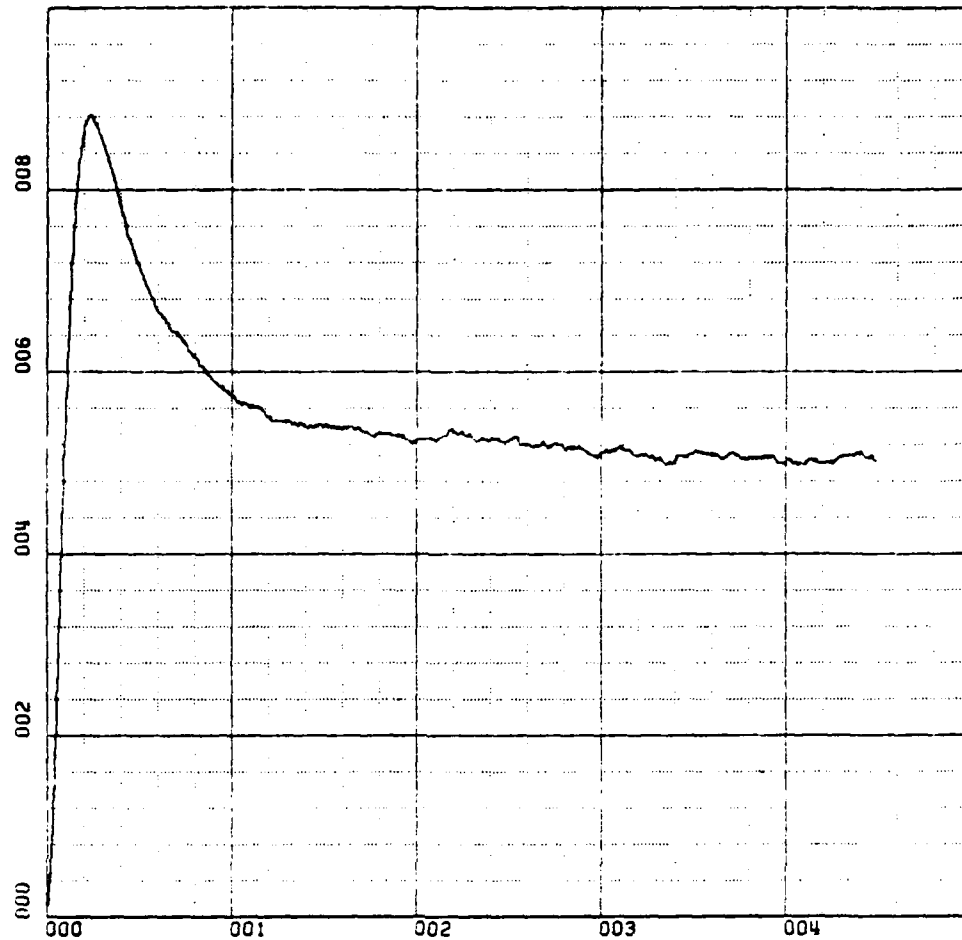
Y-SCALE=5.00E+02 UNITS INCH. [ft]

KWSTAS

RUN 2

R-HAT VS TIME

Figure 109. Case I. Predicted Position Versus Time.



X-SCALE=1.00E+01 UNITS INCH. [hours]

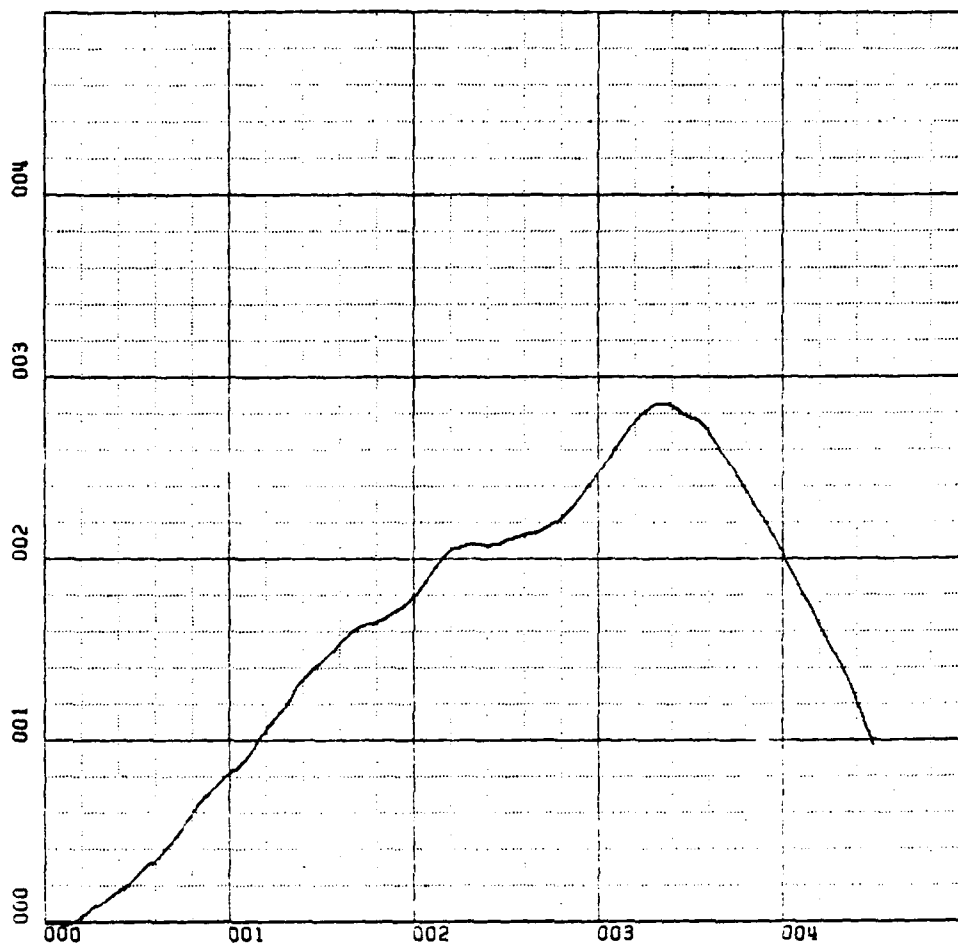
Y-SCALE=2.00E+01 UNITS INCH. [ft/sec]

KWSTAS

RUN 2

V-HAT VS TIME

Figure 110. Case I. Predicted Velocity Versus Time.



X-SCALE=1.00E+01 UNITS INCH. [hours]

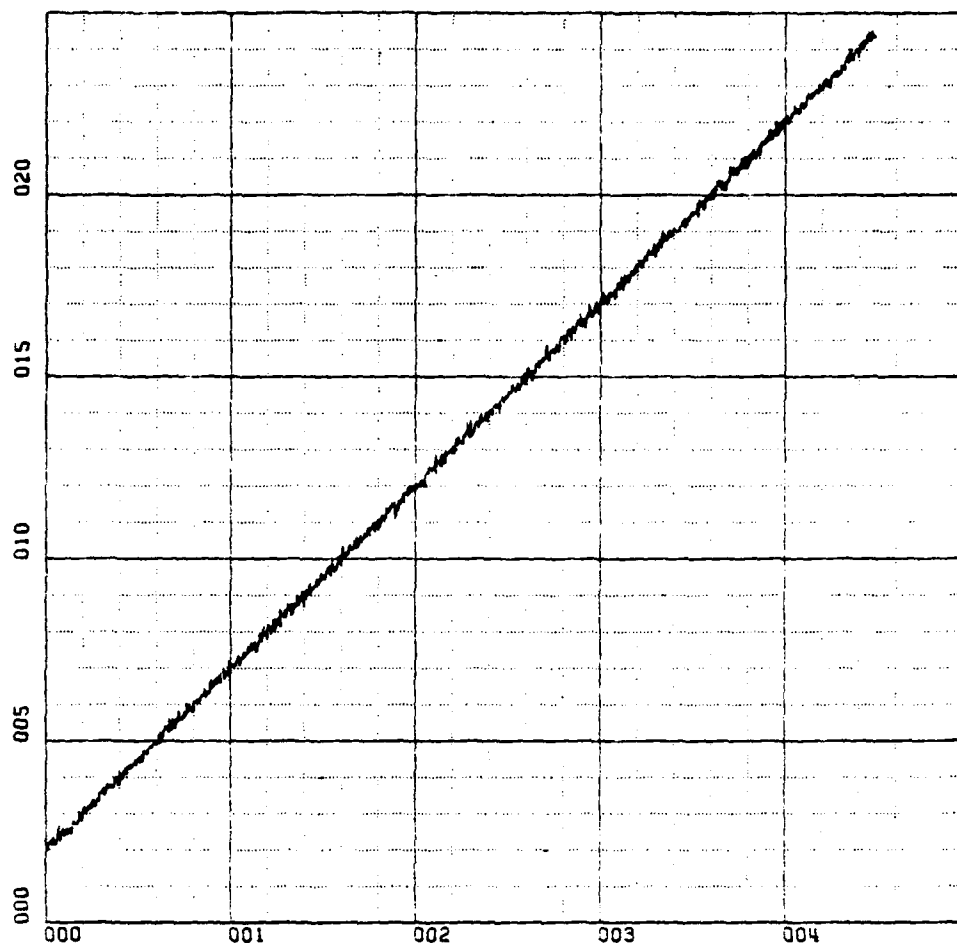
Y-SCALE=1.00E+01 UNITS INCH. [ft]

KWSTAS

RUN 3

R-INS VS TIME

Figure 111. Case I. I.N.S. Indicated Position Versus Time.



X-SCALE=1.00E+01 UNITS INCH. [hours]

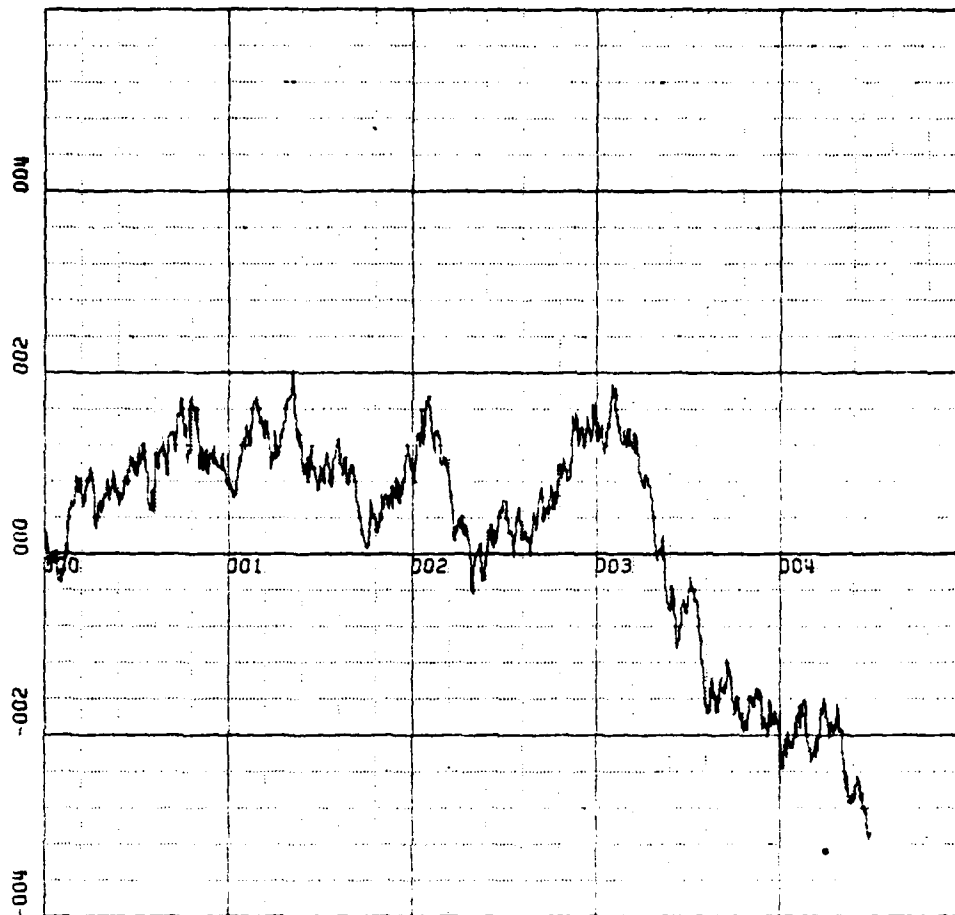
Y-SCALE=5.00E+02 UNITS INCH. [t]

KWSTAS

RUN 3

R-RADAR VS TIME

Figure 112. Case I. Radar Indicated Position Versus Time.



X-SCALE=1.00E+01 UNITS INCH. [hours]

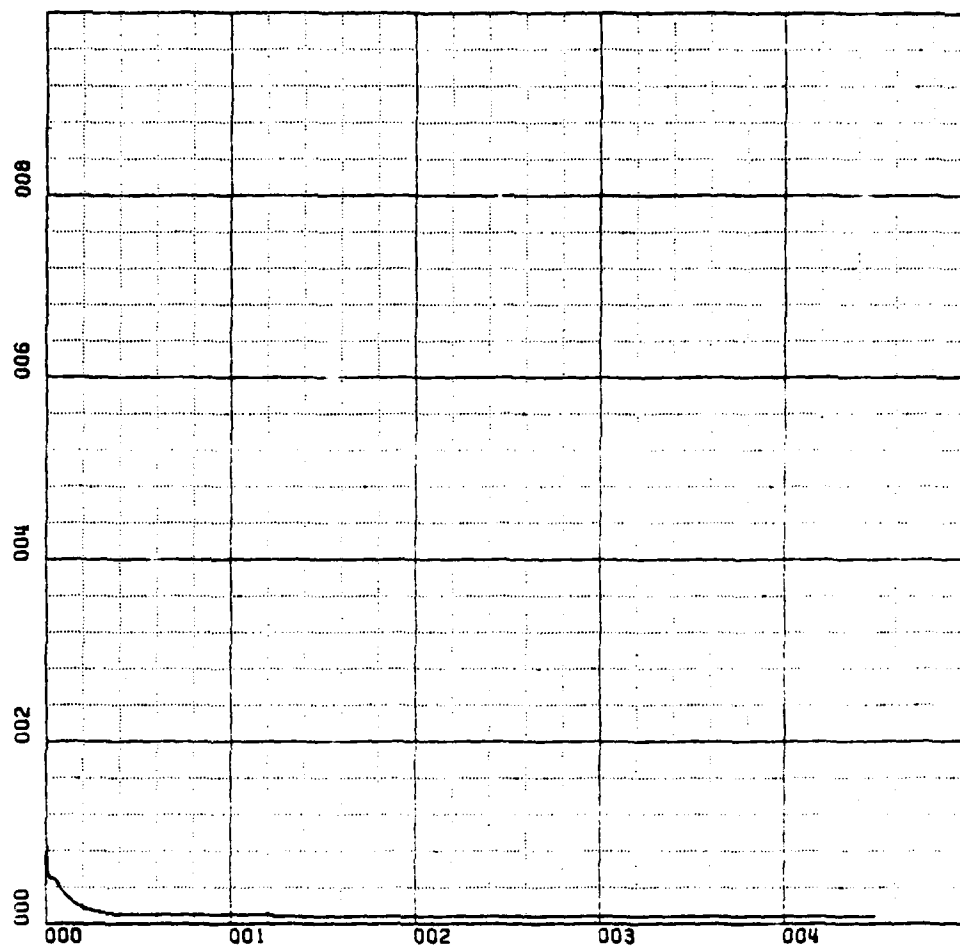
Y-SCALE=2.00E+00 UNITS INCH. [ft/sec]

KWSTAS

RUN 3

V-INS VS TIME

Figure 113. Case I. I.N.S. Indicated Velocity Versus Time



X-SCALE=1.00E+01 UNITS INCH. [hours]

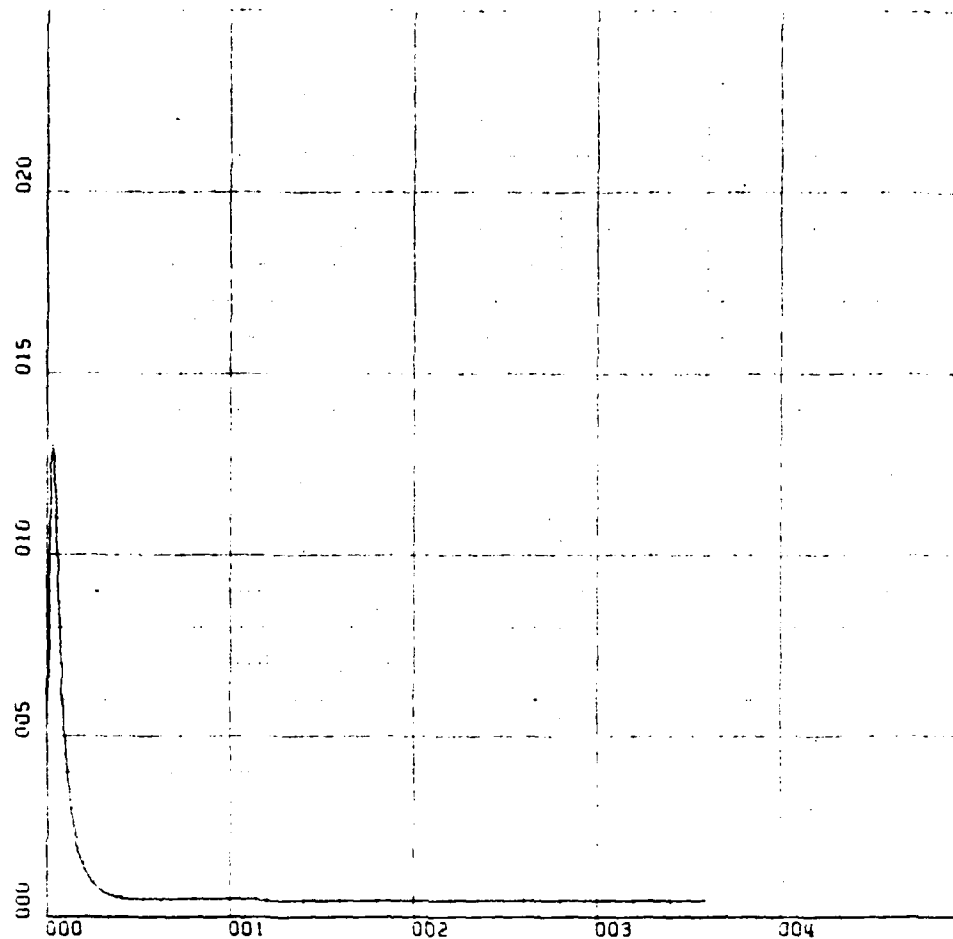
Y-SCALE=2.00E+01 UNITS INCH. [ft/sec]

KWSTAS

RUN 1

K1 VS TIME

Figure 114. Case II. Kalman Filter Gain to Velocity.



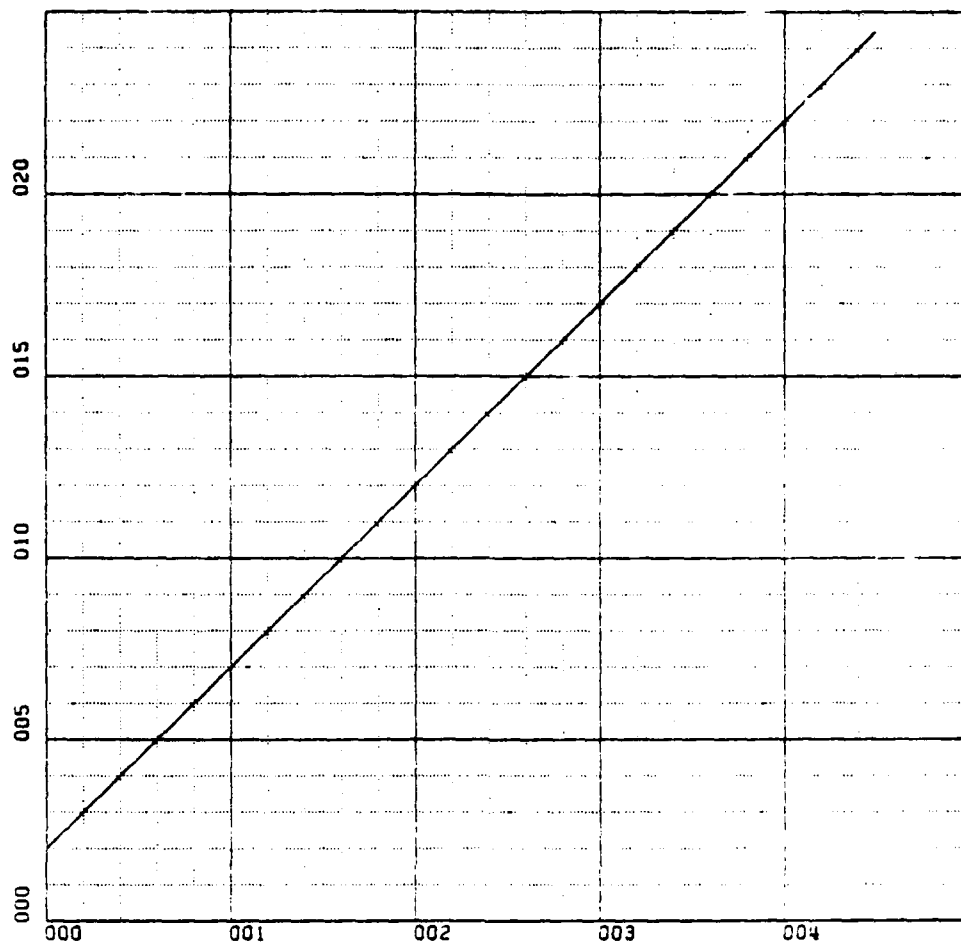
X-SCALE=1.00E+01 UNITS INCH. [hours]
Y-SCALE=5.00E+00 UNITS INCH. [ft/(sec)²]

KWSTAS

RUN 1

K2 VS TIME

Figure 115. Case II. Kalman Filter Gain to Acceleration.



X-SCALE=1.00E+01 UNITS INCH. [hours]

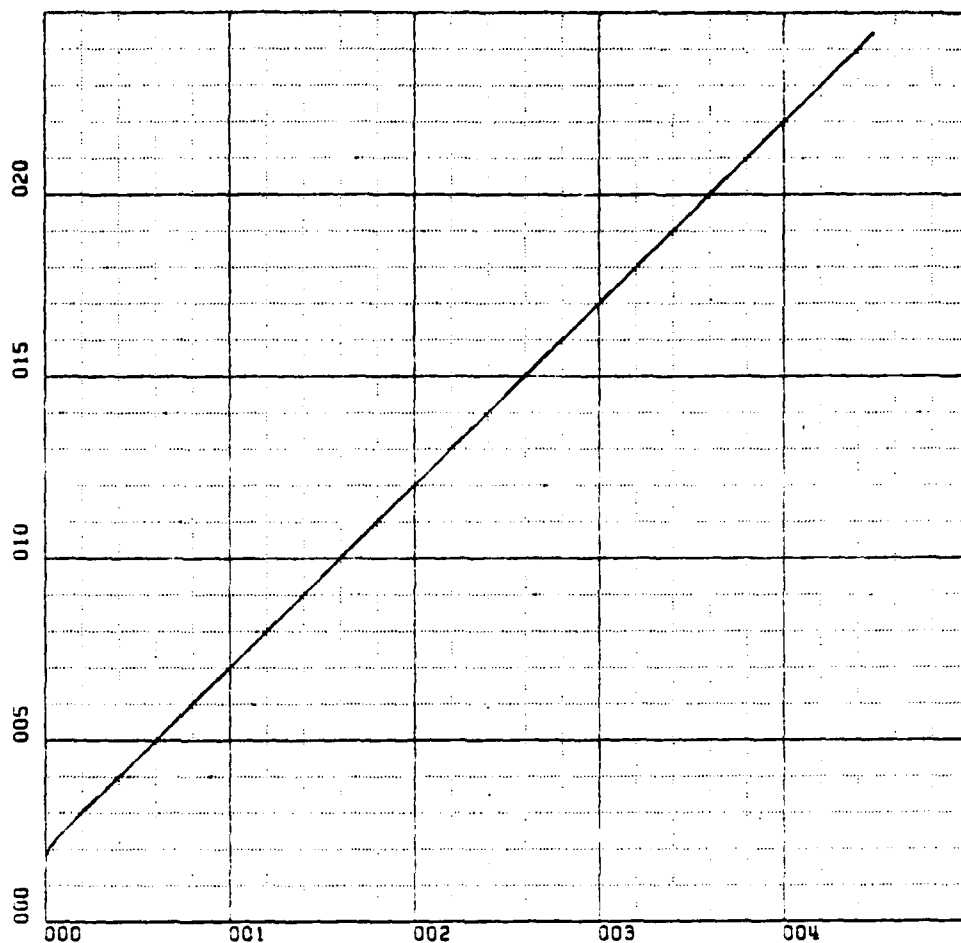
Y-SCALE=5.00E+02 UNITS INCH. [ft]

KWSTAS

RUN 2

R-TRUE VS TIME

Figure 116. Case II. True Position Versus Time.



X-SCALE=1.00E+01 UNITS INCH. [hours]

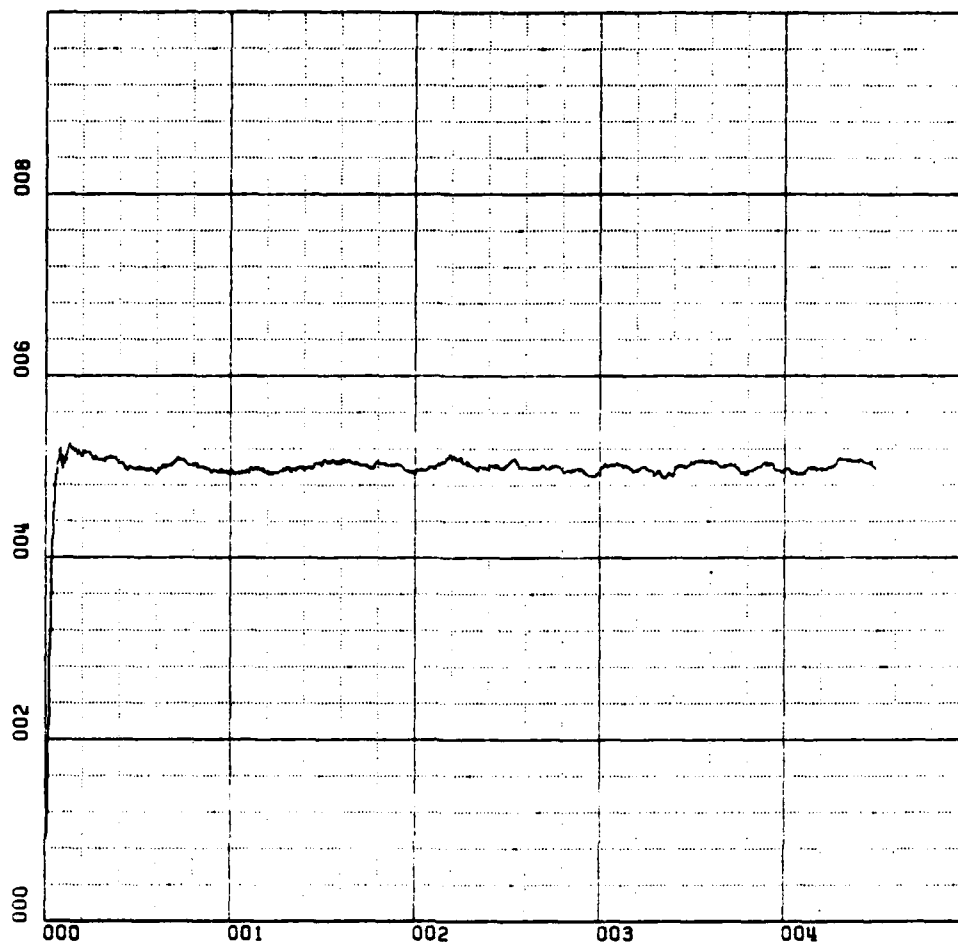
Y-SCALE=5.00E+02 UNITS INCH. [ft]

KWSTAS

RUN 2

R-HAT VS TIME

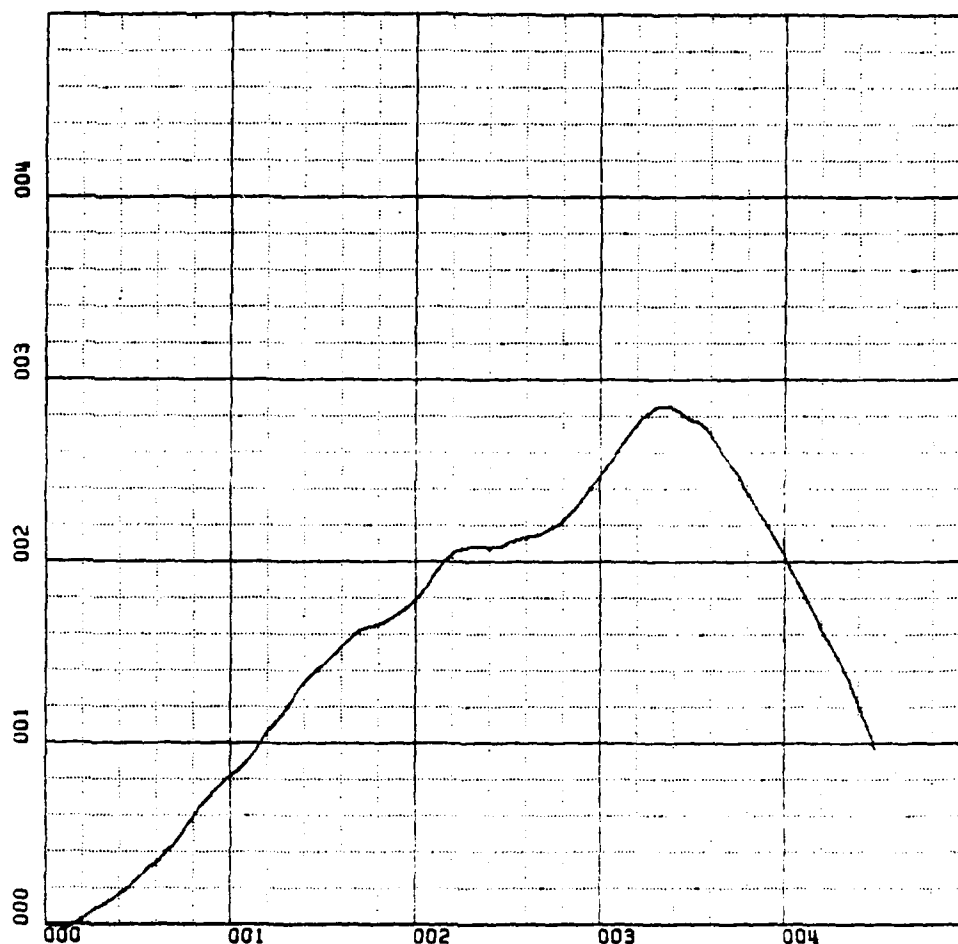
Figure 117. Case II. Predicted Position Versus Time.



X-SCALE=1.00E+01 UNITS INCH.[hours]
Y-SCALE=2.00E+01 UNITS INCH.[ft/sec]
KWSTAS
RUN 2

V-HAT VS TIME

Figure 118. Case II. Predicted Velocity Versus Time.



X-SCALE=1.00E+01 UNITS INCH. [hours]

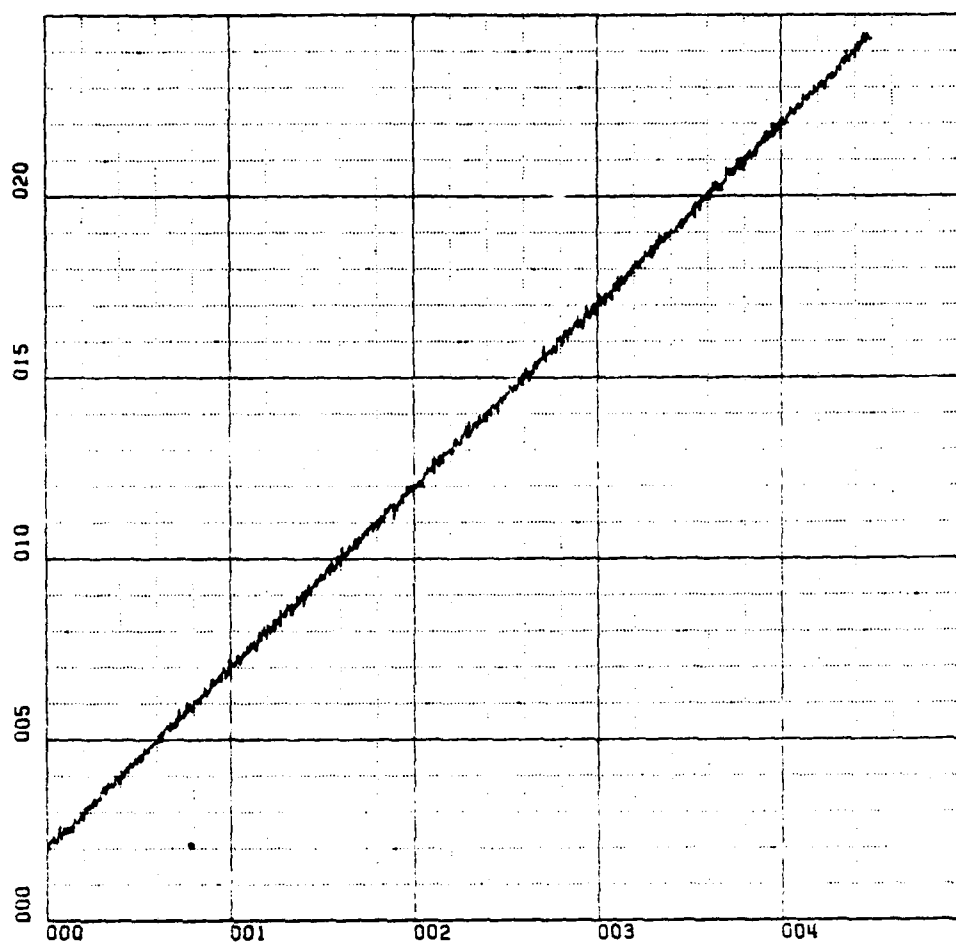
Y-SCALE=1.00E+01 UNITS INCH. [ft]

KWSTAS

RUN 3

R-INS VS TIME

Figure 119. Case II. I.N.S. Indicated Position Versus Time



X-SCALE=1.00E+01 UNITS INCH. [hours]

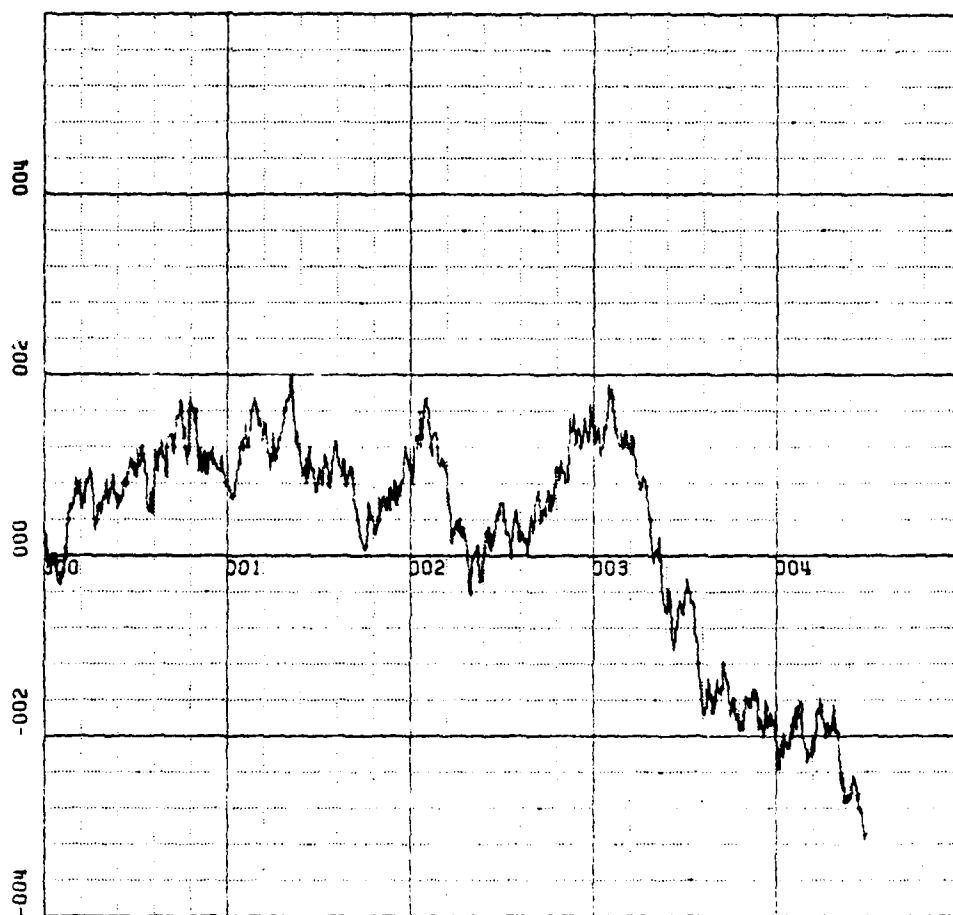
Y-SCALE=5.00E+02 UNITS INCH. [ft]

KWSTAS

RUN 3

R-RADAR VS TIME

Figure 120. Case II. Radar Indicated Position Versus Time.



X-SCALE=1.00E+01 UNITS INCH. [hours]

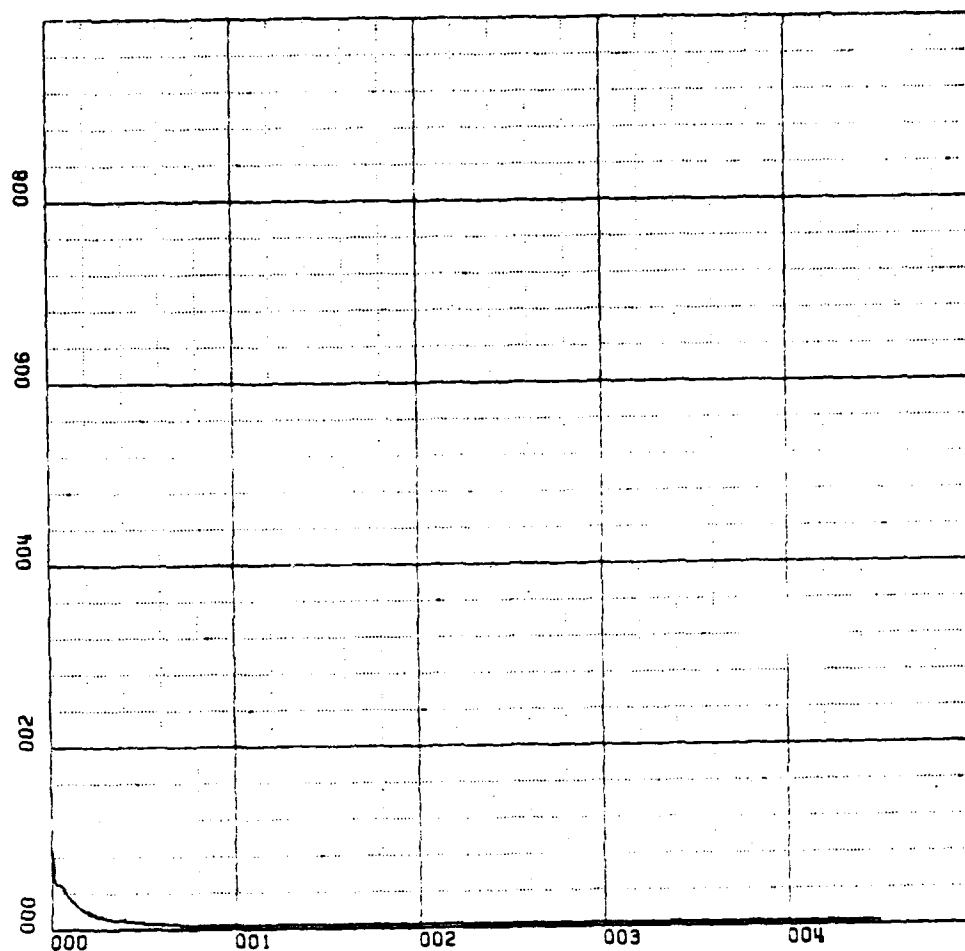
Y-SCALE=2.00E+00 UNITS INCH. [ft/sec]

KWSTAS

RUN 3

V-INS VS TIME

Figure 121. Case II. I.N.S. Indicated Velocity Versus Time.



X-SCALE=1.00E+01 UNITS INCH. [hours]

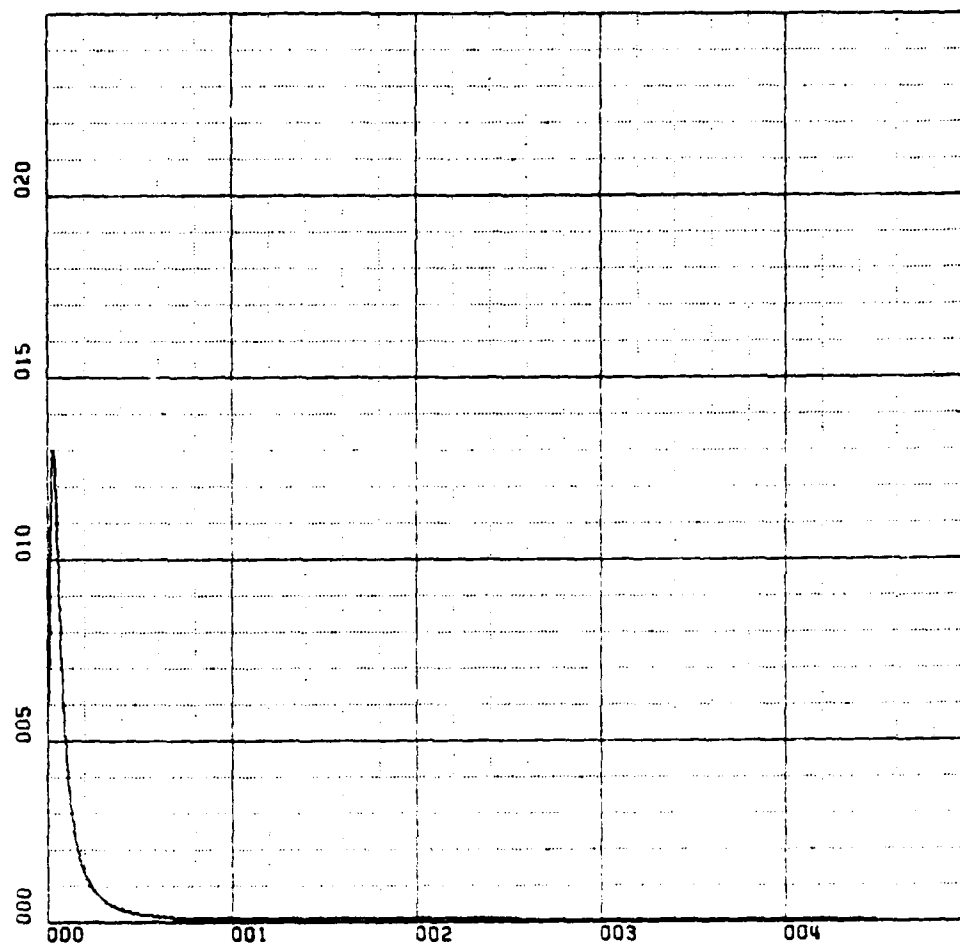
Y-SCALE=2.00E+01 UNITS INCH. [ft/sec]

KWSTAS

RUN 1

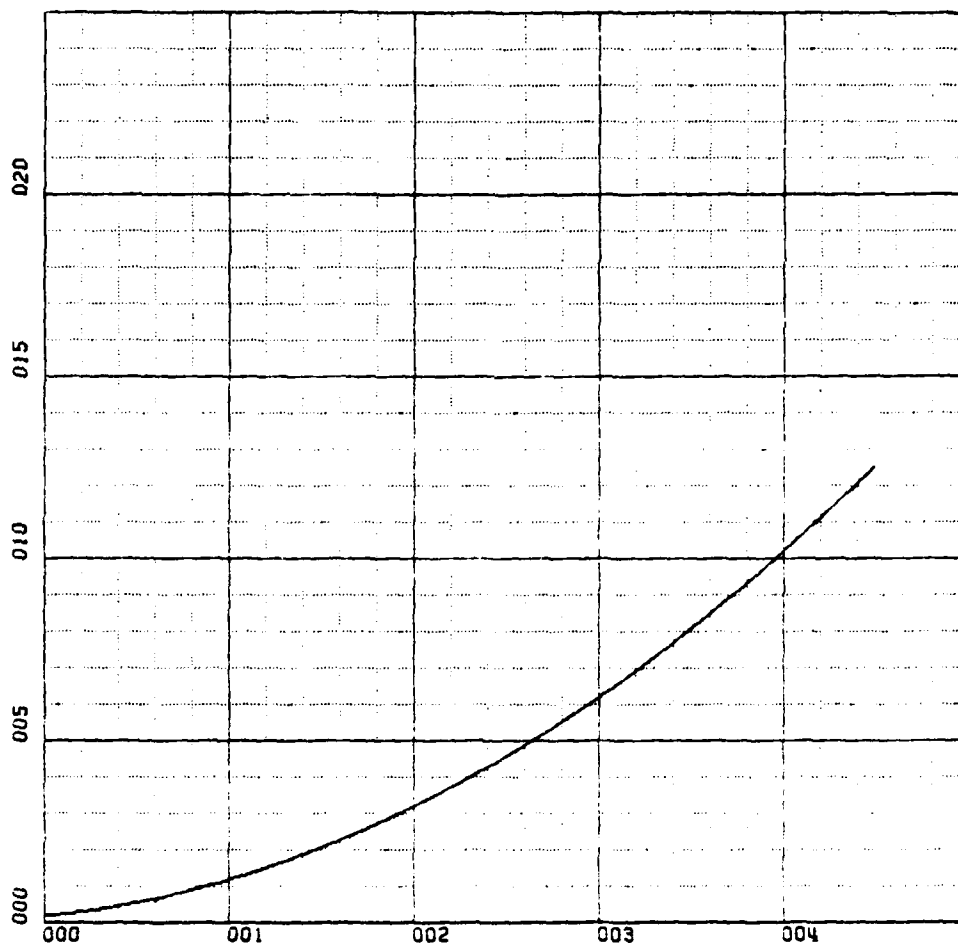
K1 VS TIME

Figure 122. Case III. Kalman Filter Gain to Velocity.



X-SCALE=1.00E+01 UNITS INCH. [hours]
 Y-SCALE=5.00E+00 UNITS INCH. [ft/(sec)²]
 KWSTAS
 RUN 1 K2 VS TIME

Figure 123. Case III. Kalman Filter Gain to Acceleration.



X-SCALE=1.00E+01 UNITS INCH. [hours]

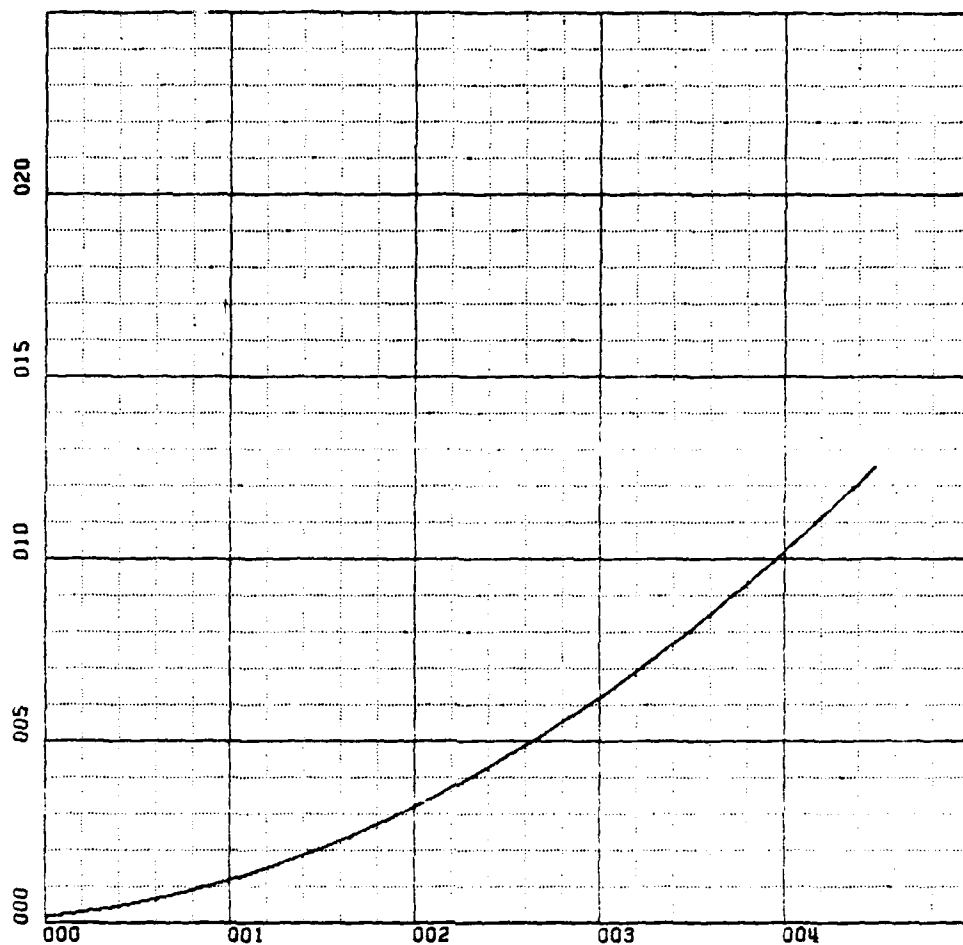
Y-SCALE=5.00E+03 UNITS INCH. [ft]

KWSTAS

RUN 2

R-TRUE VS TIME

Figure 124. Case III. True Position Versus Time.



X-SCALE=1.00E+01 UNITS INCH. [hours]

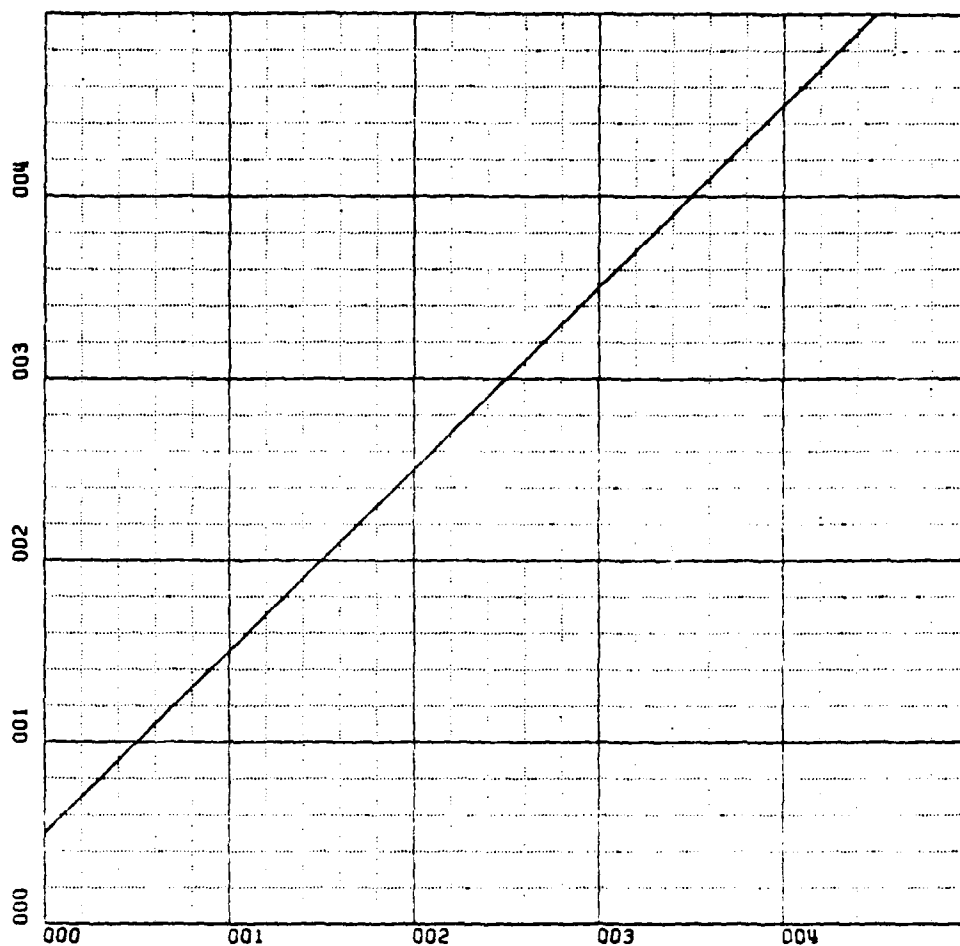
Y-SCALE=5.00E+03 UNITS INCH. [ft]

KWSTAS

RUN 2

R-HAT VS TIME

Figure 125. Case III. Predicted Position Versus Time.

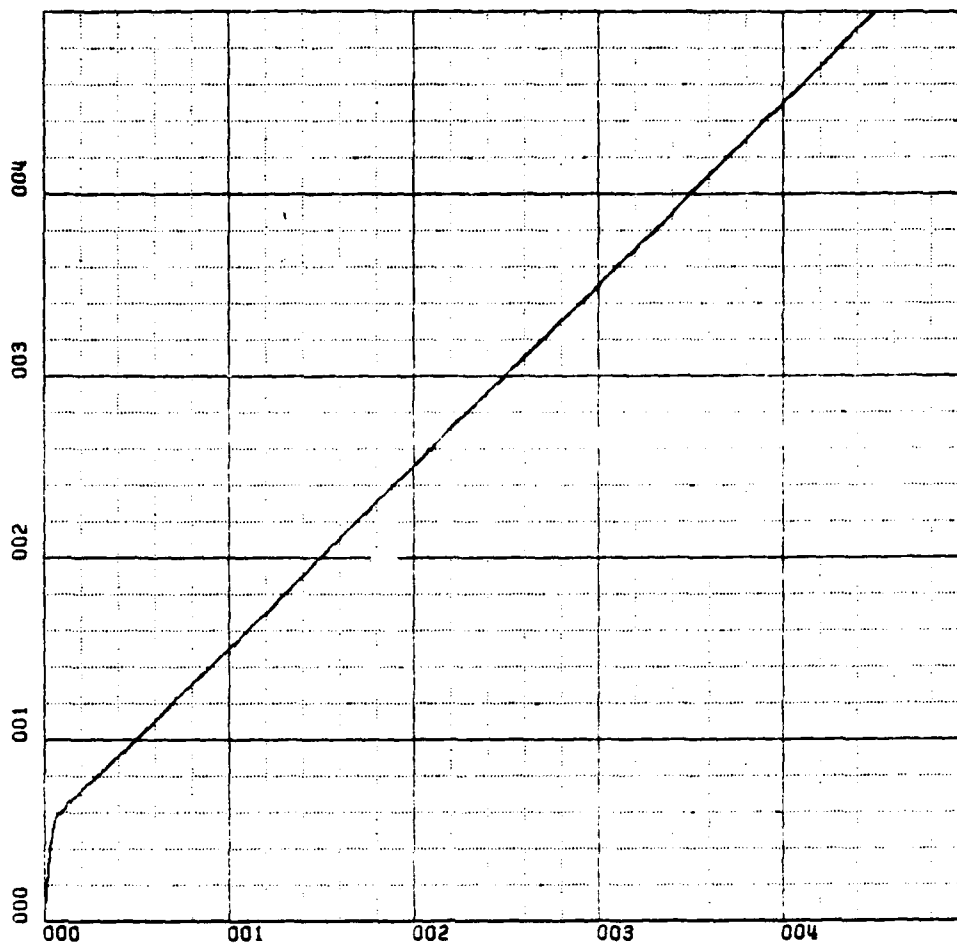


X-SCALE=1.00E+01 UNITS INCH. [hours]
Y-SCALE=1.00E+02 UNITS INCH. [ft/sec]

KWSTAS
RUN 2

V-TRUE VS TIME

Figure 126. Case III. True Velocity Versus Time.

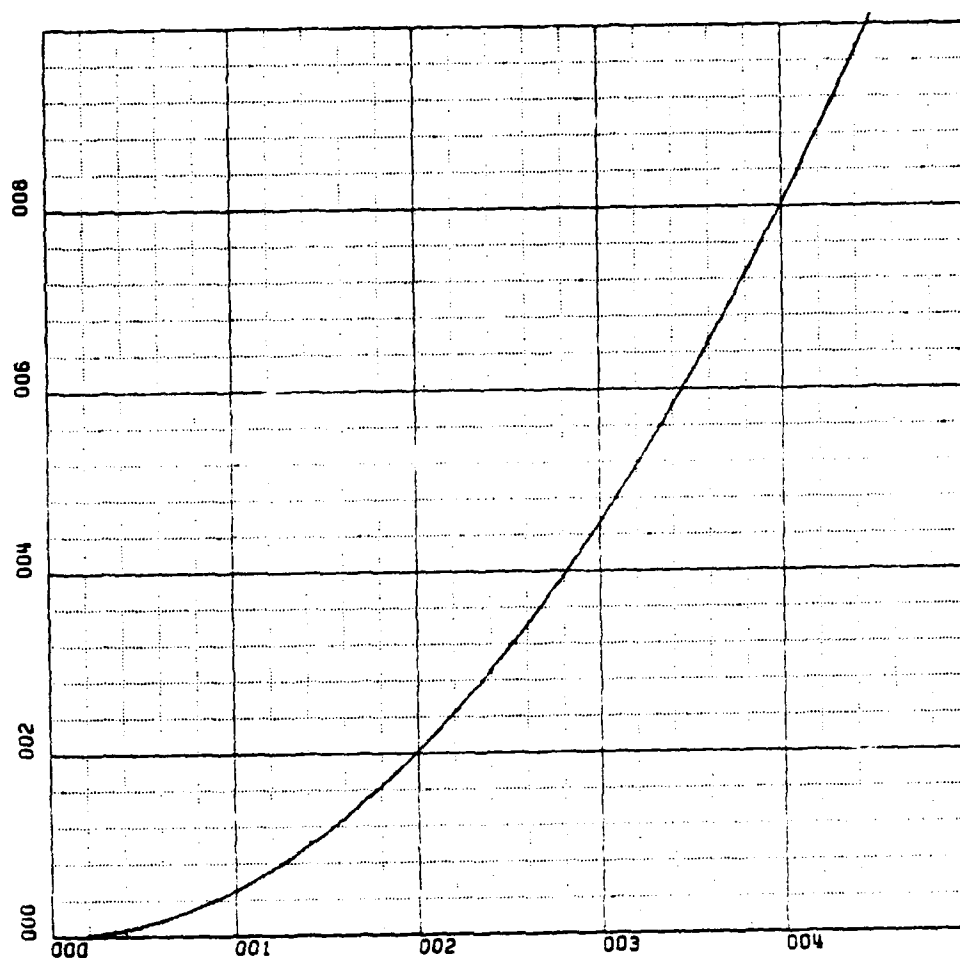


X-SCALE=1.00E+01 UNITS INCH. [hours]
 Y-SCALE=1.00E+02 UNITS INCH. [ft/sec]

KWSTAS
 RUN 2

V-HAT VS TIME

Figure 127. Case III. Predicted Velocity Versus Time.



X-SCALE=1.00E+01 UNITS INCH. [hours]

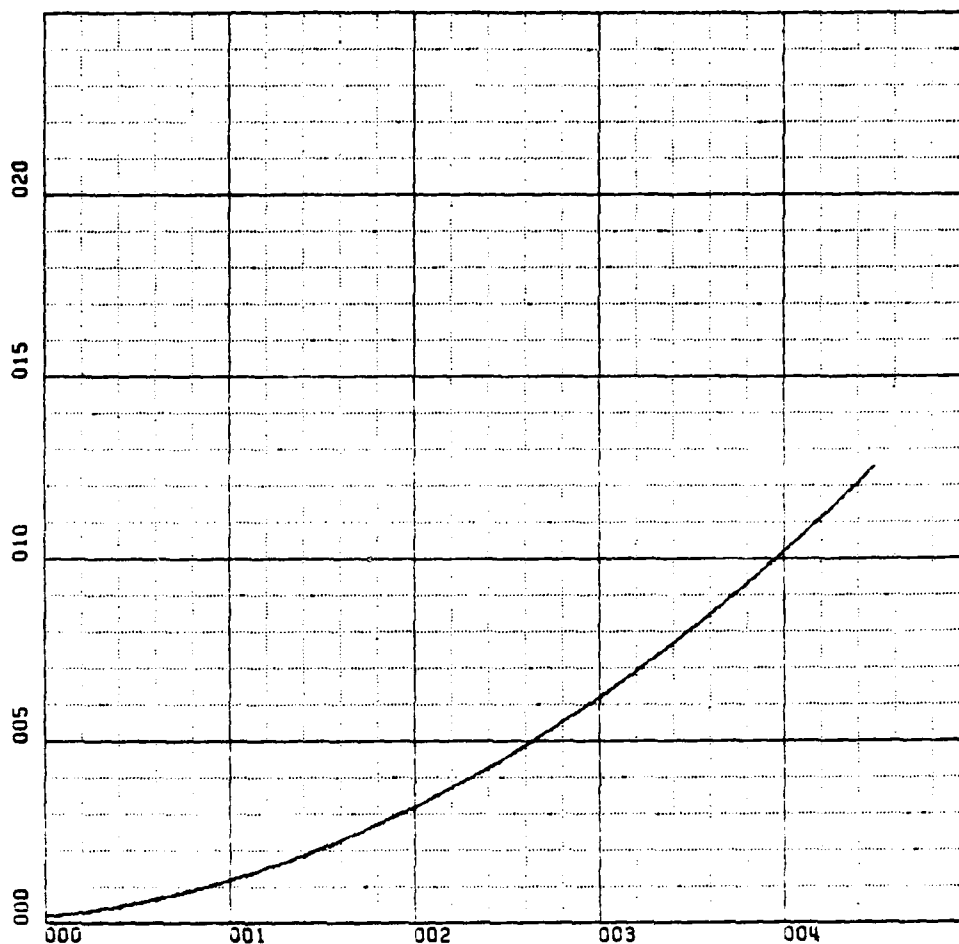
Y-SCALE=2.00E+03 UNITS INCH. [ft]

KWSTAS

RUN 3

R-INS VS TIME

Figure 128. Case III. I.N.S. Indicated Position Versus Time.



X-SCALE=1.00E+01 UNITS INCH. [hours]

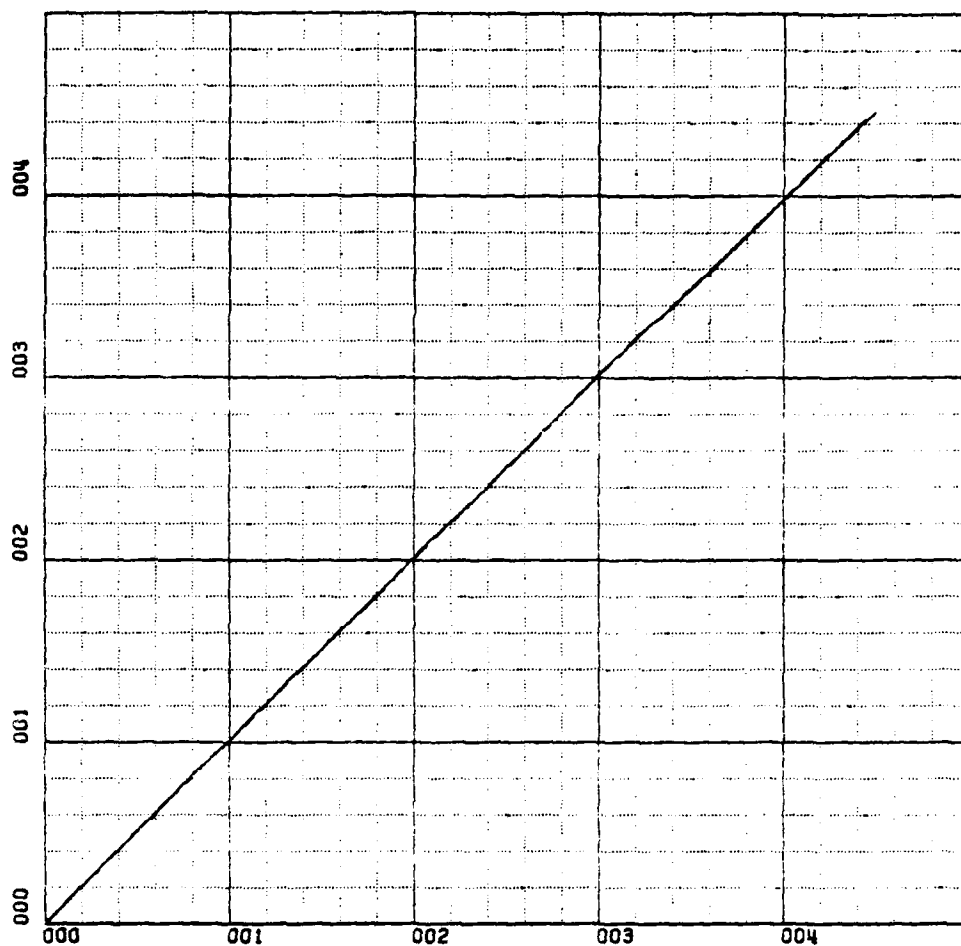
Y-SCALE=5.00E+03 UNITS INCH. [ft]

KWSTAS

RUN 3

R-RADAR VS TIME

Figure 129. Case III. Radar Indicated Position Versus Time.



X-SCALE=1.00E+01 UNITS INCH. [hours]

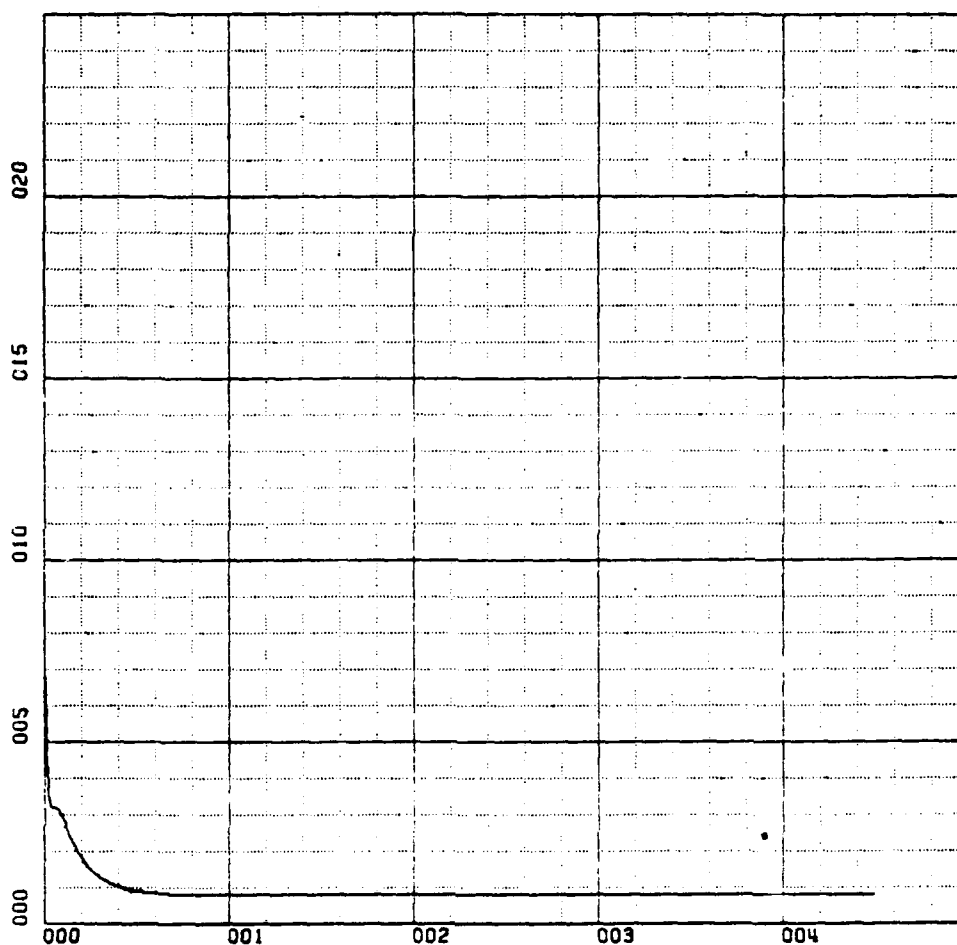
Y-SCALE=1.00E+02 UNITS INCH. [ft/sec]

KWSTAS

RUN 3

V-INS VS TIME

Figure 130. Case III. I.N.S. Indicated Velocity Versus Time.



X-SCALE=1.00E+01 UNITS INCH. [hours]

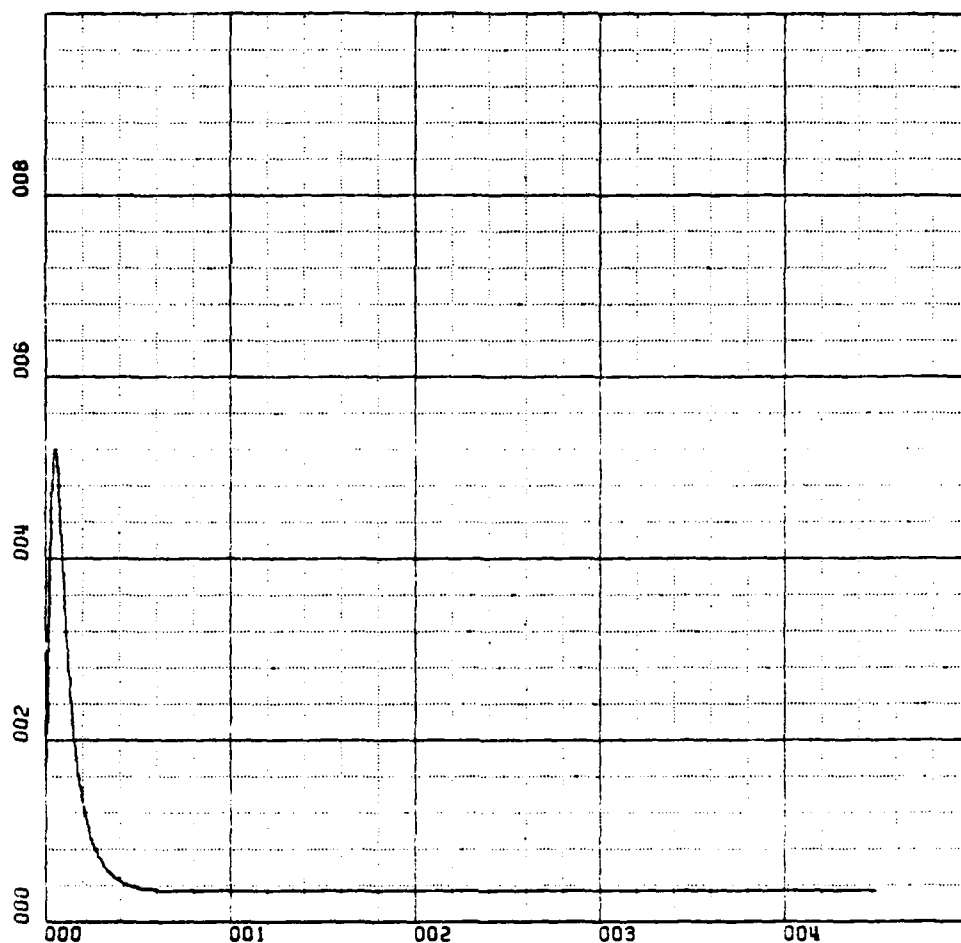
Y-SCALE=5.00E+00 UNITS INCH. [ft/sec]

KWSTAS

RUN 1

K1 VS TIME

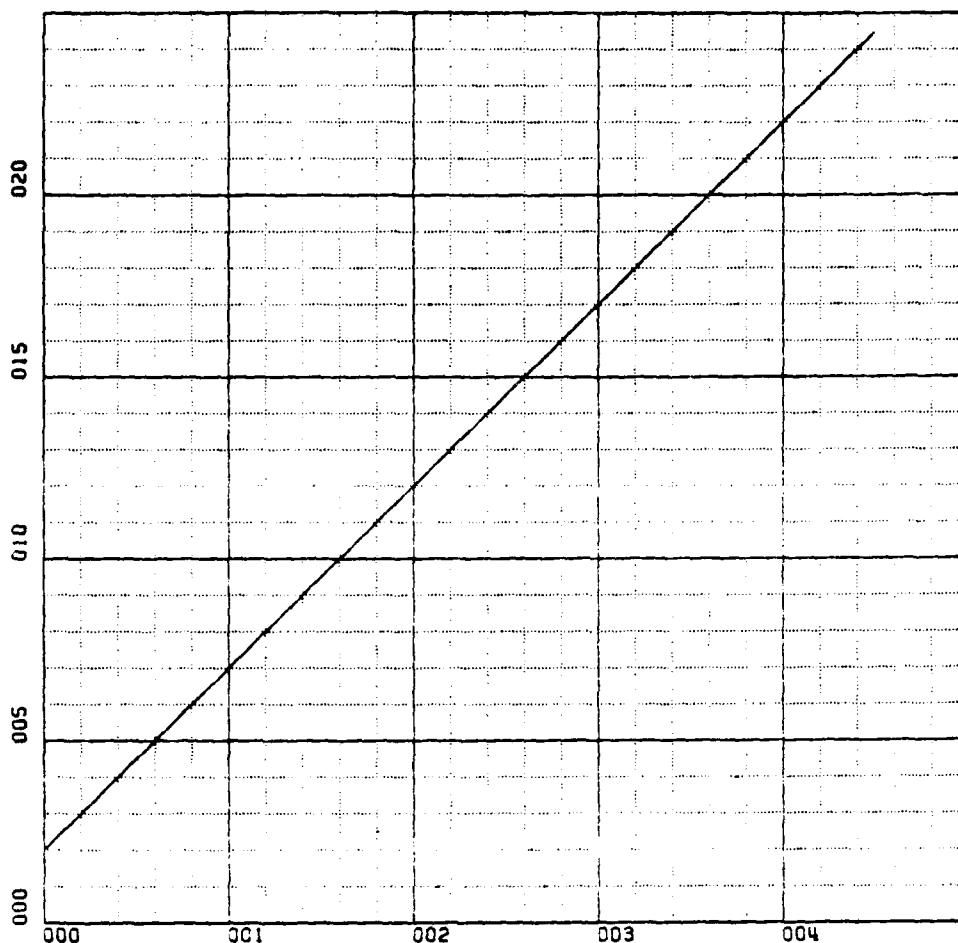
Figure 131. Case IV. Kalman Filter Gain to Velocity.



X-SCALE=1.00E+01 UNITS INCH. [hours]
 Y-SCALE=2.00E+00 UNITS INCH. [ft/(sec)²]
 KWSTAS
 RUN 1

K2 VS TIME

Figure 132. Case IV. Kalman Filter Gain to Acceleration.



X-SCALE=1.00E+01 UNITS INCH. [hours]

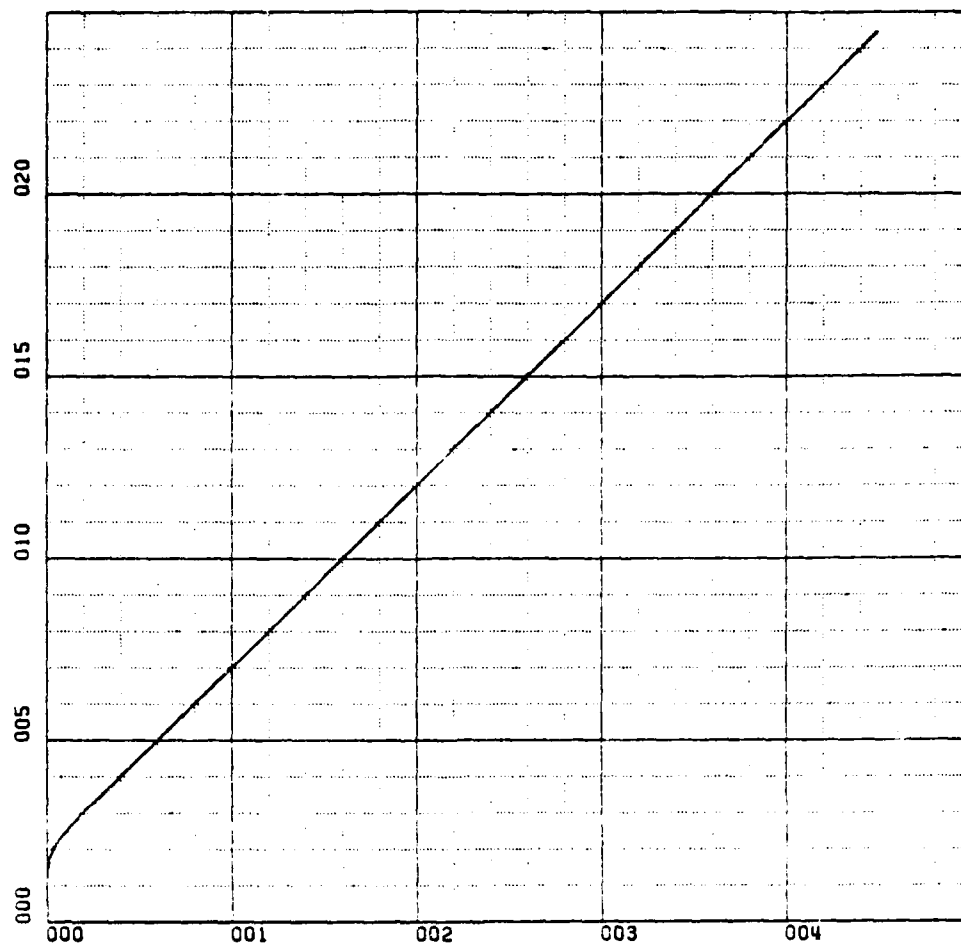
Y-SCALE=5.00E+02 UNITS INCH. [ft]

KWSTAS

RUN 2

R-TRUE VS TIME

Figure 133. Case IV. True Position Versus Time.



X-SCALE=1.00E+01 UNITS INCH. [hours]

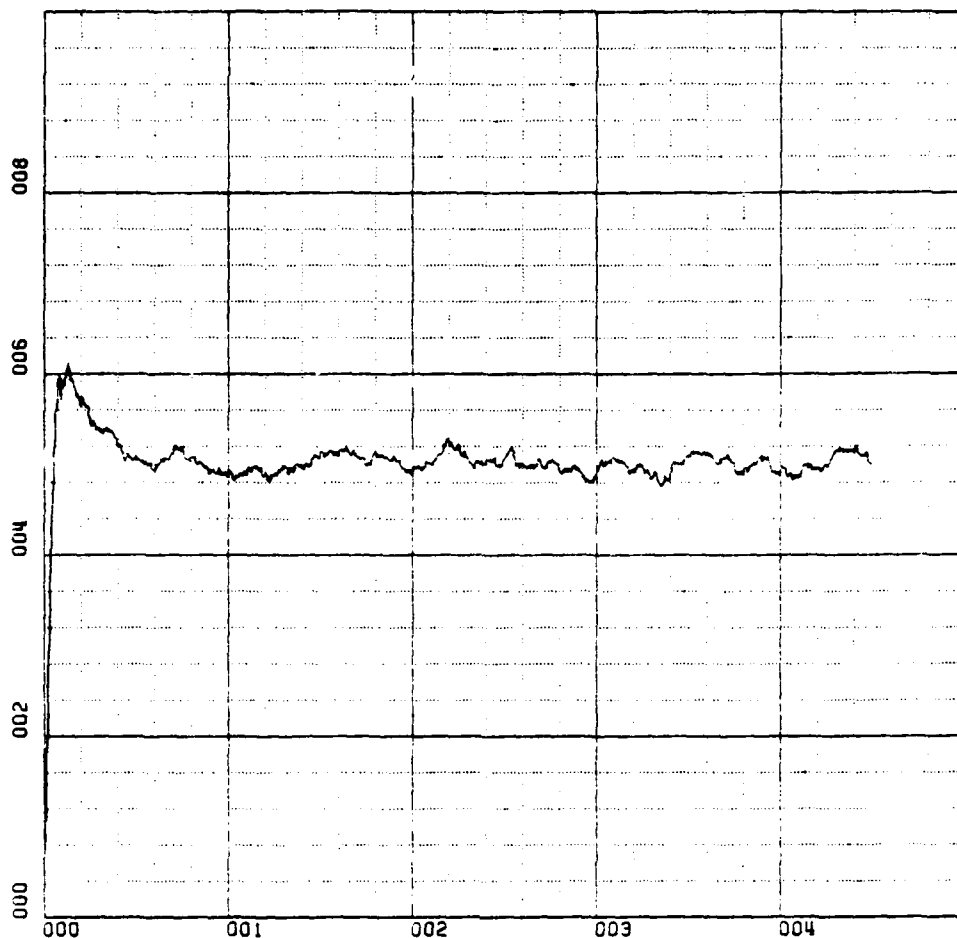
Y-SCALE=5.00E+02 UNITS INCH. [ft]

KWSTAS

RUN 2

R-HAT VS TIME

Figure 134. Case IV. Predicted Position Versus Time.



X-SCALE=1.00E+01 UNITS INCH. [hours]

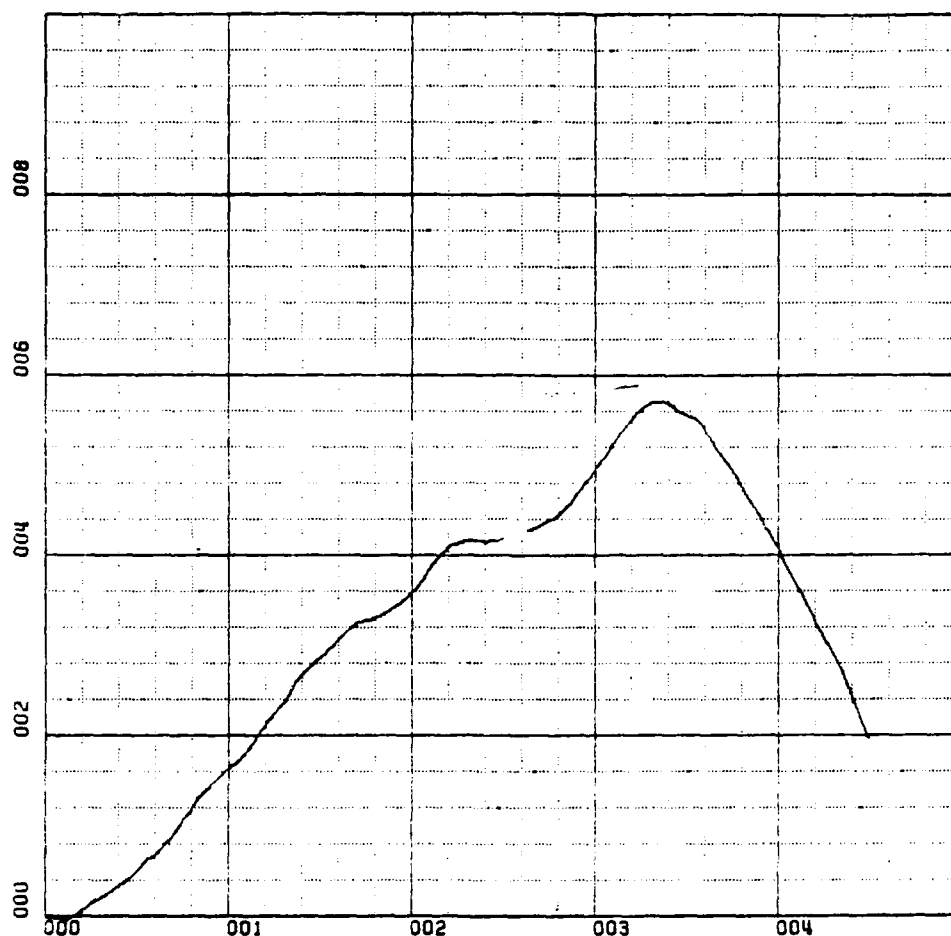
Y-SCALE=2.00E+01 UNITS INCH. [ft/sec]

KWSTAS

RUN 2

V-HAT VS TIME

Figure 135. Case IV. Predicted Velocity Versus Time.



X-SCALE=1.00E+01 UNITS INCH. [hours]

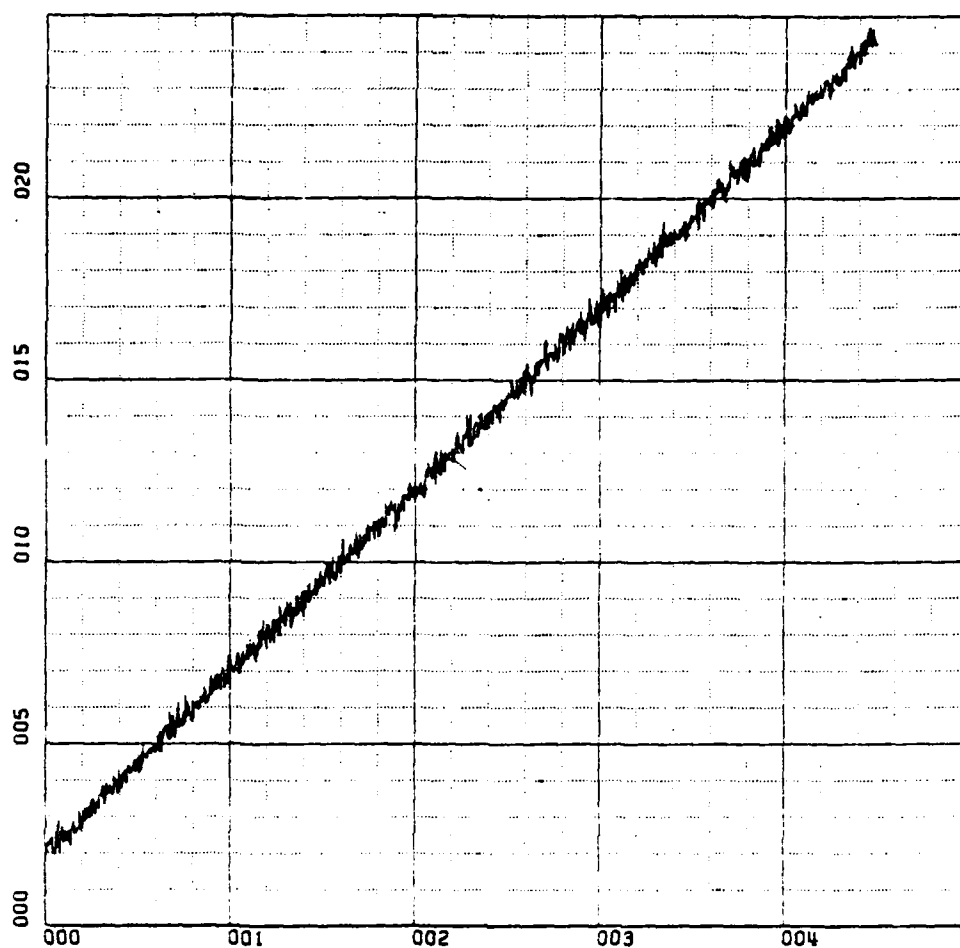
Y-SCALE=2.00E+01 UNITS INCH. [ft]

KWSTAS

RUN 3

R-INS VS TIME

Figure 136. Case IV. I.N.S. Indicated Position Versus Time.



X-SCALE=1.00E+01 UNITS INCH. [hours]

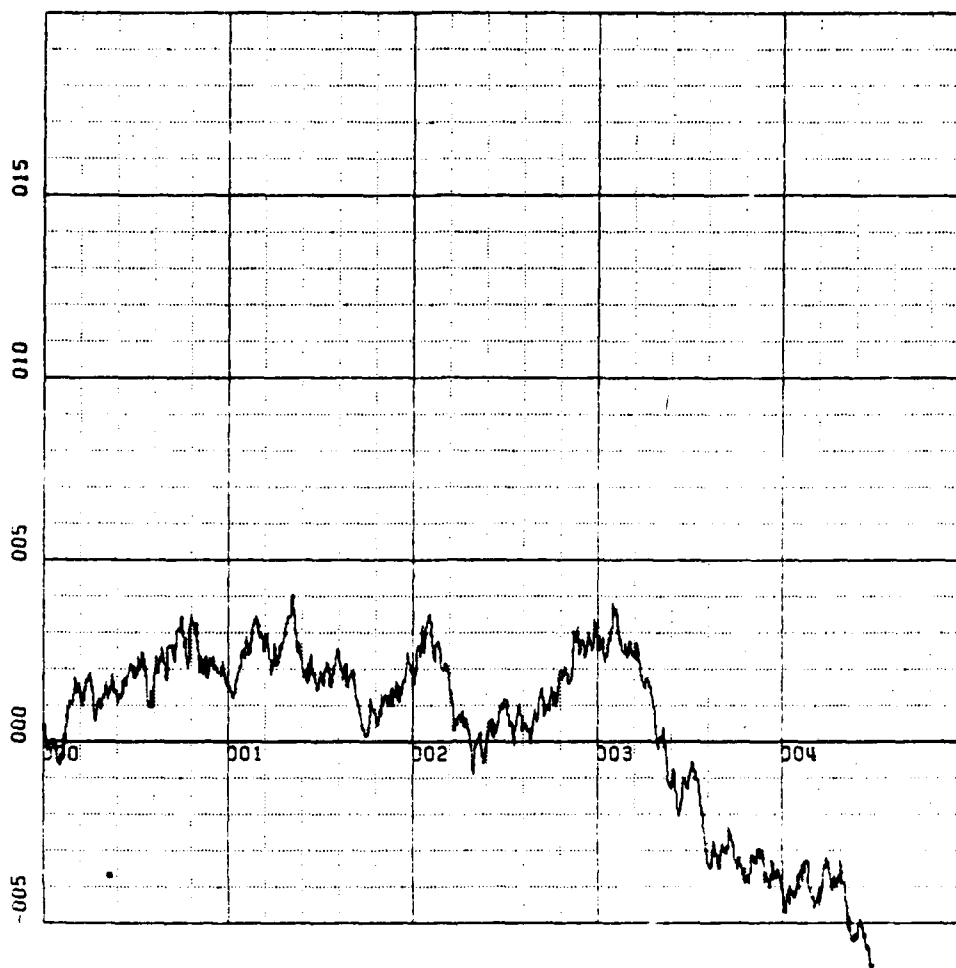
Y-SCALE=5.00E+02 UNITS INCH. [ft]

KWSTAS

RUN 3

R-RADAR VS TIME

Figure 137. Case IV. Radar Indicated Position Versus Time.



X-SCALE=1.00E+01 UNITS INCH. [hours]

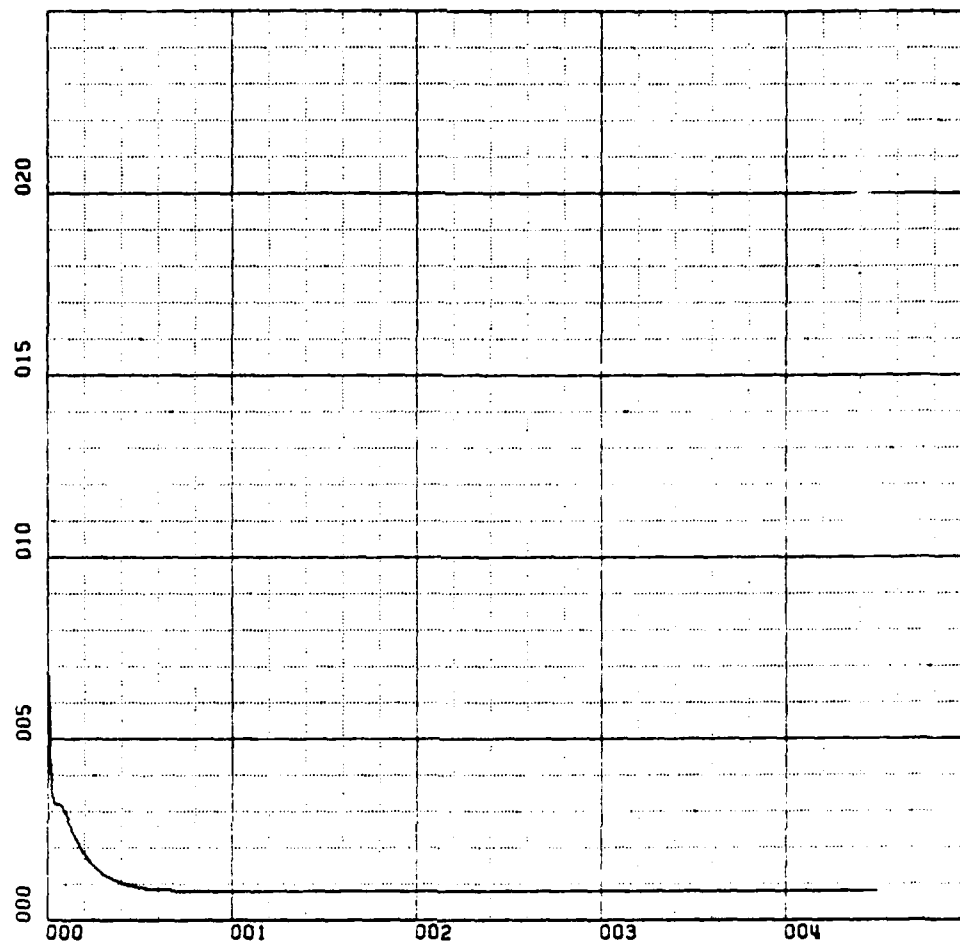
Y-SCALE=5.00E+00 UNITS INCH. [ft/sec]

KWSTAS

RUN 3

V-INS VS TIME

Figure 138. Case IV. I.N.S. Indicated Velocity Versus Time.



X-SCALE=1.00E+01 UNITS INCH. [hours]

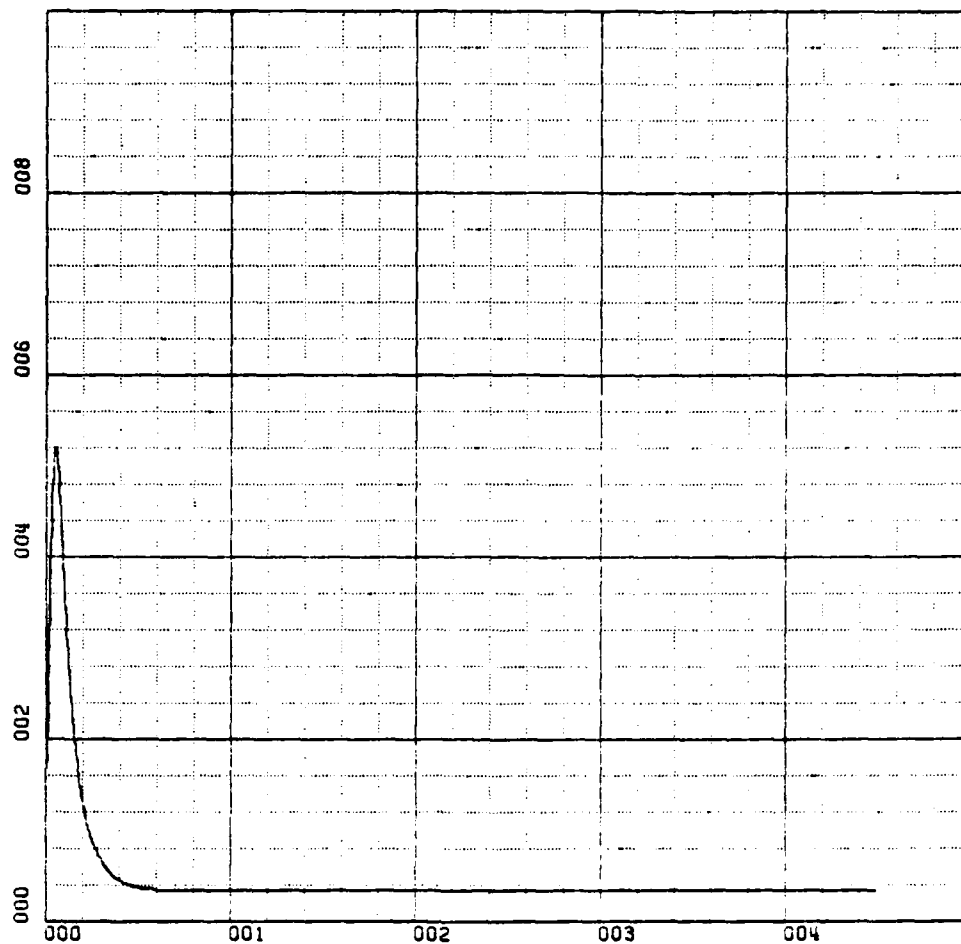
Y-SCALE=5.00E+00 UNITS INCH. [ft/sec]

KWSTAS

RUN 1

K1 VS TIME

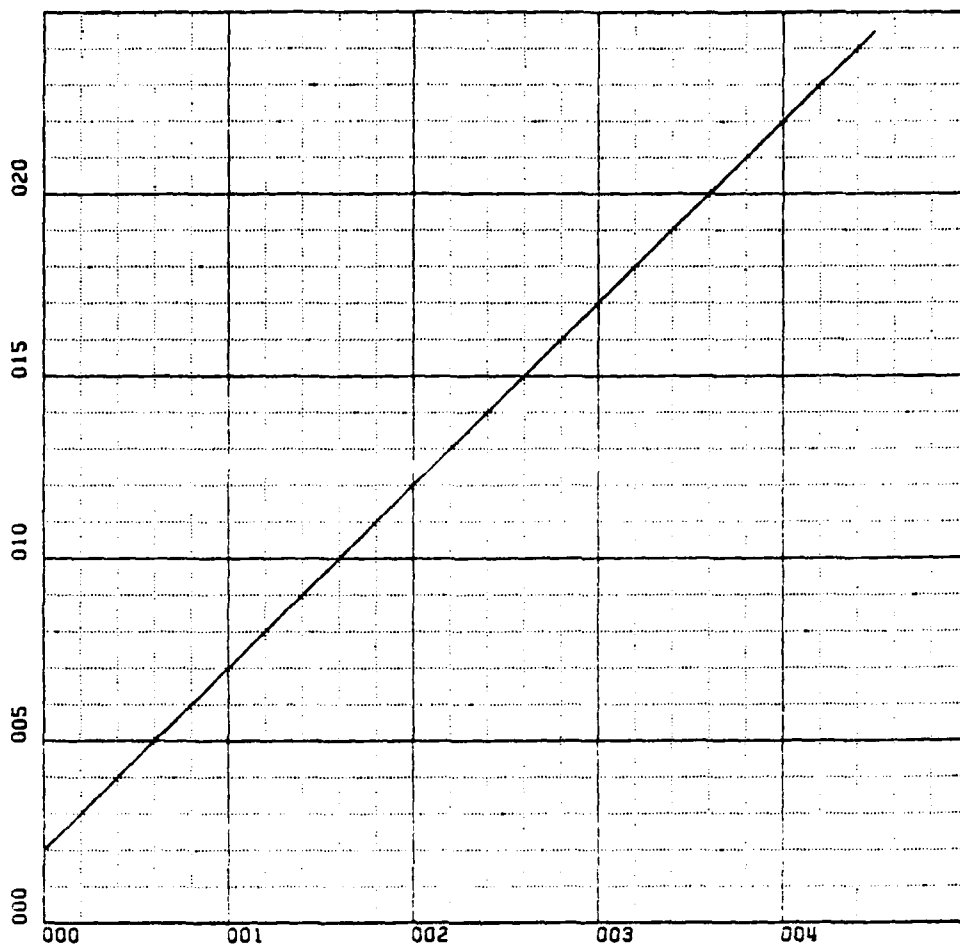
Figure 139. Case V. Kalman Filter Gain to Velocity.



X-SCALE=1.00E+01 UNITS INCH. [hours]
 Y-SCALE=2.00E+00 UNITS INCH. [ft/(sec)²]
 KWSTAS
 RUN 1

K2 VS TIME

Figure 140. Case V. Kalman Filter Gain to Acceleration.



X-SCALE=1.00E+01 UNITS INCH. [hours]

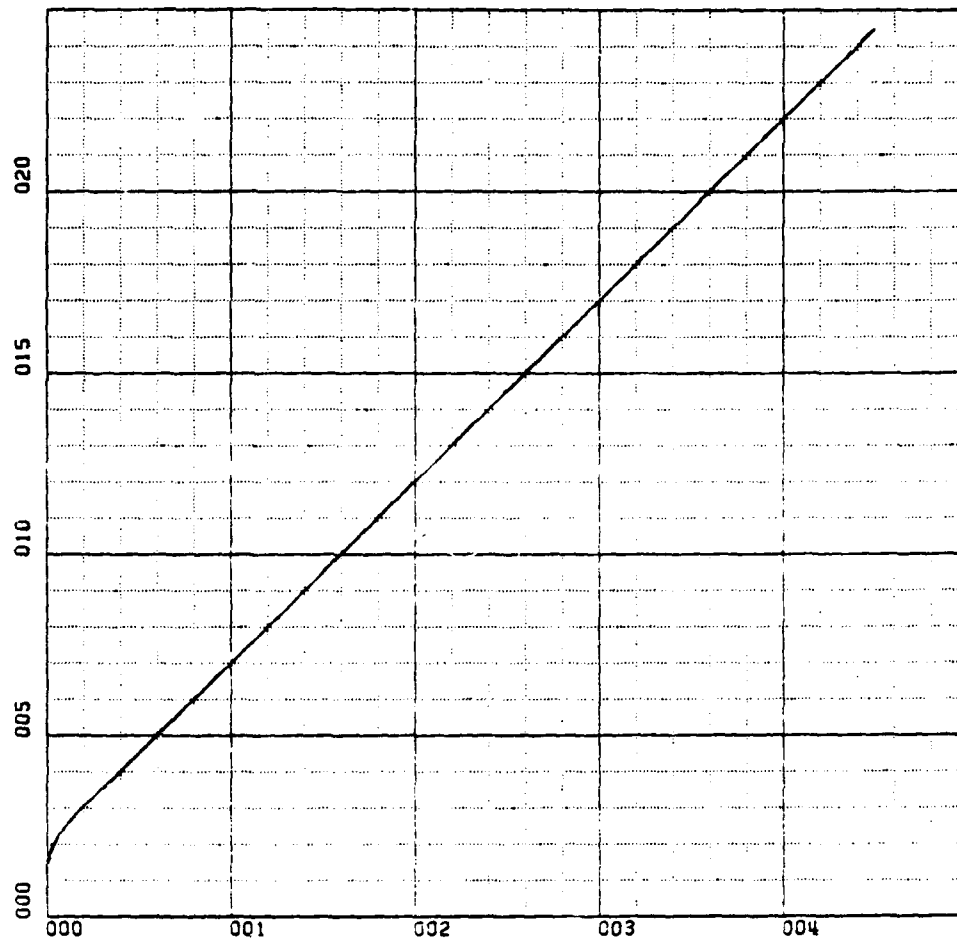
Y-SCALE=5.00E+02 UNITS INCH. [ft]

KWSTAS

RUN 2

R-TRUE VS TIME

Figure 141. Case V. True Position Versus Time.



X-SCALE=1.00E+01 UNITS INCH. [hours]

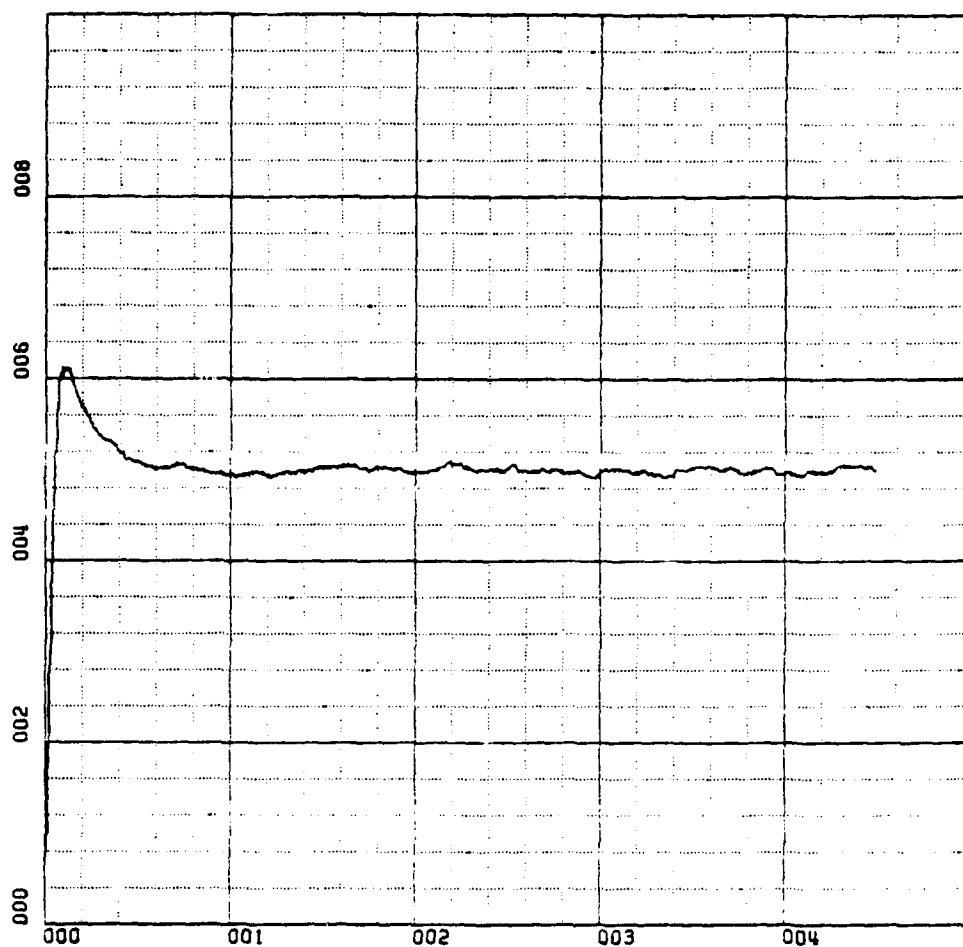
Y-SCALE=5.00E+02 UNITS INCH. [ft]

KWSTAS

RUN 2

R-HAT VS TIME

Figure 142. Case V. Predicted Position Versus Time.



X-SCALE=1.00E+01 UNITS INCH. [hours]

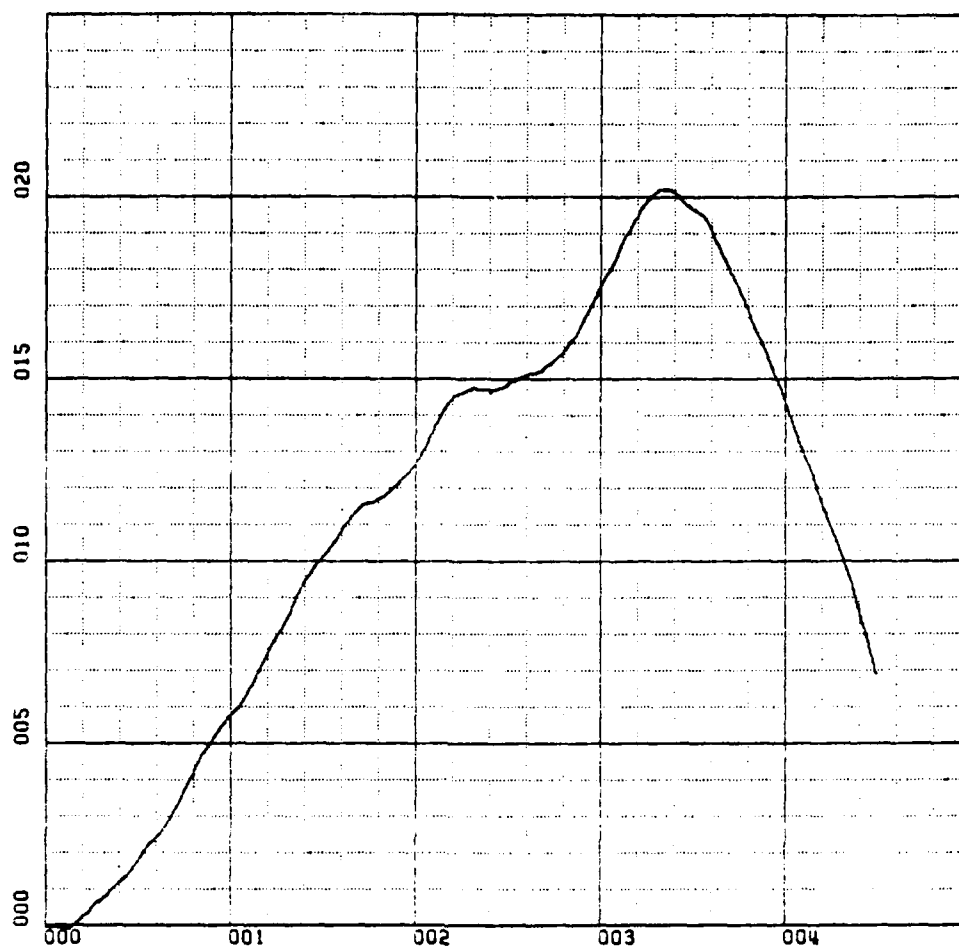
Y-SCALE=2.00E+01 UNITS INCH. [ft/sec]

KWSTAS

RUN 2

V-HAT VS TIME

Figure 143. Case V. Predicted Velocity Versus Time.



X-SCALE=1.00E+01 UNITS INCH. [hours]

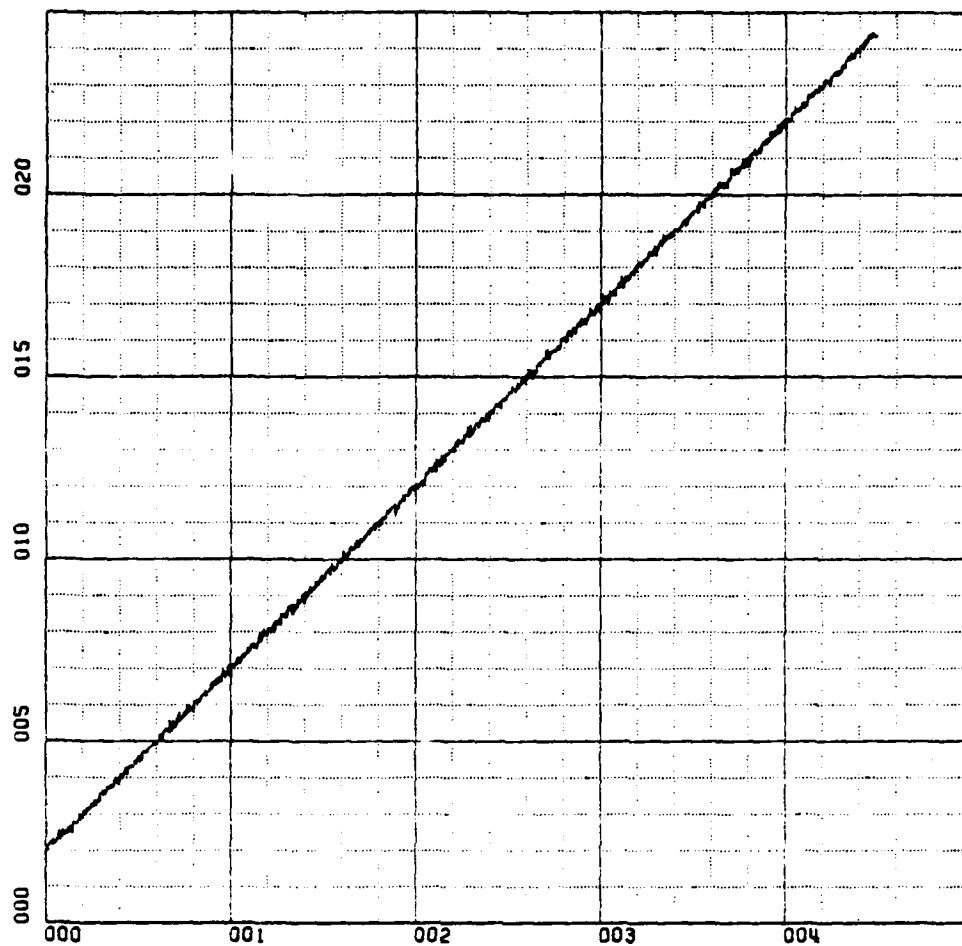
Y-SCALE=5.00E+00 UNITS INCH. [ft]

KWSTAS

RUN 3

R-INS VS TIME

Figure 144. Case V. I.N.S. Indicated Position Versus Time.



X-SCALE=1.00E+01 UNITS INCH. [hours]

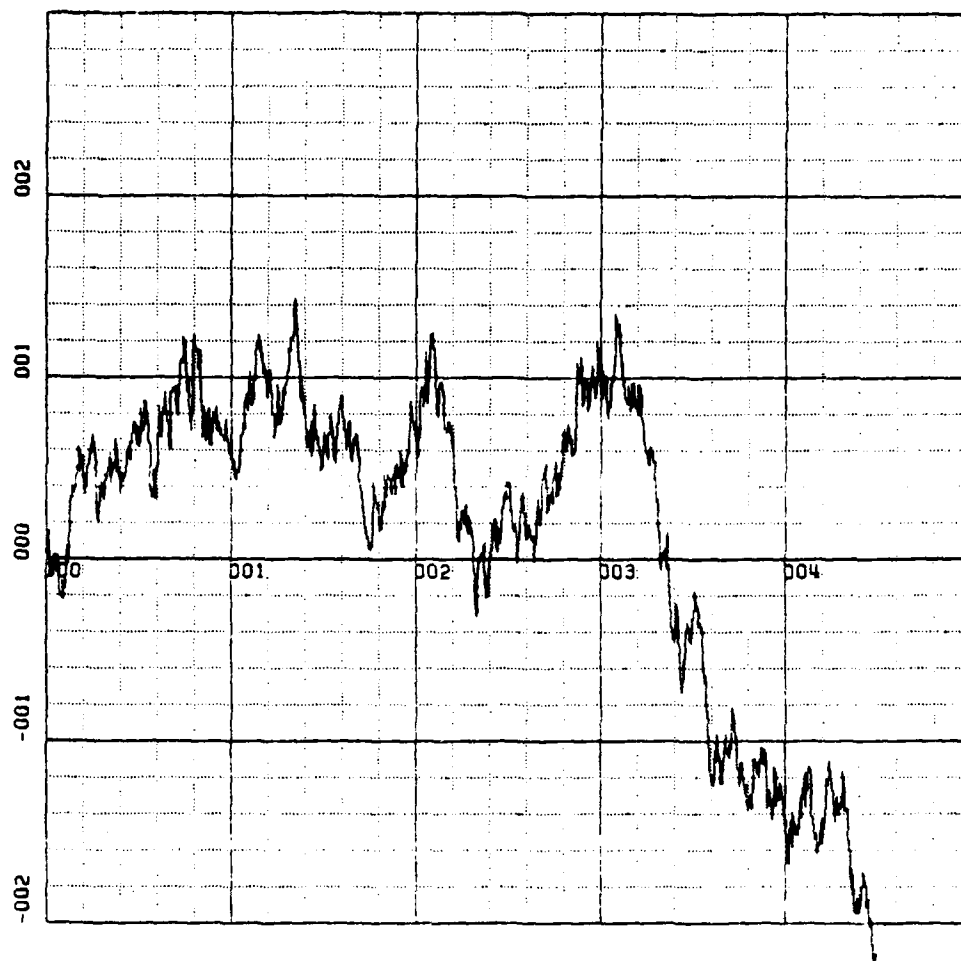
Y-SCALE=5.00E+02 UNITS INCH. [ft]

KWSTAS

RUN 3

R-RADAR VS TIME

Figure 145. Case V. Radar Indicated Position Versus Time.



X-SCALE=1.00E+01 UNITS INCH. [hours]

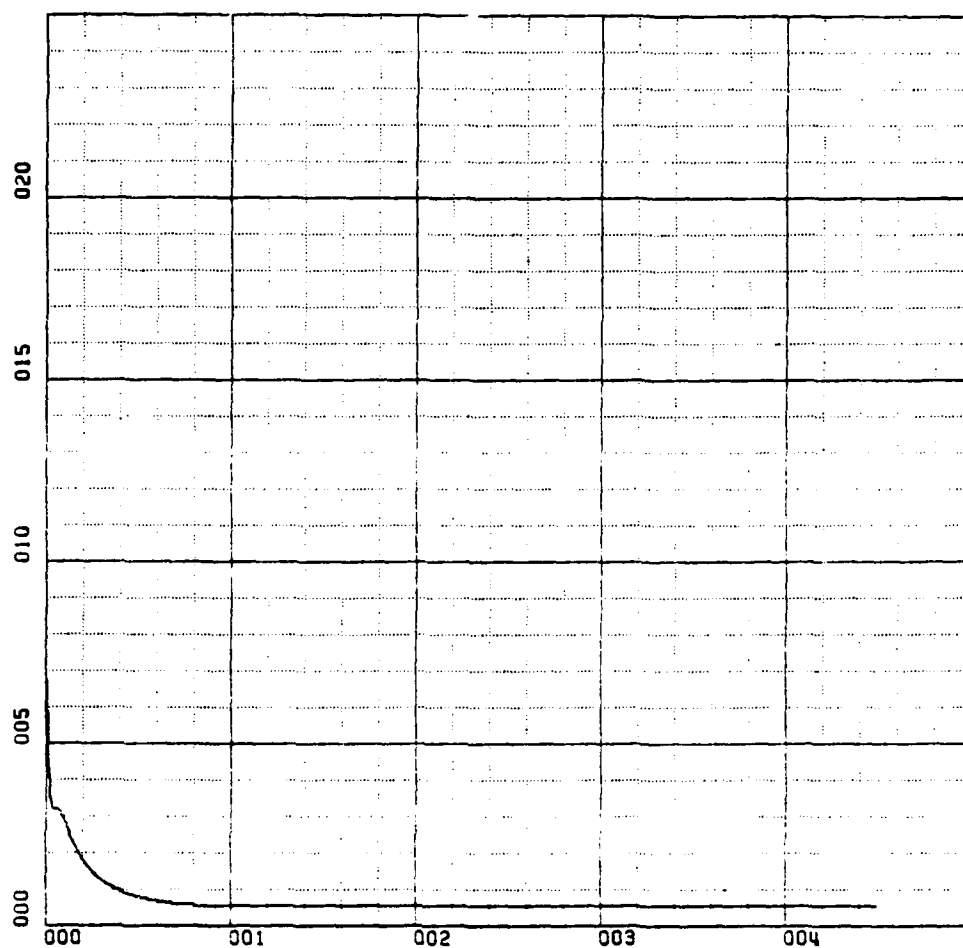
Y-SCALE=1.00E+00 UNITS INCH. [ft/sec]

KWSTAS

RUN 3

V-INS VS TIME

Figure 146. Case V. I.N.S. Indicated Velocity Versus Time.



X-SCALE=1.00E+01 UNITS INCH. [hours]

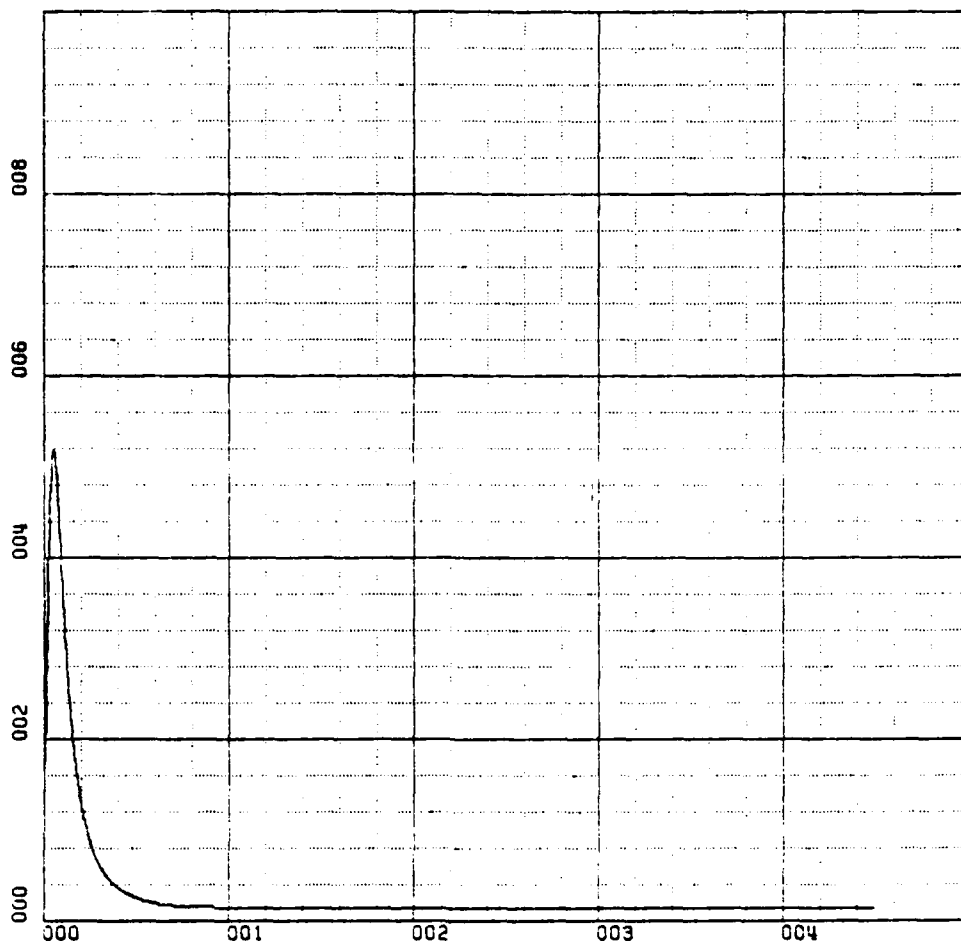
Y-SCALE=5.00E+00 UNITS INCH. [ft/sec]

KWSTAS

RUN 1

K1 VS TIME

Figure 147. Case VI. Kalman Filter Gain to Velocity.



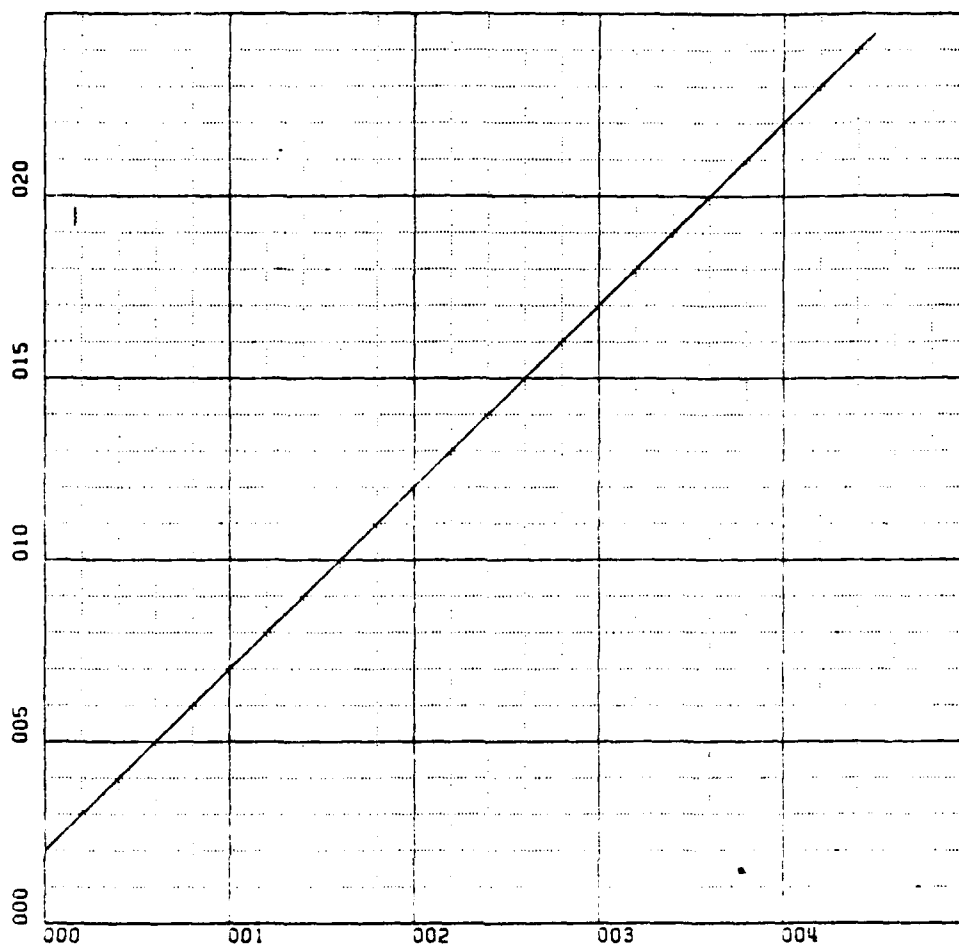
X-SCALE=1.00E+01 UNITS INCH. [hours]
Y-SCALE=2.00E+00 UNITS INCH. [ft/(sec)²]

KWSTAS

RUN 1

K2 VS TIME

Figure 148. Case VI. Kalman Filter Gain to Acceleration.



X-SCALE=1.00E+01 UNITS INCH. [hours]

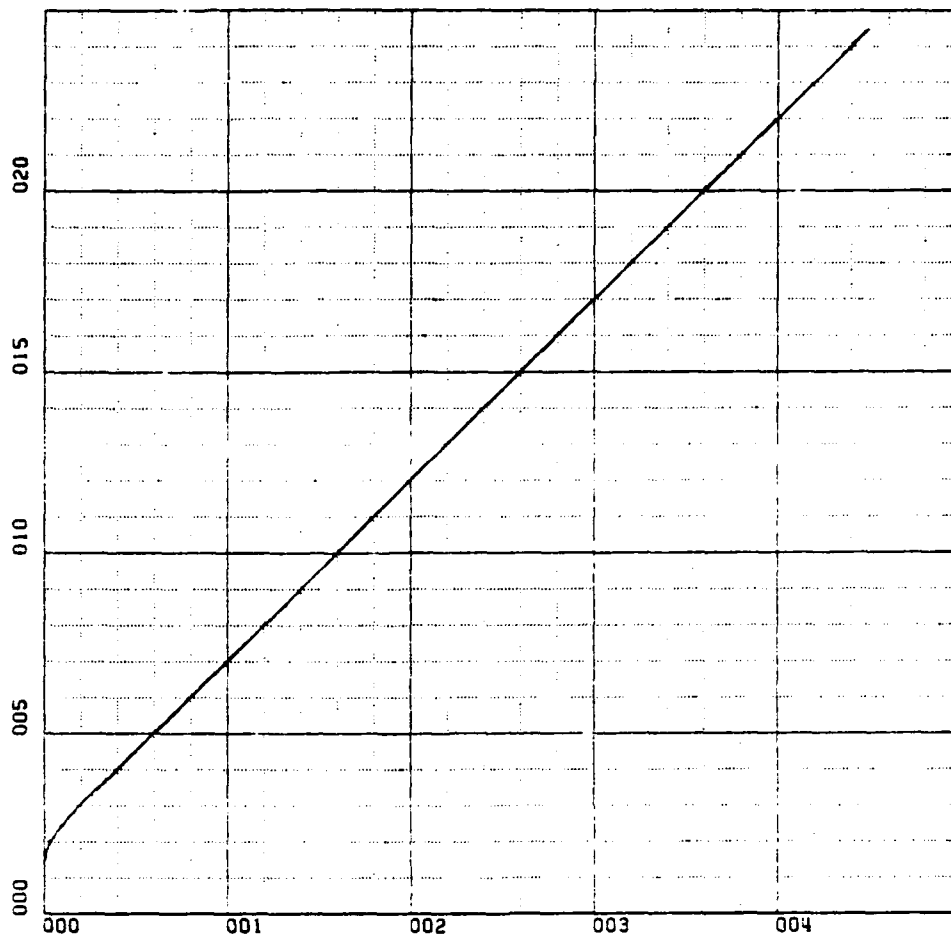
Y-SCALE=5.00E+02 UNITS INCH. [ft]

KWSTAS

RUN 2

R-TRUE VS TIME

Figure 149. Case VI. True Position Versus Time.



X-SCALE=1.00E+01 UNITS INCH. [hours]

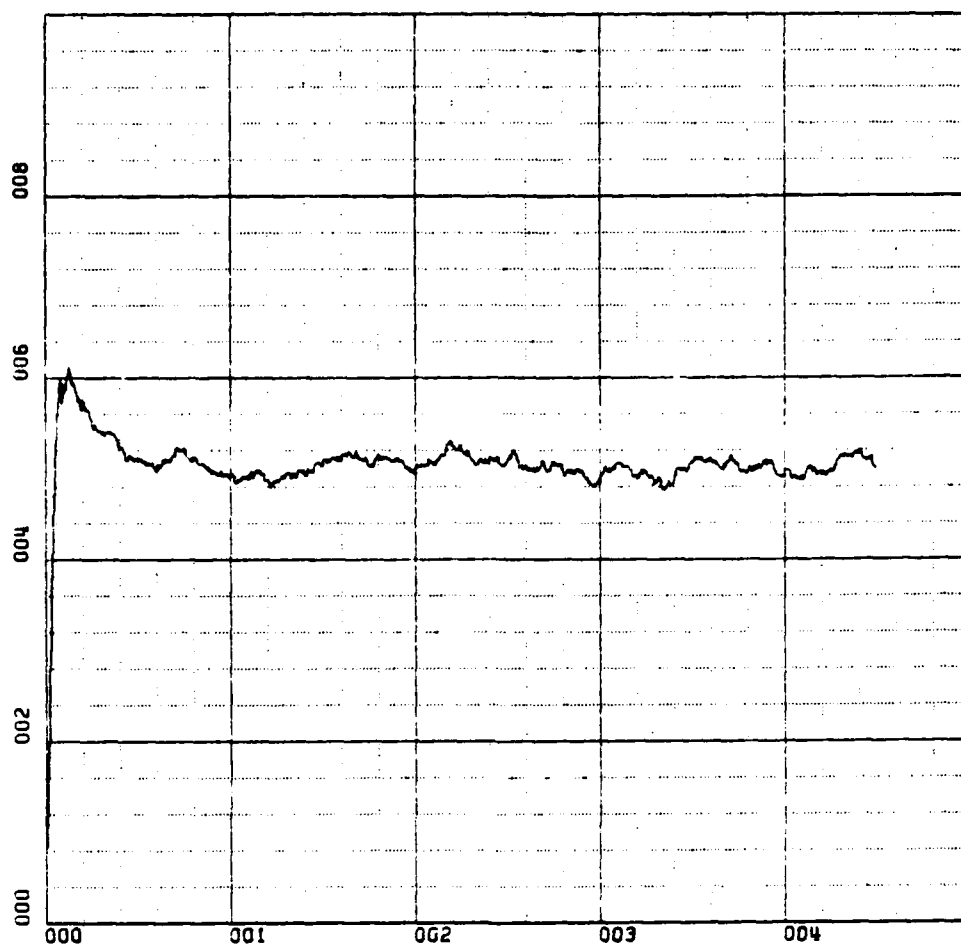
Y-SCALE=5.00E+02 UNITS INCH. [ft]

KWSTAS

RUN 2

R-HAT VS TIME

Figure 150. Case VI. Predicted Position Versus Time.



X-SCALE=1.00E+01 UNITS INCH. [hours]

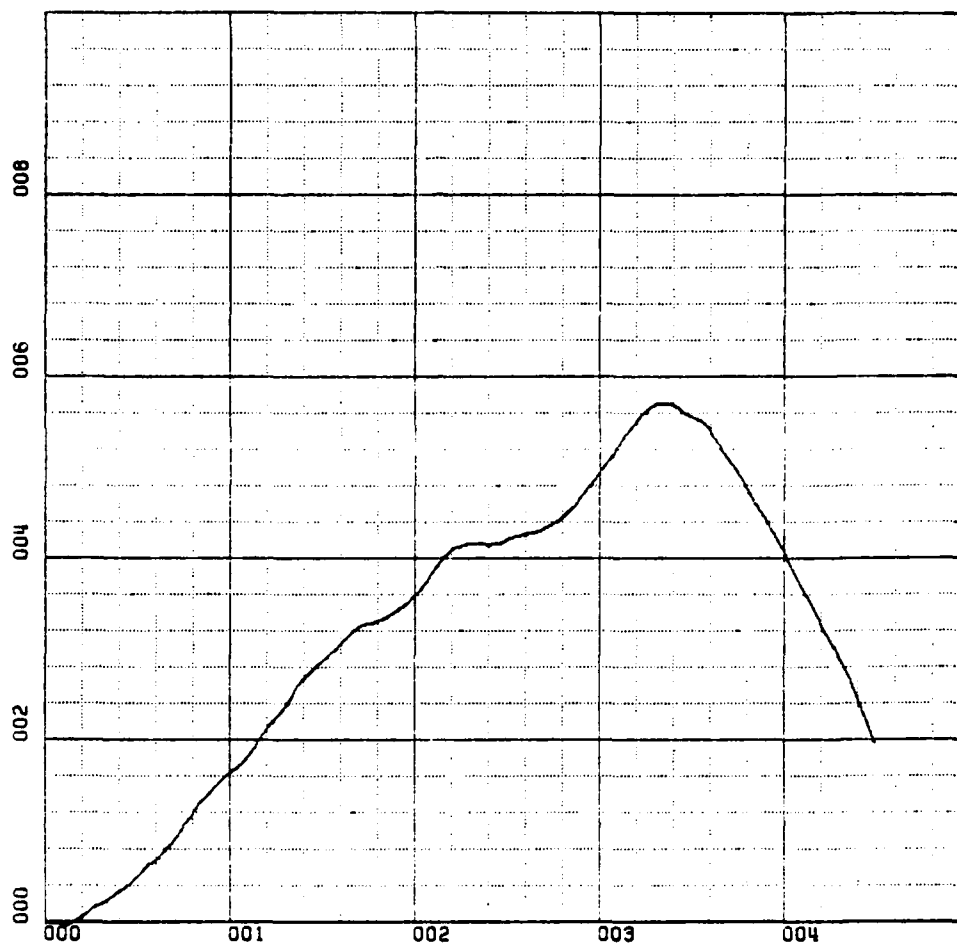
Y-SCALE=2.00E+01 UNITS INCH. [ft/sec]

KWSTAS

RUN 2

V-HAT VS TIME

Figure 151. Case VI. Predicted Velocity Versus Time.



X-SCALE=1.00E+01 UNITS INCH. [hours]

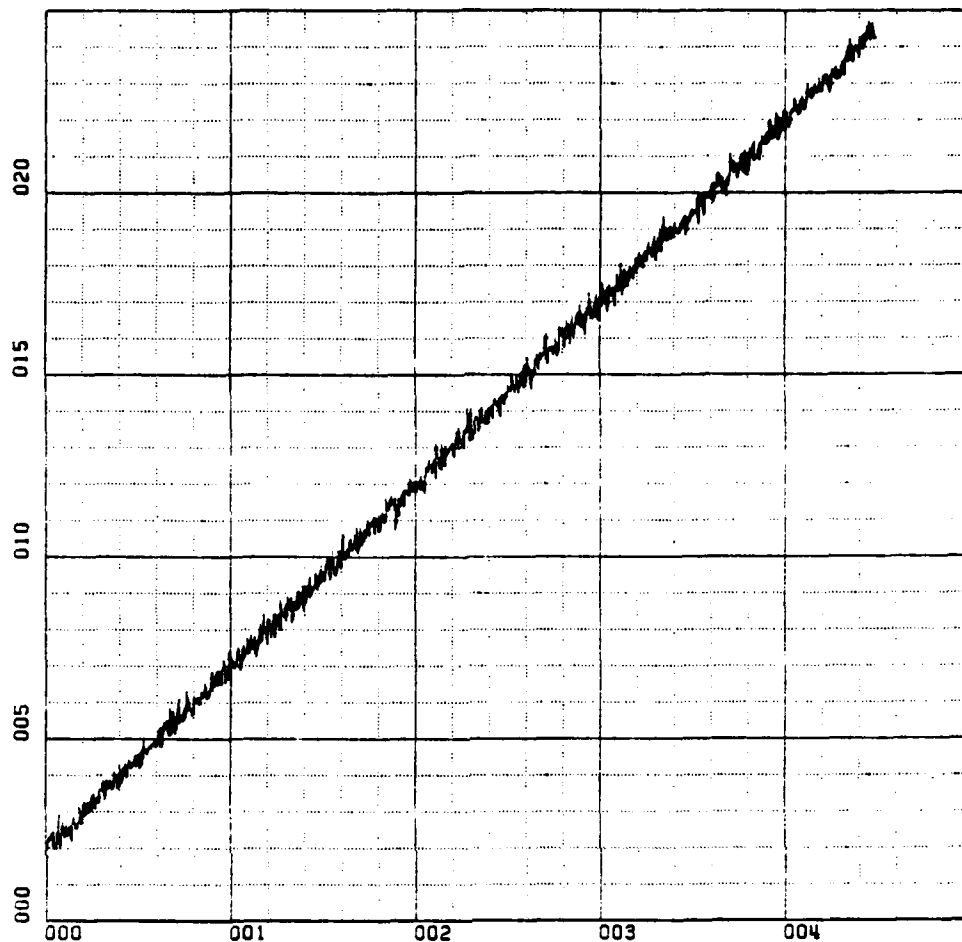
Y-SCALE=2.00E+01 UNITS INCH. [ft]

KWSTAS

RUN 3

R-INS VS TIME

Figure 152. Case VI. I.N.S. Indicated Position Versus Time.



X-SCALE=1.00E+01 UNITS INCH. [hours]

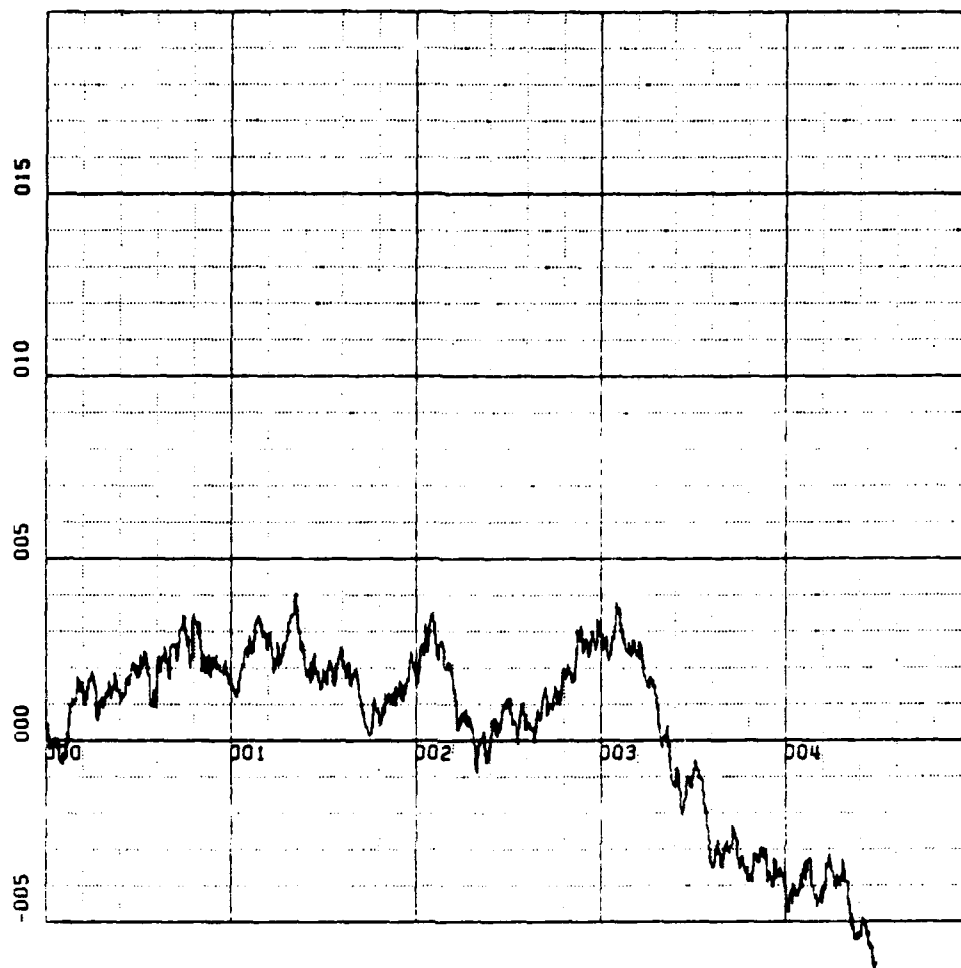
Y-SCALE=5.00E+02 UNITS INCH. [ft]

KWSTAS

RUN 3

R-RADAR VS TIME

Figure 153. Case VI. Radar Indicated Position Versus Time.



X-SCALE=1.00E+01 UNITS INCH. [hours]
Y-SCALE=5.00E+00 UNITS INCH. [ft/sec]

KWSTAS

RUN 3

V-INS VS TIME

Figure 154. Case VI. I.N.S. Indicated Velocity Versus Time.

APPENDIX B

SATELLITE GEOMETRY, VIEW AND RANGE ERRORS

The range measurement equation will first be developed. Next a simple program has been formulated to verify the "observability" and "suitability" of at least four satellites at any given time.

A. RANGE MEASUREMENT EQUATION

The range measuring process is characterized by a set of equations, called the range divergence equations, which are generated by the user from a combination of I.N.S. and satellite information. This range measurement process involves the comparison of a measured value of range against a predicted value of range.

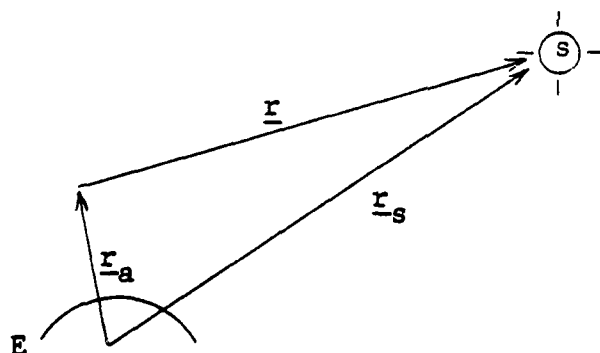
The measured range to a satellite is determined by measuring the incremental phase shift between the satellite's clock and that of the control station which supports the user. These clocks were synchronized at an earlier time. The computed range on the other hand is obtained from satellite ephemeris data and user I.N.S. supplied position information.

The fact is that both the measured and the computed range values contain in general errors; so by subtracting the computed range value from the measured one, the

different will contain only the associated errors. This difference is called "the range divergence." A Kalman filter can be constructed to estimate the errors and improve the accuracy of the raw range data if these errors can be modeled as the outputs of linear systems driven by white Gaussian noise [Ref. 8].

1. Range Divergence

The case of a single satellite will be considered, in order to avoid the notational inconvenience of using superscripts or subscripts to keep track of which satellite is being referred to. The results are identical for any one of the 18 satellites and therefore very easily extended.



- \underline{r} = User-Satellite position vector
- \underline{r}_a = Earth-User position vector
- \underline{r}_s = Earth-Satellite position vector

Figure 155. Range Vector Definition

The range vector of interest is the vector \underline{r} from the user to the satellite. It is explicitly related to the two vectors \underline{r}_a and \underline{r}_s which are defined and illustrated in the above figure. From the geometry it follows that

$$\underline{r} = \underline{r}_s - \underline{r}_a \quad (B-1)$$

where

$$r = |\underline{r}| = |\underline{r}_s - \underline{r}_a| = \underline{r} \cdot \underline{r} = (\underline{r}_s - \underline{r}_a) \cdot (\underline{r}_s - \underline{r}_a) \quad (B-2)$$

The measured range to the satellite, r' , is composed of two parts

$$r' = r + \delta r' \quad (B-3)$$

where, r is the true range and $\delta r'$ is the error in the measured range to the satellite. The computed range to the satellite, r'' , is in a similar way written:

$$r'' = r + \delta r'' \quad (B-4)$$

where, r is again the true range and $\delta r''$ is the error in the value of the computed range.

The quantity then, that is being observed, is the difference of these two range values and it is called "range divergence," Δr .

$$\Delta r = r' - r'' = \delta r' - \delta r'' \quad (B-5)$$

2. Errors in Measured Range

To model the range measurement error, a knowledge of the various error sources which are contained in the measurement is required and fitting these error sources with empirical data. The model used in our study is a simplified version of the one found in [Ref. 4] with additional information of [Ref. 5]. It is a linear combination of three components for each satellite measurement corrupted by white Gaussian noise (w). Each of the separate components is a linear system which is driven by white Gaussian noise.

The range measurement error is modeled by:

$$\delta r' = \delta b + c(\delta T_u - \delta T_s) + w \quad (B-6)$$

where

δb = range bias

c = the speed of the light

δT_u = user clock phase error

δT_s = satellite clock phase error

w = measurement noise

The error in the range measurement due to ionosphere delay is assumed to be included in the satellite clock phase/range error. This is a function of the elevation angle and on the

order of 15 feet as a good approximation. The bias term, δb , in the above equation accounts for the minor effect of both speed of light bias and tropospheric delay uncertainties in each one of the four satellite range measurements.

3. Errors in Computed Range

The computed satellite position includes error which depends on the ephemeris data errors, while the I.N.S. errors account for the uncertainty in the user's position. So far we have

$$\underline{r}_s'' = \underline{r}_s + \delta \underline{r}_s'' \quad (\text{B-7})$$

$$\underline{r}_a'' = \underline{r}_a + \delta \underline{r}_a'' \quad (\text{B-8})$$

The error equation is obtained now since,

$$(r'')^2 = \underline{r}'' \cdot \underline{r}''$$

and by taking the differential of both sides we get

$$2r''\delta r'' = \underline{r}'' \cdot \delta \underline{r}'' + \delta \underline{r}'' \cdot \underline{r}''$$

or

$$\delta r'' = \frac{1}{r''} (\underline{r}'' \cdot \delta \underline{r}'') = \left(\frac{1}{r''} \underline{r}'' \right) \cdot \delta \underline{r}'' \quad (\text{B-9})$$

We can easily notice that the quantity, $\frac{1}{r''} \underline{r}''$, of the right hand side is a unit vector from the user to the satellite.

$$\underline{i}_{r''} = \frac{1}{r''} \underline{r}'' ; \quad \underline{i}_{r''} = [i_{r_N}, i_{r_E}, i_{r_D}]^T \quad (\text{B-10})$$

and also that

$$\delta \underline{r}'' = \delta \underline{r}_s'' - \delta \underline{r}_a'' \quad (\text{B-11})$$

Finally the computed error is written as

$$\delta r'' = \underline{i}_r'' \cdot (\delta \underline{r}_s'' - \delta \underline{r}_a'') \quad (\text{B-12})$$

Without any significant accuracy loss, it is assumed that the earth-satellite range error, $\delta \underline{r}_s$ is approximately zero for the following logic sequence. Satellite orbital parameters are updated by the ground tracking network on a periodic basis and relayed to the user along with the range data. This ephemeris data is quite accurate and any uncertainties in computed satellite range can be accounted for by increasing the satellite clock phase error [Ref. 4].

Thus the computed range error can be written

$$\delta r'' = - \underline{i}_r'' \cdot \delta \underline{r}_a'' \quad (\text{B-13})$$

The computation of the above equation requires values for the unit vector from the user to the satellite and also current values for the north, east and azimuth I.N.S. position error states

$$\delta \underline{r}_a'' = [\Delta N, \Delta E, \Delta D]^T$$

Since we are dealing with a stochastic process simulation the root-mean-squared (RMS) values of the covariance of the three position errors are used.

The final form of the range divergence equation is obtained now by substitution of equations (B-6) and (B-13) into the general form equation (B-5)

$$\Delta r = \underline{\hat{r}}'' \cdot \delta \underline{\hat{r}}_a'' + c\delta T_u - c\delta T_s + \delta b + w \quad (B-14)$$

Since at least four satellites are required as observables to correct for the three components of position and the clock phase (or time difference), a minimum of four range divergence equations need to be solved simultaneously.

B. SATELLITE OBSERVABILITY

In the following development of equations we will drop out the double prime (") for notational convenience. A given satellite must be in-view by the user in order to obtain certain measurements. It is then required that the satellite must be above some specified minimum angle of the user's horizon to get a useful signal. This minimum angle depends upon the capabilities of the user-equipment and can be characterized as arbitrary. In our study the nominal value of this angle was selected of ten degrees. This observability criterion together with the suitable selection of 18 satellites as the total number of satellites for global coverage, insures that regardless of the user's

position, a sufficient and reasonable number of satellites will always be in-view, from which a "best set" of the required four satellites may be chosen.

In the following a method for determining whether or not a satellite is observable is presented.

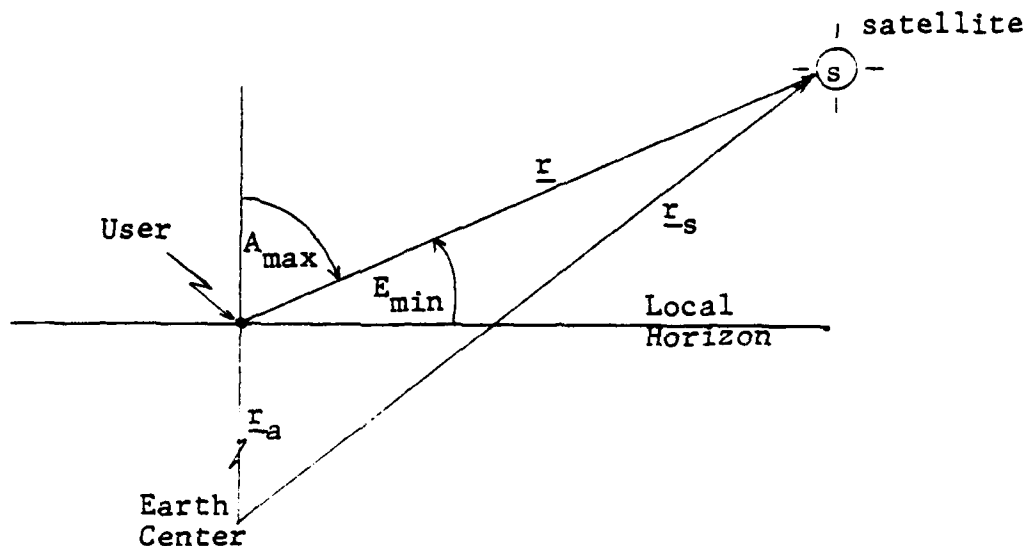


Figure 156. Observability-Criterion Geometry

From the above figure and for the following calculations:

E_{\min} = minimum angle of elevation for useful signal

$D_{\max} = 90^{\circ} - E_{\min}$

\underline{r} = User-Satellite position vector

\underline{r}_s = Earth-Satellite position vector

\underline{r}_a = Earth-User position vector

C_e^n = earth to navigation transformation matrix

The quantity \underline{r}_a is most readily expressed in the navigation frame as

$$\underline{r}_a^n = \begin{bmatrix} 0 \\ 0 \\ R+h \end{bmatrix} = \begin{bmatrix} 0 \\ 0 \\ R \end{bmatrix} \quad (B-15)$$

where

R = radius of Earth

h = altitude of user

and the superscript, n , denotes the frame in which the vector is coordinated (navigation frame).

Since the earth-satellite position vector in the earth frame, \underline{r}_s^e , is derived from the ground track latitude and longitude of the satellite in the orbit generator and is readily available, the vector \underline{r} from the user to the satellite coordinatized in the navigation frame is written as

$$\underline{r}_n = \underline{r}_s^n - \underline{r}_a^n = C_e^n \underline{r}_s^e - \begin{bmatrix} 0 \\ 0 \\ R \end{bmatrix} \quad (B-16)$$

The unit vector along \underline{r}^n is given by

$$\underline{i}_r = \frac{1}{r} \underline{r}^n ; \quad r = \underline{r}^n \cdot \underline{r}^n \quad (\text{B-17})$$

From the geometry we observe that the azimuth component of this unit vector is evaluated as the sine of the elevation angle, E, or the cosine of its complementary angle A. That is

$$\underline{i}_r \cdot \begin{bmatrix} 0 \\ 0 \\ 1 \end{bmatrix} = i_{r_D} = \cos A \quad (\text{B-18})$$

So far the observability criterion, if the unit vectors from the user to the satellite expressed in the navigation frame are computed, becomes

$$A < A_{\max}$$

or

$$\cos A > \cos A_{\max} \quad (\text{B-19})$$

or

$$\text{if } i_{r_D} > \cos A_{\max}, \text{ the satellite is observable}$$

$$\text{if } i_{r_D} \leq \cos A_{\max}, \text{ the satellite is not observable}$$

Since we arbitrarily selected for our study the minimum elevation angle of ten degrees the above criterion requires the azimuth component of this unit vector to be greater than the value of $\cos 80^\circ = 0.174$.

$$i_{r_D} > 0.174 \quad ; \quad A = 80^\circ \quad (B-20)$$

Total deployment consists of three rings or "constellations" of six satellites each. The satellite orbits are assumed to be planar and circular; in fact, the orbital speed and altitude and thus the orbital period of all satellites is assumed constant. Furthermore, since global coverage is desired, the satellites on any of the three rings are equally spaced; thus, the circular arc between any two adjacent satellites on a ring subtends a central angle of sixty degrees ($6 \times 60^\circ = 360^\circ$). The satellite identification code used is a two-digit code, the first digit denoting the particular constellation-ring (1, 2 or 3) and the second digit indicating the particular satellite (1 through 6) among the six on the denoted ring. As an example, satellite 32 is the second satellite on the third ring.

In order to specify the orientation of any one satellite with respect to the Earth-fixed frame, three parameters are required. The most convenient parameters are the Euler angle, from which the direction cosines or unit vectors to the satellite may be determined. This process is explicitly described in [Ref. 11] and here we will use directly the result for the unit vector from Earth to satellite in Earth coordinates.

$$\underline{r}_s^e = [a_{13}, a_{23}, a_{33}]^T \quad (B-21)$$

where

$$a_{13} = \sin \zeta \sin \xi$$

$$a_{23} = -(\sin n \cos \zeta + \cos n \sin \zeta \cos \xi) \quad (B-22)$$

$$a_{33} = \cos n \cos \zeta - \sin n \sin \zeta \cos \xi$$

and the three Euler angles are ξ , n , ζ .

The initial conditions are the constant orbital parameters of the satellite orbits are given in the following two tables. Note that m refers to the m th satellite on the designated n ring; for example, the entry of $2m$ represents the remaining five satellites of the second ring. The missing entries from the table, (--), are dependent upon the initial values of the Euler angles ξ , n and ζ which are specified. Finally the latitude and longitude values refer to the ground track of the satellites.

TABLE IX
ORBITAL DESIGN CONSTANTS

Orbital Period	12 hours
Angle of inclination	63° (all three rings)
Altitude	11,000 n. miles
Separation arc-angle	60° ($6 \times 60^\circ = 360^\circ$)
Ring spacing arc-angle	120° ($3 \times 120^\circ = 360^\circ$)

TABLE X
SATELLITE INITIAL CONDITIONS

<u>Satellite #</u>	<u>Initial Latitude</u>	<u>Initial Longitude</u>	<u>Angle ϵ_0</u>
11	0°	0°	0°
1m	--	--	-60(m-1)
21	0°	120° (E)	0°
2m	--	--	-60(m-1)
31	0°	-120° (W)	0°
3m	--	--	-60(m-1)

Now the sequence of equations required to compute the unit vectors for each of the 18 satellites is presented.

$$\xi = 63^\circ$$

$$n = 120^\circ(n-1) - \omega_{ie}t \quad (B-23)$$

$$\epsilon = -60(m-1) + Ct$$

where

m = satellite designator (1 through 6)

n = ring designator (1, 2 or 3)

ω_{ie} = rotational speed of earth = $15^\circ/h = 1^\circ/240 \text{ sec}$

C = orbital speed of the satellite

$$C = G_e/r_s^e = \frac{2r_s \cdot n}{T} = 2.1 \text{ n.miles/sec}$$

Using the Euler angles the components of the unit vectors of the satellite-earth range, \underline{r}_s^e , are computed [Ref. 10, 11].

$$\begin{aligned} a_{13} & \quad \sin \zeta \sin \xi \\ a_{23} & = -(\sin n \cos \zeta + \cos n \sin \zeta \cos \xi) \\ a_{33} & \quad \cos n \cos \zeta - \sin n \sin \zeta \cos \xi \end{aligned} \quad (B-24)$$

The ground track latitudes and longitudes are given by

$$\text{Latitude } \theta = \text{arc-tan} (a_{13} / \sqrt{(a_{23})^2 + (a_{33})^2}) \quad (B-25)$$

$$\text{Longitude } \Lambda = \text{arc-tan} (-a_{23}/a_{33}) \quad (B-26)$$

The required components of the unit vector of the user-satellite range, \underline{r}^n , in navigation coordinates may now be computed.

$$\begin{aligned} \underline{r}_s^n & = C_e^n \underline{r}_s^e \\ \underline{r}^n & = \underline{r}_s^n - \begin{bmatrix} 0 \\ 0 \\ R \end{bmatrix} = C_e^n \underline{r}_s^e - \begin{bmatrix} 0 \\ 0 \\ R \end{bmatrix} = \begin{bmatrix} r_N \\ r_E \\ r_D \end{bmatrix} \end{aligned} \quad (B-27)$$

$$r = (r_N)^2 + (r_E)^2 + (r_D)^2 \quad (B-28)$$

$$\underline{i}_{r_n} = \underline{r}^n / r = [i_{r_N}, i_{r_E}, i_{r_D}]^T \quad (B-29)$$

The observability-criterion requires

$$i_{r_D} > \cos 80^\circ = 0.174$$

(B-30)

A sample output from the computer program for the observability-criterion is included in the next pages listing the satellites which are in-view at a particular time instant. The output table presents in seven columns the most important calculated data. Column 1 contains the satellite number according to the previously specified code. Columns 2, 3 and 4 contain the north, east, and azimuth components of the unit vector under consideration. Columns 5 and 6 give the ground track latitude and longitude for each satellite. Finally column 7 gives the observability result denoting with "O.K." the satellites which fulfill the criterion and with "--" those satellites which do not fulfill the criterion.

```

$JOB
XREF KWSTAS SAFLIANIS
REAL * 4 H,K,F,X,Y,Z,LA,LQ,IX,IY,IZ
REAL * 8 R,IRX,IRY,IRZ,LAT,LONG
DIMENSION N(3),M(6)
PI = 3.14129
T = 3600
C = 3780
H = 63*PI/180
WRITE (6,60C)
WRITE (6,60C)
WRITE (6,60I)
DO 1 I = 1,3
  READ 1 (5,500) N(I)
DO 2 J = 1,6
  READ 2 (5,501) M(J)
R = 120*PI/180*(N(I)-1)-1/24*PI/180*T
F = 60*PI/180*(M(J)-1)+C*T
K = SIN(K)*SIN(H)
X = -(SIN(F)*COS(K)+COS(F)*SIN(K)*COS(H))
Y = COS(F)*COS(K)-SIN(F)*SIN(K)*COS(H)
Z = ATAN(X/(SQRT(Y**2+Z**2)))
LA = ATAN(-Y/Z)
LQ = COS(LQ)*SIN(LA)*Y-COS(LA)*SIN(LQ)*Z
IX = COS(LA)*Y+SIN(LA)*Z
IY = COS(LQ)*X-SIN(LQ)*COS(LA)*Y+
  SIN(LQ)*X-SIN(LA)*COS(LQ)*Z
IRX = IX/R
IRY = IY/R
IRZ = IZ/R
LAT = LA * 180/PI
LONG = LQ * 180/PI
IF (IRZ.LE.0.174) GO TO 100
  AND:(LONG.LE.0.) GO TO 10
  I,J,IRX,IRY,IRZ,LAT,LONG
  WRITE (8,602) I,J,IRX,IRY,IRZ,LAT,LONG
  TC 20
10 IF ((LAT.GE.0.) AND.(LONG.GE.0.)) GC TC 11
  I,J,IRX,IRY,IRZ,LAT,LONG
  WRITE (8,603) I,J,IRX,IRY,IRZ,LAT,LONG
  TC 20
11 IF ((LAT.LE.0.) AND.(LONG.GE.0.)) GC TC 12
  I,J,IRX,IRY,IRZ,LAT,LONG
  WRITE (8,604) I,J,IRX,IRY,IRZ,LAT,LONG
  TC 20
12 CONTINUE
  I,J,IRX,IRY,IRZ,LAT,LONG
  WRITE (8,605) I,J,IRX,IRY,IRZ,LAT,LONG

```

267

TABLE XI-1

SATELLITE POSITION AND OBSERVABILITY CRITERION							TIME = 30	S
SAT #	X-COORD	Y-COORD	Z-COORD	LATITUDE	LONGITUDE	VIEW		
11	0.21	0.13	0.97	51.47 N	39.79 E	OK		
12	0.00	0.00	1.00	0.46 N	0.24 E	OK		
13	-0.22	-0.13	0.97	-50.75 S	-38.59 W	OK		
14	-0.59	0.65	-0.49	-49.63 N	36.83 E	--		
15	-0.01	0.03	-1.00	-1.31 N	0.67 E	--		
16	0.59	-0.64	-0.49	50.08 N	-37.53 E	--		
21	0.67	-0.59	-0.45	51.47 N	-20.23 E	--		
22	-0.42	-0.87	-0.26	0.46 N	-59.78 E	--		
23	0.30	-0.47	-0.83	-50.75 N	81.41 E	--		
24	-0.47	-0.29	0.83	-49.63 S	-23.19 W	OK		
25	0.44	0.85	0.29	-1.31 S	-59.35 W	OK		
26	0.64	0.34	0.69	50.08 N	82.47 E	OK		
31	-0.28	0.47	-0.84	51.47 N	-80.25 E	--		
32	0.44	0.86	-0.24	0.46 N	60.22 E	--		
33	-0.65	0.60	-0.46	-50.75 N	21.39 E	--		
34	-0.63	-0.36	0.69	-49.63 S	-83.21 W	OK		
35	-0.42	-0.88	0.21	-1.31 N	60.65 E	OK		
36	0.49	0.30	0.82	50.08 N	22.45 E	OK		

TABLE XI-2

SATELLITE POSITION AND OBSERVABILITY CRITERION							TIME = 60	S
SAT #	X-COORD	Y-COORD	Z-COORD	LATITUDE	LONGITUDE	VIEW		
11	0.57	-0.66	-0.49	48.51 N	-35.18 E	--		--
12	0.21	0.12	0.97	51.82 N	40.40 E	OK		OK
13	0.01	0.01	1.00	0.93 N	0.47 E	OK		OK
14	-0.22	-0.14	0.97	-50.39 S	-38.01 W	OK		OK
15	-0.62	0.61	-0.49	-52.46 N	41.55 E	--		--
16	-0.02	0.05	-1.00	-1.77 N	0.90 E	--		--
21	0.60	0.39	0.70	48.51 N	84.82 E	OK		OK
22	0.67	-0.59	-0.45	51.82 N	-19.61 E	--		--
23	-0.42	-0.87	-0.26	0.93 N	-59.55 E	--		--
24	0.32	-0.47	-0.82	-50.39 N	81.99 E	--		--
25	-0.59	-0.34	0.73	-52.46 S	-18.47 W	OK		OK
26	0.45	0.84	0.30	-1.77 S	-59.11 W	OK		OK
31	0.43	0.27	0.86	48.51 N	24.80 E	OK		OK
32	-0.26	0.46	-0.85	51.82 N	-79.63 E	--		--
33	0.45	0.86	-0.24	0.93 N	60.45 E	--		--
34	-0.64	0.61	-0.47	-50.39 N	21.98 E	--		--
35	-0.69	-0.27	0.67	-52.46 S	-78.49 W	OK		OK
36	-0.42	-0.89	0.20	-1.77 N	60.89 E	OK		OK

TABLE XI-3

SATELLITE POSITION AND OBSERVABILITY CRITERION							TIME = 120 S	
SAT #	X-COORD	Y-COORD	Z-COORD	LATITUDE	LONGITUDE	VIEW		
11	-0.64	0.58	-0.51	-54.23 N	45.02 E	--		
12	-0.04	0.11	-0.99	-4.20 N	2.14 E	--		
13	0.56	-0.67	-0.49	47.74 N	-34.12 E	--		
14	0.20	0.11	0.97	52.52 N	41.60 E	OK		
15	0.04	0.04	1.00	5.04 N	2.58 E	OK		
16	-0.25	-0.16	0.95	-47.04 S	-33.18 W	OK		
21	-0.67	-0.37	0.65	-54.23 S	-15.00 W	OK		
22	0.46	0.80	0.38	-4.20 S	-57.87 W	OK		
23	0.58	0.42	0.70	47.74 N	85.88 E	OK		
24	0.69	-0.57	-0.44	52.52 N	-18.36 E	--		
25	-0.34	-0.88	-0.32	5.04 N	-57.44 E	--		
26	0.43	-0.49	-0.76	-47.04 N	86.82 E	--		
31	-0.74	-0.21	0.64	-54.23 S	-75.02 W	OK		
32	-0.39	-0.91	0.12	-4.20 N	62.13 E	--		
33	0.39	0.25	0.88	47.74 N	25.86 E	OK		
34	-0.23	0.46	-0.86	52.52 N	-78.38 E	--		
35	0.52	0.84	-0.17	5.04 N	62.56 E	--		
36	-0.57	0.65	-0.50	-47.04 N	26.81 E	--		

TABLE XI-4

SATELLITE POSITION AND OBSERVABILITY CRITERION							TIME = 360 S	
SAT #	X-COORD	Y-COORD	Z-COORD	LATITUDE	LONGITUDE	VIEW		
11	0.12	0.12	0.98	14.89 N	7.79 E	OK		
12	-0.25	-0.20	0.95	-35.39 S	-21.22 W	OK		
13	-0.21	0.52	-0.83	-22.01 N	11.89 E	--		
14	0.29	-0.62	-0.73	28.54 N	-16.09 E	--		
15	0.41	-0.21	-0.89	63.00 N	-89.39 E	--		
16	0.22	0.19	0.96	29.02 N	16.42 E	OK		
21	-0.14	-0.89	-0.43	14.89 N	-52.23 E	--		
22	-0.65	-0.58	0.49	-35.39 S	-81.24 W	OK		
23	0.37	0.41	0.83	-22.01 S	-48.13 W	OK		
24	-0.10	0.85	-0.52	28.54 N	-76.11 E	--		
25	0.96	-0.24	0.12	63.00 N	30.61 E	--		
26	0.17	-0.83	-0.52	29.02 N	-43.59 E	--		
31	0.64	0.77	0.02	14.89 N	67.77 E	--		
32	-0.31	0.78	-0.54	-35.39 N	38.76 E	--		
33	-0.06	-0.93	-0.38	-22.01 N	71.87 E	--		
34	-0.24	-0.23	0.94	28.54 N	43.89 E	OK		
35	0.77	0.45	-0.45	63.00 N	-29.40 E	--		
36	0.69	0.64	0.33	29.02 N	76.41 E	OK		

TABLE XI-5

SATELLITE POSITION AND OBSERVABILITY CRITERION							TIME = 1200 S	
SAT #	X-COORD	Y-COORD	Z-COORD	LATITUDE	LONGITUDE	VIEW		
11	-0.18	-0.11	0.98	-53.29 S	-43.12 W	OK		
12	-0.58	0.65	-0.49	-49.49 N	36.62 E	--		
13	0.56	-0.67	-0.49	47.63 N	-33.97 E	--		
14	0.15	0.08	0.99	54.91 N	46.50 E	OK		
15	0.07	0.07	1.00	8.36 N	4.30 E	OK		
16	-0.26	-0.19	0.95	-41.39 S	-26.69 W	OK		
21	0.19	-0.46	-0.87	-53.29 N	76.88 E	--		
22	-0.47	-0.29	0.84	-49.49 S	-23.39 W	OK		
23	0.58	0.42	0.70	47.63 N	86.03 E	OK		
24	0.75	-0.53	-0.40	54.91 N	-13.51 E	--		
25	-0.28	-0.89	-0.36	8.36 N	-55.72 E	--		
26	-0.56	-0.53	0.63	-41.39 S	-86.70 W	OK		
31	-0.71	0.56	-0.43	-53.29 N	16.86 E	--		
32	-0.62	-0.36	0.69	-49.49 S	-83.41 W	OK		
33	0.39	0.25	0.89	47.63 N	26.01 E	OK		
34	-0.11	0.45	-0.89	54.91 N	-73.53 E	--		
35	0.56	0.82	-0.11	8.36 N	64.28 E	--		
36	-0.44	0.72	-0.53	-41.39 N	33.30 E	--		

TABLE XI-6

SATELLITE POSITION AND OBSERVABILITY CRITERION							TIME = 3600 S
SAT #	X-COORD	Y-COORD	Z-COORD	LATITUDE	LONGITUDE	VIEW	
11	0.10	-0.28	-0.95	11.02 N	-5.70 E	--	
12	0.66	-0.52	-0.54	56.68 N	-50.81 E	--	
13	-0.03	-0.03	1.00	-3.81 S	-1.94 W	OK	
14	-0.21	-0.12	0.97	-51.59 S	-39.99 W	OK	
15	-0.61	0.63	-0.49	-51.29 N	39.48 E	--	
16	-0.03	0.09	-1.00	-3.42 N	1.75 E	--	
21	0.28	0.96	-0.08	11.02 N	-65.71 E	--	
22	0.80	0.12	0.59	56.68 N	69.19 E	OK	
23	-0.50	-0.85	-0.19	-3.81 S	-61.96 W	--	
24	0.27	-0.46	-0.84	-51.59 N	80.01 E	--	
25	-0.54	-0.32	0.78	-51.29 S	-20.53 W	OK	
26	0.46	0.82	0.35	-3.42 S	-58.27 W	OK	
31	-0.47	-0.67	0.57	11.02 N	54.29 E	OK	
32	0.77	0.41	0.50	56.68 N	9.17 E	OK	
33	0.36	0.88	-0.31	-3.81 N	58.04 E	--	
34	-0.67	0.59	-0.45	-51.59 N	19.99 E	--	
35	-0.67	-0.31	0.68	-51.29 S	-80.55 W	OK	
36	-0.40	-0.91	0.15	-3.42 N	61.73 E	--	

APPENDIX C

I.N.S. ERROR ANALYSIS COMPUTER PROGRAMS

KWS00050
KWS00051
KWS00052
KWS00053
KWS00054
KWS00055
KWS00056
KWS00057
KWS00058
KWS00059
KWS00060
KWS00061
KWS00062
KWS00063
KWS00064
KWS00065
KWS00066
KWS00067
KWS00068
KWS00069
KWS00070
KWS00071
KWS00072
KWS00073
KWS00074
KWS00075
KWS00076
KWS00077
KWS00078
KWS00079
KWS00080
KWS00081
KWS00082
KWS00083
KWS00084
KWS00085
KWS00086
KWS00087
KWS00088
KWS00089
KWS00090
KWS00091
KWS00092
KWS00093
KWS00094
KWS00095
KWS00096
KWS00097
KWS00098
KWS00099
KWS00100
KWS00101
KWS00102
KWS00103
KWS00104
KWS00105
KWS00106
KWS00107
KWS00108
KWS00109
KWS00110
KWS00111
KWS00112
KWS00113
KWS00114
KWS00115
KWS00116
KWS00117
KWS00118
KWS00119
KWS00120
KWS00121
KWS00122
KWS00123
KWS00124
KWS00125
KWS00126
KWS00127
KWS00128
KWS00129
KWS00130
KWS00131
KWS00132
KWS00133
KWS00134
KWS00135
KWS00136
KWS00137
KWS00138
KWS00139
KWS00140
KWS00141
KWS00142
KWS00143
KWS00144
KWS00145
KWS00146
KWS00147
KWS00148
KWS00149
KWS00150
KWS00151
KWS00152
KWS00153
KWS00154
KWS00155
KWS00156
KWS00157
KWS00158
KWS00159
KWS00160
KWS00161
KWS00162
KWS00163
KWS00164
KWS00165
KWS00166
KWS00167
KWS00168
KWS00169
KWS00170
KWS00171
KWS00172
KWS00173
KWS00174
KWS00175
KWS00176
KWS00177
KWS00178
KWS00179
KWS00180
KWS00181
KWS00182
KWS00183
KWS00184
KWS00185
KWS00186
KWS00187
KWS00188
KWS00189
KWS00190
KWS00191
KWS00192
KWS00193
KWS00194
KWS00195
KWS00196
KWS00197
KWS00198
KWS00199
KWS00200
KWS00201
KWS00202
KWS00203
KWS00204
KWS00205
KWS00206
KWS00207
KWS00208
KWS00209
KWS00210
KWS00211
KWS00212
KWS00213
KWS00214
KWS00215
KWS00216
KWS00217
KWS00218
KWS00219
KWS00220
KWS00221
KWS00222
KWS00223
KWS00224
KWS00225
KWS00226
KWS00227
KWS00228
KWS00229
KWS00230
KWS00231
KWS00232
KWS00233
KWS00234
KWS00235
KWS00236
KWS00237
KWS00238
KWS00239
KWS00240
KWS00241
KWS00242
KWS00243
KWS00244
KWS00245
KWS00246
KWS00247
KWS00248
KWS00249
KWS00250
KWS00251
KWS00252
KWS00253
KWS00254
KWS00255
KWS00256
KWS00257
KWS00258
KWS00259
KWS00260
KWS00261
KWS00262
KWS00263
KWS00264
KWS00265
KWS00266
KWS00267
KWS00268
KWS00269
KWS00270
KWS00271
KWS00272
KWS00273
KWS00274
KWS00275
KWS00276
KWS00277
KWS00278
KWS00279
KWS00280
KWS00281
KWS00282
KWS00283
KWS00284
KWS00285
KWS00286
KWS00287
KWS00288
KWS00289
KWS00290
KWS00291
KWS00292
KWS00293
KWS00294
KWS00295
KWS00296
KWS00297
KWS00298
KWS00299
KWS00300
KWS00301
KWS00302
KWS00303
KWS00304
KWS00305
KWS00306
KWS00307
KWS00308
KWS00309
KWS00310
KWS00311
KWS00312
KWS00313
KWS00314
KWS00315
KWS00316
KWS00317
KWS00318
KWS00319
KWS00320
KWS00321
KWS00322
KWS00323
KWS00324
KWS00325
KWS00326
KWS00327
KWS00328
KWS00329
KWS00330
KWS00331
KWS00332
KWS00333
KWS00334
KWS00335
KWS00336
KWS00337
KWS00338
KWS00339
KWS00340
KWS00341
KWS00342
KWS00343
KWS00344
KWS00345
KWS00346
KWS00347
KWS00348
KWS00349
KWS00350
KWS00351
KWS00352
KWS00353
KWS00354
KWS00355
KWS00356
KWS00357
KWS00358
KWS00359
KWS00360
KWS00361
KWS00362
KWS00363
KWS00364
KWS00365
KWS00366
KWS00367
KWS00368
KWS00369
KWS00370
KWS00371
KWS00372
KWS00373
KWS00374
KWS00375
KWS00376
KWS00377
KWS00378
KWS00379
KWS00380
KWS00381
KWS00382
KWS00383
KWS00384
KWS00385
KWS00386
KWS00387
KWS00388
KWS00389
KWS00390
KWS00391
KWS00392
KWS00393
KWS00394
KWS00395
KWS00396
KWS00397
KWS00398
KWS00399
KWS00400
KWS00401
KWS00402
KWS00403
KWS00404
KWS00405
KWS00406
KWS00407
KWS00408
KWS00409
KWS00410
KWS00411
KWS00412
KWS00413
KWS00414
KWS00415
KWS00416
KWS00417
KWS00418
KWS00419
KWS00420
KWS00421
KWS00422
KWS00423
KWS00424
KWS00425
KWS00426
KWS00427
KWS00428
KWS00429
KWS00430
KWS00431
KWS00432
KWS00433
KWS00434
KWS00435
KWS00436
KWS00437
KWS00438
KWS00439
KWS00440
KWS00441
KWS00442
KWS00443
KWS00444
KWS00445
KWS00446
KWS00447
KWS00448
KWS00449
KWS00450
KWS00451
KWS00452
KWS00453
KWS00454
KWS00455
KWS00456
KWS00457
KWS00458
KWS00459
KWS00460
KWS00461
KWS00462
KWS00463
KWS00464
KWS00465
KWS00466
KWS00467
KWS00468
KWS00469
KWS00470
KWS00471
KWS00472
KWS00473
KWS00474
KWS00475
KWS00476
KWS00477
KWS00478
KWS00479
KWS00480
KWS00481
KWS00482
KWS00483
KWS00484
KWS00485
KWS00486
KWS00487
KWS00488
KWS00489
KWS00490
KWS00491
KWS00492
KWS00493
KWS00494
KWS00495
KWS00496
KWS00497
KWS00498
KWS00499
KWS00500
KWS00501
KWS00502
KWS00503
KWS00504
KWS00505
KWS00506
KWS00507
KWS00508
KWS00509
KWS00510

//KWSSTAS JOB (2211,1196),'KWSSTAS SAFLIANIS',CLASS=A

//EXEC FRTXCLGP

//FORT.SYSIN DD *

DIMENSION X(30),XDOT(30),C(15)

REAL*8 W,WIE,K

REAL*4 SN,SN2,CO,TN,L

CONSTANTS

WIE = .2618 "RAD/HR" = 900 "ARC-MIN/HR" = EARTH RATE
K = G/R = 19.52 "1/HR**2" (K**2 = SHULER FREQ.)
C(1) = (U)W<N> = NCRTH GYRO DRIFT = 1 "MERU" = 0.015 "DEG/HR"
C(2) = (U)W<E> = EAST " " = 1 "MERU" = 0.015 "DEG/HR"
C(3) = (U)W<D> = AZIMOUTH " " = 1 "MERU" = 0.015 "DEG/HR"
L = LATITUDE "RAD"
W = LOCAL EARTH RATE

FUNCTIONS

WIE = .2618
L = 7854
K = 19.52
SN = SIN(L)
SN2 = SIN(2.*L)
CN = COS(L)
TN = TAN(L)

CASE : STATICNARY

W = WIE

C(10) = 1.
1 CALL INTEG2(T,X,XDOT,C)

EQUATIONS

XDOT(1) = -W*SN*X(2) - W*SN*X(4) + CO*X(1)
XDOT(2) = W*SN*X(1) + W*CO*X(3) - X(6) + C(2)

KMS00520
 KMS00530
 KMS00540
 KMS00550
 KMS00560
 KMS00570
 KMS00580
 KMS00590
 KMSC0600

XDNT(3) = -W*CO*X(2) - W*CO*X(4) - SN*X(7)
 XDNT(4) = X(6)
 XDNT(5) = X(7)
 XDNT(6) = K*X(2) - W*SN2*X(7) + C(1)
 XDNT(7) = -K/CO*X(1) + 2.*W*TN*X(6) + C(2)

GO TO 1
 END

C

KWS00040
KWS00050
KWS00060
KWS00070
KWS00080
KWS00090
KWS00100
KWS00110
KWS00120
KWS00130
KWS00140
KWS00150
KWS00160
KWS00170
KWS00180
KWS00190
KWS00200
KWS00210
KWS00220
KWS00230
KWS00240
KWS00250
KWS00260
KWS00270
KWS00280
KWS00290
KWS00300
KWS00310
KWS00320
KWS00330
KWS00340
KWS00350
KWS00360
KWS00370
KWS00380
KWS00390
KWS00400
KWS00410
KWS00420
KWS00430
KWS00440
KWS00450
KWS00460
KWS00470
KWS00480
KWS00490
KWS00500
KWS00510

```

//KWSSTAS JOB (2211,1196), 'KWSSTAS SAFLIANIS', CLASS=A
// EXEC FRTXCLGP
// FORT.SYSIN DD *
DIMENSION X(30), XDOT(30), C(15)
REAL*8 W, WIE, K
REAL*4 SN, SN2, CO, TN, L

CONSTANTS
WIE = .2618 "RAD/HR" = 900 "ARC-MIN/HR" = EARTH RATE
K = G/R = 19.52 "1/HR**2" ( K**2 = SHULER FREQ. )
C(1) = (U)W<N> = NORTH GYRO DRIFT = 1 "MERU" = 0.015 "DEG/HR"
C(2) = (U)W<E> = EAST " " = 1 "MERU" = 0.015 "DEG/HR"
C(3) = (U)W<D> = AZIMUTH " " = 1 "MERU" = 0.015 "DEG/HR"
L = LATITUDE "RAD"
L = LOCAL EARTH RATE

FUNCTIONS
WIE = .2618
L = .7854
K = 19.52
SN = SIN(L)
SN2 = SIN(2.*L)
CO = COS(L)
TN = TAN(L)

CASE : EASTERLY FLIGHT 600 "FT/SEC" = 355.5 "KNOTS"
W = 1.557 * WIE

C(10) = 1
1 CALL INTEG2(T,X,XDOT,C)

EQUATIONS
XDOT(1) = -W*SN*X(2) - W*SN*X(4) + CO*X(7)
XDOT(2) = W*SN*X(1) + W*CO*X(3) - X(6) + C(2)
XDOT(3) = -W*CO*X(2) - W*CO*X(4) - SN*X(7)
XDOT(4) = X(6)
XDOT(5) = X(7)
XDOT(6) = K*X(2) - W*SN2*X(7) + C(1)

```

KWS00520
KWS00530
KWS00540
KWS00550
KWS00560

XDOT(7) = -K/CO*X(1)+2.*W*TN*X(6)+C(2)

GO TO 1
END

C

KWS00520
KWS00530
KWS00540
KWS00550
KWS00560

XDOT(7) = -K/CO*X(1)+2.*W*TN*X(6)+C(2)

GO TO 1
END

C

KWS00040
 KWS00050
 KWS00060
 KWS00070
 KWS00080
 KWS00090
 KWS00100
 KWS00110
 KWS00120
 KWS00130
 KWS00140
 KWS00150
 KWS00160
 KWS00170
 KWS00180
 KWS00190
 KWS00200
 KWS00210
 KWS00220
 KWS00230
 KWS00240
 KWS00250
 KWS00260
 KWS00270
 KWS00280
 KWS00290
 KWS00300
 KWS00310
 KWS00320
 KWS00330
 KWS00340
 KWS00350
 KWS00360
 KWS00370
 KWS00380
 KWS00390
 KWS00400
 KWS00410
 KWS00420
 KWS00430
 KWS00440
 KWS00450
 KWS00460
 KWS00470
 KWS00480
 KWS00490
 KWS00500
 KWS00510

```

CCC
      //KWSSTAS JOB (2211,1196), 'KWSSTAS SAFLIANIS', CLASS=A
      // EXEC FRTXCLGP
      // FORT. SYSIN DD *
      DIMENSION X(30), XDOT(30), C(15)
      REAL*8 W, WIE, K
      REAL*4 SN, SN2, CO, TN, L
  
```

```

CONSTANTS
WIE = 2618 "RAD/HR" = 900 "ARC-MIN/HR" = EARTH RATE
K = G/R = 19.92 "1/HR**2" ( K**2 = SHULER FREQ. )
C(1) = (U)F<N> = NORTH ACCEL BIAS = 0.2E-4 "G"
C(2) = (U)F<E> = EAST
L = LATITUDE "RAD"
TN = LOCAL EARTH RATE
  
```

```

FUNCTIONS
WIE = .2618
L = .7854
K = 19.92
SN = SIN(L)
SN2 = SIN(2.*L)
CO = COS(L)
TN = TAN(L)
  
```

```

CASE : STATIONARY
W = WIE
C(10) = 1.
1 CALL INTEG2(T,X,XDOT,C)
  
```

```

EQUATIONS
XDOT(1) = -W*SN*X(2) - W*SN*X(4) + CO*X(7)
XDOT(2) = W*SN*X(1) + W*CO*X(3) - X(6) + C(2)
XDOT(3) = -W*CO*X(2) - W*CO*X(4) - SN*X(7)
XDOT(4) = X(6)
XDOT(5) = X(7)
XDOT(6) = K*X(2) - W*SN2*X(7) + C(1)
XDOT(7) = -K/CO*X(1) + 2.*W*TN*X(6) + C(2)
  
```

CCC
 CCCCCCCCCCCCCCCC
 CCC CC CCCCCC

KMS00520
KMS00530
KMS00540
KMS00550

GO TC 1
END

C

KWS00520
KWS00530
KWS00540
KWS00550

GO TO 1
END

C

KW5C0520
KW500530
KW5C0540
KW500550

GO TO 1
END

C

KWS00520
 KWS00530
 KWS00540
 KWS00550
 KWS00560
 KWS00570
 KWS00580
 KWS00590
 KWS00600

XDOT(3) = -W*CO*X(2) - W*CO*X(4) - SH*X(1)
 XDOT(4) = X(6)
 XDOT(5) = X(7)
 XDOT(6) = K*X(2) - W*SN2*X(7) + C(1)
 XDOT(7) = -K/CO*X(1) + 2.*W*TN*X(6) + C(2)

GO TO 1
 END

C

AD-A126 689

INERTIAL NAVIGATION SYSTEMS AIDED BY GPS(U) NAVAL
POSTGRADUATE SCHOOL MONTEREY CA C C SAFLIANIS DEC 82

4/4

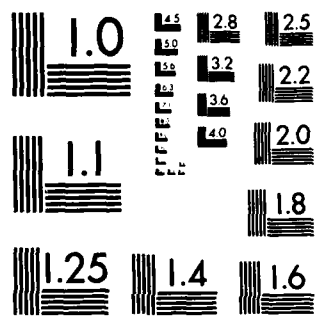
UNCLASSIFIED

F/G 17/7

NL



END
DATE
FILMED
BY
DTIC



MICROCOPY RESOLUTION TEST CHART
NATIONAL BUREAU OF STANDARDS-1963-A

```

C C C
//KWSTAS JOB (2211,1196),'KWSTAS SAFLIANIS',CLASS=A
// EXEC FRTXCLGP
//FCRT-SYSIN DC *
DIMENSION X(30),XDOT(30),C(15)
REAL*8 W,WIE,K
REAL*4 SN,SN2,CC,TN,L

CONSTANTS
WIE = .2618 "RAD/HR" = 900 "ARC-MIN/HR" = EARTH RATE
K = G/R = 19.92 "1/HR**2" ( K**2 = SHULER FREQ. )
C(1) = F<N>(0) = NORTH LEVEL ERROR = 0.14 "MIL"RAD" = 0.483 "ARC-MIN"
C(2) = E<E>(0) = EAST " " = " "
C(3) = E<D>(0) = AZIMUTH " " = " "
C(4) = CLAD(0) = LATITUDE ERROR = 0.17 "MIL"RAD" = 0.586 "ARC-MIN"
C(5) = CLAD(0) = LCNGITUDE ERROR = " "
C(6) = CLAD(0) = LAT. RATE ERROR = 2 "FT/SEC" = 1.184 "ARC-MIN/HR"
C(7) = CLAD(0) = LCNG. RATE ERROR = " "
L = LATITUDE "RAD"
W = LOCAL EARTH RATE

FUNCTIONS
WIE = .2618
L = 7854
K = 19.92
SN = SIN(L)
SN2 = SIN(2.*L)
CO = COS(L)
TN = TAN(L)

CASE : EASTERLY FLIGHT 600 "FT/SEC" = 355.5 "KNOTS"
W = 1.557 * WIE

C(10) = 1.
1 CALL INTEG2(T,X,XDOT,C)

EQUATIONS
XDOT(1) = -W*SN*X(2)-W*SN*X(4)+CO*X(7)
XDOT(2) = W*SN*X(1)+W*CO*X(3)-X(6)+C(2)

```

KMS00520
 KMS00530
 KMS00540
 KMS00550
 KMS00560
 KMS00570
 KMS00580
 KMS00590
 KMS00600

XDOT(3) = -W*CO*X(2) - W*CO*X(4) - SN*X(7)
 XDOT(4) = X(6)
 XDOT(5) = X(7)
 XDOT(6) = K*X(2) - W*SN2*X(7) + C(1)
 XDOT(7) = -K/CO*X(1) + 2.*W*TN*X(6) + C(2)
 GO TO 1
 END

KMS00520
 KMS00530
 KMS00540
 KMS00550
 KMS00560
 KMS00570
 KMS00580
 KMS00590
 KMS00600

$XDOT(3) = -W*CO*X(2) - W*CO*X(4) - SN*X(7)$
 $XDOT(4) = X(6)$
 $XDOT(5) = X(7)$
 $XDOT(6) = K*X(2) - W*SN2*X(7) + C(1)$
 $XDOT(7) = -K/CO*X(1) + 2.*W*IN*X(6) + C(2)$

GO TO 1
 END

3

[illegible]

APPENDIX E

I.N.S./G.P.S. ERROR ANALYSIS COMPUTER PROGRAMS

KMS00040
KMS00050
KMS00060
KMS00070
KMS00080
KMS00090
KMS00100
KMS00110
KMS00120
KMS00130
KMS00140
KMS00150
KMS00160
KMS00170
KMS00180
KMS00190
KMS00200
KMS00210
KMS00220
KMS00230
KMS00240
KMS00250
KMS00260
KMS00270
KMS00280
KMS00290
KMS00300
KMS00310
KMS00320
KMS00330
KMS00340
KMS00350
KMS00360
KMS00370
KMS00380
KMS00390
KMS00400
KMS00410
KMS00420
KMS00430
KMS00440
KMS00450
KMS00460
KMS00470
KMS00480
KMS00490
KMS00500
KMS00510

```

//K$T$$ JOB (2211,1196),*K$TAS SAFLIANIS*,CLASS=A
//*MAIN GRG=NPGVM1,2211P,LINES=(40)
//**FORMAT PR,DDNAME=K$T$$,DEST=LOCAL
//**FORMAT PR,CDNAME=K$T$$,DEST=NPGVM1-2211P
//**FORMAT PR,CDNAME=K$T$$,DEST=LOCAL
// EXEC FRTXCLGP
//FCRT.SYSIN DD *
DIMENSION X(30),DCT(30),C(15)
REAL*8 W,WIE,K
REAL*4 SN,SN2,CC,TN,L
IX = 6758756

CONSTANTS
WIF = 2618 "RAD/HR" = 900 "ARC-MIN/HR" = EARTH RATE
K = G/R = 19.92 "1/HR**2" ( K**2 = SIULER FREQ. )
L = LATITUDE "RAD"
W = LOCAL EARTH RATE

FUNCTIONS
WIE = 2618
L = 19.92
SN = SIN(L)
SN2 = SIN(2.*L)
TN = TAN(L)
LATRUE = 0.00000522
LOTRUE = 0.00000522

CASE : STATICNARY
W = WIE

C(10) = 1.
CALL INCRM(IX,W,1,16807,0)
CALL INCRM(IX,V,1,16807,0)
CALL INTEG2(T,X,XDOT,C)

```

KWS00520
 KWS00530
 KWS00540
 KWS00550
 KWS00560
 KWS00570
 KWS00580
 KWS00590
 KWS00600
 KWS00610
 KWS00620
 KWS00630
 KWS00640
 KWS00650
 KWS00660
 KWS00670
 KWS00680
 KWS00690
 KWS00700
 KWS00710
 KWS00720
 KWS00730
 KWS00740
 KWS00750
 KWS00760
 KWS00770
 KWS00780
 KWS00790
 KWS00800
 KWS00810
 KWS00820
 KWS00830
 KWS00840
 KWS00850
 KWS00860
 KWS00870
 KWS00880
 KWS00890
 KWS00900
 KWS00910
 KWS00920
 KWS00930
 KWS00940
 KWS00950
 KWS00960
 KWS00970
 KWS00980
 KWS00990

EQUATIONS

$XDOT(1) = -W*SN*X(2) - W*SN*X(4) + CC*X(7) + AA*X(14) + (X(8) - X(4)) + X(15) * (X(9) - X(5))$
 $XDOT(2) = W*SN*X(1) + W*SN*X(3) - X(6) + BB + X(16) * (X(8) - X(4)) + X(17) * (X(9) - X(5))$
 $XDOT(3) = -W*CO*X(2) - W*CO*X(4) - SN*X(7) + SS + X(18) * (X(8) - X(4)) + X(19) * (X(9) - X(5))$
 $XDOT(4) = X(6) + X(20) * (X(8) - X(4)) + X(21) * (X(9) - X(5))$
 $XDOT(5) = X(7) + X(22) * (X(8) - X(4)) + X(23) * (X(9) - X(5))$
 $XDOT(6) = K * X(2) - W*SN^2 * X(7) + DD + X(24) * (X(8) - X(4)) + X(25) * (X(9) - X(5))$
 $XDOT(7) = -K/CO * X(1) + 2 * H * TN * X(6) + EE + X(26) * (X(8) - X(4)) + X(27) * (X(9) - X(5))$

A = 0.00000006853
 B = 0.00000006853
 C = 0.00000006853
 D = 0.00000006853
 E = 0.00000006853
 F = 0.00000006853
 G = 0.00000006853
 $X(8) = X(10) - FF$
 $X(9) = X(11) - GG$
 $LATRUE = 0.000000522$
 $LOTRUE = 0.000000522$
 $X(11) = LOTRUE$
 $X(12) = V$
 $X(13) = X(12) * SQRT(A)$
 $AA = X(12) * SQRT(B)$
 $BB = X(12) * SQRT(C)$
 $SS = X(12) * SQRT(D)$
 $DD = X(12) * SQRT(E)$
 $EE = X(13) * SQRT(F)$
 $GG = X(13) * SQRT(G)$
 $X(14) = K11$
 $X(15) = C.0347566672$
 $X(16) = K12$
 $X(17) = 1.7201123$
 $X(18) = K21$
 $X(19) = -1.36921265$
 $X(20) = K22$
 $X(21) = -0.0401669175$

```

X(18) = K31 6555360
X(19) = K32 86193609
X(20) = -2: K41 44020611
X(21) = 3: K42 0507281520
X(22) = 0: K51 0507281520
X(23) = 0: K52 431037639
X(24) = 4: K61 2162494
X(25) = 5: K62 239257459
X(26) = -0: K71 104245351
X(27) = 1: K72 25378811
X(27) = 9: 25378811

```

```

GO TO 1
END

```

C

```

KMS01000
KMS01010
KMS01020
KMS01030
KMS01040
KMS01050
KMS01060
KMS01070
KMS01080
KMS01090
KMS01100
KMS01110
KMS01120
KMS01130
KMS01140
KMS01150
KMS01160
KMS01170
KMS01180
KMS01190
KMS01200
KMS01210
KMS01220

```

```
//KWST$$ JOB (2211,1196),'KWSTRAS SAFLIANIS',CLASS=A  
//#MAIN ORG=NPGVMI,2211P,LINES=(40)  
//FORMAT PR,CNAME=KWST$,DEST=LOCAL  
//FORMAT PR,CNAME=KWST$,DEST=NPGVMI,2211P  
//FORMAT PR,CNAME=PLOT,SYSVECTR,DEST=LOCAL  
//EXEC FBXCLGP  
//FORT.SYIN DD *  
DIMENSION X(20),XDOT(20),C(15)  
REAL*8 W,WIE,K  
REAL*4 SN,SN2,CC,TN,L  
  
IX = 6758756  
  
CONSTANTS  
  
WIE = .2618 "RAD/HR" = 900 "ARC-MIN/HR" = EARTH RATE  
K = G/R = 19.92 "1/HR**2" ( K**2 = SHULER FREQ. )  
L = LATITUDE "RAD"  
W = LOCAL EARTH RATE  
  
FUNCTIONS  
  
WIE = .2618  
L = .7854  
K = 19.92  
SN = SIN(L)  
SN2 = SIN(2.*L)  
CO = COS(L)  
TN = TAN(L)  
LATRUE = 0.000000522  
LOTRUE = 0.000000522  
  
CASE : STAGINARY  
  
W = WIE  
  
C(10) = 1.  
CALL LNCRM{IX,W,1,168C7,O}  
CALL LNORM{IX,V,1,168O7,O}  
CALL INTEG2(T,X,XDOT,C)  
  
EQUATIONS
```



```

X(20)
X(20)
X(21)
X(21)
X(22)
X(22)
X(23)
X(23)
X(24)
X(24)
X(25)
X(25)
X(26)
X(26)
X(27)
X(27)

GO TO 1
END

```

298

C

```

XDOT(1)=-W*SN*X(2)-W*SN*X(4)+CU*X(7)+AA*X(14)*(X(8)-X(4))+X(15)*(X
$ (9)-X(5))
XDOT(2)= W*SN*X(1)+W*CO*X(3)-X(6)+BB*X(16)*(X(8)-X(4))+X(17)*(X(9)
$ -X(5))
XDOT(3)=-W*CC*X(2)-W*CO*X(4)-SN*X(7)+SS*X(18)*(X(8)-X(4))+X(19)*(X
$ (9)-X(5))
XDOT(4)= X(6)+X(20)*(X(8)-X(4))+X(21)*(X(9)-X(5))
XDOT(5)= X(7)+X(22)*(X(8)-X(4))+X(23)*(X(9)-X(5))
XDOT(6)= K*X(2)-W*SN2*X(7)+DD*X(24)*(X(8)-X(4))+X(25)*(X(9)-X(5))
XDOT(7)= -K/CO*X(1)+2.*W*TN*X(6)+EE+X(26)*(X(8)-X(4))+X(27)*(X(9)
$ -X(5))
XDOT(14) = -(1./CT)*X(14) + X(12)
XDOT(15) = -(1./CT)*X(15) + X(12)
XDOT(16) = -(1./CT)*X(16) + X(12)
XDOT(17) = -(1./CT)*X(17) + X(12)
XDOT(18) = -(1./CT)*X(18) + X(12)

```

KWS00520
 KWS00530
 KWS00540
 KWS00550
 KWS00560
 KWS00570
 KWS00580
 KWS00590
 KWS00600
 KWS00610
 KWS00620
 KWS00630
 KWS00640
 KWS00650
 KWS00660
 KWS00670
 KWS00680
 KWS00690
 KWS00700
 KWS00710
 KWS00720
 KWS00730
 KWS00740
 KWS00750
 KWS00760
 KWS00770
 KWS00780
 KWS00790
 KWS00800
 KWS00810
 KWS00820
 KWS00830
 KWS00840
 KWS00850
 KWS00860
 KWS00870
 KWS00880
 KWS00890
 KWS00900
 KWS00910
 KWS00920
 KWS00930
 KWS00940
 KWS00950
 KWS00960
 KWS00970
 KWS00980
 KWS00990

3

```

A = 0.C0000CC6853
B = 0.C0000CC6853
S = 0.00000C18981
D = 0.00000C18981
E = 0.00000C02
F = 0.00000C02
G = X(10) - FF
X(8) = X(10) - GC
X(9) = X(11) - GC
LATRUE = 0.C00000522
LOTRUE = LATRUE
LOTRUE = 0.CC0000522
X(10) = W
X(11) = W
X(12) = V
X(13) = (2/CT)*(X(15)+X(12))*SQR(T(A))
AA = (2/CT)*(X(16)+X(12))*SQR(T(B))
BB = (2/CT)*(X(17)+X(12))*SQR(T(S))
SS = (2/CT)*(X(18)+X(12))*SQR(T(D))
DD = (2/CT)*(X(19)+X(12))*SQR(T(E))
EE = (2/CT)*SQR(T(F))
FF = X(13)*SQR(T(G))
GG = X(13)*SQR(T(G))

X(14) = K11
X(14) = 0.0347566672
X(15) = K12
X(15) = 1.17201123
X(16) = K21
X(16) = -1.36921265

```

C

KMS01000
 KMS01010
 KMS01020
 KMS01030
 KMS01040
 KMS01050
 KMS01060
 KMS01070
 KMS01080
 KMS01090
 KMS01100
 KMS01110
 KMS01120
 KMS01130
 KMS01140
 KMS01150
 KMS01160
 KMS01170
 KMS01180
 KMS01190
 KMS01200
 KMS01210
 KMS01220
 KMS01230
 KMS01240

K22 C401669175
 = -0.5655360
 = K31
 = 1.32
 = K32
 = -2.186193605
 = K41
 = 3.44020611
 = K42
 = 0.507281520
 = K51
 = 0.0907281520
 = K52
 = 4.31037629
 = K61
 = 5.92162494
 = K62
 = -0.339257459
 = K71
 = 1.04245351
 = K72
 = 9.2527811

X(17)
 X(18)
 X(19)
 X(20)
 X(21)
 X(22)
 X(23)
 X(24)
 X(25)
 X(26)
 X(27)
 X(27)

GO TO 1
 END

C

LIST OF REFERENCES

1. Britting, K.R., Inertial Navigation System Analysis, Wiley-Interscience, undated.
2. Maybeck, P.S., Stochastic Models, Estimation and Control, Vol. I, Academic Press, 1979.
3. Schmidt, G.T., and Brock, L.D., General Questions on Kalman Filtering in Navigation Systems, in Theory and Applications of Kalman Filtering (C.T. Leondes), Agardograph No. 139, London, February 1970.
4. D'Appolito, J.A. and Roy, K.J., Satellite/Inertial Navigation System Kalman Filter Design Study, Technical Report AFAL-TR-71-178, AFAL, Wright-Patterson AFB, Ohio, 1971.
5. Widnall, W.S. and Grundy, P.A., Inertial Navigation System Error Models, Intermetrics TR-03-73, Intermetrics Inc., Cambridge, Massachusetts, May 1973.
6. Hammett, J.E., Evaluation of a Proposed INS Kalman Filter in a Dynamic Flight Environment, Master's Thesis, Air Force Institute of Technology, Wright-Patterson AFB, Ohio, December 1974.
7. Pitman, G.R., Jr., Inertial Guidance, John Wiley & Sons, New York-London, undated.
8. The Institute of Navigation, Global Positioning System, undated.
9. Brockstein, A.J., GPS Kalman Augmented I.N.S. Performance, NAECON '76 Record, pp. 864-871, National Aerospace Electronics Conference.
10. Battin, R.H., Astronautical Guidance, New York, McGraw-Hill, 1974.
11. Synge, J.L., and Griffith, B.A., Principles of Mechanics, New York, McGraw-Hill, 1959.
12. Collins, D., Notes for the course EE 3472, Naval Postgraduate School, Monterey, California, undated.
13. Bryson, A.E., Kalman Filter Divergence and Aircraft Motion Estimators, Vol. I, AIAA Journal, January 1970.

BIBLIOGRAPHY

- AGARD-LS-82, Practical Aspects of Kalman Filtering Implementation, AD-AO 24377, March 1976.
- AGARD-LS-95, Strapdown Inertial Navigation Systems, NATO publications, France 1978.
- ADARDOGRAPH No. 139, Theory and Applications of Kalman Filtering, C.T. Leondes, February 1970.
- Andreev, V.D., Theory of Inertial Navigation Aided Systems, Translation from Russian, Israel Program for Scientific Translation, Jerusalem 1969.
- Britting, K., Error Analysis of Strapdown and Local Level Inertial Systems which Compute in Geographic Coordinates, M.I.T., Measurement Systems Laboratory, November 1969.
- Fitzgerald, R.J., Divergence of the Kalman Filter, Trans. Automatic Control, AC-16(8), pp. 736-747 (1971).
- Gelb, A., Applied Optimal Estimation, M.I.T. Press, 1974.
- Heller, W.G., Models for Aided Inertial Navigation System Sensor Errors, TASC TR-312-3, The Analytic Science Corporation, Reading, Massachusetts, February 1975.
- Hollister, W.M. and Brayard, M.C., Optimum Mixing of Inertial Navigator and Position Fix Data, Rep. RE-62, M.I.T. Measurement Systems Lab, RE-77, M.I.T., Cambridge, Massachusetts, November 1970.
- Leondes, C.T., Guidance and Control of Aerospace Vehicles, McGraw-Hill, 1963.
- Markey, W and Hovorka, J., The Mechanics of Inertial Position and Heading Information, Methuen, 1961.
- Maybeck, P.S., Applied Optimal Estimation: Kalman Filter Design and Implementation, Notes for a short course presented by the A.F.I.T., Wright-Patterson AFB, Ohio, 1972.

McRuer, Ashkenas and Graham, Aircraft Dynamics and Automatic Control, undated.

Myers, K.A. and Butler, R.R., Simulation Results for an Integrated GPS/Inertial Aircraft Navigation System, NAECON 1976 Record, pp. 841-848.

O'Donnell, C.F., Inertial Navigation Analysis and Design, McGraw-Hill, 1964.

Papoulis, A., Probability Random Variables and Stochastic Processes, McGraw-Hill, 1965.

Pyle, R.H., Defense Navigation Satellite Development Program Performance Analysis, Space and Missile System Organization, The Analytic Sciences Corporation, Massachusetts, 15 April 1974.

Pyle, R.H., and Rains, R.G., Global Positioning System (Phase I) Error Analysis, Space and Missile System Organization, The Analytic Sciences Corporation, Massachusetts, TR-428-1, August 1974.

Sandell, M.R. and Athans, Modern Control Theory Manual of Fortran Computer Subroutines for Linear Quadratic Gaussian Design, M.I.T. Press, 1965.

The Analytic Sciences Corporation, GPS Simulation Development and Analysis, Book 1 of 2, TR-428-2, 15 December 1974.

The Analytic Sciences Corporation, GPS Simulation Development and Analysis, Book 2 of 2, TR-428-2, 15 December 1974.

INITIAL DISTRIBUTION LIST

	No. Copies
1. Library, Code 0142 Naval Postgraduate School Monterey, California 93940	2
2. Department Chairman, Code 62 Department of Electrical Engineering Naval Postgraduate School Monterey, California 93940	1
3. Department Chairman, Code 67 Department of Aeronautics Naval Postgraduate School Monterey, California 93940	1
4. Professor D.J. Collins, Code 67Co Department of Aeronautical Engineering Naval Postgraduate School Monterey, California 93940	3
5. Professor H. Titus, Code 62Ts Department of Electrical Engineering Naval Postgraduate School Monterey, California 93940	2
6. Defense Technical Information Center Cameron Station Alexandria, Virginia 22314	2
7. Lt. Constantinos Ch. Saflianis Pyrrou 43 ATHENS - 505 GREECE	6
8. Hellenic General Naval Staff (HGNS) Education Department Camp Papagou ATHENS - GREECE	3
9. G.E.T.E.N. Camp Papagou ATHENS - GREECE	1

10. E.M. Polytechnion 1
Department of Electrical Engineering
ATHENS - GREECE
11. E. M. Polytechnion 1
Department of Aeronautical Engineering
ATHENS - GREECE
12. Dr. Ioannis Saflianis 1
Arivou 52
ATHENS - 505
GREECE
13. Nicolas Kalouptzidis (Ph.D.) 1
Artakis 80
Ano Nea Smyrni
ATHENS - GREECE
14. Lt. Dimitrios Pouliezios (MSES) 1
513 Athinon Street - TT89
Keratsini
ATHENS - GREECE
15. Lt. Athanasios Palikaris 1
SMC 1292
Naval Postgraduate School
Monterey, California 93940

END

DATE
FILMED

5 - 83

DTIC